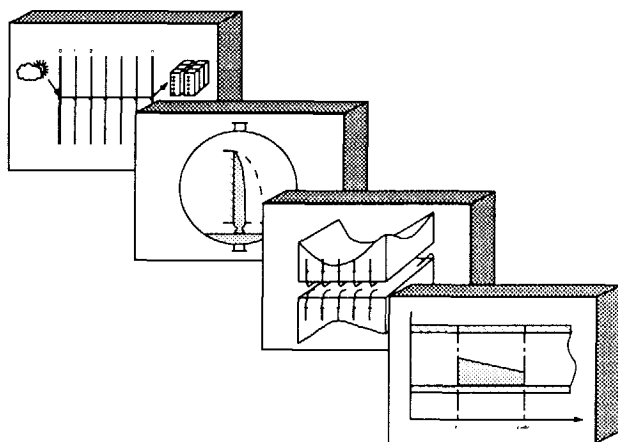


MODELLING OF A REFRIGERATING SYSTEM COUPLED WITH A REFRIGERATED ROOM

TR diss
1910



H. Wang

CIP-DATA KONINKLIJKE BIBLIOTHEEK, DEN-HAAG

Wang, H

Modelling of a refrigerating system coupled with a refrigerated room /

H. Wang. - Delft : Delft University of Technology, Faculty of Mechanical Engineering and Marine Technology. - III.

Thesis Delft. - With ref. - With summary in Dutch.

ISBN 90-370-0051-7

Subject headings: refrigerating systems / refrigerated rooms.

Copyright ©1991, Faculteit der Werktuigbouwkunde en Maritieme Techniek,
Technische Universiteit Delft.

Alle rechten voorbehouden.

Niets uit dit rapport mag op enigerlei wijze worden verveelvoudigd of openbaar gemaakt zonder schriftelijke toestemming van de auteur.

All rights reserved.

No part of this book may be reproduced by any means, or transmitted without the written permission of the authors.

Gebruik of toepassing van de gegevens, methoden en/of resultaten enz., die in dit rapport voorkomen, geschiedt geheel op eigen risico.

De Technische Universiteit Delft, Faculteit der Werktuigbouwkunde en Maritieme Techniek, aanvaardt geen enkele aansprakelijkheid voor schade, welke uit gebruik of toepassing mocht voortvloeien.

Any use or application of data, methods and/or results etc., occurring in this report will be at user's own risk. The Delft University of Technology, Faculty of Mechanical Engineering and Marine Technology, accepts no liability for damages suffered from the use or application.

STELLINGEN

1. One of the basic problems a model-maker ought to think about is how to avoid his(her) model having an excellent agreement only with the "reality" to which the validation is subjected.
2. If computer programmes form part of a promotion work, then writing a thesis is not enough to imply a finish of the work; the "promovendus" (the person to be promoted) should also clearly document his programmes, so that his successors will not get too many troubles in using the programmes.
3. Two-zone modelling of dry expansion evaporators is consistent with the Lagrangian approach in fluid mechanics (the boundary between the two-phase and single-phase flow regions is traced in order to derive the governing equations), while distributed modelling complies with the Eulerian approach (the coordinate for deriving the governing equations is fixed on the evaporator pipe). The successful application of the Eulerian approach in fluid mechanics justifies the choice of a distributed model of evaporator in chapter 2.
4. PHOENICS is a globally recognised software that almost everybody is able to operate with beautiful pictures as output. However, to obtain a practically reliable result, much more efforts are needed than just to tick the keyboards of computers. Therefore, as a third party to evaluate the PHOENICS output, people should be very careful and independent.
5. In recent years, people are desperately searching for new CFC substitute refrigerants because of the ecological concerns. However, if attention is paid only to the ozone-layer depletion with forgetting the greenhouse effect, the results may be diverse from the purpose.
6. In nowadays scientific papers, statements, such as "a lot of investigations [1], [2], [3] ... have been done in this field", are frequently encountered. In most of the cases, they can be explained as: the author didn't have enough patience or time to read those articles, but he had a lack of references.
7. A.I.O. at Delft University of Technology should be more and more interpreted as "geAvanceerd Internationale Onderwijs (advanced international education)" instead of "Assistent In Opleiding (assitant in training)".

8. Peace and war are "twins", as long as nations are existing.
9. The inability of referees to absolutely fairly judge is a big pity of today's football.
10. Today, many people claim to be environmentalists, but few know how to be a real one.
11. A good film is like a beautiful painting one can just look at; a good novel however is like a sketch one can still paint.

Hongwei Wang, April 9, 1991

MODELLING OF A REFRIGERATING SYSTEM COUPLED WITH A REFRIGERATED ROOM

Proefschrift

Ter verkrijging van de graad van doctor aan de Technische Universiteit Delft,
op gezag van de Rector Magnificus, Prof. drs P.A. Schenck
in het openbaar te verdedigen ten overstaan van
een commissie aangewezen door het College van Dekanen
op dinsdag 9 april 1991 om 14.00 uur

Hongwei Wang

geboren te Shaanxi, China
Werktuigkundig ingenieur

Dit proefschrift is goedgekeurd door de promotor
Prof. ir A.L. Stolk

dr ir S. Touber
heeft als begeleider in hoge mate bijgedragen
aan het totstandkomen van het proefschrift.
Het College van Dekanen heeft hem als zodanig aangewezen.

CONTENTS

CONTENTS	I
SUMMARY	VII
SAMENVATTING	IX
NOMENCLATURE	XI
CHAPTER 1 INTRODUCTION	1
1.1 General	1
1.2 Why a Vapour Compression Refrigerating Machine ?	2
1.3 Why a Refrigerated Room ?	3
1.4 Coupling between a Refrigerating Machine and a Refrigerated Room	4
1.5 Outline of the Thesis	6
References	8
CHAPTER 2 DYNAMIC MODELLING OF THE EVAPORATOR	9
2.1 General	9
2.2 Literature	11
2.3 Modelling Strategies	15
2.3.1 Conclusions from the literature review	15
2.3.2 Modelling strategies	16

2.4	Derivation of the Equations	17
2.4.1	Basic equations	17
2.4.2	Modification of the basic equations	23
2.5	Void Fraction Model (VFM)	26
2.5.1	Comparison of the existing void fraction models	26
2.5.2	Effects of the VFM on the evaporator behaviour	30
2.6	Off-Period Modelling	32
2.6.1	Incomplete evaporation situation	33
2.6.2	Complete evaporation situation	34
2.7	Discretization of the Equations	34
2.7.1	The refrigerant side	34
2.7.2	The pipe wall	35
2.7.3	The air side	37
2.7.4	Transformation between the two element notations	37
2.7.5	Logic diagram	38
	References	40

CHAPTER 3 DYNAMIC MODELLING OF THE CONDENSER 43

3.1	General	43
3.2	Literature	45
3.3	Division of Basic Elements	46
3.4	Conservation Equations	49
3.4.1	Superheated vapour	49
3.4.2	Liquid film	50
3.4.3	Subcooled liquid	51
3.4.4	Tube wall	52
3.4.5	Cooling water	52
3.4.6	Shell wall	53
3.4.7	Closure of the conservation equations	53
3.5	Boundary Layer Theory	54
3.5.1	Setting up of boundary layers for vertical film condensation	54
3.5.2	Calculation of the boundary layer thickness δ and δ_T	56
3.5.3	Calculation of the heat transfer to the liquid film	57
3.6	Solution of the Equations	59
3.7	Closure	60
	References	62

CHAPTER 4 STEADY-STATE MODELLING OF THE REFRIGERATING MACHINE 63

4.1	General	63
4.2	Literature	64

4.3	The Three-Zone Steady-State Evaporator Model	66
4.3.1	Assumptions	67
4.3.2	Conservation equations	68
4.3.3	Closure of the equations	71
4.3.4	Implementation of the evaporator model	71
4.4	The Two-Zone Steady-State Condenser Model	75
4.4.1	Assumptions	75
4.4.2	Conservation equations	75
4.4.3	Closure of the equations	76
4.4.4	Implementation of the condenser model	76
4.5	Coupling of the Component Models	80
4.5.1	Input and output description	80
4.5.2	The cyclic computation	82
	References	83

CHAPTER 5	MODELLING OF THE REFRIGERATED ROOM	85
5.1	General	85
5.2	Literature	86
5.3	Modelling Strategies	87
5.3.1	Solutions to reduce the long computational time	87
5.3.2	Lumped model versus distributed model	89
5.3.3	Steady-state model versus dynamic model	89
5.4	Modelling the Air Flow	90
5.4.1	Basic equations	90
5.4.2	Boundary conditions	91
5.4.3	Solution of the equations with the aid of PHOENICS	94
5.4.4	Air flow through ball-like products	100
5.5	Modelling of Heat and Mass Transport	101
5.5.1	Air	101
5.5.2	Walls	105
5.5.3	Products	107
5.6	Criterion for the De-Coupling of the Governing Equations	109
5.7	Heat and Mass Transport through Door-Opening	110
5.7.1	A simple open-door model	110
5.7.2	Combination of the open-door model with the room model	112
5.8	Computer implementation	114
5.8.1	Establishment of computational grids	114
5.8.2	Flow charts	116
5.9	Closure	116
	References	119

CHAPTER 6	HEAT, MASS AND MOMENTUM TRANSFER COEFFICIENTS	121
6.1	General	121
6.2	In the Evaporator	123
6.2.1	Between the refrigerant and pipe wall	123
6.2.2	Between the pipe walls	132
6.2.3	Between the pipe wall and air	133
6.2.4	Heat transfer coefficient in off-periods	137
6.2.5	Effects of oil presence on the inside transfer coefficients	138
6.3	In the Condenser	139
6.3.1	Condensation zone	139
6.3.2	Subcooling zone	142
6.4	On the Connection Lines	144
6.5	In the Refrigerated Room	144
6.5.1	Micro-climate	144
6.5.2	Macro-climate	147
6.5.3	Outside of the room	148
6.6	Closure	149
	References	150
CHAPTER 7	VALIDATION OF THE MODELS	153
7.1	General	153
7.2	Contents of the Experiments	154
7.3	Description of the Experiment Plant	154
7.4	Measurement Instruments	156
7.5	Determination of Several Empirical Constants	158
7.5.1	Constants A, B, m in Eqs. (6.31) and (6.32)	160
7.5.2	Constants a, b, c in Eqs. (6.4), (6.9) and (6.11)	163
7.5.3	Interfacial momentum-transport coefficient f_i in Eq. (2.9)	164
7.6	Validation of the Steady-State Model	166
7.7	Validation of the Dynamic Model	168
7.8	Validation of the Air Flow Model (PHOENICS)	177
7.8.1	Measurement of the turbulence intensity produced by the evaporator fans	178
7.8.2	Measurement of the air flow	181
	References	184
CHAPTER 8	APPLICATIONS OF THE MODELS	185
8.1	General	185
8.2	Prediction of the Steady-State Distribution of the Air Velocity, Temperature and Humidity in a Cold Store	186

8.2.1	Problem setting	186
8.2.2	Presentation of the results	188
8.2.3	Discussion and conclusions	196
8.3	Study of C.O.P. with Different Capacity Control Systems	197
8.3.1	Group G1: on-off(rpm=1195), P and PI control systems	198
8.3.2	Group G2: two-stage, on-off(rpm=700) and on-off(rpm=1195) control systems	202
8.3.3	Group G3: the effects of thermal mass on C.O.P.	202
	References	207
CHAPTER 9 CONCLUSIONS		209
9.1	About the Models	209
9.1.1	The evaporator model	209
9.1.2	The condenser model	210
9.1.3	The refrigerated room model	211
9.2	About the Validation of the Models	211
9.2.1	The steady-state validation	211
9.2.2	The dynamic validation	212
9.2.3	The validation of the air flow model (PHOENICS)	213
9.3	About the Applications of the Models	214
9.3.1	Using PHOENICS to study the air distributions in cold stores	214
9.3.2	The effects of capacity control systems on the system performance	215
9.3.3	The effects of thermal mass on the C.O.P. with on-off control	216
9.4	Recommendations for Further Investigations	216
9.4.1	Long-term simulations accounting for weather and climate changes	216
9.4.2	Modification of the lumped steady-state evaporator model into a distributed one	216
9.4.3	Extensive applications of the refrigerated room model	217
9.4.4	Simulations using substitute fluids for CFCs	217
APPENDIX 1	The Compressor Model	A1
APPENDIX 2	The TEV Model	A5
APPENDIX 3	Calculation of the Heat Transfer Areas in the Condenser	A7
CURRICULUM VITAE		A11
ACKNOWLEDGEMENT		A12

A refrigeration process is an energy transport process through which heat is removed from spaces or substances which are expected to be colder than their surroundings. Since the first compression refrigerating machine was invented 1834, it has been becoming a ultimate goal of refrigeration engineering to use as less energy as possible to produce as much refrigeration as possible; people have been searching various methods for the enhancement of refrigeration efficiency. In recent years, the environmental concerns of human being (i.e., ozone depletion and greenhouse effect) are announcing the importance of energy saving more loudly than ever. Today, mathematical modelling as one of the advanced methods is being extensively applied to design, analyze, economize and optimize refrigerating systems.

The investigation described in this thesis is aimed to develop a set of comprehensive computer models to simulate and analyze both steady-state and non-steady-state behaviour of a refrigerating system coupled with a refrigerated room. The refrigerating system is a single-stage vapour compression system consisting of four basic elements: a reciprocating piston compressor, a dry expansion evaporator (air cooler), a shell and tube water cooled condenser and a thermostatic expansion valve.

The research work is divided into three stages: theoretical modelling, experimental validation, and application. The theoretical part of the investigation includes the literature review, the determination of modelling strategies, the derivation of basic equations, the computer implementation of the mathematical models. The modelling procedure consists of the steady-state and dynamic modelling of the evaporator and condenser, the coupling of the component models with a simple description of the connection pipe lines and auxiliary devices. The steady-state evaporator model is a lumped model with dividing the

evaporator pipes into three zones. This model is mainly used as a start program for non-steady-state simulations. The dynamic evaporator model takes the form of a distributed model with slicing the evaporator pipes into small elements which are described by a set of matrices. The steady-state and dynamic condenser models are all lumped and involve a new concept of film condensation boundary layer. The compressor model was deduced from the experimental fitting and the model of the thermostatic expansion valve was established and validated by a precedent investigator. The model of the refrigerated room is added in order to have a more or less realistic dynamic "load" for the refrigerating machine when the model is used to simulate dynamic behaviour, e.g. to simulate control strategies.

To validate the computer models, a test plant was set up, on which steady-state and dynamic measurements were carried out. Experiments were firstly done to determine several empirical constants encountered in the models. Then the simulation results were compared with a series of measurements within a wide range of operation conditions. Good agreement was achieved from the comparison.

The validated models were applied for two practical purposes: 1. the prediction of the air distributions in a cold store: PHOENICS was applied to simulate the 3-D air flow pattern. Based on the predicted velocity and pressure distributions, our own model was employed to simulate the temperature and humidity distributions. The predicted temperature fields were also compared to the measurement results; 2. the study of system C.O.P with different capacity control systems: four types of capacity control systems were compared, which were on-off system, multi-stage system, proportional system and proportional plus integral system. The capability and reliability of the models have been proved by the results from the two application examples. Moreover, a number of technical findings have been obtained which could be useful in practice.

Het koelmachineproces leidt tot een energietransport waardoor warmte wordt onttrokken aan ruimten of voorwerpen die kouder zijn dan hun omgeving. Sinds de eerste compressiekoelmachine werd uitgevonden (1834), heeft men er naar gestreefd om met een zo laag mogelijk energieverbruik een zo hoog mogelijke koelcapaciteit te verkrijgen. Er is gezocht naar verschillende methoden om het nuttig effect te vergroten. In de afgelopen jaren benadrukt de zorg voor het milieu nog eens extra de belangrijkheid van de energiebesparing in verband met de ozon-reductie en het broeikas effect. Tegenwoordig worden geavanceerde methoden, meestal met behulp van wiskundige modellen, intensief toegepast bij ontwerp, analyse, economische aspecten en optimalisatie van koelsystemen.

Het in dit proefschrift beschreven onderzoek is bedoeld om een aantal uitgebreide computermodellen van koelmachine-componenten te ontwikkelen voor het simuleren en analyseren van een koelsysteem, gekoppeld aan een gekoelde ruimte. Het koelsysteem is een ééntraps dampcompressiesysteem, bestaande uit 4 componenten: een zuigercompressor, een luchtkoeler met "droge" verdamping, een watergekoelde bundel-pijpcondensor, en een thermostatisch expansieventiel.

Het onderzoek is gesplitst in 3 delen: theoretische modellering, experimentele toetsing en de toepassing. Het theoretisch deel van het onderzoek betreft het literatuuroverzicht, de bepaling van de modelleringsstrategie, het afleiden van de basisformules, en het maken van computerprogramma's voor de rekenmodellen. De modelleringsprocedure bestaat uit de stationaire en dynamische modellering van verdamper en condensor, en van de gekoelde ruimte, het koppelen van componentmodellen met een eenvoudige beschrijving van de verbindingsleidingen en verdere appendages. Het stationaire verdampermodel is een zône-model dat de verdamperpijpen in drie zônes verdeeld. Dit model wordt hoofdzakelijk gebruikt als

startprogramma voor simulaties van het niet-stationaire gedrag. Het dynamisch verdampermodel is opgezet als een gedistribueerd model dat de verdamperpijpen in korte elementen verdeelt die wiskundig door een aantal matrices wordt beschreven. De stationaire en de dynamische condensermodellen zijn beiden zône-modellen. Daarbij werd een nieuw concept voor film-condensatie toegepast. Het compressormodel is een stationair model afgeleid uit experimentele resultaten, en het model van het thermostatisch expansieventiel is opgezet en geevalueerd door een vorige onderzoeker. Het model van de gekoelde ruimte is in principe opgezet als gedistribueerd model waarin een macro-klimaat en een micro-klimaat wordt onderscheiden. Het model van de gekoelde ruimte is toegevoegd om, bij simulatie van het dynamisch gedrag van de koelmachine, over een enigszins realistische, dynamische "belasting" van de machine te kunnen beschikken.

Ten behoeve van de validatie van de computermodellen is een proefopstelling gebouwd waaraan metingen in stationaire en niet-stationaire toestand werden uitgevoerd. Eerst zijn er experimenten verricht om de verschillende empirische constanten vast te stellen, die in de modellen toegepast zijn. Daarna zijn de simulatieresultaten vergeleken met een serie metingen met een brede variatie van de bedrijfscondities. Er is een goede overeenkomst verkregen uit deze vergelijking.

De gevalideerde modellen werden voor twee praktische doeleinden toegepast:

1. Het voorspellen van de luchtstroming in een koelhuis: Hierbij werd een bestaand pakket, PHOENICS, toegepast om de 3-dimensionale luchtstroming te simuleren. Gebaseerd op de voorspelde snelheids- en drukverdelingen, werd dit model gebruikt om de temperatuur en vochtigheidsverdeling te simuleren.
2. De studie van de C.O.P. van het systeem met verschillende regelsystemen voor de koelcapaciteit: vier typen regelsystemen zijn vergeleken, te weten: aan-uit regeling, meertrapsregeling, proportionele regeling en proportionele regeling met integrerende werking.

De geschiktheid en de betrouwbaarheid van de modellen is beproefd aan de hand van de resultaten van deze twee toepassingsvoorbeelden. Een aantal uitkomsten zijn verkregen, die van praktisch nut kunnen zijn.

NOMENCLATURE

Symbols	Physical Meaning	Units
A	Area, or constant	[m ²]
a	Heat diffusivity, or constant	[m ² /s]
B	Constant	
b	Constant	
C	Constant,or coefficient	
c	Specific heat, or constant	[kJ/(kg · °C)]
D	Outer diameter of pipe	[m]
d	Inner diameter of pipe	[m]
E	Fraction of liquid flow rate entrained in the vapour stream	
F	Friction force	[N/m ³]
f	Interfacial momentum-transport coefficient	[kg/(m ³ · s)]
G	Mass flux	[kg/(m ² · s)]
g	Gravity (=9.8)	[m/s ²]
H	Height	[m]
h	Specific enthalpy	[kJ/kg]
I	Number of elements in the i direction	
IV	Input value	
i	Coordinate	
J	Number of elements in the j direction	

JP	Parameter in Eq. (6.17)	
J(s)	Parameter in Eq. (6.17)	
j	Coordinate, or factor	
K	Number of elements in k direction	
k	Turbulent kinetic energy, or adiabatic exponent, or coordinate	[J/kg]
L	Length	[m]
l	Characteristic length	[m]
M	Mass, or number of elements in the refrigerant flow direction	[kg]
\dot{M}	Interfacial mass-transport rate	[kg/(m ³ · s)]
m	Denoting the space increment in the refrigerant flow direction	
\dot{m}	Mass flow rate	[kg/s]
N	Various numbers, or number of elements in the time domain	
n	Denoting the time increment, or rotational speed	[1/min]
P	Pressure	[N/m ²]
Q	Heat transfer	[kW]
q	Heat flux	[kW/m ²]
R	Gas constant	[m ² /(s ² · K)]
S	Source term vector	
S	Surface area, or various source terms	[m ²]
s	Fin spacing	[m]
T	Absolute temperature	[K]
t	Time	[s]
U	Velocity	[m/s]
\mathbf{U}	Velocity vector (U_1, U_2, U_3)	[m/s]
u	Velocity	[m/s]
V	Velocity, or volume	[m/s] [m ³]
\mathbf{V}	Velocity vector (V_1, V_2, V_3)	[m/s]
\dot{V}	Volume flow	[m ³ /s]
v	Velocity	[m/s]
w	Water vapour concentration in air	[kg/kg]
W	Power	[kW]
x	Quality, or coordinate	[m]
y	Fin thickness, or	[m]

	distance from wall, or	[m]
	position of the adjusting screw of the TEV	[count]
z	Coordinate	[m]

Greek symbols

\dot{A}	Flux of k	[N/(m · s)]
α	Heat transfer coefficient	[kW/(K · m ²)]
$\langle \alpha \rangle$	Void fraction	
β	Mass transfer coefficient	[kg/(m ² · s)]
Γ	Transfer flux	
γ	Latent heat of water	[kJ/kg]
δ	Diffusivity of water vapour in air, or boundary layer thickness	[m ² /s] [m]
ε	Porosity of product packing, or dissipation rate of k	[J/(kg · s)]
η	Efficiency	
θ	Temperature	[°C]
Λ	Momentum flux	[N/m ²]
κ	Transfer coefficient; constant	
λ	Heat conductivity	[kW/(°C · m)]
μ	Dynamic viscosity	[N · s/m ²]
ν	Kinetic viscosity	[m ² /s]
ξ	Friction factor	
Π	Replaceable parameter	
ρ	Density	[kg/m ³]
σ	Constant, or surface tension	[N/m]
τ_s	Surface shear stress	[N/m ²]
Ω	Source term for $\langle \alpha \rangle$, or flux of ε	[N/(m · s ²)]
ω	Volumetric coefficient of thermal expansion	[1/K]
ϕ	Relative humidity, or transport quantity	[%]

Subscripts

<i>a</i>	Air
<i>abs</i>	Absorbing
<i>ad</i>	Adiabatic
<i>ai</i>	Air inlet condition
<i>amb</i>	Ambient
<i>ao</i>	Air outlet condition
<i>atm</i>	Atmospheric
<i>b</i>	Bend
<i>bou</i>	Boundary layer; boundary condition
<i>con</i>	Condensation
<i>cond</i>	Condenser
<i>comp</i>	Compressor
<i>cyl</i>	Cylinder
<i>d</i>	Dry-out
<i>dis</i>	Discharge condition
<i>door</i>	open-door
<i>E</i>	East cell
<i>e</i>	Evaporation region; east wall of cell
<i>evap</i>	Evaporator
<i>f</i>	Friction
<i>film</i>	Liquid film
<i>fin</i>	Fins
<i>fr</i>	Frost-formation
<i>g</i>	Superheated vapour
<i>H</i>	High cell
<i>h</i>	High wall of cell
<i>heat</i>	Heating system
<i>hydr</i>	Hydrolic
<i>i</i>	Interface; inside; inlet
<i>ib</i>	Inside basis
<i>in</i>	Inlet
<i>L</i>	Low cell
<i>l</i>	Saturated liquid; low wall of cell
<i>lv</i>	From liquid to vapour
<i>m</i>	Average
<i>mac</i>	Macro-climate
<i>mic</i>	Micro-climate
<i>mv</i>	Mixing vapour
<i>N</i>	North cell
<i>n</i>	North wall of cell

<i>nat</i>	Natural convection
<i>nuc</i>	Nucleate boiling
<i>o</i>	Oil; outside, outlet
<i>ob</i>	Outside basis
<i>off</i>	Off-period
<i>out</i>	Outlet
<i>P</i>	Centre of cell
<i>p</i>	At constant pressure
<i>pipe</i>	Bare pipe
<i>prod</i>	Product
<i>pw</i>	Pipe wall
<i>pwi</i>	Pipe wall at inlet
<i>pwo</i>	Pipe wall at outlet
<i>r</i>	Refrigerant
<i>ref</i>	Reflection
<i>ri</i>	Refrigerant inlet condition
<i>rl</i>	Refrigerant liquid
<i>ro</i>	Refrigerant outlet condition
<i>row</i>	Row of pipes
<i>rv</i>	Refrigerant vapour
<i>S</i>	South cell
<i>s</i>	Superheat region; sensible; south wall of cell
<i>s1</i>	Superheat zone 1
<i>s2</i>	Superheat zone 2
<i>sh</i>	Condenser shell
<i>sh1</i>	Lower part of the condenser shell
<i>sh2</i>	Upper part of the condenser shell
<i>solar</i>	Solar
<i>sp</i>	Single-phase region
<i>str</i>	Straight pipe
<i>sub</i>	Subcooling zone
<i>t</i>	Turbulence; total
<i>T</i>	Thermal boundary layer
<i>tev</i>	Thermostatic expansion valve
<i>tot</i>	Total
<i>tp</i>	Two-phase region
<i>tube</i>	Condenser tube
<i>v</i>	Saturated vapour
<i>vl</i>	From vapour to liquid
<i>vol</i>	Volumetric
<i>W</i>	West cell
<i>w</i>	Water; west wall of cell; referring to w

<i>wall</i>	room's wall
<i>wl</i>	From pipe wall to refrigerant liquid
<i>wv</i>	From pipe wall to refrigerant vapour
α	Referring to $\langle \alpha \rangle$
Π	Referring to Π
θ	Referring to θ
<i>1-d</i>	1-dimension
<i>3-d</i>	3-dimensions
<i>1</i>	x-coordinate
<i>2</i>	y-coordinate
<i>3</i>	z-coordinate

Superscripts

-	Average
+	Dimensionless
'	Next time step; correction term
*	Assumed value

Dimensionless parameters

Numbers	Symbols	Physical meanings	Formula
Reynolds	Re	$\frac{\text{inertia force}}{\text{viscous force}}$	$\frac{u l}{\nu}$
Nusselt	Nu	$\frac{\text{total heat transfer}}{\text{heat transfer by diffusion}}$	$\frac{\alpha l}{\lambda}$
Prandtl	Pr	$\frac{\text{velocity boundary layer thickness}}{\text{temperature boundary layer thickness}}$	$\frac{\nu}{a}$
Lewis	Le	$\frac{\text{temperature boundary layer thickness}}{\text{concentration boundary layer thickness}}$	$\frac{a}{\delta}$
Schmidt	Sc	$\frac{\text{velocity boundary layer thickness}}{\text{concentration boundary layer thickness}}$	$\frac{\nu}{\delta}$
Sherwood	Sh	$\frac{\text{total mass transfer}}{\text{mass transfer by diffusion}}$	$\frac{\beta l}{\delta \rho}$
Grashof	Gr	$\frac{\text{force due to density difference}}{\text{viscous force}}$	$\frac{g \rho l^3 \Delta T}{\nu^2}$
Martinelli parameter	X_{tt}	$\frac{\text{frictional pressure gradient of liquid-alone flow}}{\text{frictional pressure gradient of vapour-alone flow}}$	$\frac{\left[\rho_v^{-0.5} \right] \left[\mu_l \right]^{0.1} \left[1-x \right]^{0.9}}{\left[\rho_l \right] \left[\mu_v \right] \left[x \right]}$
Boiling number	Bo	$\frac{\text{quality change}}{\text{unit length}}$	$\frac{J \Delta x \gamma}{l}$

Rayleigh	Ra	Gr · Pr	$\frac{g\alpha\beta\Delta T}{\nu\alpha}$
----------	----	---------	--

1.1 General

In the early years of refrigeration, people could only carry out research by doing experiments or very simple calculations. The primitiveness and laboriousness of the methods seriously retarded the progress of refrigeration technology. By the early 60's of this century, a new technique entered the field of refrigeration, that is *mathematical modelling*. After nearly three decades of development, this technique has been becoming an indispensable tool for both scientific research and industrial practice in today's refrigeration. The impact of computer models in research, design, manufacturing, operation, and control of refrigerating components and systems is enormous. Optimization, intelligent control, dynamic simulation, CAD and so on are increasingly applied, as the consequence of using computer models. All these advanced methods are helping people to continuously improve the performance and reliability of refrigerating machines, the quality and profitability of refrigeration applications.

In the past years, a lot of computer models have been developed in the field of refrigeration, which varied from steady-state to dynamic, from lumped to distributed, from "black" to "white". The history of the progress was excellently recorded in [1.1]. However, with the rapid development of computer technology, the need for more accurate, more sophisticated and more realistic mathematical models is increasing. In this aspect, refrigeration is still behind the other technological areas, such as applied mechanics, hydrodynamics, control engineering. On the other hand, the modelled objects are being required to extend from components of refrigerating machines to those using refrigeration, such as refrigerated warehouses, freezing tunnels, refrigerated transport equipment, etc. One

of the reasons for this is that it is found that the dynamic behaviour of refrigerating machines is strongly influenced by their application partners. For these purposes, the involvement of other technologies in refrigeration is inevitable. For example, the application of standard computer software developed in the fields of fluid mechanics, heat transfer, numerical mathematics is gradually becoming popular in refrigeration and air conditioning. With such disciplinary interference, many unsolved problems encountered in the early years are being tackled and the modelling technique is beginning a new era in refrigeration.

As a contribution to this field, the investigation described in this dissertation is intended to make use of the new modelling methodology and strategies to model a vapour compression refrigerating machine coupled with a refrigerated room as a whole (see Fig. 1-1).

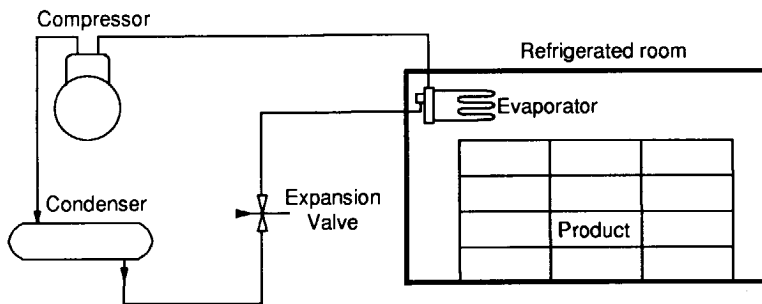


Fig. 1-1 Schematic diagram of the system consisting of a refrigerating machine and a refrigerated room.

1.2 Why a vapour compression refrigerating machine ?

In nowadays refrigeration, there are a variety of types of refrigerating machines working with different principles. Generally, they can be classified into five categories : 1. evaporative system, 2. expansion system, 3. **compression system**, 4. absorption system, 5. thermo-electric system. Among them compression system is the most commonly used, owing to its higher efficiency. Although the recent concern of human being about their environment (ozone depletion and global warming) is encouraging people to employ the other types of refrigerating systems, specially absorption systems, it seems that vapour compression systems will still be the main refrigerating systems in the foreseen future, but working with non-ozone depleting refrigerants.

A vapour compression refrigerating machine normally consists of four components: compressor, evaporator, condenser and expansion device (see Fig. 1-1).

1.3 Why a refrigerated room ?

Modern refrigeration has many applications in industries and human daily lives, which are normally classified into 5 categories: domestic refrigeration, industrial refrigeration, refrigerated transport, air conditioning, *food preservation*. As a matter of life or death of human being, refrigerated food preservation has occupied about 80% of the application area of refrigeration.

As a result of industrialization and urbanisation, today, foods are usually produced in places far from where most of them are consumed. Therefore, transportation and storage of foods over long distances and periods have become necessary. However, during transport and storage, foods are subjected to changes in quality, such as taste, shape, nutritional value and so on. Such changes are caused by biological, chemical and physical reactions. All the reactions are dependent on the temperature of foods: the lower the temperature is, the slower the reactions are. Thus, Lowering of the storage temperature has always been the most important method of diminishing detrimental changes in fresh foods. According to [1.2], in retail food distribution systems in developed countries today, about half of the product value is distributed at temperatures below ambient.

Refrigeration, as a method of producing cold, is playing a very important role in preserving food. In recent years, cold chains have been widely used to store, transport and distribute agricultural products in many countries. A cold chain consists of all stages from harvesting to retailing of food products. These stages include harvesting, processing (packing and sorting), storing, transporting, distributing, retailing and consuming of foods. In cold chains, a refrigerated room is a typical object which can be a cold store, a container, or a train wagon, etc.

In a refrigerated room, air circulation (or distribution) is one of the basic requirements of thermal protection of perishable food products. As mentioned above, in order to prevent food products from deteriorating during transportation and storage, people have to keep them under certain required conditions which are usually related to temperature, humidity, and concentrations of carbon-dioxide and oxygen. These conditions are realised normally in refrigerated rooms. To be convenient to transport, load and unload, products are stacked by using boxes or pallets in the rooms. Consequently, the conditions in the rooms are often far from uniform so that part of the products seem to be in good quality, while part of them might be already perishing. Therefore, it is very important to study the influencing factors to the distribution of the conditions in the rooms.

1.4 Coupling between a refrigerating machine and a refrigerated room

In principle, the efficiency of refrigerating systems can be increased by either designing them properly or operating them economically. The first is usually called *optimal design* and the second *optimal operation*. Optimal design actually results in an optimal choice of steady-state conditions for maximum economy. It needs steady-state models to provide the possibilities for optimization. Usually, for steady-state modelling for the purpose of optimal design, a refrigerating machine exclusive its application partner is considered, because the connections between these two parts can be easily separated.

In contrast, optimal operation results in a series of optimal adaptations of the system to time dependent working conditions. A typical example of optimal operation in refrigeration is capacity control which is realised by using the feed-back control strategy. A sensor is located on the application side and the signal obtained by the sensor is used to adjust the refrigerating capacity of the system. The adjustment could be on-off or stepwise or continuous depending on the required accuracy. The variation of the capacity can keep the refrigerated conditions within a certain required range. Such a number of actions take place under non-steady-state conditions. Thus, dynamic models are necessary to reveal the dynamic behaviour of the system. In this case, the system to be modelled should not be only the refrigerating machine itself but also its application partner, because the interactions between these two parts to a large extent influence the dynamic behaviour of the whole system.

In principle, a refrigerating machine may have more than one application partners. For example, in the case of storage warehouse, several storage rooms are usually cooled by one refrigerating unit. However, as the first attempt to model a complete system, only one application component, a refrigerated room, is assumed herein.

The coupling between a refrigerating machine and a refrigerated room can be analogued by a mechanical problem as shown in Fig. 1-2. The machine part can be represented by a small mass, because its thermal mass, defined as the product of density and specific heat, is smaller, as compared to the room which is replaced by a big mass. If the mass difference between these two objects is considerable, there will be two completely different combinations:

Short-term coupling

If the transient behaviour of the refrigerating machine with small mass is considered, its influence on the behaviour of the refrigerated room is negligible. Thus, during a short period such as several minutes or one hour, the behaviour of the room could be considered as constant (see the left side of Fig. 1-2). Based on this assumption, we may simplify the

modelling for a short-term coupling: the products and walls of the refrigerated room could be treated as time-independent elements.

Long-term coupling

If the refrigerated room is emphasized, the refrigerating machine will receive almost 100 % of influence from the room side. The machine seems to be following the room in view of a long-term observation (see the right side of Fig. 1-2). In this case, the modelling strategy could be totally different from that for a short-term coupling. A good combination of a steady-state machine model with a non-steady-state room model is then suitable. With this combination, a lot of computation times can be saved during simulations, because large time steps can be adopted for integration.

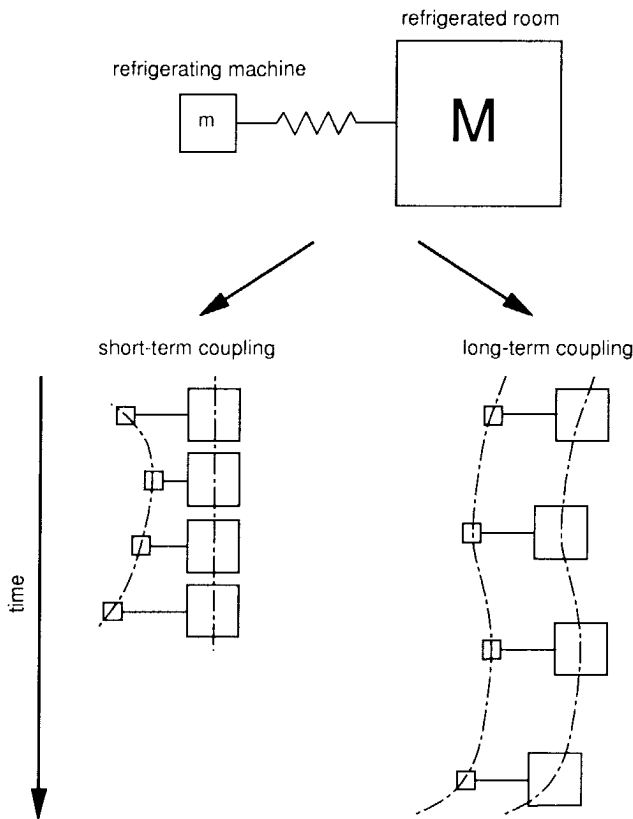


Fig. 1-2 Coupling between a refrigerating machine and a refrigerated room.

1.5 Outline of the thesis

This thesis consists of nine chapters and three appendices. The functions of each chapter are briefly described below.

Chapter 1 is the introduction part in which the motive and objective of the investigation are described. Moreover, attention is paid to the coupling between the refrigerating machine and refrigerated room, in order to distinguish two completely different simulations: short-term and long-term. Finally the organization of the text is introduced.

Chapter 2 describes the dynamic modelling of the evaporator. Following a general description of the evaporator and literature review, the basic equations are derived and modified on the basis of a series of modelling strategies. Then the solution methodology and computer implementation are reported.

Chapter 3 deals with the dynamic modelling of the condenser, which follows the same procedures as chapter 2.

Chapter 4 is about the steady-state modelling of the refrigerating machine. As the strategies of steady-state modelling are different from those of dynamic modelling, a separate chapter is specially written, in which the steady-state models of the evaporator and condenser are set up. Besides, part of the text is used to describe the coupling of the models.

Chapter 5 describes the modelling of the refrigerated room. Because the modelling method and basic equations are more or less the same in both steady-state and dynamic situations, no special treatment is made just for a steady-state model, as in chapter 4. All the equations in this chapter are, therefore, in the form of non-steady-state equations. However, simplification to be a steady-state model is just a matter of scratching those derivatives with respect to time.

Chapter 6 is a collection of all the correlations for the heat, mass and momentum transfer coefficients encountered in the previous chapters where, to be clear, only the governing equations are focused, while those auxiliary correlations are left for this chapter.

Chapter 7 describes the experimental validation of the mathematical models. Three groups of conventional experiments were carried out for three purposes: determination of several empirical constants; validation of the steady-state models; and validation of the dynamic models. Moreover, a special experiment was done to measure the air velocity distribution in the test room, in order to check the simulation results by PHOENICS.

Chapter 8 gives two examples of applying the models to solve practical problems. One is to predict the air distributions in a cold store and another is to study different capacity control systems. Some interesting conclusions obtained from the simulations are reported in this chapter.

Chapter 9 concludes the whole thesis and gives several recommendations for further investigations.

Appendices 1 and 2 describe the models of the compressor and thermostatic expansion valve respectively. Appendix 3 is about how to calculate the heat transfer areas in the condenser according to the amount of liquid refrigerant.

References

- 1.1 **Touber, S.** "Principles and methods for mathematical modelling the steady-state and dynamic behaviour of refrigeration components and installations", *I.I.F. - I.I.R. - Commission B2 - Dresden*, 1984, pp.163-175.
- 1.2 **Persson, P.-O.** "Refrigeration and its influence on the world food supply now and in the future", *International Journal of Refrigeration*, Vol 10, No 5, 1987, pp.279-284.

Dynamic Modelling of the Evaporator

2.1 General

An evaporator is a heat exchanger which realises the purpose of a refrigerating system. By evaporating refrigerants, heat can be removed from the space where lower temperature is needed. In practice there are a lot of types of evaporators which are classified in Fig. 2-1. Among them, air coolers are the most commonly used in refrigerated storage and transportation. This type of evaporators can be directly installed in places where products are stored. The fans on an air cooler act as ventilators to distribute cold air so that no extra re-circulation systems are needed in a cold store. Fig. 2-2 shows a typical air cooler which will be the object to be modelled in this chapter.

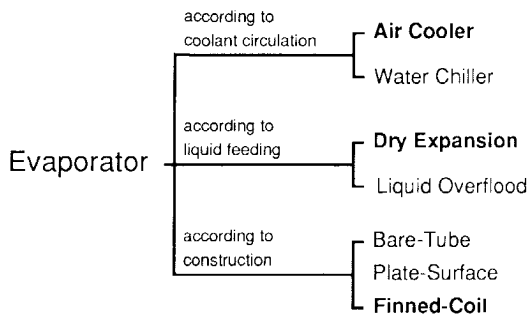


Fig. 2-1 Classification of refrigeration evaporators.

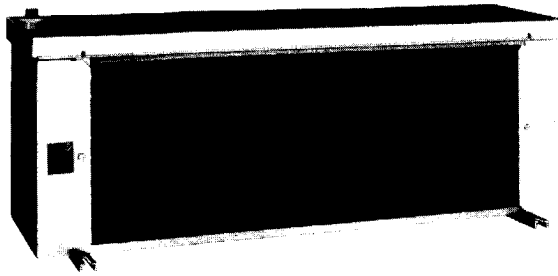


Fig. 2-2 Photograph of an air cooler which is the object to be modelled.

Usually, air coolers are also called dry expansion evaporators, because they are often accompanied by thermostatic expansion valves; the refrigerants needs to be totally evaporated and superheated so that two completely different regions appear in the evaporator coils: a two-phase flow (or evaporation) region and a single-phase flow (or superheat) region. The superheat temperature is in turn used as a feedback signal of the expansion valves. In most cases, a dry expansion evaporator may have several parallel refrigerant circuits. The refrigerant coming from the expansion valve is split into parallel streams each of which undergoes the same processes in the evaporator. At the end of the evaporator, there is a header to collect all the superheated refrigerant from every circuit. On the air side, the fans supply a forced air flow across the tube bank. Even with such a forced air flow, the heat transfer coefficient on the air side is still much lower than that on the refrigerant side. Thus extended surface is necessary to intensify the outside heat transfer. Normally plate fins are equipped on the tube bank.

Compared to the other components of refrigerating systems or other types of evaporators, dry expansion evaporators are relatively more complicated to model, due to the complexity of the two-phase flows involved. For example, in the case of a shell and tube evaporator, lumped models are fully successful in describing the mechanism. However, lumped models are inadequate for dry expansion evaporators, at least in dynamic cases. In the past, many models have been developed for compressors, expansion devices, condensers and evaporators, but air coolers are still an obstacle for model makers. Therefore, it is still necessary to investigate this problem.

On the other hand, as almost every refrigerating system operates under variable conditions, a pure steady-state does not exist. Specially if capacity controllers are fitted to the system,

investigations should not be limited only to steady-state analysis, but also to non-steady state or dynamic analysis. Dynamic modelling is a mathematical description of the system in the time domain. Mass and energy accumulate or dissipate in the system due to differences between the input and output of mass and energy to the system.

A complete dynamic model of dry expansion evaporators, such as air coolers, should include two parts: an on-period model and an off-period model. The first describes the dynamic behaviour of evaporators during on-periods and the second depicts what occurs when the refrigeration system is switched off. The reason for considering these two aspects is that most of the refrigeration systems used today are still equipped with on-off control elements. In fact, the dynamics of an evaporator are strongly influenced by the turn-on and turn-off procedures of the compressor. Therefore, ignoring of the off-period modelling is irrational.

The dynamic behaviour of an evaporator results from both energy and mass accumulations. The heat capacity of the pipes and refrigerant acts as a reservoir of heat energy. The two-phase flow taking place inside the evaporator pipes is the reason for mass accumulation. Thus the success of dynamic modelling for dry-expansion evaporators depends to a large extent on the degree of understanding of the two-phase flow mechanism.

Usually, the heat exchange process between the refrigerant and coolant in a dry expansion evaporator takes place in the form of cross-flow. However, in order to improve the heat transfer efficiency or meet the special requirements of customers, manufacturers design air coolers with various pipe circuiting methods. This diversity makes the modelling of air coolers even more difficult. Accordingly distributed models are increasingly required to maintain flexibility and applicability.

2.2 Literature

In the last few years there have been many publications related to the dynamic modelling of dry expansion evaporators. These can be classified into four categories: black box models, one-zone models, two-zone models and distributed models. The following section will give a detailed review.

Black box models

Black box modelling is actually an idea from system control theory. It has the advantage of simplicity, but does not reveal the mechanism of dynamic behaviour. With this type of modelling, an evaporator system can be represented by a set of transfer functions with several constants which are determined through experiments. Black box models are commonly used to investigate control problems in refrigeration. Several models have appeared in the past.

As an attempt to apply system control theory to an evaporator-expansion valve control loop, **Stoecker** [2.1, 2.2] made one of the pioneering black box models for a refrigerant-in-tube evaporator. He assumed two linear elements for the evaporator: the motion of the boundary between the evaporation and superheat regions; and the thermal capacity of the coils. One linear element was set up for the expansion valve. With this assumption, the whole system could be represented by one time-lag and three time constants and three zero-frequency magnitude ratios. Then various combinations of the constants were compared subjected to the stability of the system. It was also found that the time constant for the boundary motion was longer for step increases in flow rate than that for step decreases.

Najork [2.3] investigated the possibilities for improvement of the stability of an evaporator control loop. Similar to **Stoecker**, he also made use of a black box model to represent every part of the evaporator and expansion valve. Through the experiments, it was found that different pipe configurations of the evaporator could lead to different stabilities of the control loop.

One-zone models

One-zone models are suitable for both type or shell and tube evaporators. However, in dry expansion evaporators, the refrigerants mostly flow through long coils and undergo two different flow regions. Thus, one-zone models have not been widely used. Below are some exceptions.

Chi and Didion [2.4] developed one of the first dynamic models of heat pumps. The evaporator was modelled as lumped. All the refrigerant in the evaporator was considered as one zone with inlet and outlet mass flows. The average density of liquid-vapour mixture was a time-dependent variable which could describe the phase change process occurring in the evaporator. By setting up mass, momentum and heat balances for the lumped zone, three ordinary differential equations were derived. Apparently, this is a very simple evaporator model which cannot completely reveal the dynamic behaviour of the evaporator.

Marshall and James [2.5] modelled a non-dry evaporator by using one-zone model. The evaporator was followed by a liquid separator. The mixture refrigerant inside tubes was considered as compressible medium with an assumed relationship between the inlet pressure and quality and the average density. Moreover, constant heat transfer coefficients inside and outside the tubes were used.

Another one-zone model for a dry expansion evaporator was made by **Hargreaves and James** [2.6] when they investigated a marine chilled water plant for microprocessor control development. The model is an overall lumped parameter type and does not distinguish between the two-phase and single-phase regions. The overall heat transfer coefficient was assumed as

a function of the inlet refrigerant mass flow rate and the mass storage of the refrigerant was neglected because the internal volume of the chiller tubes was small.

Two-zone models

Two-zone evaporator models are very popular. With the division of an evaporator into two zones, the two-phase and single-phase flow regions are considered separately so that the mass and energy conservations can be reasonably described. Nevertheless, a discontinuity of variables between the two regions is inevitably rooted in this type of models. This requires some artificial "repairs" to make the model sufficiently realistic (see [2.14]). Two-zone models need an average heat transfer coefficient in the two-phase flow region, and because the correlations for the heat transfer coefficient are usually in the form of local values, mathematical integration has to be worked out to calculate the average value. Some assumptions are necessary for this, for instance, linear distribution of quality. Another disadvantage of the two-zone models is that they are not flexible for different pipe circuiting arrangements.

Wedekind and **Stoecker** [2.7, 2.8] firstly proposed the two-zone model consisting of a two-phase region and a single-phase region to predict the transient responses of the motion of the boundary between the two regions in a horizontal evaporating flow, in which the system mean void fraction concept was introduced. Following this research, **Wedekind** et al [2.9] continued to investigate the system mean void fraction model. The assumption that the system mean void fraction is time-invariant de-couples the problem from the transient form of the momentum principle. That is an analytical simplification of considerable magnitude. However, as the model is inherently a lumped parameter model, it is impossible to predict the time delay effect caused by the propagation of the step change signal from the beginning to the end of the evaporator pipe.

Dhar and **Soedel** [2.10] made a simple two-zone model to study the dynamic behaviour of a vapour compression refrigeration system during start-up of the system. To be general, an accumulator was also included in the model. However, it was not clearly shown how to identify the two control volumes, that is, the calculation of the length of the two-phase region was not concerned. It seems to be that the two zones have fixed volumes. Such a simplification may make the simulation results unrealistic.

Bruijn et al [2.11] developed a two-zone model with a moving boundary. It was assumed that the mean void fraction in the evaporator was time-independent and the axial pipe heat conduction and refrigerant pressure drop were negligible. This model was later improved by **Yasuda** et al [2.12, 2.13] with adding pressure drop and dividing the pipe metal into small elements to take the axial heat conduction into account. It is obvious that, with this model, the boundary between the two-phase and single-phase regions moves immediately when there is a step change in flow rate at the inlet of the coil.

Such a consequence apparently contradicts the reality. Therefore, **van der Meer** [2.14] in his Ph.D. thesis spent a lot of efforts to modify this model. He used several transportation times to delay various parameters which influence the length of the two-phase region. The **Chawla** correlation for the slip effect between refrigerant liquid and vapour was used, when these transportation times were calculated. Meanwhile, he found that the correlations for heat transfer, pressure drop, void fraction in the two-phase flow region were strongly dependent on the geometrical dimensions and configurations of the modelled evaporators. He also pointed out a combination of theory and empiric were necessary for modelling of evaporators. He mentioned in his conclusions that a distributed model of a dry expansion evaporator could not increase the simulation accuracy, compared to a simple two-zone lumped model, due to the complexity of the two-phase flow.

Bonte and Veldhoven [2.15] made a two-zone model with a fixed boundary between the two regions. The energy balance equations for refrigerant and pipe were simplified into exponent equations with time constants and gain factors. Thus the dynamic effects were largely considered as a black box model. The block-diagram method was used to analyze the dynamic behaviour of the evaporator coupled with a thermostatic expansion valve. Experiments were carried out to check the model.

Broersen and van der Jagt [2.16] followed the idea introduced in [2.9] that the system mean void fraction was time-independent and assumed the distribution of the refrigerant liquid over the two-phase region behaved as a first-order element. They then made linearization and Laplace transformation of the energy and mass balance equations and finally obtained a single-input single-output transfer function to relate the liquid flow entering the evaporator and the opening of the expansion valve. The simple transfer function can be used to analyze the hunting problem of evaporators controlled by thermostatic expansion valves.

Distributed models

Distributed models have gained in importance in recent years. However, one of the key problems in these models is the description of void fraction and two-phase flow. The momentum exchange between refrigerant liquid and vapour causes a slip-effect which influences the mass distribution of the refrigerant. A better void fraction model could make the distributed models more realistic.

James [2.17] employed the modelling method previously used for steam generators. He proposed to divide the liquid chiller into small sections to represent the distributive behaviour of the liquid surrounding the tubes, the refrigerant boiling inside the tubes and the metal tubes themselves. Equations can be derived from energy and mass balance on each zone in turn. He considered the refrigerant vapour-liquid mixture as a compressible medium. However, no attention was paid to the void fraction distribution and therefore his equations in the model were not closed. Besides, there were no simulation and experiment results presented.

Gruhe and Isermann [2.18] developed a theoretical model for a refrigerant evaporator by using distributed parameter process. Three partial differential equations were derived respectively based on the balance equations for enthalpy, mass and momentum for the refrigerant. Discretization of the partial differential equations was made by dividing the evaporator pipe into n sections. The final unknown variables consists of vapour content, pressure and mass flow rate. However, a mistake was made in the model: a mis-defined average refrigerant velocity was used in the enthalpy balance equation. This mistake concealed the slip effect occurring in the two-phase flow region. The model was not validated with experiments.

MacArthur [2.19] only used the energy and mass balance equations to describe the phenomena taking place in the evaporator, the pipe of which was divided into small sections. The implicit finite difference method was made use of. In order to avoid the flow field calculation, he imposed an enthalpy constraint on the equations: the enthalpy of vapour-liquid mixture defined with quality is equal to that defined with void fraction, that is, $xh_v + (1-x)h_l = \langle \alpha \rangle h_v + (1-\langle \alpha \rangle)h_l$. It is obvious that such an assumption is far from the reality, when the slip effect between vapour velocity and liquid velocity plays a role. This model was improved by the author himself in [2.20] in which a void fraction model was introduced. Experiments were carried out to check the modified model and good agreement between the model and laboratory data has been obtained for the cases shown. However, he neglected a very important fact: pressure drop.

2.3 Modelling strategies

2.3.1 Conclusions from the literature review

From the literature review in 2.2, The following conclusions can be drawn:

- Two-zone models are the most popular. This type of models can properly describe the energy conservation mechanism in dry expansion evaporators. Because the refrigerant temperature does not change very much in the two-phase flow region, an average temperature can be used to represent the whole evaporation region. But a two-zone model is poor in predicting the refrigerant mass distribution in the pipe and the behaviour of the boundary between the two regions. This failure will lead to an incorrect prediction of the superheat temperature. While, superheat is substantial in case of a thermostatic expansion valve.
- Two-zone models need an average heat transfer coefficient for the two-phase flow region. Because the correlations for the heat transfer coefficient in the literature are usually given in the form of local values, mathematical integration has to be worked out to calculate the average value. To do this, some assumptions are necessary, for example, linear distribution of quality, even distribution of mass flow rate.

- Two-zone models cannot easily tackle the heat conduction between pipes which are connected by fins, when air coolers are concerned. The attempt to solve this problem in [2.14] seems to be not successful, as the calculation is strongly dependent on the pipe configurations of evaporators.

- Distributed models are gaining the field in recent years, thanks to the enhanced computer abilities. Anyway, the weak point still exists in solution of the momentum equation for the two-phase flow. The momentum exchange between liquid and vapour causes slip effect which influences the mass distribution of refrigerant in the evaporator. The existing distributed models paid too much attention to the energy equation that is actually possible to be lumped and intended to avoid a deep analysis of void fraction behaviour, perhaps because of the complexity of it.

2.3.2 Modelling strategies

It has been made clear that several possibilities exist for non-steady-state modelling of dry-expansion evaporators. The choice normally depends on a compromise between the accuracy and complexity of the model to be made. However, for a relatively flexible model of dry expansion evaporators, a basic demand may be that the model has to be applicable to as many types of evaporator pipe configurations as possible. This requires the model to be distributed. Moreover, the mass transport process gradually takes place inside the evaporator pipe. To predict a correct refrigerant mass distribution, the model should be also distributed. Another advantage of a distributed model is that the two-phase heat transfer coefficient can be calculated locally according to the local quality and mass flow rate. Starting from this point of view, the following modelling strategies can be made.

Strategy 1

The model to be set up will be distributed in structure and the mass balance equation will be solved in the form of partial differential equations. In the meantime, the heat transfer between refrigerant and tubes, tubes and other tubes, tubes and air will be calculated locally.

Strategy 2

Because the refrigerant temperature in the two-phase flow region is almost constant, except for the effect of pressure drop, the energy balance equation can be easily integrated in this region so that it will be solved by the lump method. The temperature decrease caused by the pressure drop will be added on later. This strategy avoids the simultaneous solution of the mass balance and energy balance equations which are otherwise all partial differential equations. In the single-phase flow region, the refrigerant has little mass and heat content and it is possible to consider the refrigerant temperature as a zero-order parameter (no heat and mass accumulations in the region), while the pipe wall of this region still plays a dynamic role.

Strategy 3

The momentum equation in the two-phase flow region is the most difficult equation to solve compared to the other two. This equation determines the pressure drop — mass flow rate correlation as well as the slip factor: it is the void fraction model. Owing to the quick equilibrium of the momentum transport, the momentum equation can be assumed as time-independent. The overall momentum equation for both liquid and vapour together will be replaced by a pressure drop — mass flow rate correlation which is derived semi-empirically. The separated equations for each of the two phases will be solved beforehand by using standard computer packages, such as PHOENICS. The results will be fitted into a void fraction — slip factor function.

2.4 Derivation of the equations

2.4.1 Basic equations

Two-phase flow region on the refrigerant side

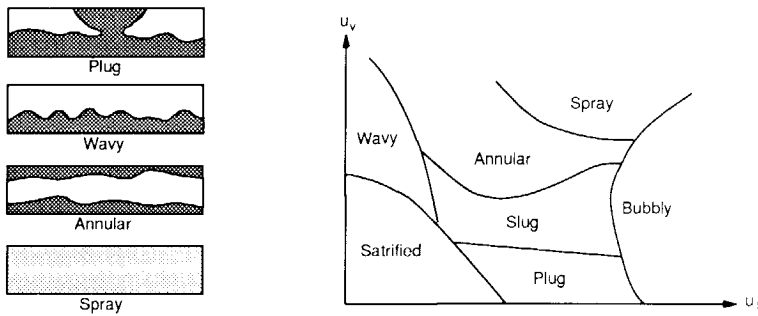


Fig. 2-3 Two-phase flow regimes (left) and the **Baker's** flow regime map (right).

If we exclude the possibility that subcooling exists in the evaporator, a dry expansion evaporator can always be divided into two completely different regions: two-phase flow region (evaporation region) and single-phase flow region (superheat region). Most of the length of the evaporator tube passed by the refrigerant belongs to the two-phase flow region. The behaviour of two-phase flows is complex but can be classified in terms of flow regimes which are often recognised from visual or photographic observations. The most commonly encountered flow regimes are shown in Fig. 2-3.

In refrigeration system evaporators, the flow patterns are mostly annular flow (see [2.17]). One-dimensional two-phase annular flows can be mathematically described with the so-called separated flow model which takes account of the fact that the two phases can have different properties and velocities. The separated flow model consists of 7 equations: continuity, momentum and energy equations for both phases and an interphase transfer rate equation describing how the phases interact with each other. However, a detailed description of the interphase energy transfer mechanism is impossible. The energy equation is usually written for the combined flow of the mixture.

Assumptions

- 1) the refrigerant vapour and liquid are incompressible and in saturated thermal equilibrium.
- 2) the refrigerant flow is one-dimensional, i.e. the vapour and liquid each have an average cross-sectional velocity and the void fraction is used to describe the ratio of cross-sectional area occupied by the vapour to the total cross-sectional area.
- 3) the vapour and liquid saturation physical properties are spatially and temporally invariant.
- 4) the pressures of the vapour and liquid are equal in one cross-section.
- 5) the kinetic energy and potential energy are all neglected in the energy equation.
- 6) the interface between the vapour and liquid moves at the liquid velocity.

With the listed assumptions, a simplified one-dimensional two-phase flow model can be made by considering the system shown in Fig. 2-4 (see [2.21]).

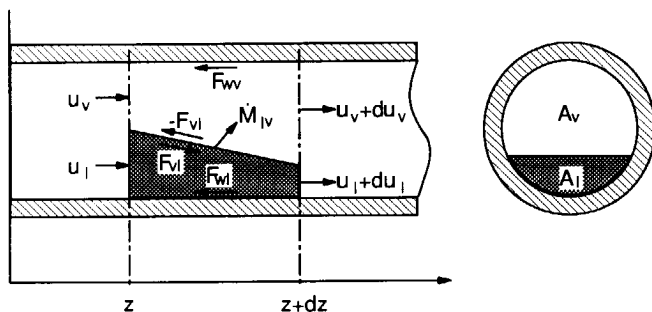


Fig. 2-4 Control volume for the refrigerant inside the evaporator pipe.

Continuity equation for the vapour phase:

$$\frac{\partial}{\partial t} (\langle \alpha \rangle \rho_v) + \frac{\partial}{\partial z} (\langle \alpha \rangle \rho_v u_v) = \dot{M}_{lv} \quad (2.1)$$

where $\langle \alpha \rangle = A_v / A$ and $A = A_v + A_l$.

Continuity equation for the liquid phase:

$$\frac{\partial}{\partial t} [(1 - \langle \alpha \rangle) \rho_l] + \frac{\partial}{\partial z} [(1 - \langle \alpha \rangle) \rho_l u_l] = -\dot{M}_{lv} \quad (2.2)$$

Energy equation for the mixture:

$$\begin{aligned} & \frac{\partial}{\partial t} [\langle \alpha \rangle \rho_v h_v + (1 - \langle \alpha \rangle) \rho_l h_l] + \frac{\partial}{\partial z} [\langle \alpha \rangle \rho_v u_v h_v + (1 - \langle \alpha \rangle) \rho_l u_l h_l] \\ & = (\pi d/A) q_{tp} \end{aligned} \quad (2.3)$$

As the equilibrium process of momentum transport is rapid, the momentum equation will be considered as time-independent.

Momentum equation for the vapour phase:

$$\frac{\partial}{\partial z} [\langle \alpha \rangle \rho_v u_v u_v] = -\langle \alpha \rangle \frac{\partial P}{\partial z} - (F_{vl} + F_{wv}) \quad (2.4)$$

In case of annular flows, F_{wv} is zero since there is no contact surface between the pipe wall and the vapour refrigerant.

Momentum equation for the liquid phase:

$$\frac{\partial}{\partial z} [(1 - \langle \alpha \rangle) \rho_l u_l u_l] = -(1 - \langle \alpha \rangle) \frac{\partial P}{\partial z} + (F_{vl} - F_{wl}) \quad (2.5)$$

By definition

$$\dot{m}_v = \langle \alpha \rangle A \rho_v u_v \quad (2.6)$$

$$\dot{m}_l = (1 - \langle \alpha \rangle) A \rho_l u_l \quad (2.7)$$

With using (2.6) and (2.7), the addition of (2.4) and (2.5) gives

$$\frac{1}{A} \frac{\partial}{\partial z} (\dot{m}_v u_v + \dot{m}_l u_l) = - \frac{\partial P}{\partial z} - F_{pw,tp} \quad (2.8)$$

which is the momentum equation for the vapour-liquid mixture and will be replaced later by an empirical correlation for calculating the pressure drop in the two-phase flow region.

Interfacial friction equation:

The interfacial friction force in (2.4) and (2.5) is calculated as follows (see [2.22], [2.27]),

$$F_{vl} = \frac{4}{d} \frac{1}{2} \left[\rho_v \xi_i (u_v - u_l)^2 \right] = f_i (u_v - u_l) \quad (2.9)$$

where the interfacial momentum-transport coefficient f_i is dependent on the interface conditions. A correlation for the case of wavy-interfaces has been given in [2.23].

Single-phase flow region on the refrigerant side

The situation in this region is relatively simple, because there is no phase change. As the heat capacity of the superheated vapour is small, the refrigerant can be considered as a system without mass and energy accumulations as well as incompressible.

Continuity equation:

$$\frac{dm}{dz} = 0 \quad (2.10)$$

Energy equation:

$$\frac{d(\dot{m} h)}{dz} = (\pi d) q_s \quad (2.11)$$

where $\frac{dh}{dz} = \frac{\partial h}{\partial T} \frac{dT}{dz} + \frac{\partial h}{\partial P} \frac{dP}{dz}$.

Momentum equation:

$$\rho_s u_s \frac{du_s}{dz} = - \frac{dP}{dz} - F_{pw,s} \quad (2.12)$$

The pipe wall

The metal pipes of the evaporator are the very important elements which possess considerable mass and heat capacities. The heat transfer process in the pipes is three-dimensional. Usually the evaporator pipes are assembled with extended fins in order to intensify the outside heat transfer. Thus, the concept of pipe wall always involves the evaporator pipes as well as the fins. Fig. 2-5 shows one nodal point of the plate-finned pipes of an evaporator. The basic equations will be subjected to this point.

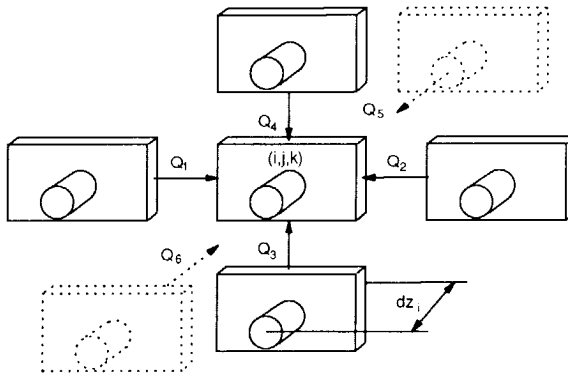


Fig. 2-5 A pipe wall element with its neighbors.

Assumptions

- 1) the radial heat resistance of the pipe wall is neglected.
- 2) the fin temperature is supposed to be equal to that of the pipe wall. To compensate for the error caused by this assumption, a fin efficiency is used in calculating the heat transfer between the air and pipe wall.

Energy equation:

$$c_{p,pw} M_{pw} \frac{\partial T_{pw}}{\partial t} = \sum_{i=1}^{\xi} Q_i + Q_r + Q_a \quad (2.13)$$

Because the pipes and fins normally consist of different materials, the specific heat should be averaged according to the masses of the materials.

$$c_{p,pw} = \frac{c_{p,pipe} M_{pipe} + c_{p,fin} M_{fin}}{M_{pw}} \quad (2.14)$$

The air side

The air flowing through the evaporator usually includes air and water vapour. Thus the problem on the air side is actually a diffusion problem which comprises concentration and energy equations. Again, because of the small heat capacity of air, this side is considered as a system without mass and energy accumulations.

Concentration equation:

$$\frac{d(\dot{m}_w \frac{a}{z_k})}{dz_k} = (\pi D) \dot{m}_w \quad (2.15)$$

The flux \dot{m}_w is calculated based on the outside area of bare pipes. The fin surface area is taken into account in the flux term by using a fin efficiency and weighted transfer coefficient. For (2.16), the same treatment is made.

Energy equation:

$$\frac{d(\dot{m} h)}{dz_k} = (\pi D) q_a \quad (2.16)$$

By the enthalpy definition:

$$h_a = c_{p,a} \theta_a + c_{p,w} \frac{\theta_a}{w_a} + \gamma w_a \quad (2.17)$$

2.4.2 Modification of the basic equations

The above basic equations governing the dynamic processes of the evaporator have been derived based on physical principles, such as the conservation laws. However, some of the equations are still too implicit and complex to be used for the computer simulation. Therefore simplification is necessary, which includes deriving a void fraction propagation equation from (2.1), (2.2) and integrating (2.3).

First consider the continuity equations. Multiplying (2.1) and (2.2) by ρ_l and ρ_v respectively, addition of them results in (see [2.24]):

$$\frac{\partial \langle u \rangle}{\partial z} = \frac{\Delta \rho \dot{M}_{lv}}{\rho_v \rho_l} \quad (2.18)$$

where $\Delta \rho = \rho_l - \rho_v$ and

$$\langle u \rangle = \langle \alpha \rangle u_v + (1 - \langle \alpha \rangle) u_l \quad (2.19)$$

Integration of (2.18) gives the following expression for the average velocity distribution in the z-direction:

$$\langle u \rangle = \langle u \rangle_{in} + \int_0^z \frac{\Delta \rho \dot{M}_{lv}}{\rho_v \rho_l} dz \quad (2.20)$$

Let

$$C_0 = \frac{u_v}{\langle u \rangle} \quad (2.21)$$

Employing (2.18) and rearranging, (2.1) may be expanded into

$$\frac{\partial \langle \alpha \rangle}{\partial t} + C_0 \langle u \rangle \frac{\partial \langle \alpha \rangle}{\partial z} + \langle \alpha \rangle \langle u \rangle \frac{\partial C_0}{\partial z} = \left(1 - C_0 \langle \alpha \rangle \frac{\Delta \rho}{\rho_l} \right) \frac{\dot{M}_{lv}}{\rho_v} \quad (2.22)$$

Because C_0 is a function of the void fraction $\langle \alpha \rangle$:

$$\frac{\partial \langle \alpha \rangle}{\partial t} + U_\alpha \frac{\partial \langle \alpha \rangle}{\partial z} = \Omega_\alpha \quad (2.23a)$$

where

$$U_\alpha = \left[C_0 + \frac{\partial C_0}{\partial \langle \alpha \rangle} \langle \alpha \rangle \right] \langle u \rangle \quad (2.23b)$$

$$\Omega_\alpha = \left[1 - C_0 \langle \alpha \rangle \frac{\Delta \rho}{\rho_l} \right] \frac{\dot{M}_{lv}}{\rho_v} \quad (2.23c)$$

(2.23a) has the form of a propagation equation. U_α and Ω_α correspond to the velocity of void fraction propagation and the source to the flow, respectively.

Then consider the energy equation for the mixture. As pointed out above, because the temperature of the refrigerant does not change much, the energy equation can be integrated without causing serious problems.

Assuming $\frac{\partial h_v}{\partial z} = 0$, $\frac{\partial h_l}{\partial z} = 0$, substituting (2.1) and (2.2), and rearranging, (2.3) becomes:

$$\dot{M}_{lv} (h_v - h_l) + \langle \alpha \rangle \rho_v \frac{\partial h_v}{\partial t} + (1 - \langle \alpha \rangle) \rho_l \frac{\partial h_l}{\partial t} = (\pi d/A) q_{tp} \quad (2.24)$$

As the refrigerant is saturated, thus $\frac{\partial h_v}{\partial t} = \frac{dh_v}{dT_e} \frac{\partial T_e}{\partial t}$ and $\frac{\partial h_l}{\partial t} = \frac{dh_l}{dT_e} \frac{\partial T_e}{\partial t}$.

Integration of (2.24) in the domain of $z = (0, Le)$ gives:

$$\begin{aligned} \frac{\partial T}{\partial t} \left[\frac{dh_v}{dT_e} \int_0^{Le} \rho_v <\alpha> dz + \frac{dh_l}{dT_e} \int_0^{Le} \rho_l (1-<\alpha>) dz \right] \\ = \int_0^{Le} (\pi d/A) q_{tp} dz - \int_0^{Le} \dot{M}_{lv} (h_v - h_l) dz \end{aligned} \quad (2.25)$$

Therefore

$$\frac{\partial T}{\partial t} = \frac{Q_e - (h_v - h_l) \dot{m}_{lv}}{M_v \frac{dh_v}{dT_e} + M_l \frac{dh_l}{dT_e}} \quad (2.26a)$$

where

$$Q_e = \int_0^{Le} \pi d \alpha (T_w - T_e) dz \quad (2.26b)$$

$$M_v = \int_0^{Le} A \rho_v <\alpha> dz \quad (2.26c)$$

$$M_l = \int_0^{Le} A \rho_l (1-<\alpha>) dz \quad (2.26d)$$

Integrating (2.1):

$$\begin{aligned} \dot{m}_{lv} &= \int_0^{Le} A \dot{M}_{lv} dz \\ &= \frac{\partial}{\partial t} \left[\int_0^{Le} A <\alpha> \rho_v dz \right] + \int_0^{Le} A \frac{\partial}{\partial z} [<\alpha> \rho_v u_v] dz \\ &= \frac{\partial M_v}{\partial t} + \dot{m}_v(Le) - \dot{m}_v(0) \end{aligned}$$

$$= \frac{\partial M}{\partial t} + \dot{m}_{comp} - x_{in} \dot{m}_{ev} \quad (2.26e)$$

Now, the dynamic evaporator system is composed of 6 differential equations: (2.23), (2.26), (2.11), (2.13), (2.15), (2.16) to solve 6 unknown variables : $\langle \alpha \rangle$, T_e , T_s , T_{pw} , w_a , θ_a .

However, solution of this system still needs more auxiliary equations which are the void fraction model, the correlations for heat and mass transfer coefficients and pressure drops. They will be described below and in chapter 6

2.5 Void fraction model (VFM)

2.5.1 Comparison of the existing void fraction models

In equation (2.23), C_o is still not known, that should be calculated from the void fraction model (VFM). The purpose of the VFM is to account for the fact that the vapour and liquid travel at different velocities in the two-phase flow region. The void fraction distribution is determined by Equations (2.4) and (2.5). However, solution of these two equations is difficult. From the literature, three methods can be found to tackle the problem. 1) empirical method; 2) analytical method; 3) numerical method. Before the void fraction models are discussed, several basic relationships between the following important parameters should be made clear.

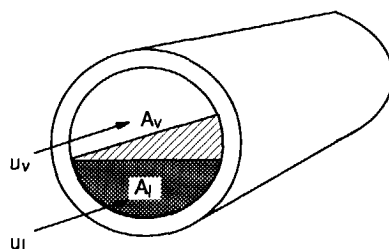


Fig. 2-6 Cross-section of the two-phase flow in the evaporator pipe.

u_v / u_l — $\langle \alpha \rangle$ — C_o correlation (see Fig. 2-6):

$$C_o = \frac{u_v}{\langle u \rangle}$$

$$\begin{aligned}
&= \frac{u_v}{\langle \alpha \rangle u_v + (1 - \langle \alpha \rangle) u_l} \\
&= \frac{1}{\langle \alpha \rangle + (1 - \langle \alpha \rangle) u_l / u_v} \quad (2.27)
\end{aligned}$$

u_v / u_l — $\langle \alpha \rangle$ — x correlation:

$$\begin{aligned}
\frac{u_v}{u_l} &= \frac{\frac{x m}{\rho_v \langle \alpha \rangle A}}{\frac{(1 - x) m}{\rho_l (1 - \langle \alpha \rangle) A}} \\
&= \frac{x (1 - \langle \alpha \rangle) \rho_l}{(1 - x) \langle \alpha \rangle \rho_v} \quad (2.28)
\end{aligned}$$

It is obvious that if any two of the four parameters: C_0 , $\langle \alpha \rangle$, x , u_v / u_l are well known, the others can be calculated. In the literature, different correlations between different parameters are given. Below are several examples.

Hancox's correlation [2.24] is an empirical one between C_0 and $\langle \alpha \rangle$:

$$C_0 = \frac{1 - \exp(-c_1 \langle \alpha \rangle)}{1 - \exp(-c_1)} (1 + c_2) - c_2 \langle \alpha \rangle \quad (2.29)$$

where $c_1 = 19$, $c_2 = 0.2$ (for water steam)

Levy's correlation [2.25] is an analytical one between x and $\langle \alpha \rangle$:

$$\begin{aligned}
x &= \quad (2.30) \\
&= \frac{\langle \alpha \rangle (1 - 2\langle \alpha \rangle) + \langle \alpha \rangle \{ (1 - 2\langle \alpha \rangle)^2 + \langle \alpha \rangle [2\rho_l / \rho_v (1 - \langle \alpha \rangle)^2 + \langle \alpha \rangle (1 - 2\langle \alpha \rangle)] \}^{0.5}}{2\rho_l / \rho_v (1 - \langle \alpha \rangle)^2 + \langle \alpha \rangle (1 - 2\langle \alpha \rangle)}
\end{aligned}$$

Zivi's correlation [2.26] is also an analytical one but between u_v/u_l and x :

$$\frac{u_v}{u_l} = \left(\frac{\rho_v}{\rho_l} \right)^{1/3} \left[\frac{1 + E(\rho_v/\rho_l) \left(\frac{1-x}{x} \right)}{1 + E \left(\frac{1-x}{x} \right)} \right]^{1/3} \quad (2.31)$$

However, all these models are subjected to certain required conditions and cannot cover the whole range encountered in the two-phase flows of refrigeration evaporators. The most accurate method is to solve the governing differential equations numerically with a small number of assumptions. With the development of computational fluid mechanics and computer science, numerical solution of one-dimensional two-phase flows can be obtained by using advanced computer packages. In this thesis, PHOENICS [2.27] has been made use of. The following is the output of the application of PHOENICS.

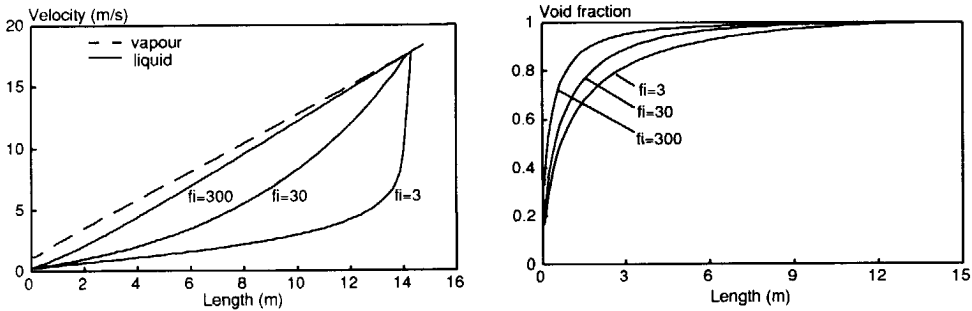


Fig. 2-7 Output of PHOENICS simulation.
left: vapour and liquid velocity distributions along the evaporator pipe.
right: void fraction distributions in the pipe.

As an example problem, the refrigerant with an inlet velocity of 0.2 m/s and quality of 0.0 flows through a tube of 15 m, under constant evenly distributed heat flux. Fig. 2-7 shows the vapour and liquid velocity, as well as the void fraction distribution along the tube. Given a different interfacial transport coefficient f_i , the distribution is different from another.

Based on the numerical solutions, a function between u_v/u_l and $\langle \alpha \rangle$ can be fitted for a f_i value by using the least-square root method. The following equation is in the form of a polynomial.

$$\frac{u}{u_l} = \sum_{i=0}^{l-1} B_i <\alpha>^i \quad (2.32)$$

where B_i is given in Table 2-1.

Table 2-1 Constants in Equation (2.32).

	$fi = 300$	$fi = 30$	$fi = 3$
$B_0 =$	0.9792383e+00	0.8314189e+00	0.8317894e+00
$B_1 =$	0.1611848e+01	0.1908810e+02	0.1923208e+02
$B_2 =$	0.4663572e+02	-0.2538455e+03	0.3954346e+01
$B_3 =$	-0.7387211e+03	0.3897408e+04	0.2028107e+04
$B_4 =$	0.5674294e+04	-0.2843790e+05	-0.2638837e+05
$B_5 =$	-0.2372763e+05	0.1114197e+06	0.1348492e+06
$B_6 =$	0.5765007e+05	-0.2580514e+06	-0.3688698e+06
$B_7 =$	-0.8404353e+05	0.3657613e+06	0.5897648e+06
$B_8 =$	0.7261648e+05	-0.3123267e+06	-0.5533253e+06
$B_9 =$	-0.3432190e+05	0.1477399e+06	0.2826817e+06
$B_{10} =$	0.6842722e+04	-0.2976721e+05	-0.6076239e+05

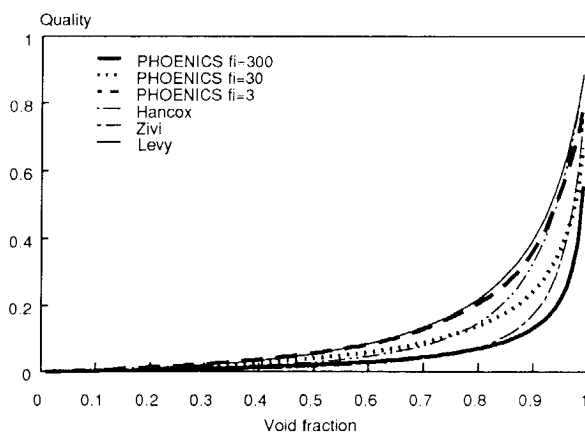


Fig. 2-8 Comparison of several void fraction models. This shows the influence of the interfacial transport coefficient fi .

The comparison of the obtained correlation to the others introduced above is illustrated in Fig. 2-8. It can be found that the range of $f_i = 3$ to 300 almost covers all of the models. However, selection of the f_i value has to be carried out experimentally.

2.5.2 Effects of the VFM on the evaporator behaviour

a) On the U_α and Ω_α values of Equation (2.23)

Equation (2.23) is the void fraction propagation equation in which the wave speed U_α and source Ω_α are dependent on the void fraction model.

$$U_\alpha = [C_0 + \frac{\partial C_0}{\partial \langle \alpha \rangle} \langle \alpha \rangle] \langle u \rangle = C_v \langle u \rangle \quad (2.33)$$

$$\Omega_\alpha = [1 - C_0 \langle \alpha \rangle \frac{\Delta \rho}{\rho_l}] \frac{\dot{M}_{lv}}{\rho_v} = C_s \dot{M}_{lv} \quad (2.34)$$

Clearly, the smaller C_v is, the slower the propagation speed is. Fig. 2-9 shows the variations of C_v and C_s as functions of $\langle \alpha \rangle$.

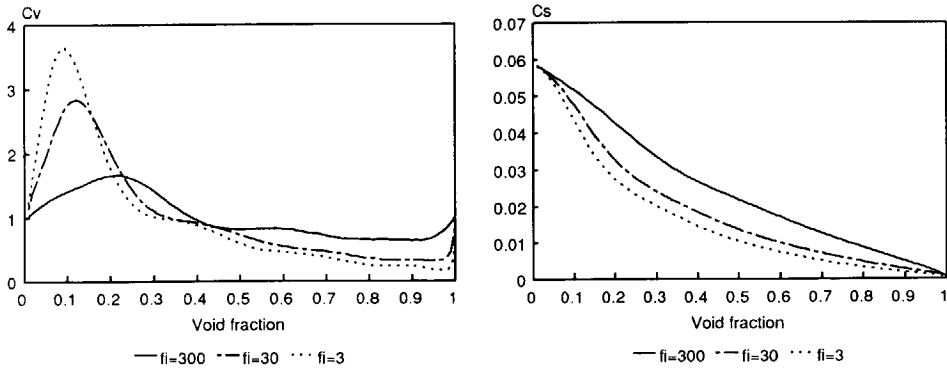


Fig. 2-9 Effect of the f_i value on the coefficients of Eqs. (2.33), (2.34).
left: variations of C_v as a function of $\langle \alpha \rangle$.
right: variations of C_s as a function of $\langle \alpha \rangle$.

On the other hand, the propagation speed is directly related to the position of the boundary between the two-phase and single-phase flow regions. Fig. 2-10 shows the responses of the two-phase flow region length L_e to a step change of the inlet mass flow rate and a step change of the heat flux added to the refrigerant. It can be found that the smaller the interfacial transport coefficient f_i , the slower the response of the two-phase flow region length L_e .

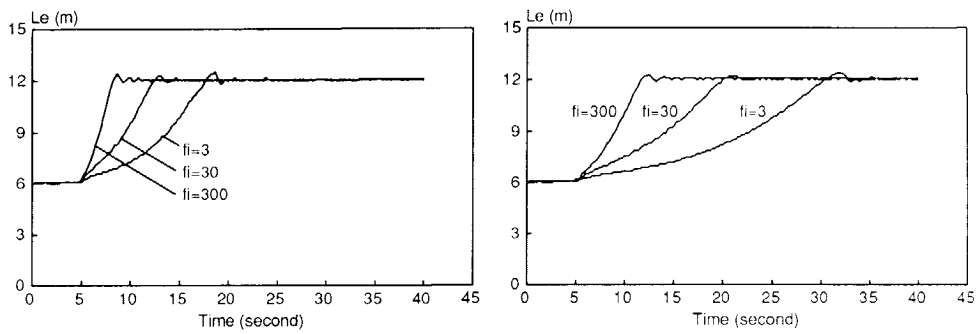


Fig. 2-10 Responses of the evaporation region length L_e with different f_i values:
left: when the inlet mass flow rate is increased with a factor of 2;
right: when the heat flux is decreased with a factor of 2.

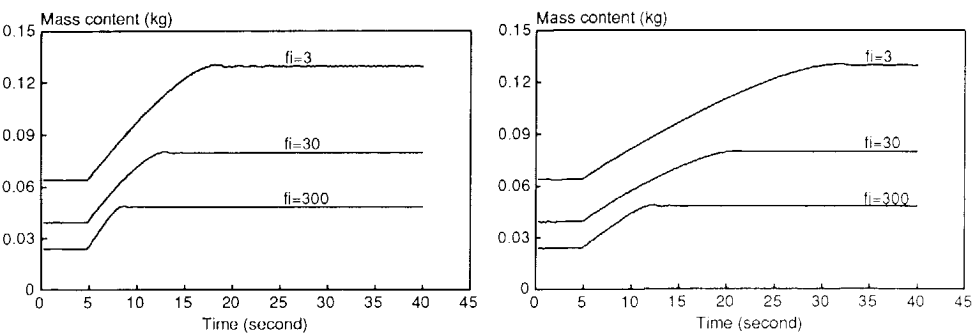


Fig. 2-11 Responses of the total refrigerant mass content with different f_i values:
left: when the inlet mass flow rate is increased with a factor of 2;
right: when the heat flux is decreased with a factor of 2.

b) On the refrigerant mass content inside the evaporator pipe

The refrigerant mass content in the evaporator pipe is important when the refrigerant charge and inventory are calculated. It also affects the off-period behaviour of the evaporator. Different void fraction models can result in different refrigerant mass content distributions in the evaporator. Fig. 2-11 illustrates the responses of the total vapour and liquid mass content to a step change of inlet mass flow rate and a step change of the heat flux. It can be found that the smaller the interfacial transport coefficient f_i , the slower the response of the refrigerant mass content in the evaporator. Moreover, the total refrigerant mass content is more for a smaller f_i in steady-state situations.

2.6 Off-period modelling

As during off-periods no refrigerant mass flow is present, the modelling on the refrigerant side can be treated differently. While, on the air side and the pipe wall, there is no difference between on-periods and off-periods, provided that the evaporator's fans keep running.

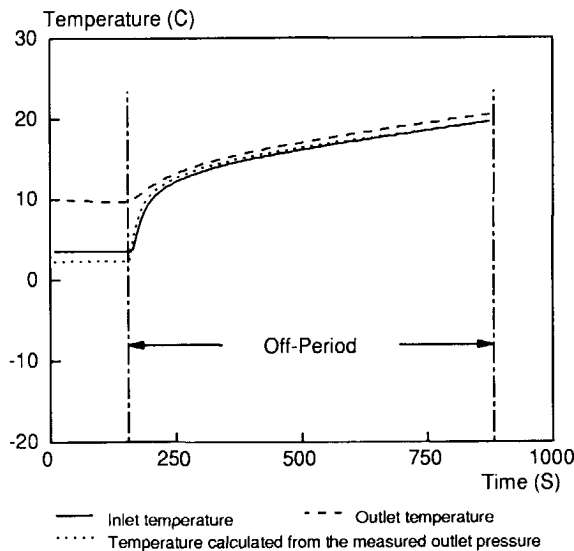


Fig. 2-12 *Experimental result to verify the assumption that a saturated equilibrium state is immediately reached throughout the whole evaporator pipe, as soon as the compressor is stopped.*

Experiments (see [2.28]) have demonstrated that as soon as the compressor stops, the inlet and outlet refrigerant temperatures in the evaporator immediately reach the saturated temperature corresponding to the measured pressure (see Fig. 2-12). This phenomenon supports the assumption that a saturated equilibrium state is immediately reached throughout the whole evaporator pipe. This assumption allows to consider the refrigerant as homogeneous, that is, a lumped model (see Fig. 2-13).

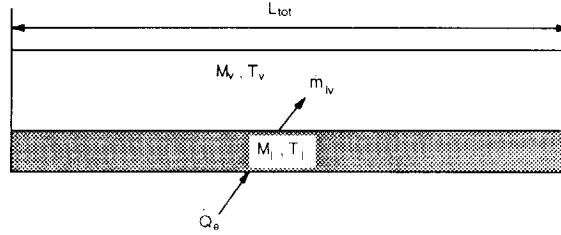


Fig. 2-13 An evaporator "tank" which is assumed to represent the off-period evaporator.

2.6.1 Incomplete evaporation situation

When the refrigerant liquid is not yet completely evaporated, the vapour and liquid co-exist at saturated equilibrium state.

Continuity equation for the vapour:

$$V \frac{d(\langle \alpha \rangle \rho_v)}{dt} = \dot{m}_{lv} \quad (2.35)$$

where the vapour is considered to be compressible and saturated

Continuity equation for the liquid:

$$\rho_l V \frac{d(1 - \langle \alpha \rangle)}{dt} = - \dot{m}_{lv} \quad (2.36)$$

Substituting (2.36) into (2.35) and using $\frac{d\rho_v}{dt} = \frac{d\rho_v}{dT} \frac{dT}{dt}$ and neglecting ρ_v / ρ_l :

$$\dot{m}_{lv} = V \langle \alpha \rangle \frac{d\rho_v}{dT_e} \frac{dT_e}{dt} \quad (2.37)$$

Energy equation for the mixture (the same as Equation (2.26)):

$$\frac{dT_e}{dt} = \frac{Q_e - (h_v - h_l) \dot{m}_{lv}}{M_v \frac{dh_v}{dT_e} + M_l \frac{dh_l}{dT_e}} \quad (2.38)$$

Thus Equations (2.37) and (2.38) determine two unknown variables T_e and \dot{m}_{lv}

2.6.2 Complete evaporation situation

If the off-period is long enough, the refrigerant liquid may be totally evaporated. Then the situation becomes a single-phase problem which can be described by only one equation.

$$\frac{dT_g}{dt} = \frac{Q_g}{M_g \frac{\partial h}{\partial T_g}} \quad (2.39)$$

where the vapour is superheated and its density is constant.

2.7 Discretization of the equations

2.7.1 The refrigerant side

To discretize (2.23), the coil circuit needs to be sub-divided into small elements as shown in Fig. 2-14. In order to obtain a stable solution, the implicit finite difference method has to be used, which results in the finite difference equation below:

$$\frac{\langle \alpha \rangle_m^{n+1} - \langle \alpha \rangle_m^n}{\Delta t} = \Omega_{\alpha m}^n - \frac{U_{\alpha m}^n}{4 \Delta z} [\langle \alpha \rangle_{m+1}^{n+1} - \langle \alpha \rangle_{m-1}^{n+1} + \langle \alpha \rangle_{m+1}^n - \langle \alpha \rangle_{m-1}^n] \quad (2.40)$$

where n is for time and m is for position.

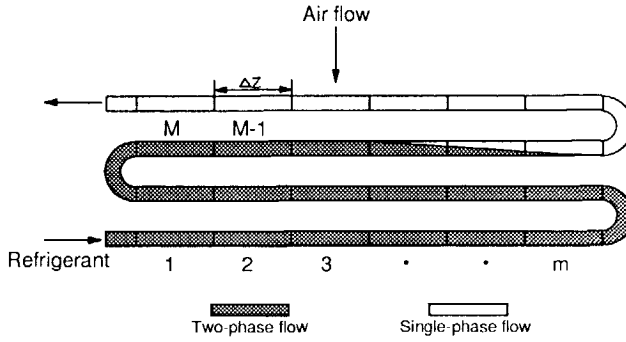


Fig. 2-14 Sub-division of elements in the refrigerant flow direction.

The following initial conditions are necessary:

- 1) $\langle \alpha \rangle_m^0 \quad (m = 0, 1, 2, \dots, M)$
- 2) $\langle \alpha \rangle_0^n \quad (n = 0, 1, 2, \dots, N)$

The solution of (2.40) determines the length L_e of the two-phase flow region. With L_e , (2.26) can be solved. However, the assumption has to be made that $\partial Mv/\partial t$ is very small, otherwise (2.23) and (2.26) need to be solved simultaneously, which requires long computation times.

2.7.2. The pipe wall

The evaporator pipes are normally arranged in three dimensions. Thus discretization of (2.13) requires the evaporator to be sub-divided into a 3-dimensional network with small elements, each of which centres around the corresponding pipe. The element number in the i direction can be arbitrary, while the subdivision in the j and k directions must be the same as the arrangement of the pipes. Fig. 2-15 shows the element division of an air cooler.

(2.13) can then be discretized on this element network as follows,

$$\frac{T_{i,j,k}^{n+1} - T_{i,j,k}^n}{\Delta t} = \frac{1}{c M_{p,i,j,k}} \left[(\lambda \Lambda)_i \frac{T_{i+1,j,k}^n + T_{i-1,j,k}^n - 2T_{i,j,k}^n}{\Delta z_i} \right]$$

$$\begin{aligned}
 & + (\lambda A)_j \frac{T_{i,j+1,k}^n + T_{i,j-1,k}^n - 2T_{i,j,k}^n}{\Delta z_j} + (\lambda A)_k \frac{T_{i,j,k+1}^n + T_{i,j,k-1}^n - 2T_{i,j,k}^n}{\Delta z_k} \Big] \\
 & + \dot{Q}_a + \dot{Q}_r
 \end{aligned}
 \tag{2.41}$$

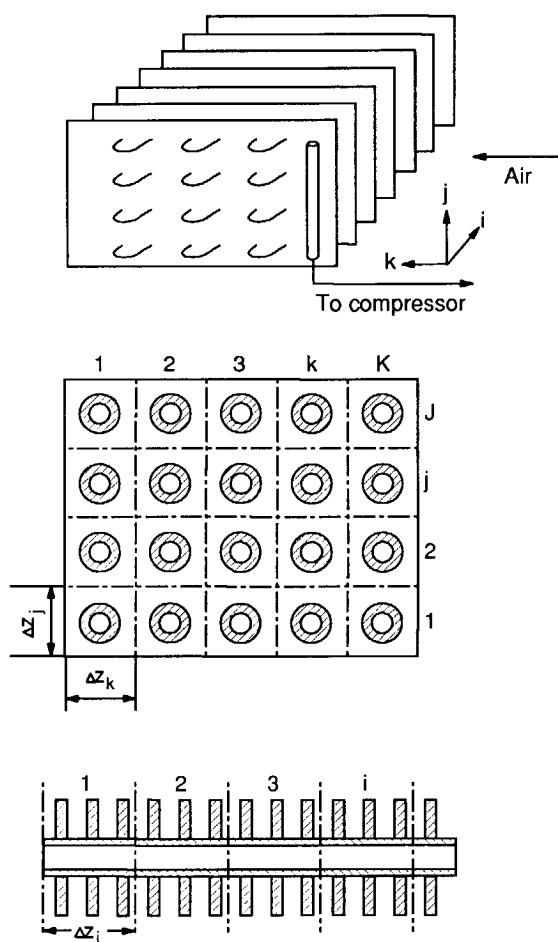


Fig. 2-15 Sub-division of elements in three-dimensional space.

where $(\lambda A)_i$, $(\lambda A)_j$, $(\lambda A)_k$ will be calculated in chapter 6. For sake of simplicity, the boundary of the element network is assumed insulated.

2.7.3 The air side

Although the air flow is in one dimension, the air temperature and humidity distributions are still space-dependent owing to their interaction with the pipe wall. The division of the air is the same as that of the pipe wall. Therefore (2.15) and (2.16) have the following finite difference equations:

$$\frac{w_{i,j,k} - w_{i,j,k-1}}{\Delta z_k} = (\pi D) \dot{m}_{w,i,j,k} / \dot{m}_{i,j,k} \quad (2.42)$$

$$\frac{h_{i,j,k} - h_{i,j,k-1}}{\Delta z_k} = (\pi D) \dot{q}_{i,j,k} / \dot{m}_{i,j,k} \quad (2.43)$$

The boundary conditions are the air inlet conditions:

- 1) $w_{i,j,0}$ ($i = 1, I$ and $j = 1, J$)
- 2) $h_{i,j,0}$ ($i = 1, I$ and $j = 1, J$)

2.7.4 Transformation between the two element notations

Above, two types of element divisions have been described. One is according to the refrigerant flow direction and another is according to the arrangement of the pipes. To facilitate the programming procedure, transformation between the two element notations is necessary. This can be realized by using a transformation matrix Π which is input according to the coil circuitry of the evaporator concerned. Fig. 2-16 illustrates the way in which Π is filled. With this matrix, the pipe wall temperature can be notated in both one and three dimensions. The transformation from one to another is as follows:

$$T_{pw,3-d}(i,j,k) = T_{pw,1-d}(\Pi(i,j,k)) \quad (2.44)$$

Such a method makes the data transfer between the inside and outside of the pipes much easier.

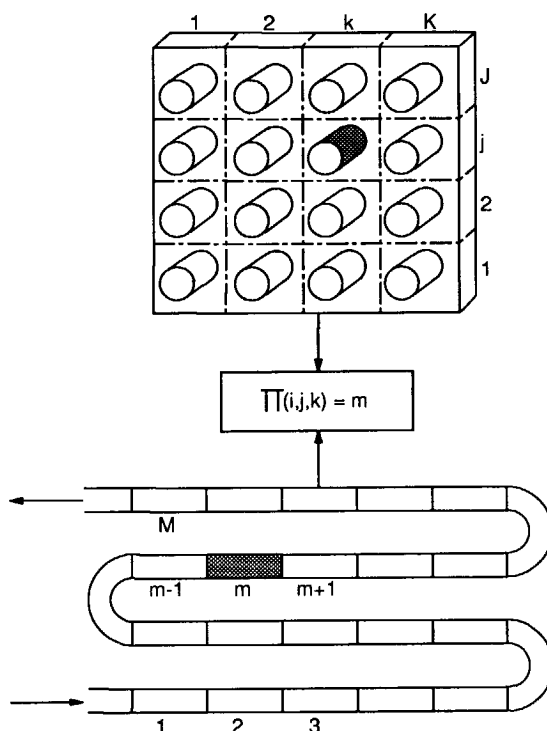


Fig. 2-16 Transformation between the two element notations.

2.7.5 Logic diagram

Fig. 2-17 gives a logic diagram to implement the dynamic model on computers. The computer program starts with initial values which are the output of a steady-state model. The simulation time is at this moment set to be zero. If the compressor is running, then the subroutine for on-periods on the refrigerant side is called with which (2.23), (2.26), (2.11) are solved. If the compressor is stopped, the subroutine for off-periods on the refrigerant side is called with which (2.37) and (2.38) or (2.39) are solved. Afterwards the subroutine for the air side is called with which (2.15), (2.16) are solved. Finally the subroutine for the pipe wall is called with which (2.13) is solved. Meanwhile, the auxiliary subroutines for the heat transfer coefficients and pressure drops as well as the physical properties are called. Such a computational loop is repeated until the total simulation time is reached.

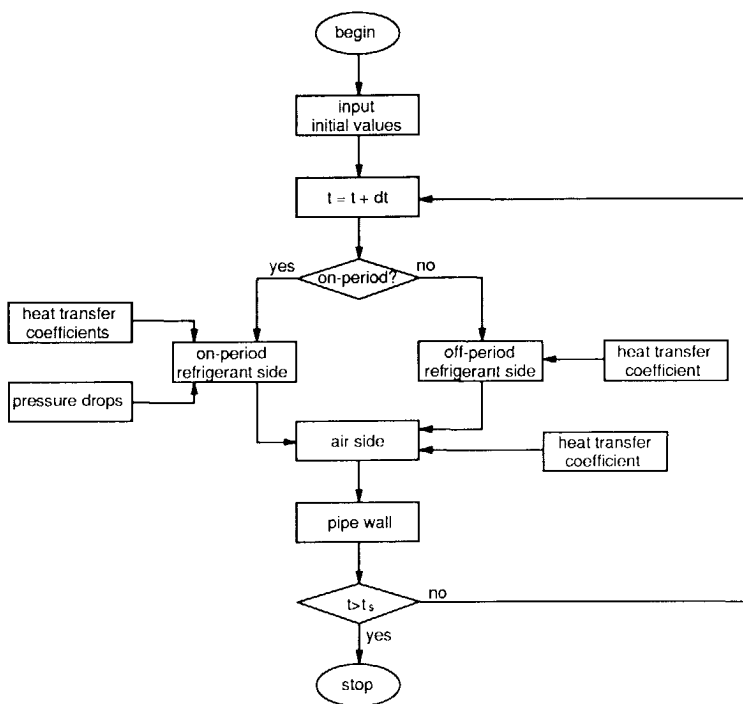


Fig. 2-17 Flow chart of the computer program of the non-steady-state model.

References

- 2.1 **Stoecker, W.F.** "Stability of an evaporator-expansion valve control loop", *ASHRAE Annual Meeting, Toronto, 1966, No.2007*, ASHRAE Atlanta, GA, pp.4.1-4.8
- 2.2 **Stoecker, W.F., Shahan, J.E., Mumma, S.A.** "Dynamic response of a finned coil refrigerant evaporator to step changes in refrigerant flow rate", Research Report No.2199 RP-51, *ASHRAE Annual Meeting, Washington D.C. August 1971*, pp.80-87
- 2.3 **Najork, H.** "Investigation on the dynamic behaviour of evaporators with thermostatic expansion valve", *Proceedings IIR, Commission B2, Moscow 1975*, pp.1021-1028
- 2.4 **Chi, J., Didion, D.** "A simulation model of the transient performance of a heat pump", *International Journal of Refrigeration*, Vol.5, No.3, May 1982, pp.176-180
- 2.5 **Marshall, S.A., James, R.W.** "Dynamic analysis of an industrial refrigeration system to investigate capacity control", *Proc Instn Mech Engrs.* Vol.189, 1975, pp.437-444
- 2.6 **Hargreaves, M.R.O., James, R.W.** "A model of a marine chilled water plant for microprocessor control development", *the Institute of Refrigeration at the Institute of Marine Engineering, 76 Mark Lane, London, Session 1979-1980*, pp.1-10
- 2.7 **Wedekind, G.L., Stoeker, W.F.** "Transient response of the mixture-vapour transition point in horizontal evaporating flow", *ASHRAE Journal*, November 1966, pp.74-77
- 2.8 **Wedekind, G.L., Stoeker, W.F.** "Theoretical model for prediction the transient response of the mixture-vapour transition point in horizontal evaporating flow", *Journal of Heat Transfer*, February 1968, pp.165-174
- 2.9 **Wedekind, G.L., Bhatt, B.L., Beck, B.T.** "A system mean void fraction model for predicting various transient phenomena associated with two-phase evaporating and condensing flows", *International Journal of Multiphase Flow*, Vol.4, 1978, pp.97-114
- 2.10 **Dhar, M., Soedel, W.** "Transient analysis of a vapour compression refrigeration system", *Proceedings I.I.R. - Commission B2, Venice, 1979*, pp.1035-1068
- 2.11 **de Bruijn, M., van der Jagt, M.F.G., Machielsen, C.H.M.** "Simulation experiments on a compression-refrigerator system", *Proceedings IMACS, Congress on Simulation Systems, Sorrento, 1979*, pp.645-665
- 2.12 **Yasuda, H., Machielsen, C.H.M., Touber, S.** "Simulation of transient behaviour of a compression-expansion refrigeration system", *I.I.F. - I.I.R. - Commissions B2, C2, D1, Sofia, 1982*, pp.147-154
- 2.13 **Yasuda, H., Machielsen, C.H.M., Touber, S., Brok, S.W., de Bruijn M.** "Simulation of transient behaviour of a compression-expansion system", Report WTHD 133, Delft University of Technology, Delft, March 1981
- 2.14 **Van der Meer, J.S.** "Simulation of a refrigerant evaporator", *Ph.D. Thesis*, Delft University of Technology, Delft, October 1987
- 2.15 **Bonte, A., Veldhoven, B.V.** "Dynamic behaviour of a refrigerating plant", *I.I.F. - I.I.R. - Commissions B 2.4, Paris, 1983*, pp.321-326
- 2.16 **Broersen, P.M.T., van der Jagt, M.F.G.** "Hunting of evaporators controlled by a thermostatic expansion valve", *Journal of Dynamic Systems, Measurement, and Control*, vol.102, June 1980, pp.130-135

- 2.17 **James, R.W.** "Refrigeration and air conditioning systems", *Modelling of Dynamic Systems*, book edited by H. Nicholson, University of Sheffield, England, pp.62-96
- 2.18 **Gruhle, W.D., Isermann, R.** "Modelling and control of a refrigerant evaporator", *Journal of Dynamic Systems, Measurement, and Control*, vol.107, 1985, pp.235-240
- 2.19 **MacArthur, J.W.** "Transient heat pump behaviour: a theoretical investigation", *International Journal of Refrigeration*, Vol.7, No.2, 1984
- 2.20 **MacArthur, J.W., Grald, E.W.** "Unsteady compressible two-phase flow model for predicting cyclic heat pump performance and a comparison with experimental data", *International Journal of Refrigeration*, Vol. 12, 1989, pp.29-41
- 2.21 **Collier, J.G.** "Convective boiling and condensation", McGraw-Hill Book Company, 1972
- 2.22 **Wallis, G.B.** "One-dimensional two-phase flow", McGraw-Hill Book Company, 1969
- 2.23 **Prakash, C.** "Prediction of some complex multi-dimensional two-phase flow phenomena" using PHOENICS code (1) phase distribution in ducts (2) phase separation in tee junctions and (3) condensation in stratified flow", *Proceedings of 2nd International PHOENICS User Conference*, London, November, 1987
- 2.24 **Hancox, W.T., Nicoll, W.B.** "A general technique for the prediction of void distributions in non-steady two-phase forced convection", *Int. J. Heat mass Transfer*, Vol.14, 1971, pp.1377-1394
- 2.25 **Levy, S.** "Steam slip - theoretical prediction from momentum model", *Journal of Heat Transfer*, May 1960, pp.113-123
- 2.26 **Zivi, S.M.** "Estimation of steady-state steam void-fraction by means of the principle of minimum entropy production", *Journal of Heat Transfer*, May 1964, pp.247-252
- 2.27 **Rosten, H.I., Spalding, D.B.** "The PHOENICS reference manual", Cham Tr/200, October, 1987, Document Revision 06, Software Version 1.4
- 2.28 **Grul, Q.** "Dynamic simulation model of a refrigeration system with on-off control", Rapport No.s-888, Delft University of Technology, April 1989

Chapter
THREE
Dynamic Modelling of the Condenser

3.1 General

The function of a condenser is to remove heat from a refrigerating system to its surrounding. In the case of a simple vapour compression refrigeration cycle, the total removed heat is the summation of the heat received by the evaporator and the work charged to the compressor. The thermal process in the condenser can be divided into three phases: de-superheating, condensing and subcooling. To fulfill this function, several types of condenser are used in practice. According to their constructions and cooling mediums, they are classified as shown in Fig. 3-1. Among them, water-cooled shell-and-tube condensers (see Fig. 3-2) are often used in the places where cooling water is available. Therefore this type of condenser is chosen as the object of this study.

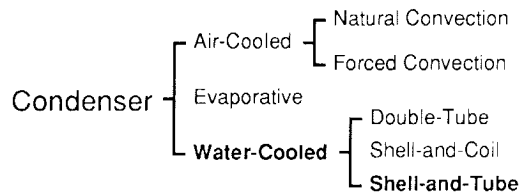


Fig. 3-1 Classification of refrigeration condensers.

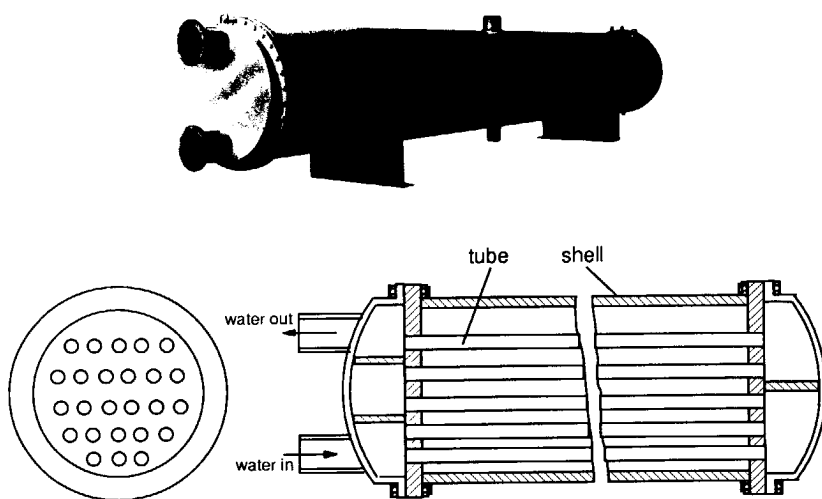


Fig. 3-2 Photograph and internal structure of a shell-and-tube condenser.

In a shell-and-tube condenser, the superheat vapour from the compressor enters the shell at the top and condenses on the outside of the pipes. At the bottom of the shell, the condensed refrigerant is further cooled to be subcooled liquid which leaves for the expansion valve. For improving the refrigerant side heat transfer coefficient during condensation, most shell-and-tube condensers are provided with low-finned tubes. The cooling water flows through the pipes. In order to increase the velocity of the flowing water, the pipes are grouped into passes by using partitioning plates. Since the number of pipes in each pass is different from another, the water velocity in the pipes of each pass is also different from another.

In contrast to the evaporator, the shell-and-tube condenser is of a bath-type and does not involve two-phase flows. Moreover, there usually exists a clear boundary between the vapour and liquid phases of refrigerant in the condenser. Under such a particular condition, the approach of lumped modelling can be utilized to model the condenser. The advantage of a lumped model is that no partial differential equations appear in the model and accordingly the numerical solution of the equations becomes easy. However, a lumped model has to be on the basis of some necessary assumptions which determines the quality of the model. Because, in reality, pure homogeneous systems do not exist, any attempt to lump a distributed system needs certain amounts of assumptions. In the case of the condenser, the main assumption is the boundary layer concept which allows to limit the space-dependency of the problem within a small region near to the boundary between the refrigerant and tube wall. The partial differential governing equations can be analytically integrated in this small region and the analytical solution can be directly used in the model.

Therefore, the emphasis of this chapter will be laid on the application of the boundary layer theory to modelling of shell-and-tube condensers. Besides the modelling strategies, the derivation and solution of the conservation equations will also be described. The modelling ideas created in this chapter will be also used in chapter 4 where the steady-state model is developed.

3.2 Literature

Modelling of shell-and-tube condensers has been a hot subject, since the technique of mathematical modelling was introduced to the field of refrigeration. Taking it for granted that such type of condensers are more or less like a well-stirred tank, almost everybody models them as lumped. Differences between each other exist in two aspects: the treatment of vapour phase of refrigerant; the zone-division of tubes. Below, several representative models are assessed.

James and Marshall [3.1] developed a dynamic model for a shell-and-tube condenser in 1973. Their "conceptual model" represented the condenser by using 5 zones: 1) vapour outside the boundary layer, 2) boundary layer, 3) liquid refrigerant, 4) water in the tubes above the refrigerant liquid level, 5) water in the tubes submerged in the refrigerant liquid. The refrigerant vapour outside the boundary layer was considered to be superheated with a temperature between the inlet and saturated temperatures. The most interesting concept is that a certain amount of vapour was assumed to be cooled down in the boundary layer and then to escape to the vapour space. This is a phenomenon taking place in reality. However, as they did not go deeply towards the boundary layer, the mass flow rate of the escaping vapour was impossible to calculate. They could not help but assumed an artificial ratio of the mass flow of the escaping vapour to that condensed. This model was later applied by **Wong** [3.2] to analyze capacity control of refrigeration systems.

Yasuda et al [3.3] presented another dynamic condenser model in 1981. The condenser was described by one lumped zone that included four thermal elements: refrigerant, cooling water, tube, shell. The refrigerant vapour and liquid were considered together as a homogeneous and saturated medium. The proportion between vapour and liquid was fixed by rule of thumb and assumed independent of time. Apparently, this model is much rougher than that of **James**.

van der Meer [3.4] improved the model of **Yasuda** by dividing the condenser into two zones: condensation region and subcooling region. Respectively, the cooling water, tubes and shell were split into two distinguished portions. However, as he did not think about the boundary layer around the liquid film on the tubes, there was always a lack of a governing equation. He then had to suppose the refrigerant vapour in the condensation region was saturated instead of superheated. This assumption is obviously far from reality.

Comparing the three existing condenser models, it is found that the model of **James** is the most realistic. However, because of the lack of a further consideration of the boundary layer, some artificial treatment had to be imposed to calculate the amount of escaping vapour. On the other hand, all the three models adopted a simple way to tackle the cooling water and tubes which were not divided or just divided into two parts. Such assumptions undoubtedly decreased the quality of the models. Based on the conclusions drawn from the literature study, we decide to establish a new model with the emphasis on the consideration of boundary layer and with a more precise zone division of cooling water and tubes.

3.3 Division of basic elements

As has been done by all other model makers, the model to be developed in this chapter will also take the form of a lumped model. To set up a lumped model, the division of basic elements is decisive as a prolusion of modelling.

Refrigerant side

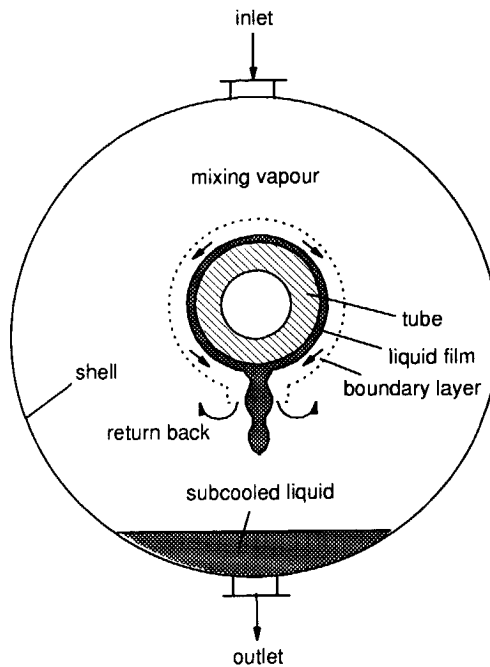


Fig. 3-3 Inside vision of a shell-and-tube condenser

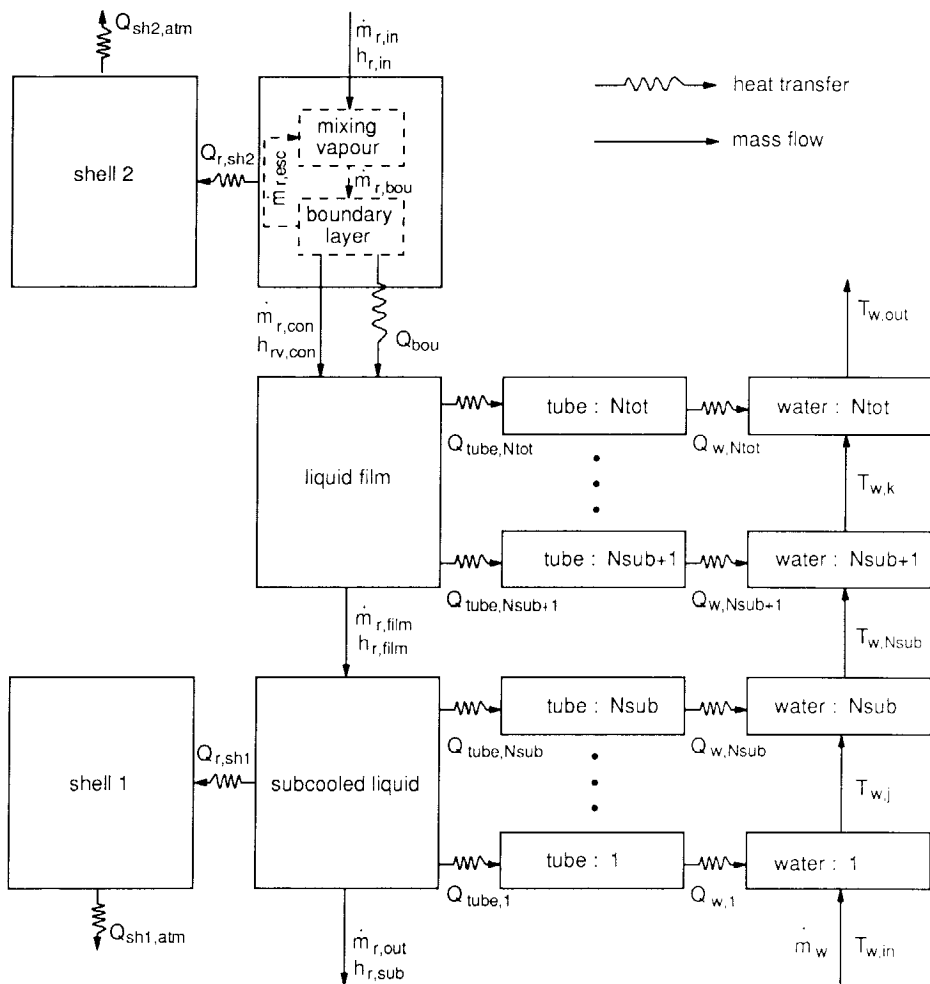


Fig. 3-4 Division of the lumped elements for modelling the condenser

Consider a condenser system shown in Fig. 3-3, the superheated refrigerant vapour enters the shell at the top and is then mixed with the vapour standing still inside the shell. As an assumption, the mixing process is thought so perfect that the temperature of the refrigerant vapour in the region above the liquid level and outside the boundary layer is independent of spatial position. At the same time, a proportion of the vapour in this region enters the thermal boundary layer and is cooled. It is assumed again that the temperature gradient appears only in the thermal boundary layer. This amount of cooled vapour partly condenses on the outside surface of the tube wall and partly returns back to the main region and mixes with the rest. The condensed refrigerant usually forms a liquid film around the tube wall. Such a condensation process is called film condensation. In our case, we always assume a film condensation. The liquid film finally drops down to the bottom of the shell and form another distinguished region: subcooling region. At the bottom there is an exit where the refrigerant liquid leaves the condenser.

Fig. 3-4 shows the division of basic elements. It needs to be pointed out that the mixing vapour and the thermal boundary layer are combined into one element, because the mass flow rate of the escaping vapour from the boundary layer is difficult to determine. Such a combination can be justified with the following explanations: 1) as the boundary layer contains very small amount of refrigerant, the temperature of the combined element can be represented by the mixing vapour temperature; 2) although the escaping vapour to a large extent influences the mixing vapour temperature, the effect is automatically taken into account if they are put together in one control volume; 3) Although the boundary layer and the mixing vapour are regarded as one element, the significance of defining a boundary layer still exists: to calculate Q_{bou} (see section 3.5). With the above consideration, the refrigerant side of the condenser can be represented by three lumped elements:

- a) the superheated mixing vapour including the thermal boundary layer
- b) the condensed liquid film that may have some degrees of subcooling near to the surface of the tube wall
- c) the subcooled liquid at the bottom of the condenser

Cooling water and tubes

The refrigerant side is divided into three sections, because the velocity of refrigerant is almost zero. However, the cooling water flows inside the tubes and its temperature varies along the flow direction. Thus lumping the cooling water into one or two sections seems to be unrealistic. In practice, the tubes are grouped in passes each of which has the same water flow. All the tubes in one pass share the water flow and have the same temperature profile of water. Therefore, it is easy to think about regarding one pass as one element. To account for the total heat transfer area and cross-sectional areas of the tubes in one pass, a virtual tube can be used to replace the element, as illustrated in Fig. 3-5. The relations among the elements are also shown in Fig. 3-4.

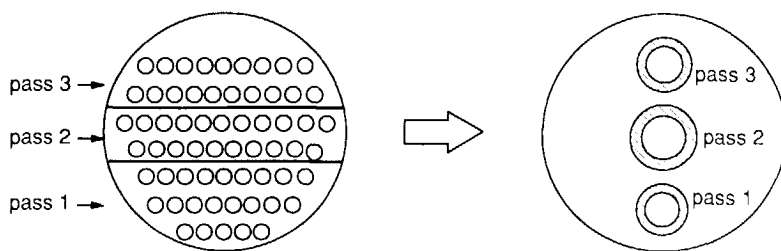


Fig. 3-5 Element division of the cooling water and tubes.

Shell wall

The condenser shell is in contact with the mixing vapour and subcooling liquid. Respectively, it can also be divided into two parts between which no heat conduction is assumed to occur. As the shell wall is made of heavy metal and possesses rather large heat capacity, the effect on the dynamic behaviour of the condenser is quite important.

3.4 Conservation equations

3.4.1 Superheated vapour

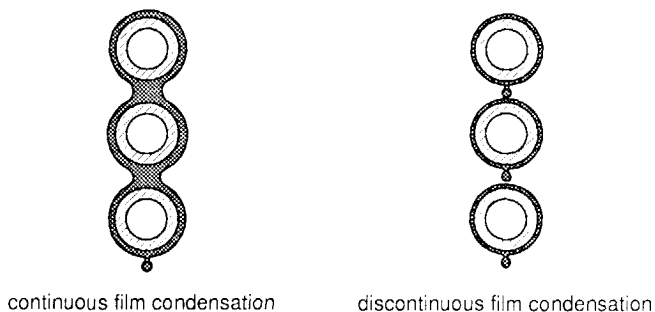


Fig. 3-6 Two modes of refrigerant liquid flows around the condenser pipes.

As shown in Fig. 3-4, the element of superheated vapour consists of two proportions of vapour: the mixing vapour in the bulk region and the vapour in the boundary layer. If the

falling process of the refrigerant liquid from one tube to another is discontinuous (see Fig. 3-6), a boundary layer is built up on each tube. The refrigerant vapour in the boundary layer escapes from each tube to the bulk region. In this case, the temperature distribution of the mixing vapour is nearly homogeneous all over the bulk region. If the liquid film is continuously formed around the tube bundle as shown on the left side of Fig. 3-6, the refrigerant vapour would escape more from the lower tubes. Then the mixing in the bulk region would be uneven and the upper part of the region may have a different temperature from the lower part. In this situation, a lumped model for the mixing vapour would not be suitable. More information about this problem can be founded in [3.6]. Hereafter, we only assume a discontinuous film condensation. The conservation equations for the superheated mixing vapour are then as follows:

Mass balance:

$$\frac{d(\rho_{r,mv} V_{mv})}{dt} = \dot{m}_{r,in} - \dot{m}_{r,con} \quad (3.1)$$

Energy balance:

$$\frac{d(\rho_{r,mv} V_{mv} h_{r,mv})}{dt} = \dot{m}_{r,in} h_{r,in} - \dot{m}_{r,con} h_{rv,con} - Q_{r,sh2} - Q_{bou} \quad (3.2)$$

where Q_{bou} is the heat transfer from the thermal boundary layer to the liquid film and causes a cooling-down of the mixing vapour to a saturated state. The details on the calculation of Q_{bou} will be described in 3.5.

$$Q_{r,sh2} = \alpha_{r,sh2} A_{r,sh2} (T_{r,mv} - T_{sh2}) \quad (3.3)$$

The concerned heat transfer coefficients will be specially introduced in chapter 6 and the heat transfer areas will be calculated in Appendix 3. The inlet conditions of the condenser are determined by the compressor model which will be described in Appendix 1.

3.4.2 Liquid film

The liquid film is a very thin layer of refrigerant liquid. As a temperature difference is needed for heat transfer, there must be a temperature gradient in the liquid film from the condensation temperature to the tube wall temperature. The average temperature of the liquid film was empirically given by **Henrici** [3.5] as below:

$$T_{r,film} = T_{r,con} - 0.528 (T_{r,con} - T_{tube}) \quad (3.4)$$

Because of the little amount of refrigerant, the heat and mass accumulations in the film are negligible. Then the conservation equations for it becomes:

Mass balance:

$$\dot{m}_{r,film} = \dot{m}_{r,con} \quad (3.5)$$

Energy balance:

$$\dot{m}_{r,con} h_{rv,con} - \dot{m}_{r,film} h_{r,film} + Q_{bou} - \sum_{k=Nsub+1}^{Ntot} Q_{tube,k} = 0 \quad (3.6)$$

where

$$Q_{tube,k} = \alpha_{con} A_{tube,r,k} (T_{r,con} - T_{tube,k}) \quad (3.7)$$

3.4.3 Subcooled liquid

In a dynamic process, the level of the subcooled liquid changes with the refrigerant mass deposited at the bottom of the shell. Thus the heat transfer areas between the refrigerant and tubes, the refrigerant and shell, changes also, that is, N_{sub} , the number of tubes (virtual tubes) merged in the liquid is changeable. The calculation of these areas, N_{sub} , as well as the height of the liquid level is a matter of geometry, if the liquid mass and density are well known. The details about the calculation will be given in Appendix 3.

Mass balance:

$$\rho_{r,sub} \frac{d(V_{sub})}{dt} = \dot{m}_{r,film} - \dot{m}_{r,out} \quad (3.8)$$

Energy balance:

$$\rho_{r,sub} \frac{d(V_{sub} h_{r,sub})}{dt} = \dot{m}_{r,film} h_{r,film} - \dot{m}_{r,out} h_{r,sub} - Q_{r,shl} - \sum_{j=1}^{N_{sub}} Q_{tube,j} \quad (3.9)$$

where the heat transfer rates are calculated as follows:

$$Q_{r,shl} = \alpha_{r,shl} A_{r,shl} (T_{r,sub} - T_{shl}) \quad (3.10)$$

$$Q_{tube,j} = \alpha_{sub\ tube,r,j} A_{sub\ tube,r,j} (T_{r,sub} - T_{tube,j}) \quad (3.11)$$

The outlet mass flow rate of refrigerant is calculated by the TEV model which will be described in Appendix 2.

3.4.4 Tube wall

The tube elements are defined according to water flow passes. The conservation equations of them are all similar to each other. Therefore, hereafter only one of them is considered. Moreover, the mass of tubes does not change and the mass conservation is not interesting. The energy conservation equation for element j is then as follows:

Energy balance:

$$M_{tube,j} \frac{d(h_{tube,j})}{dt} = Q_{tube,j} - Q_{w,j} \quad (3.12)$$

As the temperature increase of water in one pass is not big, an arithmetic temperature difference is used to calculate the heat transfer between the tube and water.

$$Q_{w,j} = \alpha_{w,j} A_{tube,w,j} (T_{tube,j} - T_{w,j}) \quad (3.13)$$

3.4.5 Cooling water

Assume the cooling water is incompressible. Each of the water elements (one water pass) should have the same mass flow rate. The energy balance equation for element j is then as follows:

Energy balance:

$$M_{w,j} \frac{d(h_{w,j})}{dt} = \dot{m}_w (h_{w,in,j} - h_{w,out,j}) + Q_{w,j} \quad (3.14)$$

where $h_{w,j} = 0.5 (h_{w,in,j} + h_{w,out,j})$.

3.4.6 Shell wall

The condenser shell is divided into two elements as shown in Fig. 3-4. The volumes of the two elements change with the height of the liquid level. However, because the change of the liquid level is very slow, the volumes of the shell elements can be assumed independent of time in deriving the equation. However, they are not constant at all during simulations, because they are calculated using the height of liquid level which actually changes with time. But this change is assumed not to have a dynamic effect. If one of the two elements is only considered, then:

Energy balance:

$$\rho_{sh} V_{sh} \frac{d(h_{sh})}{dt} = Q_{r,sh} - Q_{sh,atm} \quad (3.15)$$

$$Q_{sh,atm} = \alpha_{sh,atm} A_{sh} (T_{sh} - T_{atm}) \quad (3.16)$$

3.4.7 Closure of the conservation equations

Until now, all the conservation equations for the lumped elements divided in 3.3 have been set up. It is necessary to check whether the set of equations is closed or not. Below the unknown variables to be solved as well as the equations to be used are listed.

Unknown variables		Equations	
1. $T_{r,con}$	condensation temperature	(3.1)	mass balance for the mixing vapour
2. $T_{r,mv}$	temperature of the mixing vapour	(3.2)	energy balance for the mixing vapour
3. $\dot{m}_{r,film}$	mass flow rate of the dropping liquid	(3.5)	mass balance for the liquid film
4. $\dot{m}_{r,con}$	condensation rate of refrigerant	(3.6)	energy balance for the liquid film
5. V_{sub}	volume of the subcooled liquid	(3.8)	mass balance for the subcooled liquid
6. $T_{r,sub}$	temperature of the subcooled liquid	(3.9)	energy balance for the subcooled liquid
7. $T_{tube,j}$	temperature of the tube wall	(3.12)	energy balance for the tube wall
8. $T_{w,j}$	temperature of cooling water	(3.14)	energy balance for the cooling water
9. T_{sh}	temperature of the shell wall	(3.15)	energy balance for the shell wall

It is clear that the set of equations is closed, which forms a dynamic system of the condenser. The numerical solution of these equations will be discussed in 3.6.

3.5 Boundary layer theory

In equation (3.2) and (3.6), there is a term Q_{bou} which is the heat transfer from the thermal boundary layer to the liquid film. To calculate this heat transfer, knowledge about the boundary layer theory is required. This section is intended to describe how to use the ordinary boundary layer theory in the case of film condensation.

The concept of boundary layer was firstly proposed by **Prandtl** in 1904. He assumed that friction force plays a role only in a very thin layer of fluid near to its boundary which is often a plate standing still. Outside the layer, he just assumed a potential flow. With his assumptions, the Navier-Stokes equations can be simplified and solved analytically. The **Prandtl's** boundary theory was later applied to solve the energy equation and the concept of thermal boundary layer was accordingly brought out. However, the original boundary theory is subjected to transport processes between flowing fluids and solid boundaries. **Collet** [3.6] extended the ordinary boundary theory to a particular case: film condensation of superheated refrigerant vapour in a shell-and-tube condenser. Hereafter a summary of her work is given.

3.5.1 Setting up of boundary layers for vertical film condensation

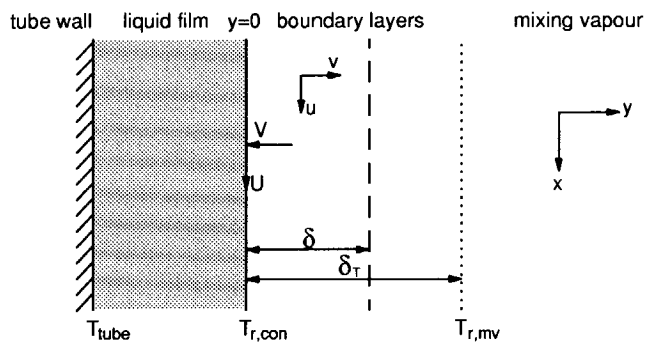


Fig. 3-7 Boundary layers for vertical film condensation

Fig. 3-7 illustrates a velocity boundary layer (thickness = δ) and a thermal boundary layer (thickness = δ_T) outside the liquid film of a condenser tube. In contrast to the ordinary concept of boundary layer, these two boundary layers are established on a moving liquid film instead of a solid plate. The vapour on the surface of the liquid film has a saturated

temperature $T_{r,con}$ and velocity (U,V). In the space far from the liquid film, the vapour has a temperature with high superheat, $T_{r,mv}$ and a velocity of zero. Following the basic assumption made for a boundary layer, it is assumed that the velocity gradient completely takes place in the velocity boundary layer and the temperature gradient in the thermal boundary layer. Thus, on the inner and outer surfaces of the two boundary layers, there exist the following relations

$$u \Big|_{y=0} = U; v \Big|_{y=0} = -V; T \Big|_{y=0} = T_{r,con}; u \Big|_{y=\delta} = 0; T \Big|_{y=\delta} = T_{r,mv}$$

$v \Big|_{y=\delta}$ is however determined through the mass balance over the whole velocity boundary layer. As the temperature and velocity outside the boundary layers are assumed constant, to ensure a continuity of gradient, there should be

$$\frac{\partial v}{\partial y} \Big|_{y=\delta} = 0; \quad \frac{\partial T}{\partial y} \Big|_{y=\delta} = 0$$

The vapour velocity (U,V) on the liquid film can be obtained by using the **Nusselt** theory (see [3.7]).

$$U = A x^{1/2}; \quad V = B x^{-1/4} \quad (3.17a)$$

where

$$A = \left[\frac{\lambda_l (T_{r,con} - T_{tube}) g}{\mu_l \gamma} \right]^{1/2} \quad (3.17b)$$

$$B = \frac{\lambda_l (T_{r,con} - T_{tube})}{\rho_v \gamma} \left[\frac{\rho_l^2 g \gamma}{4 \mu_l \lambda_l (T_{r,con} - T_{tube})} \right]^{1/4} \quad (3.17c)$$

With all these boundary conditions, the energy and momentum equations can be analytical integrated over the boundary layers.

3.5.2 Calculation of the boundary layer thicknesses δ and δ_T

By using the assumptions made above as well as an order-of-magnitude analysis, we are able to derive the boundary equations as follows (see [3.7])

Continuity equation:

$$\frac{\partial u}{\partial x} + \frac{\partial v}{\partial y} = 0 \quad (3.18)$$

Momentum equation in the x direction:

$$u \frac{\partial u}{\partial x} + v \frac{\partial u}{\partial y} = \nu \frac{\partial^2 u}{\partial y^2} \quad (3.19)$$

Energy equation:

$$u \frac{\partial T}{\partial x} + v \frac{\partial T}{\partial y} = a \frac{\partial^2 T}{\partial y^2} \quad (3.20)$$

Boundary conditions:

$$u \Big|_{y=0} = U; \quad v \Big|_{y=0} = -V; \quad T \Big|_{y=0} = T_{r,con}; \quad u \Big|_{y=\delta} = 0;$$

$$T \Big|_{y=\delta_T} = T_{r,mv}; \quad \frac{\partial v}{\partial y} \Big|_{y=\delta} = 0; \quad \frac{\partial T}{\partial y} \Big|_{y=\delta_T} = 0$$

Solutions:

The integration of (3.18) and (3.19) over $y=(0,\delta)$ results in (see [3.6])

x-velocity distribution in the velocity boundary layer:

$$u = U \left(1 - \frac{y}{\delta} \right)^3 \quad (3.21)$$

thickness of the velocity boundary layer:

$$\delta = R x^{1/4} \quad (3.22a)$$

where R is calculated as follows:

$$R = -\frac{14}{5A} \frac{B}{2} + \frac{7}{5} \left[\left(\frac{B}{A} \right)^2 + \frac{105}{A} \nu \right]^{1/2} \quad (3.22b)$$

Then the integration of (3.18) and (3.20) over $y=(0, \delta_T)$ results in

temperature distribution in the thermal boundary layer:

$$T = (T_{r,mv} - T_{r,con}) \left[\zeta (3 - 3\zeta + \zeta^2) \right] + T_{r,con} \quad (3.23)$$

where $\zeta = \frac{y}{\delta_T}$

thickness of the thermal boundary layer:

$$\delta_T = E \delta \quad (3.24a)$$

where E is calculated as follows:

$$\left[\frac{4B}{3AR} - \frac{1}{4} \right] E^3 + \frac{3}{20} E^2 - \frac{1}{20} E + \frac{1}{140} - \frac{4a}{AR^2} = 0 \quad (3.24b)$$

3.5.3 Calculation of the heat transfer to the liquid film

As soon as the temperature gradient of refrigerant in the thermal boundary layer is determined, the heat transfer from the boundary layer to the liquid film can be calculated as follows (see Fig. 3-8):

$$Q_{bou} = L \int_0^H \lambda_v \frac{\partial T}{\partial y} \bigg|_{y=0} dx \quad (3.25)$$

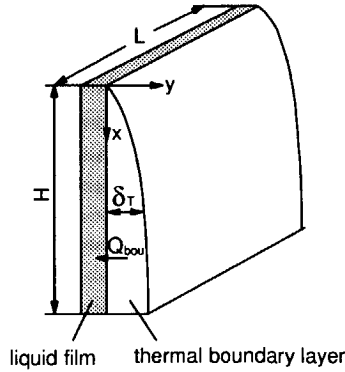


Fig. 3-8 Thermal boundary layer on the liquid film.

According to (3.23), the temperature gradient at $y=0$ is then:

$$\left. \frac{\partial T}{\partial y} \right|_{y=0} = \frac{3 (T_{r,mv} - T_{r,con})}{\delta_T} \quad (3.26)$$

As the thickness of the thermal boundary layer is given by (3.24), thus:

$$Q_{bou} = 3 L \lambda_v (T_{r,mv} - T_{r,con}) \int_0^H \frac{1}{E R x^{1/4}} dx \quad (3.27)$$

$$= \frac{4 L H \lambda_v (T_{r,mv} - T_{r,con})}{E R x^{1/4}} \quad (3.28)$$

In the case of a condenser tube (which is not a vertical plate), analogue can be made as below:

$$Q_{bou} = \frac{4 A_{tube} \lambda_v (T_{r,mv} - T_{r,con})}{E R (0.5 \pi D)^{1/4}} \quad (3.29)$$

Above, we have made an analogue between a horizontal tube and a vertical plate. Basically there must be a difference of the liquid film velocity between them — the direction of

gravity is always the same as the liquid flow direction for a vertical plate; but the direction of the liquid film velocity on a horizontal tube takes the tangential direction of the tube and is thus not align to the gravity direction. Nevertheless, **Collet** [3.6] suggested that the tangential liquid velocity of a round tube be not considerably different from the velocity of a vertical plate in three quarters of the contour of tube. She proposed that the direct adoption of (3.28) to a horizontal tube will not result in large deviation.

3.6 Solution of the equations

In 3.4 a set of ordinary differential equations have been derived, which determine 9 unknown variables together with a number of auxiliary equations for calculating the physical properties and heat transfer coefficients. The solution of these equations is usually carried out on a digital computer. To do so, two problems have to be solved. One is to have a set of initial conditions and another is to select a numerical method. Normally initial conditions are estimated by a steady-state model that will be described in chapter 4. The numerical methods for solving sets of ordinary equations are diverse. However, the simplest is the **Euler** integration method that we decide to use. Hereafter a summary of this method is stated.

Given a set of equations consisting of n differential and m algebraic equations:

Differential equations:

$$\frac{dx_1}{dt} = f_1(x_1, \dots, x_n, y_1, \dots, y_m)$$

$$\frac{dx_2}{dt} = f_2(x_1, \dots, x_n, y_1, \dots, y_m)$$

.

.

.

$$\frac{dx_n}{dt} = f_n(x_1, \dots, x_n, y_1, \dots, y_m)$$

Algebraic equations:

$$y_1 = g_1(x_1, \dots, x_n, y_1, \dots, y_m)$$

$$y_2 = g_2(x_1, \dots, x_n, y_1, \dots, y_m)$$

$$y_m = g_m(x_1, \dots, x_n, y_1, \dots, y_m)$$

the solution of the set of equations is given in the form of a sequence formula:

$$x_1(t+\Delta t) = x_1(t) + \Delta t f_1(x_1(t), \dots, x_n(t), y_1(t), \dots, y_m(t))$$

$$x_2(t+\Delta t) = x_2(t) + \Delta t f_2(x_1(t), \dots, x_n(t), y_1(t), \dots, y_m(t))$$

.

.

.

$$x_n(t+\Delta t) = x_n(t) + \Delta t f_n(x_1(t), \dots, x_n(t), y_1(t), \dots, y_m(t))$$

$$y_1(t+\Delta t) = g_1(x_1(t+\Delta t), \dots, x_n(t+\Delta t), y_1(t), \dots, y_m(t))$$

$$y_2(t+\Delta t) = g_2(x_1(t+\Delta t), \dots, x_n(t+\Delta t), y_1(t), \dots, y_m(t))$$

.

.

.

$$y_m(t+\Delta t) = g_m(x_1(t+\Delta t), \dots, x_n(t+\Delta t), y_1(t), \dots, y_m(t))$$

Such a calculation process is repeated until a required simulation time is reached. The recording of (x_1, \dots, x_n) at every time step is then the mathematical description of dynamic behaviour of the system.

3.7 Closure

This chapter has given a detailed description of the dynamic model of a shell-and-tube condenser which will be coupled with the models of the other components to simulate the whole refrigeration system in chapter 8. The condenser model is applicable for both on- and off-periods. Thus it is not necessary to make a separate model specially for off-periods, as made in the previous chapter.

For sake of simplicity, the heat transfer coefficients and physical properties of refrigerant and water were not discussed in this chapter. The heat transfer coefficients will be treated together with the other coefficients in chapter 6. And the physical properties are calculated by calling the subroutines in a STOFBANK available at the author's laboratory.

As pointed out before, a dynamic simulation requires a certain number of initial conditions which should be firstly estimated by a steady-state model. Therefore, the next chapter will be concerned with developing a simple steady-state model.

References

- 3.1 **James, R.W., Marshall, S.A.** "Dynamic analysis of a refrigeration system", *The Institute of Refrigeration*, Session 1973-1974, pp.1-9.
- 3.2 **Wong, A.K.H.** "An investigation into control of refrigeration systems with the emphasis on capacity control", Ph.D. Thesis, CNAA, South Bank Polytechnic, London, 1988.
- 3.3 **Yasuda, H., Machielsen, C.H.M., Touber, S., Brok, S.W., de Bruijn, M.** "Simulation of transient behaviour of a compression-evaporation refrigeration system", WTHD No. 133, Delft University of Technology, the Netherlands, March 1981.
- 3.4 **Van der Meer, J.S.** "Simulation of a refrigerant evaporator", Ph. D. Thesis, Delft University of Technology, the Netherlands, October 1987.
- 3.5 **Henrici, H.H.** "Kondensation von frigen 12 und frigen 22 an glatten und berippten rohren", Dissertation, Technischen Hochschule Karlsruhe, Karlsruhe, Germany, July 1961 (in German).
- 3.6 **Collet, I.C.** "De invloed van oververhitting bij filmcondensatie", Report No. S-850, Delft University of Technology, the Netherlands, May 1988 (in Dutch).
- 3.7 **Özisik, M.N.** "Heat transfer (a basic approach)", McGraw-Hill, Inc., 1985.

Steady-State Modelling of the Refrigerating Machine

4.1 General

In the preceding two chapters, the dynamic models of the evaporator and condenser were described. As the compressor responds quickly, it can be considered as an instantaneous model. In another word, for a dynamic simulation of the refrigerating machine, only the evaporator, condenser and TEV models are needed to be dynamic, while the compressor model could be steady-state. Because the TEV model has been established and validated by **van der Meer** in his Ph.D. thesis [4.1] and the compressor model is simple and experimentally fitted, they will be introduced in Appendices 1 and 2.

This chapter is written for another type of modelling: steady-state modelling. There are two motivations to develop a steady-state model for the refrigerating machine: 1) as pointed out in chapter 1, for a long-term simulation of the complete system consisting of a machine and a room, a good combination of a steady-state machine model with a non-steady-state room model is suitable. This forms the first motivation; 2) on the other hand, a steady-state model is also required to determine initial values for dynamic simulations which are usually started with a steady state in order to clean up initial "noise". In principle, the dynamic model is also able to reach a steady state, provided that it is run for a quite long time. However, this proved not to be economical. It is also found that arbitrary initial values given to the dynamic model often lead to divergent solutions. Therefore, a better way is to use the output of a steady-state model as the input initial values for the dynamic model.

The importance of steady-state models for optimal design and manufacturing of refrigerating systems has been stressed already in [4.2, 4.3]. Herein we will not go further on it.

In contrast to the dynamic modelling in the previous chapters, in which the emphasis was put on the derivation and solution of the governing equations, this chapter is intended to pay more attention on the implementations, iteration processes and coupling of the component models, besides the modelling strategies and the derivation of the conservation equations. The input and output relations and coupling among the components are also valid for dynamic simulations. To make the context clear, the heat transfer coefficients and pressure drops encountered in this chapter are also left for chapter 6.

4.2 Literature

Conde [4.4] developed a steady-state mathematical simulation model for air-to-water heat pumps in 1985. The modelled system included a reciprocating compressor, a thermostatic expansion valve, a direct-expansion evaporator, a liquid-cooled condenser and control devices. For the compressor and TEV models, the manufacturers' catalogues were used to derive the necessary parameters.

The evaporator model is sophisticated — the evaporator is sub-divided into a three dimensional network of small control volumes. The reason for this is that when dehumidification or frost-formation takes place, a better understanding of the local conditions is necessary. The **Lockhart-Martinelli** correlation [4.5] is used to calculate the local heat transfer coefficient in the evaporation region. The superheat region heat transfer coefficient is calculated using the **Sieder-Tate** correlation. The **McQuiston** correlation [4.6] is used to calculate the sensible and total heat transfer coefficients on the air-side. The pressure losses in the evaporation region are considered in two parts: in straight tubes and return bends. The results of **Thom** [4.7], **Goldstein** [4.8], **Chisholm** [4.9] and **Geary** [4.10] are used. Besides dehumidification, frost-formation is also taken into account. A quasi-steady-state model is proposed to tackle the essentially transient process of frost-formation, that is, the conservation equations in the model are independent of time and only the equations for the density, thickness, and thermal conductivity of frost are time-dependent. The outside heat and mass transfer coefficients are assumed not influenced by the frost-formation except the geometrical effects.

The condenser model is a one-zone lumped model. A so-called weighted LMTD (logarithmic mean temperature difference) is assumed, that makes the condenser a single-to-single phase heat exchanger. Then no distinguish is made between the condensation zone and subcooling zone. On the refrigerant side, the **Kirkbride** correlation [4.11] is used to calculate the heat transfer coefficient. The enthalpy of the entering vapour from the compressor is added to the heat transfer coefficient to account for the heat transfer resulting from de-superheating. On the water side, the **Dittus-Boelter** correlation is used for calculating the heat transfer coefficient. The refrigerant-side pressure drop across the tube bank is neglected. However,

the pressure drops due to the sudden expansion and contraction at the inlet and outlet are considered. The thermal resistance of the tube wall is neglected.

Although **Conde** considered almost every theoretical aspect about modelling of a steady-state vapour compression cycle and also gave the logic diagrams for the computer implementation of the model, no simulation results and experimental validation are presented in his work.

Domanski and Didion [4.12] developed a computer model for a vapour compression cycle with constant flow area expansion device in 1983. The compressor is of a reciprocating hermetic type and the evaporator and condenser are heat exchangers with coiled tubes and air as coolant.

Because of the similarity between the evaporator and condenser, both of them are treated in the same way. The so-called tube-by-tube simulation method is applied so that the general finned-coil problem is reduced to a single tube problem. This method allows to divide the whole heat exchanger into elements each of which is one tube. A certain coding has to be worked out according to the coil circuitry of the heat exchanger, in order to re-assemble the separated tubes. To perform the tube-by-tube simulation, two basic parameters are necessary to be determined: the refrigerant mass flow rate for each tube and the fraction of the tube length in the two-phase flow region. The first is calculated by using iteration processes to check the equality of pressure drops, while the second is based on the heat balance of the inside and outside of the tube. The heat transfer coefficient for the two-phase forced convection with evaporation is calculated using the **Pierre** correlation [4.13]. On the air side, the **Briggs and Young** correlation is adopted. When dehumidification is concerned, the Lewis number is chosen to 1. The effect of frost thickness is also taken into account. For the pressure drop in the two-phase flow with evaporation, the **Pierre** correlation [3.14] is used.

The verification of the model has been conducted against the laboratory test data from three heat pump systems. The maximum discrepancy of the model was found to be 3.4% for capacity and 5.5% for coefficient of performance.

Van der Meer [4.1] studied a dry expansion evaporator accompanied with a thermostatic expansion valve. He divided the evaporator into 3 zones (1 evaporation zone and 2 superheat zones). The reason to split the superheat region into 2 zones was because the modelled evaporator is of an "E-flow" type as shown in Fig. 4-1. The **Dembi** correlation [4.15] was integrated to obtain an average form for calculating the two-phase flow heat transfer coefficient. The **Brauer** correlation [4.16] was used to calculate the two-phase flow pressure drop. On the air side, the **Kutateladze** correlation [4.17] was adopted for calculating the heat transfer coefficient. However no dehumidification was considered. The model was validated with the experimental data.

4.3 The three-zone steady-state evaporator model

In the previous section, three types of models for dry expansion evaporator have been reviewed. The models made by **Conde, Domanski** are distributed and complex, while the model of **van der Meer** is lumped and simple but relatively flexible as compared to two-zone models. As our original purpose of the steady-state modelling was to determine initial values for dynamic simulations, it was intended to develop a simple and economical evaporator model. Moreover, the model of **van der Meer** was available at the author's laboratory. Considering the continuity between the projects at the laboratory, it was decided to use and modify **van der Meer's** model for the evaporator.

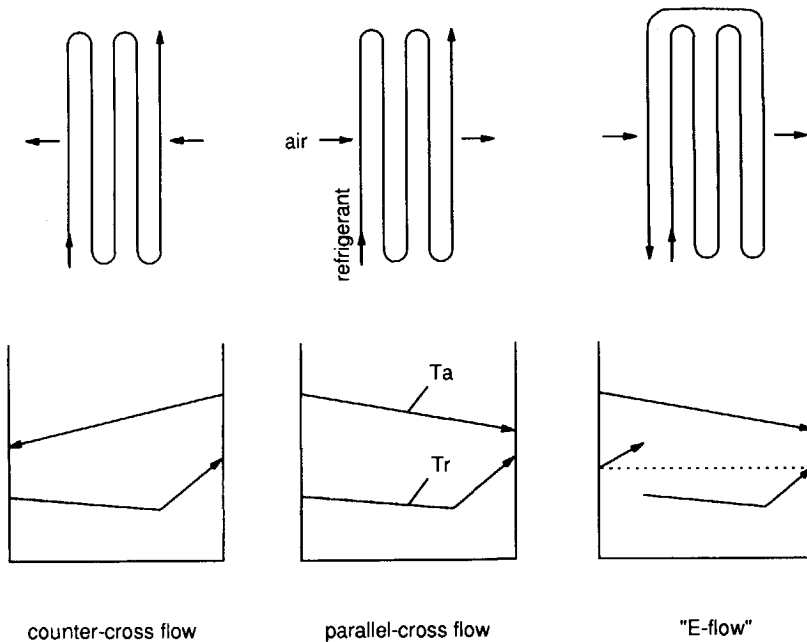


Fig. 4-1 Three types of circuiting methods and their temperature profiles.

As pointed out in chapter 2, dry expansion evaporators are often manufactured in various circuiting ways. However, the following three types are the most encountered: 1. counter-cross flow, 2. parallel-cross flow, 3. "E-flow". Fig. 4-1 gives the diagrams of these three types of circuiting methods and their temperature profiles. Below it will be found that if the three-zone division is applied, the modelling of the three types can be identified.

Let us first consider the most complicated situation — "E-flow" (see Fig. 4-2). The evaporator can be split into two regions: evaporation region (two-phase flow) and superheat region (single-phase flow), according to the refrigerant flow patterns. However since the superheat region has pipes returning back to the front of the evaporator, it is necessary to divide it further into two zones. Therefore the whole evaporator is finally divided into three zones. Such a division of the evaporator enhances the flexibility of the model. For example, in the case of a counter-cross flow, superheat zone 1 is just set to be zero without modifying the model itself. While, in the case of a parallel-cross flow, superheat zone 2 is just zero.

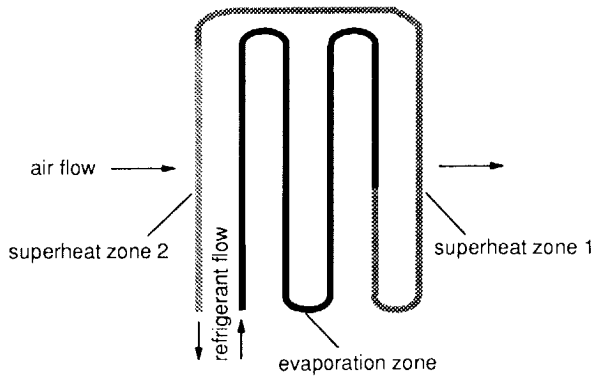


Fig. 4-2 Zone division of an "E-flow" evaporator.

4.3.1 Assumptions

Lumped modelling is in fact an assumed description of reality. The integration of distributed parameters into lumped ones needs some reasonable assumptions to simplify the problems. To develop a three-zone steady-state model for the evaporator, the following postulations are necessary:

- 1) the temperature differences between the air and pipe wall, pipe wall and refrigerant are logarithmic in each of the three zones (see Fig. 4-3);
- 2) the heat resistance in the radial direction of the pipe wall is neglected, because of the small thickness and large conductivity of the pipe wall;
- 3) no frost-formation takes place on the outside surface of the evaporator. However, dehumidification may occur in the zone where the pipe wall temperature is below the dew

point of the wet air. This assumption is made because of the large uncertainty of the thermal properties of frost layers, such as heat conductivity;

- 4) The air is equally distributed over the total free-flow area of the evaporator
- 5) The refrigerant is equally distributed to each parallel circuit. Thus, attention will be paid only to one circuit. About uneven distribution situations, [4.1] can be consulted.

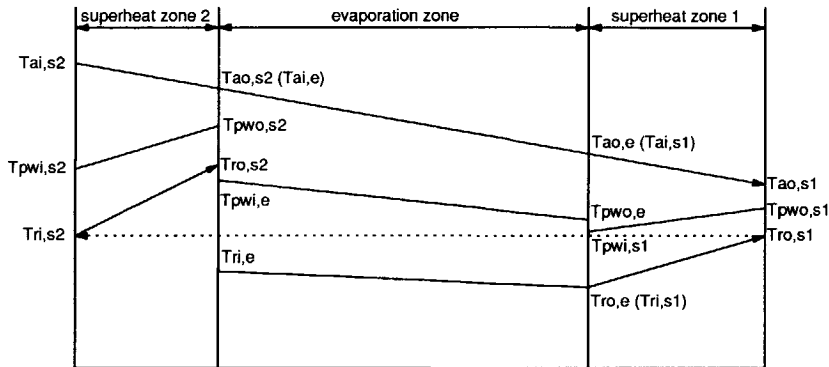


Fig. 4-3 Temperature profiles in the three zones of the "E-flow" evaporator.

4.3.2 Conservation equations

As described above, the dry expansion evaporator is divided into three zones. Each of the zones consists of three basic elements: refrigerant, pipe wall, air (see Fig. 4-4). The conservation equations can be therefore set up for every basic element. In principle, the conservation equations include energy-, momentum- and mass-balance equations. However, the momentum- and mass-balance equations can be substituted by the correlations for pressure drops and the consideration of equal mass flow rate throughout the system for both the refrigerant and air. Thus the conservation equations in this section only involve the energy balance equations (except the moisture balance equation for the wet air). As the three zones have the same form of conservation equations, one of them is just considered below. The heat transfer coefficient and pressure drop correlations used in the equations will be described in chapter 6.

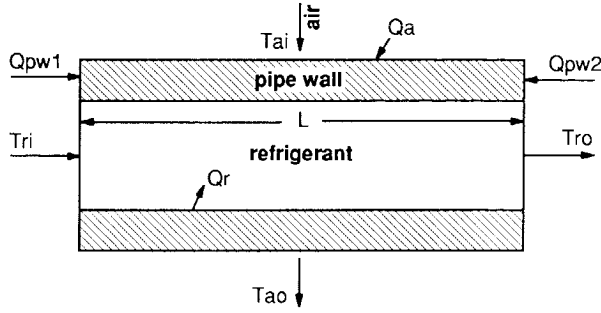


Fig. 4-4 Basic elements in one zone: refrigerant, pipe wall and air.

Energy balance for the refrigerant:

If neglecting the kinetic and potential energy, the heat transferred from the pipe wall to the refrigerant must be equal to the enthalpy increase of the refrigerant over the concerned zone.

$$\alpha_{pw,r} \pi d L \Delta T_{pw,r} = \dot{m}_r (h_{ro} - h_{ri}) \quad (4.1)$$

where (see [4.18])

$$\Delta T_{pw,r} = \frac{(T_{pwi} - T_{ri}) - (T_{pwo} - T_{ro})}{\ln[(T_{pwi} - T_{ri}) / (T_{pwo} - T_{ro})]} \quad (4.2)$$

$$T_{pwi} = \frac{\alpha_{a,s} D T_{ai} + \alpha_r d T_{ri}}{\alpha_{a,s} D + \alpha_r d} \quad (4.3)$$

Energy- and moisture-balance for the air:

The transport phenomenon between the wet air and the pipe wall involves two aspects: sensible heat transfer and water vapour condensation or evaporation. The moisture transfer due to water vapour condensation or evaporation on the outside surface of the evaporator also makes a contribution to the heat transfer which is called latent heat. To be convenient, enthalpy differences are usually used to calculate the total heat transfer (sensible heat plus latent heat).

Total energy balance equation:

$$\alpha_{a,t} (A_{pipe} + \eta_{fin} A_{fin}) \Delta h_{a,pw} = \dot{m}_a (h_{ao} - h_{ai}) \quad (4.4)$$

where

$$\Delta h_{a,pw} = \frac{(h_{ai} - h_{pwi}) - (h_{ao} - h_{pwo})}{\ln[(h_{ai} - h_{pwi})/(h_{ao} - h_{pwo})]} \quad (4.5)$$

h_{pwi} and h_{pwo} are calculated based on the corresponding pipe wall temperature and relative humidity of 100 %, if the pipe wall temperature is below the dew point of the air. The air enthalpy is defined as:

$$h_a = c_{p,a} \theta_a + c_{p,w} w_a \theta_a + \gamma w_a \quad (4.6)$$

Sensible energy balance equation:

$$\alpha_{a,s} (A_{pipe} + \eta_{fin} A_{fin}) \Delta T_{a,pw} = \dot{m}_a c_{p,a} (T_{ao} - T_{ai}) \quad (4.7)$$

where

$$\Delta T_{a,pw} = \frac{(T_{ai} - T_{pwi}) - (T_{ao} - T_{pwo})}{\ln[(T_{ai} - T_{pwi})/(T_{ao} - T_{pwo})]} \quad (4.8)$$

Energy balance for the pipe wall:

Because there is no energy accumulation in the pipe wall in steady-state situations, the summation of the heat transfer from the air, refrigerant and the adjacent pipe walls must be zero:

$$\alpha_r \pi d L (T_r - T_{pw}) + \alpha_{a,t} (A_{pipe} + \eta_{fin} A_{fin}) (h_a - h_{pw}) + Q_{pw,1} + Q_{pw,2} = 0 \quad (4.9)$$

where $Q_{pw,1}$ and $Q_{pw,2}$ are calculated according to the method given in [4.1] as follows:

$$Q_{pw,1} = c L_{leak} S_l (T_{pw,1} - T_{pw}) \quad (4.10)$$

where c is an empirical constant; L_{leak} is the effective heat leakage length between the concerned two zones (the calculation of L_{leak} can be found on page 86 of [4.1]); S_l is calculated in chapter 6. The calculation of $Q_{pw,2}$ is similar to that of $Q_{pw,1}$.

4.3.3 Closure of the equations

It can be found above that each of the three zones has four basic equations: (4.1), (4.4), (4.7), (4.9). Therefore the evaporator system totally includes 3x4 equations which can only solve 12 unknown variables. However, there are 13 unknown variable to be determined which are Tri,e , $Tro,s1$, $Tro,s2$, Le , $Tpwo,e$, $Tpwo,s1$, $Tpwo,s2$, Tao,e , $Tao,s1$, $Tao,s2$, wao,e , $wao,s1$, $wao,s2$. In order to make the set of equations closed, the models of the other components are necessary. In our case, the TEV model is put in use for the purpose. The interactions between the TEV and evaporator models are described in section 4.5.

4.3.4 Implementation of the evaporator model

Input and output description

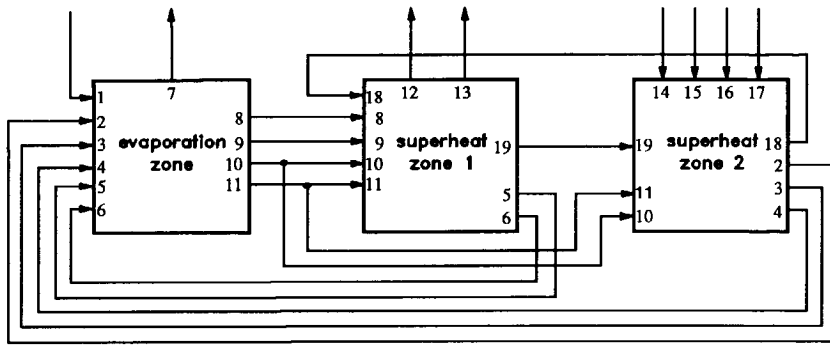
To facilitate the computer programming procedures, it is important to define the input and output of every zone clearly before writing programmes. Fig. 4-5 gives a detailed description of the input and output of the three zones and their inter-relations.

Logic of solution

As the steady-state equations derived in 4.3.2 are implicit, the solution of them requires several iterative processes at different levels.

Iterative level 1

Fig. 4-6 shows the flow diagram of the first level iteration. As the length of the evaporation zone is not known, starting a computation from any of the superheat zones is inappropriate. Therefore we chose the evaporation zone as the starting point. However, the air temperature and humidity at the inlet of the evaporation zone are not known, because the air firstly passes the second superheat zone. To solve the problem, assumption has to be made for the air temperature and humidity at the very beginning. With the assumed values, the three zones can be sequentially computed. The output air temperature and humidity of the second superheat zone are in turn used to compare the assumed values. If they are not in agreement, the iteration is continued until the required accuracy is reached.



- | | | |
|----|-------------|---|
| 1 | \dot{m}_r | refrigerant mass flow rate through the evaporator (output from the Compressor model); |
| 2 | $T_{ai,e}$ | air inlet temperature of the evaporation zone, or |
| | $T_{ao,s2}$ | air outlet temperature of superheat zone 2; |
| 3 | $w_{ai,e}$ | air inlet absolute humidity of the evaporation zone, or |
| | $w_{ao,s2}$ | air outlet absolute humidity of superheat zone 2; |
| 4 | $T_{pw,s2}$ | pipe wall temperature of superheat zone 2; |
| 5 | $P_{ro,e}$ | refrigerant outlet pressure of the evaporation zone, or |
| | $P_{ri,s1}$ | refrigerant inlet pressure of superheat zone 1; |
| 6 | $T_{pw,s1}$ | pipe wall temperature of superheat zone 1; |
| 7 | $T_{ri,e}$ | refrigerant inlet temperature of the evaporation zone (output of the evaporator model); |
| 8 | $T_{ao,e}$ | air outlet temperature of the evaporation zone, or |
| | $T_{ai,s1}$ | air inlet temperature of superheat zone 1; |
| 9 | $w_{ao,e}$ | air outlet absolute humidity of the evaporation zone, or |
| | $w_{ai,s1}$ | air inlet absolute humidity of superheat zone 1; |
| 10 | $T_{pw,e}$ | pipe wall temperature of the evaporation zone; |
| 11 | L_e | length of the evaporation zone; |
| 12 | $T_{ao,s1}$ | air outlet temperature of superheat zone 1; |
| 13 | $w_{ao,s1}$ | air inlet absolute humidity of superheat zone 1; |
| 14 | $P_{ro,s2}$ | refrigerant outlet pressure of superheat zone 2 (output of the TEV model); |
| 15 | $T_{ai,s2}$ | air inlet temperature of superheat zone 2 (input parameter); |
| 16 | $w_{ai,s2}$ | air inlet absolute humidity of superheat zone 2 (input parameter); |
| 17 | \dot{m}_a | air mass flow rate through the evaporator; |
| 18 | $P_{ro,s1}$ | refrigerant outlet pressure of superheat zone 1, or |
| | $P_{ri,s2}$ | refrigerant inlet pressure of superheat zone 2. |
| 19 | $T_{ro,s1}$ | refrigerant outlet temperature of superheat zone 1, or |
| | $T_{ri,s2}$ | refrigerant inlet temperature of superheat zone 2. |

Fig. 4-5 Input and output for the three zones of the evaporator.

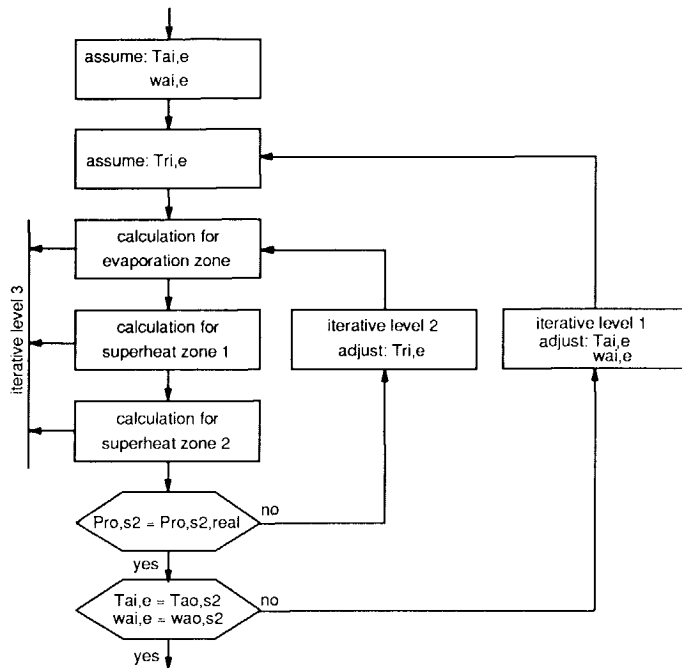


Fig. 4-6 Flow diagram of the first and second level iterations.

Iterative level 2

Because the refrigerant inlet temperature of the evaporation zone is also unknown, the second level iteration is required to determine it, as shown in Fig. 4-6. The refrigerant outlet pressure of superheat zone 2, which is output from the TEV model, is used as the checked value in this iteration.

Iterative level 3

Besides the first and second iterative levels, each of the three zones has to undergo an iteration at the third level for calculating its pipe wall temperature. Because the inside and outside heat transfer coefficients are dependent on the pipe wall temperature, assumption for the pipe wall temperature is necessary. The energy balance for the pipe wall forms the checking criterion of this iteration. Fig. 4-7 is the flow diagram of the third level iteration.

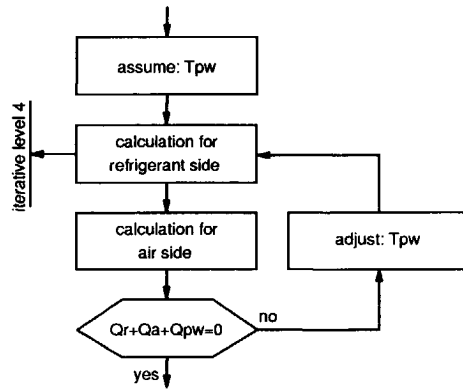


Fig. 4-7 Flow diagram of the third level iteration.

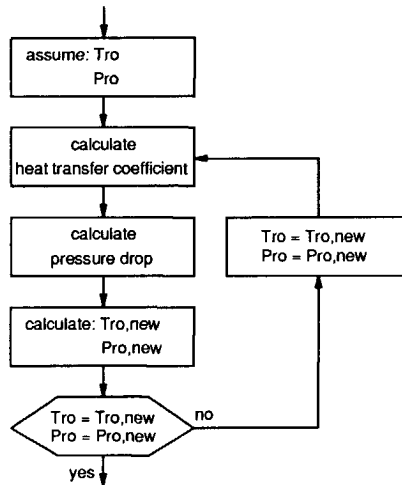


Fig. 4-8 Flow diagram of the fourth level iteration.

Iterative level 4

Due to the dependency of the heat transfer coefficients and pressure drop upon the average refrigerant temperature and pressure in the concerned zone, the fourth level iteration is needed. In principle, this iteration could be combined with the third level iteration.

However, it has been found that one iteration for more unknown variables often leads to a divergence. Thus it is decided to separate them, although such a method requires more computational times. In contrast to the two superheat zones, for the evaporation zone, an extra parameter Le is calculated in this iteration. Fig. 4-8 is the flow chart of the fourth level iteration.

4.4 The two-zone steady-state condenser model

The shell-and-tube condenser has a characteristic that there exists a clear boundary between the superheated vapour and subcooled liquid. If the inlet mass flow rate of the refrigerant is high enough to make the entering hot vapour well mixed with the rest in the shell, a 2-zone model is very suitable for the bath-type condenser. This modelling strategy has been clearly described in chapter 3 where the dynamic modelling of the condenser was dealt with. Because the zone or element divisions on both the refrigerant side and water side for the steady-state modelling is the same as those for the dynamic modelling, hereafter more attention will be paid to the iteration processes for solving the conservation equations. The details about the zone divisions can be found in section 3.3.

On the basis of the modelling strategy, the conservation principles can be applied to build up a mathematical model. Similar to the treatment to the evaporator, some assumptions are necessary to facilitate the derivation of equations.

4.4.1 Assumptions

- 1) the vapour in the condensation zone is perfectly mixed so that its thermodynamic state is able to be expressed by a temperature T_{mv} and a pressure P_{mv} or the condensation temperature T_c which is the corresponding saturated temperature of P_{mv} ;
- 2) the heat resistance in the radial direction of the tubes is neglected;
- 3) de-superheating, condensation and subcooling may take place simultaneously on the outside surface of the tubes. The liquid droplets from the tubes do not have any heat exchange with their surrounding vapour;
- 4) pressure drops at the inlet, outlet and inside of the condenser shell are all neglected;
- 5) the heat transfer between the mixing vapour and subcooled liquid is neglected.

4.4.2 Conservation equations

Energy balance for the mixing vapour:

$$\dot{m}_{r,in} h_{r,in} - \dot{m}_{r,v,con} h_{r,v,con} - Q_{r,sh2} - Q_{bou} = 0 \quad (4.11)$$

Energy balance for the liquid film:

$$\dot{m}_r h_{rv,con} - \dot{m}_r h_{r,film} + Q_{bou} - \sum_{k=Nsub+1}^{Ntot} Q_{tube,k} = 0 \quad (4.12)$$

where $h_{r,film}$ is calculated according to the **Henrici** correlation (see section 3.4.2).

Energy balance for the subcooled liquid:

$$\dot{m}_r h_{r,film} - \dot{m}_r h_{r,sub} - Q_{r,shl} - \sum_{j=1}^{Nsub} Q_{tube,j} = 0 \quad (4.13)$$

Energy balance for the pipe wall:

$$Q_{tube,j} - Q_{w,j} = 0 \quad (4.14)$$

Energy balance for the cooling water:

$$\dot{m}_w (h_{w,in,j} - h_{w,out,j}) + Q_{w,j} = 0 \quad (4.15)$$

Energy balance for the shell:

$$Q_{r,sh} - Q_{sh,atm} = 0 \quad (4.16)$$

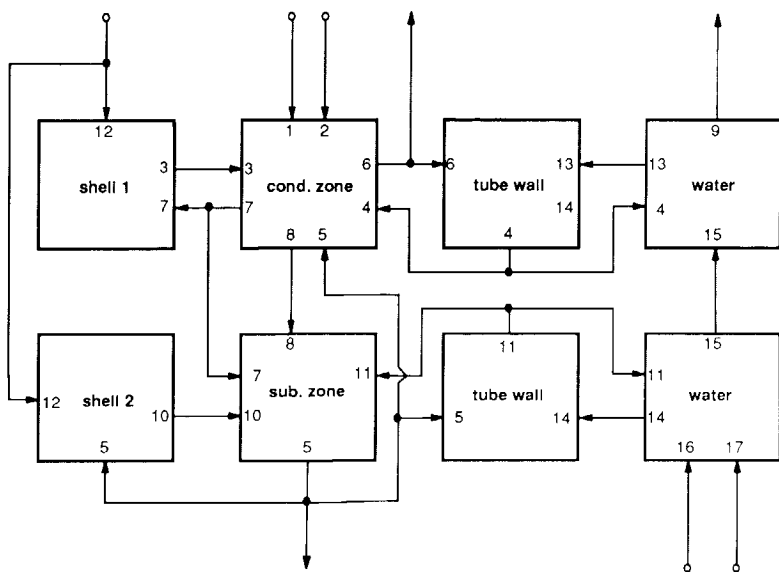
The heat transfer terms involved in the above conservation equations are all calculated in chapter 3. The concerned heat transfer coefficients will be specially introduced in chapter 6 and the heat transfer areas will be calculated in Appendix 3. The refrigerant mass flow rate results from the compressor model which will be described in Appendix 1.

4.4.3 Closure of the equations

Above, 6 equations have been derived based on the energy conservation principle. They are (4.11), (4.12),, (4.16) which compose the whole condenser system and determine 6 unknown variables: Tr,mv , Tr,con (or Pr,mv), Tr,sub , $Ttube,j$, Tw,j , Tsh . Solution of the set of algebraic equations needs iterations which will be described below.

4.4.4 Implementation of the condenser model

Input and output description



- 1 \dot{m}_r refrigerant mass flow rate (output from the compressor model);
- 2 $T_{r,in}$ inlet refrigerant temperature of the condenser (output from the compressor model);
- 3 T_{sh2} temperature of the upper part of the shell;
- 4 $T_{tube,con}$ temperature of the tube wall in the condensation zone;
- 5 $T_{r,sub}$ temperature of the subcooled refrigerant liquid;
- 6 $T_{r,con}$ condensation temperature;
- 7 $T_{r,mv}$ temperature of the mixing refrigerant vapour;
- 8 $T_{r,film}$ temperature of the liquid film;
- 9 $T_{w,out,tot}$ outlet water temperature of the last pass;
- 10 T_{sh1} temperature of the lower part of the shell;
- 11 $T_{tube,sub}$ temperature of the tube wall in the subcooling zone;
- 12 T_{amb} ambient temperature;
- 13 $T_{w,con}$ water temperature of the passes in the condensation zone;
- 14 $T_{w,sub}$ water temperature of the passes in the subcooling zone;
- 15 $T_{w,out,sub}$ outlet water temperature of the last pass in the subcooling zone;
- 16 $T_{w,in,l}$ inlet water temperature of the first pass;
- 17 \dot{m}_w water mass flow rate through the condenser.

Fig. 4-9 Input and output of the elements in the condenser system.

Fig. 4-9 gives a detailed description of the input and output of every element of the condenser system.

Logic of solution

The output of each element is calculated by solving the concerned equations based on the input. From Fig. 4-9 it can be found that one's input may be another's output. The input-output interactions among the elements make the calculation rather complicated. Therefore it is better to divide the iterative processes into several levels in which different unknown variables are calculated.

Iterative level 1

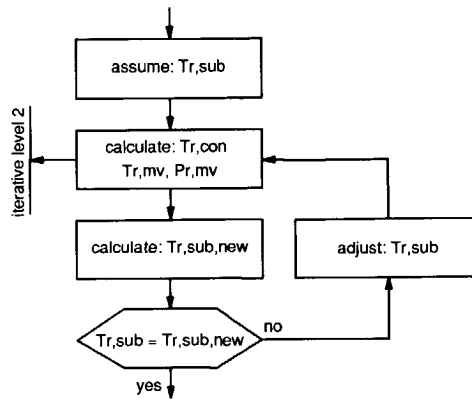


Fig. 4-10 Flow diagram of the first level iteration for the condenser model.

The first level iteration is aimed at solving for Tr_{sub} . The refrigerant enters at the top of the condenser and the water does at the bottom. Assumption for Tr_{sub} is necessary to start the calculation from the bottom. As soon as the other unknowns are worked out with the assumed Tr_{sub} , equation (4.13) can be used to determine a new Tr_{sub} . An iteration is then needed to ensure the new value of Tr_{sub} is equal to the old value. Fig. 4-10 is the flow diagram of the first level iteration.

Iterative level 2

The second level iteration is to solve for Tr_{con} . In equation (4.12), the heat transfer coefficient of condensation depends on Tr_{con} . Direct solution for Tr_{con} is then impossible.

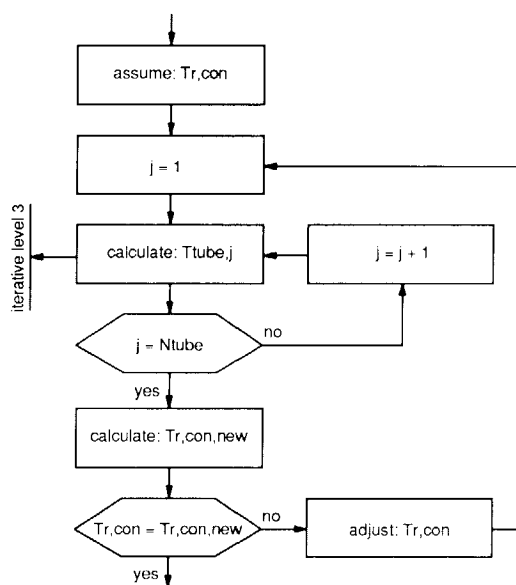


Fig. 4-11 Flow diagram of the second level iteration in the condenser model.

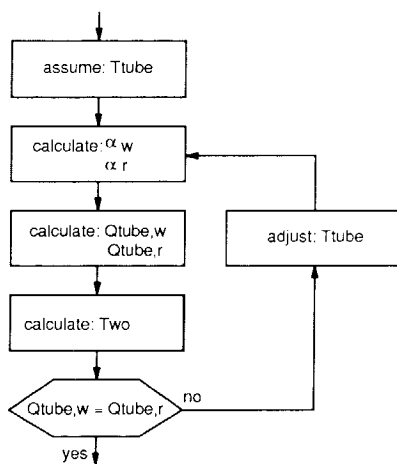


Fig. 4-12 Flow diagram of the third level iteration in the condenser model.

Thus an extra iteration is needed. Besides, a do-loop is required to repeat the calculation for all the tube elements. Fig. 4-11 is the flow diagram. Together with Tr_{con} , Tr_{mv} , Tr_{film} , and T_{sh} are also obtained from this iterative level.

Iterative level 3

Fig. 4-12 is the flow diagram of the third level iteration which is intended to calculate $T_{tube,j}$. The reason of this iteration is because the inside and outside heat transfer coefficients are also the functions of the tube wall temperature. Depending on the liquid level, a tube element may be in the condensation zone or in the subcooling zone. Thus at the beginning of the iteration, a position check should be made by comparing the height of the tube element with the liquid level. If a certain element is transected by the liquid level, two tube wall temperatures are assumed for the part sunk in the liquid and the part in the vapour. The heat conduction between the two parts is neglected.

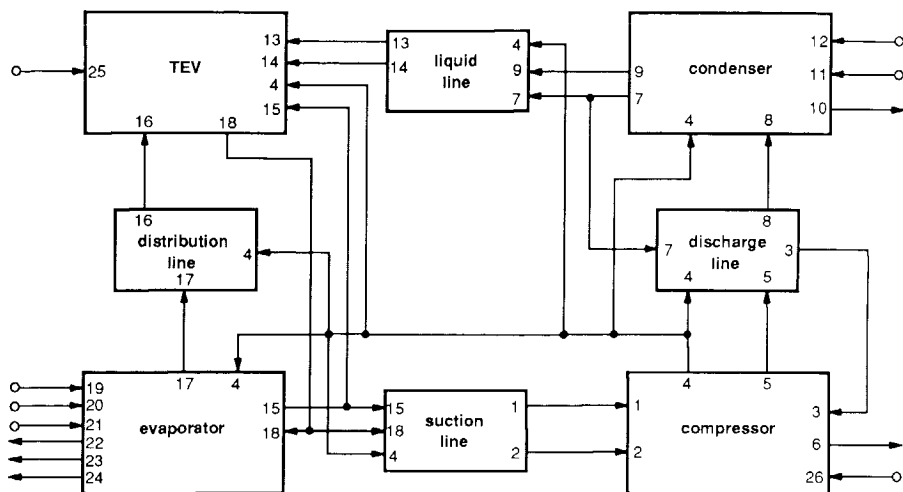
4.5 Coupling of the component models

By so far, the steady-state models of the evaporator and condenser have been described. As mentioned before, because the TEV model has been developed by **van der Meer** [4.1] and the compressor model is simple and experimentally obtained, they are all introduced in the appendices. Herein, only the coupling of them with the evaporator and condenser models are described so that a cyclic simulation becomes possible. Besides the components, the connection lines between the components should be taken into account. However, as the connection lines are too complicated and changeable according installation requirements, we decided to use two simple equations to represent each of the connection lines. These two equations account for the pressure drops and heat transfer taking place on the connection lines. Nevertheless, experiments are needed to determine the empirical constants in the two equations. The details about this problem can be found in chapters 6 and 7.

For sake of simplicity, every component or connection line is represented by a black box with specific input and output hereafter. In such a way, a module-type computer program can be made. If necessary in the future, more components can be easily added to the system without changing the contents of other component models.

4.5.1 Input and output description

Fig. 4-13 shows the input and output as well as their relations of all the components in the refrigerating machine system. There are 8 modules connected with each other. The input and output of the refrigerating machine are also identified, which form an interface with the refrigerated room model to be introduced in chapter 5.



- 1 T_{suc} suction temperature of the compressor;
- 2 P_{suc} suction pressure of the compressor;
- 3 P_{dis} discharge pressure of the compressor;
- 4 \dot{m}_r refrigerant mass flow rate through the system;
- 5 T_{dis} discharge temperature of the compressor;
- 6 W_{comp} shaft power of the compressor;
- 7 P_c condensation pressure;
- 8 $T_{ri,con}$ refrigerant temperature at the inlet of the condenser;
- 9 $T_{r,sub}$ refrigerant temperature at the outlet of the condenser;
- 10 $T_{wo,con}$ water temperature at the outlet of the condenser;
- 11 $T_{wi,sub}$ water temperature at the inlet of the condenser;
- 12 \dot{m}_w water mass flow rate of the condenser;
- 13 $P_{ri,tev}$ refrigerant pressure at the inlet of the TEV;
- 14 $T_{ri,tev}$ refrigerant temperature at the inlet of the TEV;
- 15 $T_{ro,evap}$ refrigerant temperature at the outlet of the evaporator;
- 16 $P_{ro,tev}$ refrigerant pressure at the outlet of the TEV;
- 17 $P_{ri,evap}$ refrigerant pressure at the inlet of the evaporator;
- 18 $P_{ro,evap}$ refrigerant pressure at the outlet of the evaporator;
- 19 \dot{m}_a air mass flow rate through the evaporator;
- 20 $T_{ai,evap}$ air temperature at the inlet of the evaporator;
- 21 $w_{ai,evap}$ air absolute humidity at the inlet of the evaporator;
- 22 $T_{ao,evap}$ air temperature at the outlet of the evaporator;
- 23 $w_{ao,evap}$ air absolute humidity at the outlet of the evaporator;
- 24 Q_{evap} refrigeration capacity;
- 25 DTSS screw position of the TEV;
- 26 RMP rotational speed of the compressor.

Fig. 4-13 Input and output of the components in the refrigeration system.

4.5.2 The cyclic computation

To be clear, the cyclic computation is designed to follow the thermodynamic cycle of the refrigerating system as shown in Fig. 4-14. Because fewer input parameters are required by the compressor model, the computation is started from the compressor model with assuming the following input parameters:

- T_{suc} : suction temperature at the inlet of the compressor
- P_{suc} : suction pressure at the inlet of the compressor
- P_{dis} : discharge pressure at the outlet of the compressor

Moreover, at the very beginning of a cyclic computation, two input parameters for the TEV model are also required:

- $T_{ro,tev}$: refrigerant temperature at the outlet of the TEV
- $T_{ro,evap}$: refrigerant temperature at the outlet of the evaporator

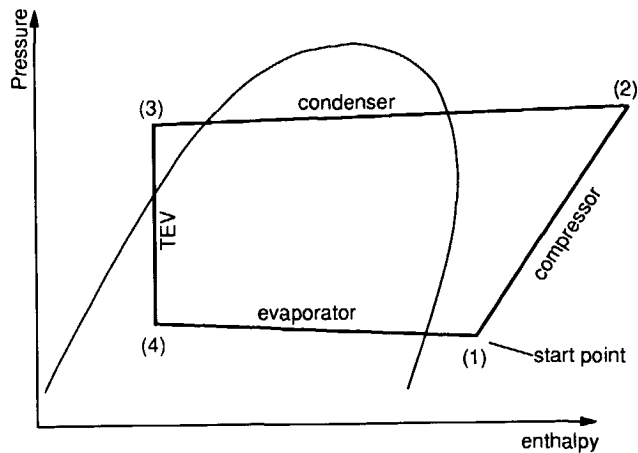


Fig. 4-14 Thermodynamic cycle of a vapour compression refrigeration system.

After a computational cycle: *compressor — discharge line — condenser — liquid line — TEV — distribution line — evaporator — suction line*, new values of the five initial input parameters can be obtained. Comparison between the old and new values results in a decision whether or not the computation is stopped. If the old and new values are not close

to each other, the old values are replaced by the new values and the same computational cycle is repeated. Fig. 4-15 is the flow diagram of the cyclic computation.

The steady-state model of the refrigerating machine has been validated by using the laboratory test data. The details about the experiments and test results will be given in chapter 7.

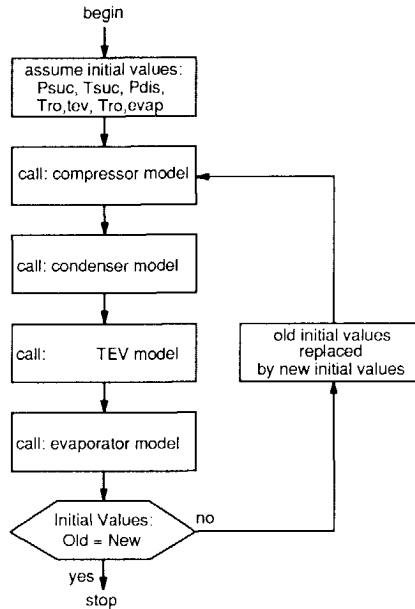


Fig. 4-15 Flow diagram of the cyclic computation.

References

- 4.1 **Van der Meer, J.S.:** "Simulation of a refrigerant evaporator", Ph.D. thesis, Delft University of Technology, the Netherlands, October 1987
- 4.2 **Touber, S.:** "Energiebesparing bij compressie-koelinstallaties", *Koeltechniek*, nr 11, November 1987, pp.11-20 (in Dutch)

- 4.3 **Kruse, H., Upmeier, B.:** "Saving of energy by applying optimum conditions to steady-state and dynamic behaviour of refrigeration components and installations", *IIR, Commission B 2*, Dresde, September 1984, pp.239-261
- 4.4 **Conde, R.M.:** "A steady-state mathematical simulation model for air-to-water heat pumps", Report, EHT Zurich, July 1985
- 4.5 **Chaddock, J.B., Noerager, J.A.:** "Evaporation of refrigerant 12 in a horizontal tube with a constant wall heat flux", *ASHRAE Transactions*, Vol.82, Part 2, 1966
- 4.6 **McQuiston, F.C.:** "Finned tube heat exchangers: state of the art for the air side", *ASHRAE Transaction*, Vol.87, Part 1, 1981, pp.1077-1085
- 4.7 **Thom, J.R.S.:** "Prediction of pressure drop during forced circulation boiling of water", *International Journal of Heat and Mass Transfer*, Vol.7, 1964, pp.709-724
- 4.8 **Goldstein, S.D.:** "On the calculation of R22 pressure drop in HVAC evaporators", *ASHRAE Transaction*, Vol.81/1, 1975
- 4.9 **Chisholm, G.:** "Pressure gradients due to friction during the flow of evaporating two-phase mixtures in smooth tubes and channels", *International Journal of Heat and Mass Transfer*, Vol.16, 1973, pp.347-358
- 4.10 **Geary, D.F.:** "Return bend pressure drop in refrigeration systems", *ASHRAE Transaction*, Vol.81/1, 1975
- 4.11 **Kirkbride, C.G.:** "Heat transfer by condensing vapour on vertical tubes", *Industrial and Engineering Chemistry*, 26/4, 1934
- 4.12 **Domanski, P., Didion, D.:** "Computer modelling of the vapour compression cycle with constant flow area expansion device", *NBS Building Science Series 155*, Washington DC, May 1983
- 4.13 **Pierre, B.:** "Stromningsmotstand vid kikande koldmedier", *Kylteknisk Tidskrift*, No. 6, December 1957
- 4.14 **Pierre, B.:** "Flow resistance with boiling refrigerants", *ASHRAE Journal*, September, 1964
- 4.15 **Dembi, N.J., Dhar, P.L., Arora, C.P.:** "Statistical analysis of heat transfer data for convective boiling of refrigerants in a horizontal tube", *Letters in Heat and Mass Transfer*, Vol.5, 1978, pp.287-296
- 4.16 **Brauer, H.:** "Grundlagen der einphasen- und mehrphasenströmungen", *Verlag Sauerlander, Aarau und Frankfurt am Main*, 1971, pp.756-758
- 4.17 **Kutateladze, S.S., Borishanskii, V.M.:** "A concise encyclopaedia of heat transfer", Pergamon press, Oxford, 1966
- 4.18 **Dikken, R.A.:** "A dynamic simulation of a refrigerated room, using a steady-state model of the refrigerating machine", Report No. S-866, Delft University of Technology, the Netherlands, September 1988

Chapter
FIVE

Modelling of the Refrigerated Room

5.1 General

In the previous chapters, the modelling of the refrigerating machine has been accomplished. The task of this chapter is to model another part of the system: the refrigerated room. Following the same procedures as adopted in modelling the machine, this chapter also involves literature review, modelling strategies, derivation of governing equations, solution of equations.

A **refrigerated room** is an abstract concept which is defined as a confined space with air flowing inside, with objects producing heat and moisture, with cooling units refrigerating, with heat or mass transferred through walls or doorways. Generally speaking, a refrigerated room can be a cold storage warehouse, a refrigerated container, a refrigerated display cabinet, or even an air conditioned room. Fig. 5-1 is a two-dimensional schematic diagram of a refrigerated room.

Basically, the phenomenon taking place in a refrigerated room can be classified into three types: **momentum transport, heat transport, mass transport**. The three modes of transport are represented by three physical parameters: velocity, temperature, concentration. The aim of mathematical modelling is then the prediction of the behaviour of these three parameters in the room. If a model is static, the prediction is merely in a spatial domain. If a model is dynamic, the prediction is however in both spatial and time domains.

Mathematical modelling for the prediction of air motion and thermal behaviour in rooms is well established in air conditioning. However, in the field of cold storage, modelling of

refrigerated space is not widespread and is generally still in the development stage. This is not surprising from the point of view of a model maker. The mathematical description of an office or living room is that of an almost empty room with few obstacles to air motion; these rooms can be described by control volumes of a rather simple shape. However, a cold store, a refrigerated container or a truck is filled almost completely with produce, often on pallets or in boxes. The remaining air space has a complicated shape, leading to complicated and time consuming mathematical simulation models. In addition, in the case of refrigerated storage of living produce, such as apples or pears, the definition of two climates is required: the *macro-climate* (in the air space between the boxes) and the *micro-climate* (around the produce in the boxes). The products themselves in the micro-climate are also difficult to be modelled, because they are not bulks of continuous solid but small ball-like "particles". A micro analysis to every single "particle" seems to apply the second Newton law to a single molecule in fluid mechanics. All these problems have not yet been solved until now, which can be clearly seen from the following literature review.

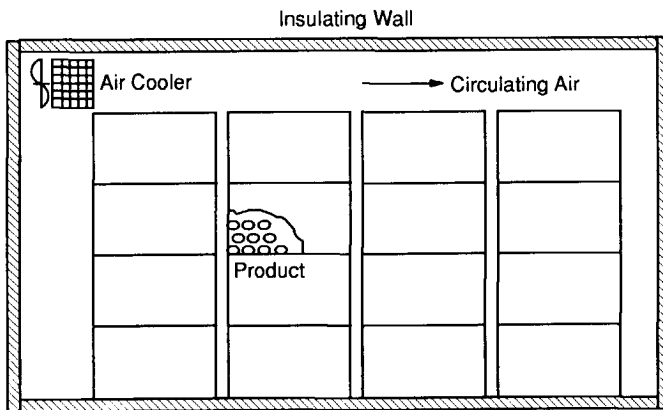


Fig. 5-1 Two-dimensional schematic diagram of a refrigerated room.

5.2 Literature

Only a few models relating to refrigeration storage have appeared to date, and most of these still have limitations because of the assumptions adopted in developing the models, and most are steady-state models. For example, **van der Ree** et al [5.1] developed a computer program based on the finite element method for the prediction of temperature distributions in loaded refrigerated rooms. Heat transmission in the load was considered to be non-steady-state and

spatially distributed. The model for the air flow was simplified and did not account for momentum. Water vapour transport was also neglected.

Marshall and James [5.2] modelled a quick freezing tunnel. The refrigerated space was divided into several sub-spaces or zones, each considered as a homogeneous model. The application of the elementary laws of conservation of mass and of energy gives a comfortable small number of equations for non-steady-state thermal behaviour. By connecting the zones in series, the model is basically one-dimensional.

Cleland [5.3] developed a lumped dynamic model for refrigerated stores. The model accounted for variable heat load conditions. Heat and moisture transport processes were all taken into account. The products stored in the cold store were described just with an ordinary differential equation with respect to time. The simulation could have applications in both refrigeration system and control system design. It now forms part of the commercial RADS package.

Van Gerwen and Oort [5.4] applied the advanced PHOENICS simulation package for the simultaneous, interactive solution of the three-dimensional momentum equations and the energy equation for a large number of nodal points in a refrigerated room. This gives a prediction of the velocity and temperature distributions. The required calculation times are high and so are the costs, and the work has so far been limited to steady-state conditions.

From the work having been done by the precedent investigators, we find a main problem is all still not solved, that is a combination between the simulations of air flow patterns in refrigerated spaces and the modelling of non-steady-state behaviour with accounting for the spatial distributions of parameters. No one of the authors mentioned above seems to have dealt with the two problems simultaneously. Therefore, further investigations in these aspects are still necessary and more advanced modelling techniques are needed.

5.3 Modelling strategies

5.3.1 Solutions to reduce the long computational time

As described before, our purpose is to develop a dynamic as well as distributed model for the refrigerated room. The model is hoped to be useful in optimizing the refrigerated room and simulating long-term non-steady-state operations. However, long computational times are not practical if many runs have to be made with changing input variables to optimize the system. The experience of **van Gerwen** and **Oort** tells us that even a steady-state simulation, by solving the governing equations interactively, requires extremely long computational time. If we follow their approach to carry out dynamic simulations, the computational times would not be allowed, at least under the present circumstance of computer science. Hence, in order to

develop a model practically workable, solutions have to be found to reduce the long computational time.

In this work, two elements are introduced to reduce the long computational time: de-coupling of the governing equations, and linearization of the energy equation.

Let us first look at the possibility of de-coupling the governing equations in a refrigerated room. The basic equations governing the transport phenomenon in the refrigerated room are the continuity, momentum (or Navier-Stokes), energy, diffusion equations. Strictly speaking, these equations are a set of coupled non-linear partial differential equations, which should be simultaneously and interactively solved. However, carefully studying the equations we can find that the effect of heat and mass transport on momentum transport is only the buoyancy force caused by temperature gradients. Thus, if the real situations can allow to neglect this effect, the momentum equations can be de-coupled from the energy and diffusion equations. Then the interactive solution of all the governing equations is not necessary.

In the case of a refrigerated room in which the air flow is mainly dominated by the forced convection caused by the fans assembled on the air coolers, such a possibility may exist. Different from air conditioned rooms where the air velocity is rather low in order to keep a certain comfort for human being, the refrigerated room is normally supplied with high air circulation by using rather powerful fans in order to keep an even distributed indoor climate and to prevent the stored products from deteriorating. The high air velocity due to forced convection often suppresses that due to free convection. Thus the buoyancy force term in the equations governing the momentum transport in the refrigerated room is able to be neglected. The air flow pattern in the refrigerated room is then independent of temperature. This assumption makes the problem much simpler, because the two transport phenomena can be treated separately. Hence the modelling of the refrigerated room can be carried out in two steps. The first step is to model the flow pattern without considering any heat and mass transfer. As long as the fans blowing the air work at a constant speed, the air flow pattern can be recognized as independent of time. The second step is to model the heat and mass transport based on the predicted flow pattern, which is now sequential and is not interactive with the first step. Such a strategy can strongly reduce the computational time in the case of dynamic simulation, because the non-linear momentum equations only need to be solved once during the simulation. On the other hand, the transport equations for heat and mass can be linearized using reasonable modelling assumptions, and can then be solved without iteration for every time step. This also saves computational time dramatically. Fig. 5-2 indicates the relation between the two modes of transport. The criterion for de-coupling the forced and free convections will be given in section 5.6.

In spite of this, it is still a difficult task to solve the non-linear three-dimensional momentum equations. Much research has been carried out in this area and some standard computer software packages have been released. After a thorough investigation of the

possibilities of simple methods [5.5], it was decided to make use of an available, comprehensive program to fulfill the first step of the modelling. However, comprehensive packages for the prediction of air flow patterns are not generally designed for cold storage rooms in which the model for air space is to be coupled with the models of living products such as fruit and of insulating walls. These tasks can nevertheless be performed in the second step.

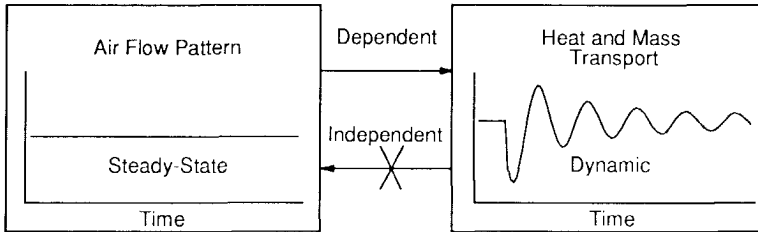


Fig. 5-2 Relationship between the flow pattern and the heat and mass transport in the refrigerated room.

5.3.2 Lumped model versus distributed model

The choice of a lumped or distributed model is very decisive in saving computation times and obtaining reliable and useful results. Generally speaking, lumped models (zero-dimension) are the simplest and also the roughest. For the purpose of finding global values of time constants of a refrigerated room, this type of models could be employed (see [5.6]). However, in the case of refrigerated storage, specially where large cold stores are concerned, lumped models are not accurate enough. In a cold store, where the air motion is caused by the fans and the room itself is usually filled with products, the assumption of perfect air mixing in certain parts or 'lumps' of the room is far from reality. This fact makes the distributed model necessary, which should be in three-dimensions.

5.3.3 Steady-state model versus dynamic model

Dynamic simulation is interesting in studying the influence of variable heat load conditions on the performance of the refrigerating machine and the behaviour of the products. A refrigerated room is always under variable conditions. Not only the weather changes but also loading and unloading processes can make the behaviour of the room dependent on time. This in turn makes the load conditions of the refrigerating machine variable. When the complete system is considered, the dynamic behaviour of the room is essential for studying the

influence of variable load conditions on the performance of the refrigerating machine and its capacity control. On the other hand, the long-term simulation of the dynamic behaviour of the room can show the energy consumption variation of the system. The result can be used by operators to decide when and how products must be loaded. However, because of the different thermal capacities possessed by the elements in the refrigerated room, the dynamic behaviour of the elements are considerably different. For example, the air in the macro-climate and micro-climate has much quicker behaviour than the walls and products. In order to ensure a reasonable integration time step, the air can be considered as a thermally instantaneous element. Such a treatment does not essentially decrease the quality of the model and however can help save computation time.

5.4 Modelling the air flow

5.4.1 Basic equations

As pointed out above, the modelling of the refrigerated room is divided into two steps. This section describes the first step to model the air flow in the room. As natural convection is neglected and the air flow is assumed to be steady-state and incompressible, the air flow in the room is governed by the continuity and momentum equations accompanied by the turbulence model, which take the following form (see [5.7]). Note that the parameters which are not distinguished by a subscript all refer to the case of air.

Continuity equation:

$$\text{div}(\mathbf{V}) = 0 \quad (5.1)$$

Momentum equation:

$$\text{div}[\rho \mathbf{V} \mathbf{V}_i - (\mu + \mu_t) \text{grad}(\mathbf{V}_i)] = - \frac{\partial P}{\partial x_i} \quad (5.2)$$

k-ε turbulence model:

k-ε-μ_t relation:

$$\mu_t = C_\mu \rho k^2 / \epsilon \quad (5.3)$$

Equation for turbulent kinetic energy:

$$\text{div}(\rho \mathbf{V} \mathbf{k} - \Gamma_{k,eff} \text{grad}(\mathbf{k})) = S_k \quad (5.4)$$

where

$$\Gamma_{k,eff} = (\mu + \mu_t) / \sigma_k \quad (5.5)$$

$$S_k = \sum_{i=1}^3 \sum_{j=1}^3 \left\{ \mu_t \left(\frac{\partial V_i}{\partial x_j} + \frac{\partial V_j}{\partial x_i} \right) \frac{\partial V_i}{\partial x_j} \right\} - \rho \epsilon \quad (5.6)$$

Equation for turbulent energy dissipation rate:

$$\text{div}(\rho \mathbf{V} \epsilon - \Gamma_{\epsilon,eff} \text{grad}(\epsilon)) = S_\epsilon \quad (5.7)$$

where

$$\Gamma_{\epsilon,eff} = (\mu + \mu_t) / \sigma_\epsilon \quad (5.8)$$

$$S_\epsilon = \sum_{i=1}^3 \sum_{j=1}^3 \left\{ C_\mu \mu_t \frac{\epsilon}{k} \left(\frac{\partial V_i}{\partial x_j} + \frac{\partial V_j}{\partial x_i} \right) \frac{\partial V_i}{\partial x_j} \right\} - C_2 \rho \frac{\epsilon^2}{k} \quad (5.9)$$

where $C_\mu = 0.09$; $\sigma_k = 1.0$; $\sigma_\epsilon = 1.3$; $C_1 = 1.44$ from equilibrium wall layers; $C_2 = 1.92$ from decay of grid turbulence (see [5.8]).

Equations (5.1) — (5.9) completely depict the air flow phenomenon without natural convection.

5.4.2 Boundary conditions

Given the necessary boundary conditions for the refrigerated room, the numerical solution of equations (5.1) — (5.9) will be the mathematical simulation of the flow pattern in the room. However, to obtain the numerical solution is not easy. Fortunately, as numerical computational fluid mechanics develops, some standard software packages developed for the solution of the Navier-Stokes equations have been produced. One of the most commonly used packages is PHOENICS developed by CHAM Ltd, UK. With this computer software, it is not necessary to tackle the numerical analysis of the equations themselves. The only task of users of the software is to define their own specified boundary conditions. Two types of boundary conditions involved in the refrigerated room are discussed in the next section.

Boundary conditions along the fans on the air cooler:

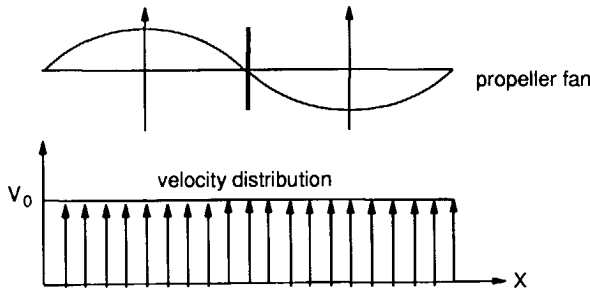


Fig. 5-3 Boundary condition along the fan on the air cooler.

The function of the fans on the air cooler is to maintain a certain volume flow of air through the air cooler. However, from a physical point of view, the action of the fans on the air is to add a certain amount of momentum to the air in the axial direction of the fans. The added momentum flux is defined as ρV^2 . The downstream-air velocity distribution of the propeller fan can be of any chosen distribution, but is assumed to be even in this case (see Fig. 5-3). Besides the added momentum flux, the stirring action of the fans also causes some enhancement of the turbulence energy k and the dissipation rate of turbulence energy ϵ . As no k and ϵ values for air cooler fans have been found in the literature, the following correlations for free jets given in [5.9] are used for the time being. However, experiments are needed to check these values, which will be described in chapter 7.

k and ϵ values for free jets (see [5.9]):

$$k_o = 0.02 V_o^2 \quad \epsilon_o = 0.0016 V_o^3 / H_{fan} \quad (5.10)$$

Therefore, the boundary conditions along a fan can be defined as a kind of fixed fluxes (see [5.10]).

$$\text{Flux of momentum:} \quad \Lambda = \rho V_o V_o \quad (5.11a)$$

$$\text{Flux of } k: \quad \dot{A} = \rho V_o k_o \quad (5.11b)$$

Flux of ϵ :

$$\Omega = \rho \sum_{\theta} V_{\theta} \epsilon_{\theta} \quad (5.11c)$$

Boundary conditions along the walls:

As very little air can flow through the boxes containing the products, the air flow model in the macro-climate assumes the boxes to be unpenetrated blocks. Thus the boundary conditions around the boxes and along the room walls can be generalised as the boundary condition along a plate (see Fig. 5-4).

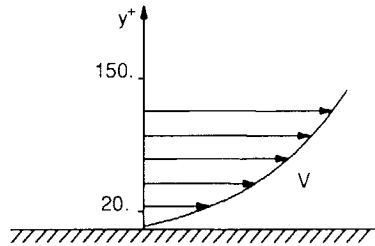


Fig. 5.4 Boundary condition along a plate. A logarithmic velocity profile is assumed with y^+ between 20 and 150.

$$V_y = 0 \quad (5.12)$$

Because the computer program does not solve the full partial differential equations in a fine-grid region close to a wall, the logarithmic velocity profile for V_x and V_z is deduced from the boundary layer theory (see [5.11]).

$$V^+ = \frac{1}{\kappa} \ln(y^+) + c \quad (5.13a)$$

where $\kappa = 0.435$; $c = 5.05$

$$y^+ = y \rho (\tau_s / \mu)^{0.5} \quad (5.13b)$$

$$V^+ = V / (\tau_s / \rho)^{0.5} \quad (5.13c)$$

$$\tau_s = \xi \rho V^2 \quad (5.13d)$$

The wall friction factor ξ is deduced from the logarithmic law

$$\xi = \left\{ \frac{0.435}{\ln(1.01 + 9.0 \operatorname{Re} \xi^{0.5})} \right\}^2 \quad (5.14)$$

The k and ε values at the near-wall cells are calculated as follows

$$k = \tau_s / \left[\rho C_\mu^{0.5} \right] \quad (5.15)$$

$$\varepsilon = C_\mu^{3/4} k^{3/2} / (\kappa y) \quad (5.16)$$

(5.13) is called wall function in PHOENICS. To ensure the validity of the approximation by the wall function, it is required that y^+ must be between 20 and 150. This means that the grids near to the walls should be fine enough.

5.4.3 Solution of the equations with the aid of PHOENICS

Although the governing equations for the air flow pattern have been derived above, the solution of them is not easy at all, because they are non-linear partial differential equations. In the past years, a lot of research in the field of fluid mechanics has been carried out with the purpose to develop standard computer software which can be applied in other fields without necessarily knowing details about the numerical procedures of the solution. Some packages have already been released in the 1980's. The most famous are PHOENICS, FLUENT, FLOW3D, FIDAP and so on. In the Netherlands, PHOENICS is the most commonly used for engineering purposes. Hereafter we will give a brief description of PHOENICS, which includes the numerical method, the program structure, the treatment of boundary conditions.

5.4.3.1 Numerical method of PHOENICS

The numerical method employed by PHOENICS is the finite control volume method. the numerical solution consists of two procedures: 1) integrating the partial differential equations over the finite control volume of a computational cell and (for transient problems) over a finite time; 2) solving a set of non-linear algebraic equations resulting from the first procedure.

The integration of (5.2), (5.4), (5.7) can result in a set of algebraic equations with the following form

$$\phi_P = \frac{a_E \phi_E + a_W \phi_W + a_N \phi_N + a_S \phi_S + a_L \phi_L + a_H \phi_H + S}{a_E + a_W + a_N + a_S + a_L + a_H} \quad (5.17)$$

where ϕ stands for the unknown variable in question, that can be V_x , V_y , V_z , k or ϵ ; the subscripts P , E , W , N , S , L , H denote the locations at which this variable is computed, in accordance with the east-west-north-south-low-high convention indicated in Fig. 5-5. It has to be pointed out that PHOENICS uses a "staggered grid" convention (the control volume with dashed lines in Fig. 5-5) for computing the values of velocity. Thus, for a single cell with four of its neighbours being shown in plane view, the west-to-east velocities are located on walls e and w of the cell; and south-to-north velocities are on walls s and n of the cell. However, the formulation of the discretization equation for the momentum equations is the same as Eq. (5.17).

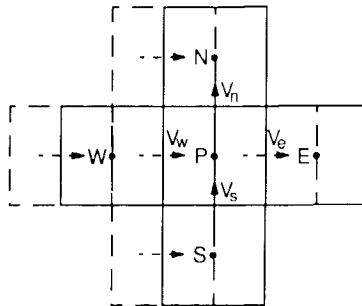


Fig. 5-5 A cell with its four neighbours in the so-called 'staggered' grid for air (the high and low neighbours are omitted).

The real difficulty in the solution of (5.17) lies in the unknown pressure field. The pressure gradient is included in the source term S of (5.17), when the momentum equation is concerned. However, the pressure field is indirectly specified via the continuity equation (5.1). In PHOENICS a so-called pressure correction method proposed by **Patankar** [5.12] is applied to formulate the continuity equation into a discretization equation for pressure.

According to **Patankar**, the correct pressure field P is equal to a guessed pressure field P^* plus a correction term P' called *pressure correction*

$$P = P^* + P' \quad (5.18)$$

Corresponding to the pressure field, the correct velocity are also expressed by an imperfect field V^* plus a velocity correction V' , that is,

$$V = V^* + V' \quad (5.19)$$

With some assumptions and mathematical manipulations (see [5.12]), the following correlations can be derived

$$V'_e = \frac{A}{a_E} (P'_P - P'_E) \quad V'_w = \frac{A}{a_W} (P'_P - P'_W) \quad (5.20)$$

$$V'_n = \frac{A}{a_N} (P'_P - P'_N) \quad V'_s = \frac{A}{a_S} (P'_P - P'_S) \quad (5.21)$$

$$V'_l = \frac{A}{a_L} (P'_P - P'_L) \quad V'_h = \frac{A}{a_H} (P'_P - P'_H) \quad (5.22)$$

These correlations are called velocity-correction formulas. If the velocity-formulas are substituted into the continuity equation (5.1), the following discretization equation for P' can be obtained

$$P'_P = \frac{b_E P'_E + b_W P'_W + b_N P'_N + b_S P'_S + b_L P'_L + b_H P'_H + B}{b_E + b_W + b_N + b_S + b_L + b_H} \quad (5.23)$$

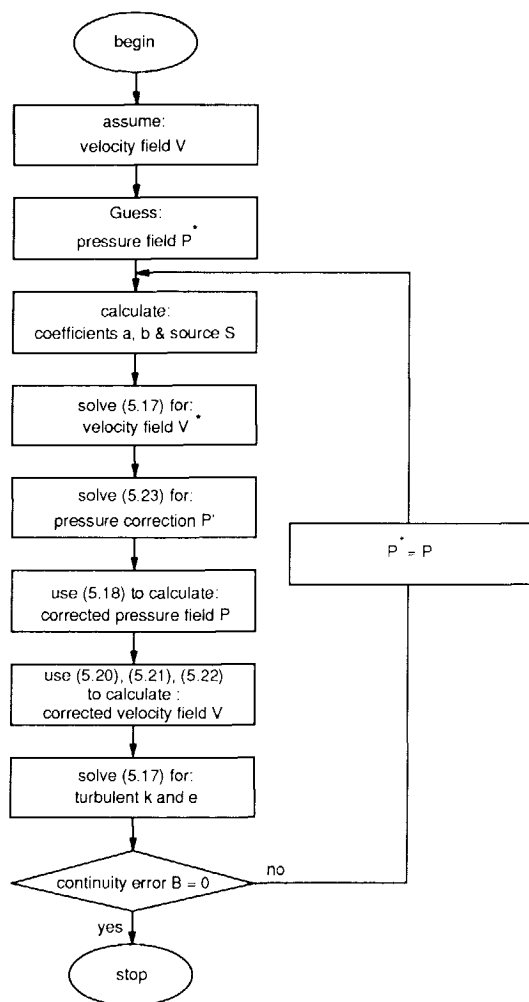


Fig. 5-6 Flow chart for the numerical solution of the Navier-Stokes equations in PHOENICS.

where the source term B is actually the continuity error produced by the imperfect velocity field V^* .

So far, the set of algebraic equations (5.17), (5.23) are closed. The solution of the set of algebraic equations is then the prediction of the flow pattern. Fig. 5-6 gives the iterative operations used in PHOENICS.

5.4.3.2 Program structure of PHOENICS

PHOENICS consists of two essential computer codes and two auxiliary ones (see [5.13]). The essential ones are a pre-processor called SATELLITE and a processor called EARTH. The auxiliary ones are a post-processor called PHOTON and a separate self-instruction program called GUIDE. The relationship among them is illustrated in Fig. 5-7.

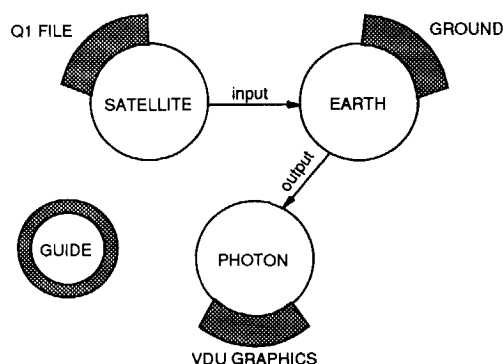


Fig. 5-7 Structure of the programmes of PHOENICS.

SATELLITE is an interpreter which turns instructions provided by a user into a data file containing instructions which EARTH can understand and obey. The normal way for a user to give SATELLITE instructions is to establish a Q1 file which is written in the PHOENICS Input Language (PIL). In the Q1 file one can define his own problem and boundary conditions. For example, in our case, the problem is a three-dimensional, steady-state, incompressible, turbulent, one-phase, forced-convective, air flow problem.

EARTH contains the main flow-simulation software. It reads the data file provided by SATELLITE and executes the corresponding computations and then produces output files which

can be read by the user and also by PHOTON, or by EARTH itself for further computations. Besides, EARTH possesses Fortran subroutines which are accessible to the user. These subroutines are stored in GROUND standing for "ground station". The main function of GROUND is to supply necessary boundary conditions, source, fluid properties and output control features which are not contained within EARTH. If the user's needs are not satisfied by what the standard GROUND subroutines already contain, he may attach the Fortran subroutines and insert programmes of his own, thereafter re-compiling and re-linking before execution.

PHOTON code is an interactive program which picks up the output file written by EARTH and then, in response to the instructions entered by the user through a VDU keyboard, represents the computed grid and flow pattern graphically on a computer screen or a printer.

GUIDE is the computer code which provides a source of helpful information about PHOENICS and its usage, for both beginners and advanced users.

5.4.3.3 Treatment of the boundary conditions in PHOENICS

Setting up a flow-simulation computation through PHOENICS involves two steps of work: specifying the concrete problem; defining the boundary conditions. These two tasks can all be fulfilled through the Q1 file mentioned above. Generally speaking, the specification of problems is comparatively easier than that of boundary conditions in PHOENICS. Therefore, it is necessary to devote one section to describing how to define the boundary conditions encountered in 5.4.2 in PHOENICS.

Along the fans on the air cooler:

PHOENICS always treats a boundary condition as a kind of source of the entity in question (mass, momentum, energy, turbulent energy, etc) by using the following equation

$$S_{boundary} = C_{\phi} (IV_{\phi} - \phi_P) \quad (5.24)$$

The boundary source $S_{boundary}$ is added as a source term to (5.17). C_{ϕ} and IV_{ϕ} are specified by the user in the Q1 file. Then (5.17) becomes

$$\phi_P = \frac{a_E \phi_E + a_W \phi_W + a_N \phi_N + a_S \phi_S + a_L \phi_L + a_H \phi_H + S + C_{\phi} IV_{\phi}}{a_E + a_W + a_N + a_S + a_L + a_H + C_{\phi}} \quad (5.25)$$

As mentioned in 5.4.2, the boundary conditions along the fans on the air cooler are of the fixed flux kind. If C_ϕ in (5.25) is given a very small value, it is negligible in comparison with the other terms in the denominator and $C_\phi IV_\phi$ in the numerator is the desired flux. Hence, substituting ϕ with V_x , k , ϵ , and $C_\phi IV_\phi$ with $\rho V_o V_o$, $\rho V_o k_o$, $\rho V_o k_o$ respectively, will result in a proper definition of the the boundary conditions along the fans on the air cooler.

Along the walls:

For an impenetrable wall, PHOENICS sets the velocity on the against-wall faces of the near-wall cells to be zero, and the k and ϵ values at the centre of the near-wall cells as calculated by (5.15) and (5.16). For the velocities parallel to the wall at the near-wall cells, the corresponding discretization momentum equation is modified by adding the following source of momentum

$$S_{boundary} = \mu \left. \frac{\partial V}{\partial y} \right|_{y=0} \quad (5.26)$$

where V is determined by (5.13).

So far, with the aid of PHOENICS, we have solved the governing equations for the macro-climate air flow patterns in the refrigerated room. However, the problem has not yet been solved completely, because the micro-climate air flow is still unknown, which is essentially important to the products themselves. The following paragraph is mainly about it.

5.4.4 Air flow through ball-like products

When the macro-climate flow pattern is calculated as above, the flow of air through the voids between the ball-like products is neglected, because its influence on the macro-climate flow pattern is very small. However, it becomes important when the heat and mass transport inside the product boxes is dealt with. As soon as the macro-climate flow pattern is determined, the pressure distribution in the room is also well known. As the air velocity in the boxes are very low, it can be calculated based on the pressure-velocity relation as follows,

$$\Delta P = \frac{1}{2} \xi \rho V^2 \quad (5.27)$$

where ξ is a coefficient depending on the surface roughness and shape of the products. The calculation of the coefficient will be described in chapter 6.

5.5 Modelling of heat and mass transport

5.5.1 Air

Following the strategy that the flow pattern is predicted independently of the temperature and concentration distributions, and the heat and mass transport is modelled on the basis of the predicted flow pattern, this section describes the second step of the modelling, which comprises the modelling of the temperature and humidity distributions.

5.5.1.1 Basic equations

The transport of a scalar quantity, such as heat or mass, in a turbulent flow of an incompressible fluid is governed by the following equation,

$$\frac{\partial \Pi}{\partial t} + \text{div} [\mathbf{V} \cdot \Pi - (a + a_t) \text{grad}(\Pi)] = S_{\Pi} / \rho \quad (5.28)$$

where a_t is the turbulent diffusivity and a is very small compared with a_t and thus can be neglected. For the time being, we assume the turbulent Prandtl number and Schmidt number are equal to 1, that is, $a_t = \delta_t = \nu_t$. In case of heat and mass transport, Π is replaced by h and w respectively.

Because temperature is usually used as an output quantity, h is usually replaced by θ . There exists a relation between h, θ and w

$$d(h) = \frac{\partial h}{\partial \theta} d(\theta) + \frac{\partial h}{\partial w} d(w) = C d(\theta) + \gamma d(w) \quad (5.29)$$

where $\frac{\partial h}{\partial \theta}$ and $\frac{\partial h}{\partial w}$ are supposed to be constant.

Because the air possesses a very small heat capacity compared to the walls and products, it can be regarded as a steady-state model. Substituting (5.29) into (5.28) and omitting the derivative term with respect to time, the heat and mass balance equations become equations for temperature and water vapour concentration (absolute humidity):

$$\text{div} [\mathbf{V} \cdot \theta - a_t \text{grad}(\theta)] = S_\theta / \rho \quad (5.30)$$

$$\text{div} [\mathbf{V} \cdot \mathbf{w} - \delta_t \text{grad}(\mathbf{w})] = S_w / \rho \quad (5.31)$$

The constants $\frac{\partial h}{\partial \theta}$ and $\frac{\partial h}{\partial w}$ (specific heat at constant pressure and latent heat of evaporation) are included in the source term S_θ .

After the flow pattern has been determined, the velocity distribution is known and not dependent on θ and w , so that the energy and mass balance equations become linear. This fact makes the problem much simpler, because the solution of linear equations does not need iteration.

5.5.1.2 Finite difference equations

The finite difference method is a typical approach to solve partial differential equations. The first step of this approach is to define the grid on which the differential equations can be discretized. Fig. 5-5 shows one nodal point (P) of the grid which also uses "staggered-grid" convention, that is, the velocities are located on the walls of the cells, while temperature and humidity are at the centres. Equations (5.30), (5.31) can be transformed into finite difference equations at this nodal point,

$$\begin{aligned} & \frac{\psi(V_e, \theta_E, \theta_P) - \psi(V_w, \theta_W, \theta_P)}{\Delta x} + a_t \frac{\theta_E + \theta_W - 2\theta_P}{\Delta x^2} + \\ & \frac{\psi(V_n, \theta_N, \theta_P) - \psi(V_s, \theta_S, \theta_P)}{\Delta y} + a_t \frac{\theta_N + \theta_S - 2\theta_P}{\Delta y^2} + \\ & \frac{\psi(V_h, \theta_H, \theta_P) - \psi(V_l, \theta_L, \theta_P)}{\Delta z} + a_t \frac{\theta_H + \theta_L - 2\theta_P}{\Delta z^2} + \\ & S_\theta / \rho = 0 \end{aligned} \quad (5.32)$$

$$\begin{aligned}
& \frac{\psi(V_e, w_E, w_P) - \psi(V_w, w_W, w_P)}{\Delta x} + a_t \frac{w_E + w_W - 2w_P}{\Delta x^2} + \\
& \frac{\psi(V_n, w_N, w_P) - \psi(V_s, w_S, w_P)}{\Delta y} + a_t \frac{w_N + w_S - 2w_P}{\Delta y^2} + \\
& \frac{\psi(V_h, w_H, w_P) - \psi(V_l, w_L, w_P)}{\Delta z} + a_t \frac{w_H + w_L - 2w_P}{\Delta z^2} + \\
& S_w / \rho = 0
\end{aligned} \tag{5.33}$$

where function ψ is defined as below

$$\psi(V, \phi_1, \phi_2) = \begin{cases} V \cdot \phi_1 & V > 0 \\ 0 & V = 0 \\ V \cdot \phi_2 & V < 0 \end{cases} \tag{5.34}$$

V is positive when it is towards point P and ϕ can be θ or w . The above finite difference scheme is also called upwind-difference scheme.

(5.32) and (5.33) form a set of linear algebraic equations which can be solved by using **Gauss-Seidel** method. To apply this method, (5.32) and (5.33) need to be changed into another form. Similar to the treatment in PHOENICS, the two discretization equations can always be represented in the form of (5.17). Thus

$$a_P \theta_P + a_E \theta_E + a_W \theta_W + a_N \theta_N + a_S \theta_S + a_L \theta_L + a_H \theta_H + S_\theta = 0 \tag{5.35}$$

$$b_P w_P + b_E w_E + b_W w_W + b_N w_N + b_S w_S + b_L w_L + b_H w_H + S_w = 0 \tag{5.36}$$

where the constants $a_E \dots a_H$ and $b_E \dots b_H$ are calculated from (5.32) and (5.33). To be convenient, we represent the left sides of (5.35) and (5.36) with Q_P and W_P respectively.

According to the **Gauss-Seidel** rule (see [5.14]), the following sequence formulas can be used to solved (5.35) and (5.36)

$$\theta_P^{(k+1)} = \theta_P^{(k)} - Q_P^{(k)} / a_P^{(k)} \tag{5.37}$$

$$w_P^{(k+1)} = w_P^{(k)} - W_P^{(k)} / w_P^{(k)} \quad (5.38)$$

where k denotes the iteration number.

5.5.1.3 Boundary conditions

The solution of the above equations requires necessary boundary conditions. In the refrigerated room, the air is in contact with the air cooler, products and walls. Thus there are three kinds of boundary conditions.

Air cooler

The air cooler acts as a heat and moisture remover in the refrigerated room. In principle, the boundary condition related to the air cooler can be defined as an additional heat and moisture source. However, the amount of heat and moisture transfer on the air cooler is impossible to calculate without using the evaporator model. In order to make a module-like model, we would not prefer the model of the refrigerated room interacting with the evaporator model at this moment. Therefore, for the time being, we define the boundary condition of the air cooler as follows

$$\theta_P = \theta_o \quad w_P = w_o \quad (5.39)$$

where θ_o and w_o are the output values from the evaporator models which have been described in chapters 2 and 4.

Walls

Heat transport between the air and the room walls is by convection. The boundary conditions along the room walls can be defined as: 1) an extra source term to (5.35); 2) impervious to water vapour. The extra source term is calculated with a heat transfer coefficient as follows

$$S_{\theta, bou, wall} = \alpha_{wall, i} A_{wall, i} (\theta_{wall, i} - \theta_P) \quad (5.40)$$

where the heat transfer coefficient $\alpha_{wall, i}$ is calculated in 6.5.2

Products

The boundary conditions around the products are similar to those along the walls. The only difference is that there is moisture transfer from the products to the air. Hence, besides an extra source term to (5.35), an extra source term should be added to (5.36).

$$S_{\theta,bou,prod} = \alpha_{prod} A_{prod} (\theta_{prod,P} - \theta_P) \tag{5.41}$$

$$S_{w,bou,prod} = \beta_{prod} A_{prod} (w_{prod,P} - w_P) \tag{5.42}$$

where the heat and mass transfer coefficients α_{prod} , β_{prod} are calculated in 6.5.1.

5.5.2 Walls

5.5.2.1 Basic equation

The refrigerated room commonly has six walls made from insulation materials. Just considering the heat transfer perpendicular to the wall, the one-dimensional heat conduction equation (Fourier equation) can be applied,

$$\frac{\partial \theta_{wall}}{\partial t} = a_{wall} \frac{\partial^2 \theta_{wall}}{\partial x^2} + S_{\theta} / \rho_{wall} \tag{5.43}$$

5.5.2.2 Finite Difference Equation

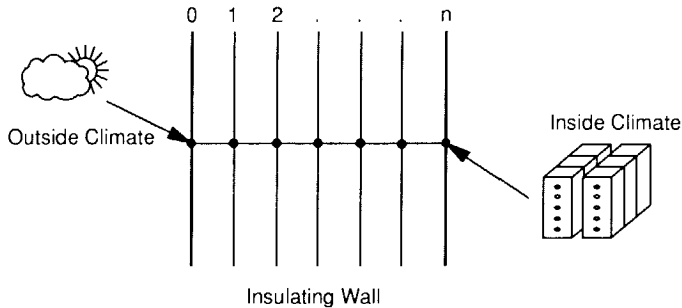


Fig. 5-8 Nodal points and boundary conditions of one-dimensional insulating walls.

When the finite difference method is applied to a wall (see Fig. 5-8), the finite difference equation of (5.43) becomes a matrix equation,

$$\underline{D}_1 \theta'_{wall} + \underline{D}_2 \theta_{wall} + \underline{D}_3 \theta_{bou} + \underline{D}_4 S_{\theta} = 0 \quad (5.44)$$

where

$$\theta_{wall} = [\theta_{wall,1}, \theta_{wall,2}, \dots, \theta_{wall,n}]$$

and the matrices $\underline{D}_1, \underline{D}_2, \underline{D}_3, \underline{D}_4$ are dependent on the material properties and the boundary conditions of the wall. Details on the calculation of these matrices can be found in [5.15]. Because (5.44) is obtained by using the implicit finite difference method, its solution is always stable.

5.5.2.3 Steady-state model

Because we do not arrange a separate chapter for the steady-state modelling of the refrigerated room, we treat the steady-state model as a particular case of the dynamic model.

In a steady-state case, assuming there is no internal heat source in the walls, (5.43) can be integrated analytically as follows

$$\theta_{wall} = a x + b \quad (5.45)$$

where the constants a and b are determined by the boundary conditions and the material properties.

5.5.2.4 Boundary conditions

The boundary conditions on the inner and outer sides of the walls are given by the following formulas

Inner side

$$S_{\theta,i} = \alpha_{wall,i} (\theta_{mac} - \theta_{wall} \Big|_{x=0}) \quad (5.46)$$

Outer side

$$S_{\theta,o} = \alpha_{wall,o} (\theta_{atm} - \theta_{wall} \Big|_{x=l}) + Q_{solar,abs} \quad (5.47)$$

The heat transfer coefficients are calculated in 6.5.2. These two source terms should be added to the corresponding elements in the matrices $\underline{D}_3, \underline{D}_4$.

5.5.3 Products

5.5.3.1 Basic equation

Generally the products stored in cold stores like apples or pears are in small pieces. The application of the heat and mass balance equations to each small piece is laborious and not generally applicable. Therefore, a bulk of products is modelled like a porous solid. Then the heat and mass balance equations for the product bulk can be derived,

$$\frac{\partial \theta_{prod}}{\partial t} = a_{prod} \nabla^2 \theta_{prod} + S_{\theta} / \rho_{prod} \quad (5.48)$$

$$\frac{\partial m_{prod}}{\partial t} = S_w \quad (5.49)$$

where, for the example of apples, the following source term S_{θ} based on the metabolism of the fruits can be used (see [5.16]):

$$S_{\theta} = [B_1 e^{-B_2 / \theta_{prod}} + (A/V)_{prod} \alpha_{prod} (\theta_{mic} - \theta_{prod})] / c_{p,prod} \quad (5.50)$$

where the constants B_1, B_2 and α_{prod} will be described in chapter 6. The porosity of product packing, defined as the ratio of the real volume occupied by the ball-like products to the volume of the box, is involved in the parameter $(A/V)_{prod}$.

5.5.3.2 Finite difference equation

The corresponding finite difference equations for (5.48) and (5.49) on nodal point P (see Fig. 5-9) are then,

$$\frac{\theta'_{prod,P} - \theta_{prod,P}}{\Delta t} = a_{prod} \left(\frac{\theta_{prod,E} + \theta_{prod,W} - 2\theta_{prod,P}}{\Delta x^2} + \right.$$

$$\frac{\theta_{prod,N} + \theta_{prod,S} - 2\theta_{prod,P}}{\Delta y^2} + \frac{\theta_{prod,L} + \theta_{prod,H} - 2\theta_{prod,P}}{\Delta z^2} + S_{\theta} / \rho_{prod} \quad (5.51)$$

$$\frac{m'_{prod,P} - m_{prod,P}}{\Delta t} = S_w \quad (5.52)$$

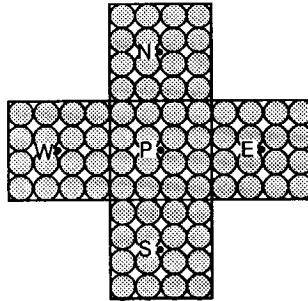


Fig. 5-9 A cell with four of its six neighbours in the grids for bulk products.

As the explicit finite difference method is adopted above, the following condition must be satisfied to ensure that the solution is stable (see [5.15])

$$0 < a_{prod} \frac{\Delta t}{[\max(\Delta x, \Delta y, \Delta z)]^2} < 1/2 \quad (5.53)$$

5.5.3.3 Steady-state model

For the products which loses moisture, a pure steady-state does not exist. However, as the moisture transport process is rather slow, a quasi steady-state can be assumed, that is, the mass of the products does not change, even though they release water vapour to the micro-climate. If the derivative with respect to time on the left side is scratched, (5.48) can be modified into a linear algebraic equation

$$\begin{aligned}
 & a_P \theta_{prod,P} + a_E \theta_{prod,E} + a_W \theta_{prod,W} + a_N \theta_{prod,N} + \\
 & a_S \theta_{prod,S} + a_L \theta_{prod,L} + a_H \theta_{prod,H} + S_\theta = 0
 \end{aligned} \tag{5.54}$$

The **Guass-Seidel** iteration method can also be used to solve (5.54).

5.5.3.4 Boundary conditions

The products are only in contact with the air in the micro-climate. Therefore the boundary condition is determined as heat and mass sources which should be added to (5.51) and (5.52).

$$S_{\theta,bou,air} = \alpha_{prod} A_{prod} (\theta_P - \theta_{prod,P}) \tag{5.55}$$

$$S_{w,bou,air} = \beta_{prod} A_{prod} (w_P - w_{prod,P}) \tag{5.56}$$

5.6 Criterion for de-coupling of the governing equations

Above it has been explained that, if the momentum equation is de-coupled from the mass and energy equations, our problem can be dramatically simplified. The de-coupling strategy has lead to two successful modelling approaches: 1) the prediction of air flow patterns does not participates dynamic simulations; it only needs to be worked out once — not for every time step; 2) the energy and mass balance equations are linearized, which makes the solution of the equations much easier. However, the de-coupling of the governing equations is conditional, that is, some criterion has to be satisfied. This section is intended to give a general criterion.

Precisely speaking, the transport processes in the refrigerated room occur in the form of combined free and forced convections. The forced convection is caused by the fans on the air cooler and the free convection results from unstable density gradients due to the temperature gradients in the room. From examination of the dimensionless form of the governing equations, the relative importance of free convection in relation to forced convection is able to be evaluated by checking the relative magnitude of the dimensionless parameter Gr/Re^2

$$\frac{Gr}{Re^2} = \frac{g \omega \Delta T L}{V^2} \tag{5.57}$$

The parameter can be used as a criterion parameter to judge whether or not the de-coupling is allowed. There exists the following principle (see [5.17])

$$\frac{Gr}{Re^2} \gg 1 \quad \text{free convection is dominant}$$

$$\frac{Gr}{Re^2} \approx 1 \quad \text{free and forced convections are of comparable magnitude}$$

$$\frac{Gr}{Re^2} \ll 1 \quad \text{forced convection is dominant}$$

If the criterion is not satisfied in practice, the model having been established above is not applicable. Then, further investigations towards combined free and forced convection flows are necessary.

5.7 Heat and mass transport through door-opening

Heat and mass exchanges between the inside and outside of the room through door-opening during loading and unloading of products are very considerable. Some attention should be paid to this aspect. In principle, heat and mass transport through doorways is of free convection. The air motion caused by free convection to a certain extent influences the main flow pattern inside the room. Accounting for such an effect requires a more sophisticated model for simulating combined free and forced convection flows. However, with some assumptions, the model developed above can still be used to simulate the room behaviour with door-opening. Herein, we will show how to combine the open-door model developed by Gosney [5.18] with the model of ourselves.

5.7.1 A simple open-door model

Considering a opened door shown in Fig. 5-10, the pressure difference between the inside and outside at a distance x above the ground is

$$P_i - P_o = P_{ib} - P_{ob} - g x (\rho_i - \rho_o) \quad (5.58)$$

Suppose the pressure difference is equal to zero at $x = x_0$, then (5.58) results in

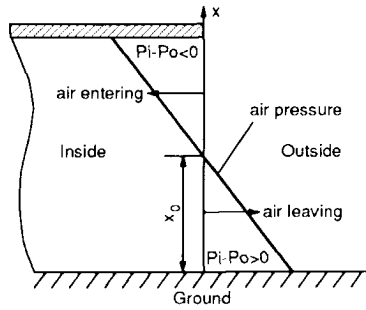


Fig. 5-10 Pressure difference distribution on an open door.

$$x_0 = \frac{P_{ib} - P_{io}}{\rho_i - \rho_o} \quad (5.59)$$

where P_{ib} and P_{ob} are the basis pressure inside and outside the room respectively. Below x_0 , the air flows from the inside to the outside; above x_0 , the air enters the room. The volume flow rate of air into the room is calculated by the equation derived by **Tamm** [5.19]

$$\dot{V}_i = - \frac{2 B}{3 (\rho_i - \rho_o)} [2 (P_{ib} - P_{ob})^3 / \rho_i]^{0.5} \quad (5.60)$$

where B is the width of the door.

The volume flow rate of air leaving the room is

$$\dot{V}_o = + \frac{2 B}{3 (\rho_i - \rho_o)} \{ 2 [P_{ob} - P_{ib} + H (\rho_i - \rho_o)]^3 / \rho_i \}^{0.5} \quad (5.61)$$

According to the mass conservation law, the amount of exiting air must be equal to that of entering air. Multiplying (5.60) and (5.61) with appropriate densities and equating them

$$\dot{V}_i \rho_i = \dot{V}_o \rho_o \quad (5.62)$$

$$P_{ib} = P_{ob} + \frac{H(\rho_i - \rho_o)}{1 + (\rho_o/\rho_i)^{1/3}} \quad (5.63)$$

Substituting (5.62) into (5.59)

$$x_o = \frac{H}{1 + (\rho_i/\rho_o)^{1/3}} \quad (5.64)$$

Thus the mass flow rate, in or out, is finally calculated by the following equation with an empirical coefficient C_d :

$$\dot{m}_{door} = \frac{2}{3} C_d \rho_i B H \left\{ \frac{2 H (1 - \rho_o/\rho_i)}{[1 + (\rho_i/\rho_o)^{1/3}]^3} \right\}^{1/2} \quad (5.65)$$

where C_d is a discharge coefficient, determined experimentally as 0.663 (see [5.18]).

5.7.2 Combination of the open-door model with the room model

Although the open-door model is based on the consideration of free convection and the model of the refrigerated room is in accordance with the assumption that forced convection is dominant, a combination of those two models is still possible. However, some assumptions are needed.

Assumptions:

- 1) The air motion due to the free convection through door-opening only influences the air flow patterns of the cells adjacent to the door. Fig. 5-11 shows the assumed flow patterns for the near-door cells.
- 2) The transport process through door-opening is regarded as steady-state. Thus the inflow and outflow of air volume should be equal.
- 3) The inflow air is evenly distributed over the cells above the neutral level $x = x_o$ and the outflow air is evenly distributed over the cells below the neutral level. This assumption is not 100% correct but the influence may be small.

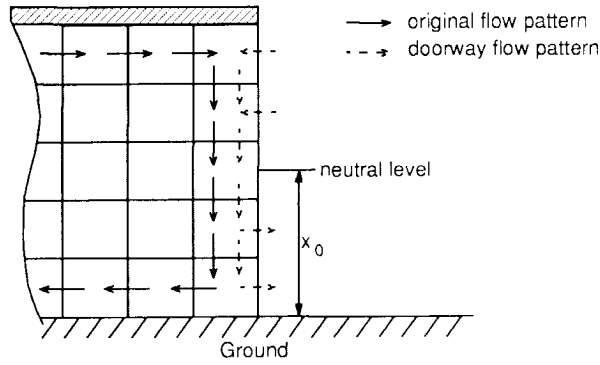


Fig. 5-11 Air flow patterns around the open door.

With all these assumptions, to combine the open-door model with the room model is then all but a matter of changing the boundary conditions for the near-door cells. Following the same way defining boundary conditions as in section 5.5, we just add an extra source term to the discretized energy and mass balance equations for the near-door cells. The extra source terms for the cells above the neutral level are calculated as follows

$$S_{\theta,door} = \dot{m}_{door} h_o \Delta x/H \quad (5.66)$$

$$S_{w,door} = \dot{m}_{door} w_o \Delta x/H \quad (5.67)$$

The extra source terms for the cells below the neutral level are calculated as follows

$$S_{\theta,door} = \dot{m}_{door} h_i \Delta x/H \quad (5.68)$$

$$S_{w,door} = \dot{m}_{door} w_i \Delta x/H \quad (5.69)$$

where h_i , h_o , w_i , w_o are the enthalpy and humidity of air inside and outside the door respectively.

5.8 Computer implementation

5.8.1 Establishment of computational grids

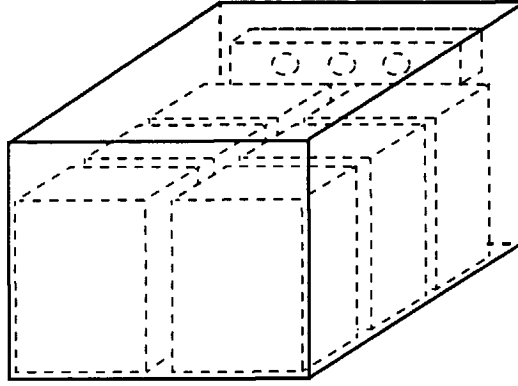


Fig. 5-12 Diagram of a cold store as an example for defining computational grids.

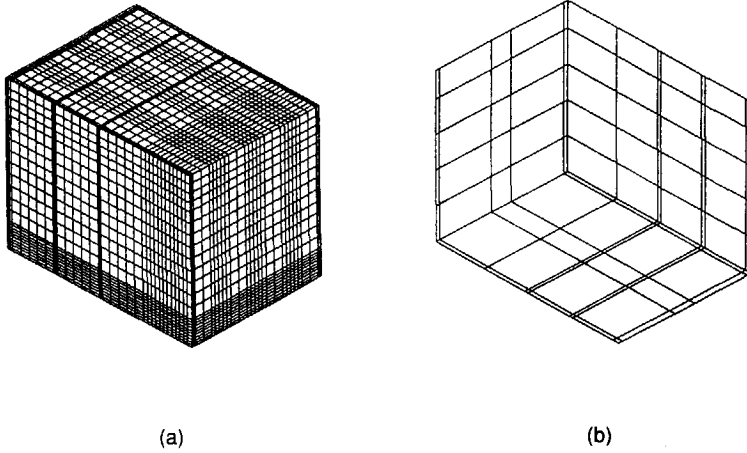


Fig. 5-13 Two computational grids for both predictions of velocity and temperature.
(a) a very fine grid for velocity; (b) a coarse grid for temperature.

Both PHOENICS for the prediction of air flow patterns and our own model for the prediction of temperature and humidity distributions are all implemented on a well-specified grid. To ensure that the solution by PHOENICS is reliable, a rather fine grid is necessary, specially in the channels between product boxes. Let us take a refrigerated room shown in Fig. 5-12 as an example. The corresponding grid is given in Fig. 5-13a. The specification of the grid should make sure that the near-wall cells must meet the requirement in 5.4.2, that is, $20 < y^+ < 150$. However, the grid for the simulation of temperature and humidity distributions may be more coarse than that for PHOENICS, as shown in Fig. 5-13b. The difference between the two computational grids results in a necessity to calculate the mass flow rates on the coarse grid from the velocities on the fine grid. Fig. 5-14 illustrates the relation between the two grids on a plane view. Hence, the mass flow rates on the six faces of cell (I,J,K) on the coarse grid are calculated as follows

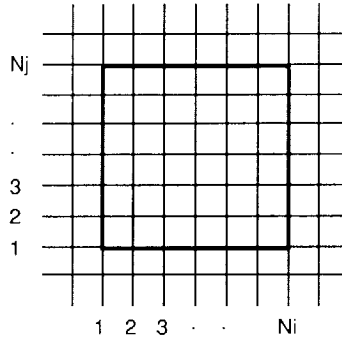


Fig. 5-14 Relationship between the two different grids.

$$\dot{m}_W = \rho \sum_{j=1}^{Nj} \sum_{k=1}^{Nk} \Delta y_j \Delta z_k V_{I,j,k,W} \quad (5.70)$$

$$\dot{m}_E = \rho \sum_{j=1}^{Nj} \sum_{k=1}^{Nk} -\Delta y_j \Delta z_k V_{Ni,j,k,E} \quad (5.71)$$

$$\dot{m}_S = \rho \sum_{k=1}^{Nk} \sum_{i=1}^{Ni} \Delta z_k \Delta x_i V_{i,I,k,S} \quad (5.72)$$

$$\dot{m}_N = \rho \sum_{k=1}^{Nk} \sum_{i=1}^{Ni} -\Delta z_k \Delta x_i V_{i,Nj,k,N} \quad (5.73)$$

$$\dot{m}_L = \rho \sum_{i=1}^{Ni} \sum_{j=1}^{Nj} \Delta x_i \Delta y_j V_{i,j,L} \quad (5.74)$$

$$\dot{m}_H = \rho \sum_{i=1}^{Ni} \sum_{j=1}^{Nj} -\Delta x_i \Delta y_j V_{i,j,Nk,H} \quad (5.75)$$

where it is defaulted that the mass flow towards the centre of cell is positive and vice versa. On the basis of the well defined grids, the flow pattern can be simulated by employing PHOENICS. The simulated results will be presented in chapter 8. The procedures of running the package are described in the PHOENICS Manual [5.11]. Hereafter the emphasis is put on the computer implementation of our own model.

5.8.2 Flow charts

Fig. 5-15 is the flow chart of a dynamic simulation. It is started with the prediction of flow pattern by PHOENICS. Then, the steady-state behaviour of the room is simulated by the own model. Using the steady-state simulation output as initial values, a dynamic simulation can be carried out. However, because the refrigerated room is filled with boxes of produce, one cell in Fig. 5-13b can be an air cell or a product cell. Thus, the interactions between the air and product models could be very complicated. In order to make more systematic computer codes, it is necessary to arrange a good indexing notation.

We propose to make use of an identifier ID for every cell element on the coarse grid. The identifier ID carries 7 items of information about the thermal characteristic of the concerned cell through 7 information channels. ID can be pre-set as input. With the aid of ID, the computer can judge whether the cell is an air cell or product cell and with which the cell is in contact. Fig. 5-16 gives the logic of judgment

5.9 Closure

In this chapter, we have developed a distributed model of the refrigerated room. In combination with the models of the components of the refrigerating machine, which have been made in chapters 2, 3, 4, the room model forms a basic tool for the simulation of the steady-state and dynamic behaviour of the whole refrigeration system. The models can be applied to analyze and optimize the system, which will be described in chapter 8. However, as we have

made lots of assumptions when those models were established, the models might to some extent be inconsistent with the reality. Moreover, a certain amount of empirical constants which were encountered in the modelling still need to be re-evaluated through experiments. Therefore, we will devote the next chapter to the experimental validation of the models.

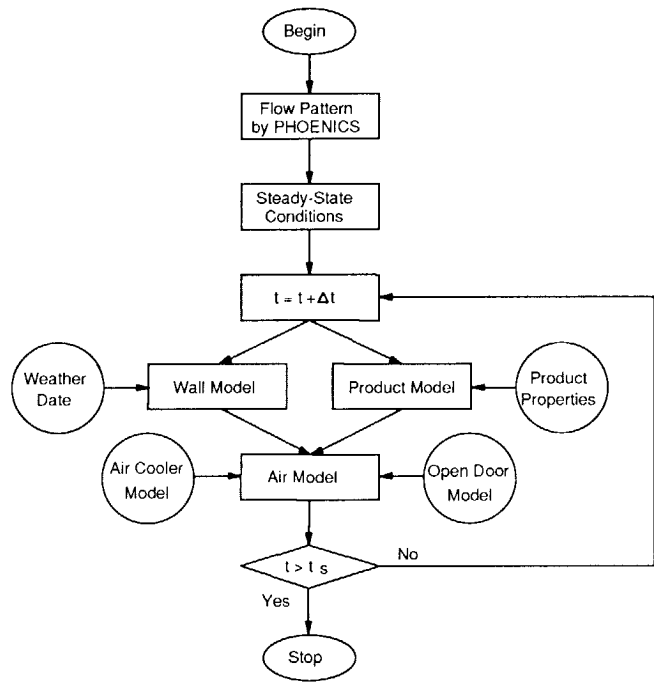


Fig. 5-15 Flow chart of a dynamic simulation of the refrigerated room.

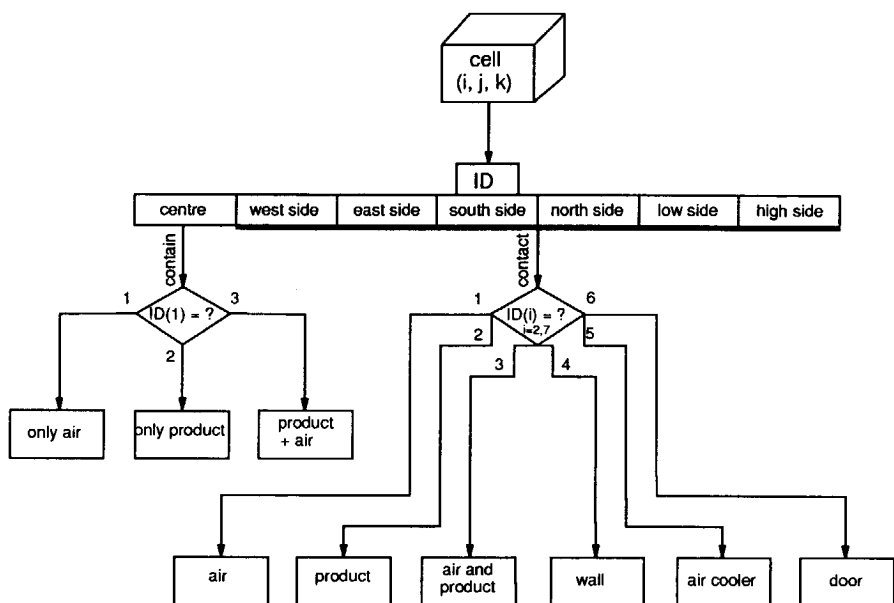


Fig. 5-16 Usage of the identifier ID for judging the heat and mass transfer forms of the cells in the grid.

References

- 5.1 **Van der Ree, H., Basting, W.J., Nievergeld, P.G.M.** "Prediction of temperature distributions in cargoes with the aid of a computer program using the method of finite elements", *I.I.F.-I.I.R.-Commission D2*, Wageningen, 1974-2, pp.195-220.
- 5.2 **Marshall, S.A., James, R.W.** "Dynamic analysis of an industrial refrigeration system to investigate capacity control", *Pro. Instn. Mech. Engrs.*, Vol189, 1975, pp.437-444
- 5.3 **Cleland, A.C.**, "Simulation of industrial refrigeration plants under variable load conditions", *International Journal of Refrigeration*, Vol 6, Jan. 1983, pp.11-19.
- 5.4 **Van Gerwen, R.J.M., Van Oort, H.** "The use of fluid dynamics simulation models in cold store design", *I.I.F.-I.I.R.-Commission B2*, Bristol (United Kingdom), July 1989, Preprints, pp.163-169.
- 5.5 **Wang, H., Toubert, S.** "Simple non-steady state modelling of a refrigerated room accounting for air flow and temperature distributions", *Proceeding IIR Meeting, Section B, Comm. C2 and Section D*, Wageningen (Netherlands), 1988.
- 5.6 **Dikken, R.A.** "Dynamic single point model of a refrigerated room", Report s-839, Delft University of Technology, The Netherlands, March 1988.
- 5.7 **Chen, Q.** "Indoor airflow, air quality and energy consumption of buildings", Ph. D. Thesis, Delft University of Technology, Netherlands, Nov. 1988.
- 5.8 **Markatos, N.C.** "The mathematical modelling of turbulent flows", *Encyclopaedia of Fluid Mechanics*, Vol. 6, 1985, Gulf Publishing Co.
- 5.9 **Sini, J.F., Dekeyser, I.** "Numerical prediction of turbulent plane jets and forced plumes by use of the k- ϵ model of turbulence", *Int. J. Heat Mass Transfer*, Vol.30, No.9, 1987, pp.1787-1801
- 5.10 **Shah, P.** a private communication about the definition of boundary conditions of an air cooler in a closed room. Cham Ltd, London, April, 1990
- 5.11 **Rosten, H.I., Spalding, D.B.** "The PHOENICS reference manual", CHAM TR / 200, Software version 1.4, Oct. 1987.
- 5.12 **Patankar, S.** "Numerical heat transfer and fluid flow", Hemisphere Publishing Corporation, McGraw-Hill Book Company, 1980.
- 5.13 **Rosten, H.I., Spalding, D.B.** "The PHOENICS beginner's guide", CHAM TR / 100, Software version 1.4, Oct. 1987.
- 5.14 **van Kan, J.** "Numerieke analyse", C II / B II, 2e deel, 3e herziene druk, Delft University of Technology, 1982 (in Dutch)
- 5.15 **van Paassen, A.H.C.** "Berekening warmte- en koellast en binnentemperatuur-overschrijdingen", Aanvulling College Klimaatregeling A i 90, Laboratory for Refrigeration and Outdoor climate Engineering, Delft University of Technology, 1985 (in Dutch).
- 5.16 **Rudolph, J.W.** "Listing of the product properties", private letter, January, 1987.
- 5.17 **Özisik, M.N.** "Heat transfer: a basic approach", McGraw-Hill Book Company, 1985.

- 5.18 **Gosney, W.B., Olama, H.A.L.** "Heat and enthalpy gains through cold room doorways", The Institute of Refrigeration at the Faculty of Environmental Science and Technology, The Polytechnic of the South Bank, London, December, 1975.
- 5.19 **Tamm, W.** "Kälteverluste durch kühlraumöffnungen", *Kältetechnik - Klimatisierung*, vol.18, Jahrgang, Heft 4, 1966, pp.142-144 (in German).

Chapter
SIX

Heat, Mass and Momentum Transfer Coefficients

6.1 General

By so far, both the steady-state and dynamic models of the system have been already described. For sake of simplicity and explicitness, the heat, mass and momentum transfer coefficients used in the models were just put aside in the previous several chapters, although the importance of them to the success of the models is obvious. This chapter is aimed at giving a detailed description about the coefficients encountered in the modelling of the refrigerating machine and refrigerated room. In principle, the acquisition of the correlations pertinent to heat, mass and momentum transfer coefficients is the assignment of those who are concerned with fundamental investigations. The job of model makers is to select the existing correlations which are suitable to their own specific purposes. Sometimes, modifications to the selected correlations are also required, if the application range is beyond the validation range of the correlations. Therefore, the main effort of this chapter is paid to comparing and choosing correlations from the literature.

Physical transport phenomena by convection are often associated with energy and mass exchange between a surface and an adjacent fluid. The rate equation for convection is expressed by the following formula

$$\Gamma = \kappa (\phi_1 - \phi_2) \quad (6.1)$$

where ϕ_1 is the value of transport quantity of the surface and ϕ_2 is that of the main stream of fluid. With respect to the three modes of transport, Γ , κ and ϕ have the following specific meanings

	heat transfer	mass transfer	momentum transfer
Γ	heat flux	mass flux	pressure drop
κ	heat transfer coefficient	mass transfer coefficient	momentum transfer coefficient
ϕ	temperature	concentration	velocity

This simple equation is the defining relation for the convective transfer coefficient κ . The determination of the coefficient is however not a simple undertaking at all. It is related to the mechanism of the fluid flow, the properties of the fluid, and the geometry of the specific system of interest. There are four methods of evaluating the convective transfer coefficient:

- a) dimensional analysis, which to be useful requires experiments
- b) exact analysis using the boundary layer theory
- c) approximate integral analysis of boundary layer
- d) analogy between the three modes of transport

Although the analysis approaches are very meaningful, they may not offer a practical solution to every engineering problem. There are many situations for which no mathematical models have as yet been successfully applied. Thus people cannot help but conduct experiments to obtain empirical correlations for various transfer coefficients, on the basis of dimensional analysis. By utilizing the method of dimensional analysis, one is able to correlate certain dimensionless parameters to construct basic equations. The purpose of experiments is then to determine the constants in the basic correlations. This can help save a lot of experimental costs. Due to the way of fundamental research, almost all the correlations to calculate transfer coefficients in the literature are in the forms indicated by dimensional analysis and involve dimensionless parameters. The correlations pertinent to the heat, mass and momentum transfer coefficients, as will be described below, are then in the forms of algebraic combinations of these dimensionless numbers. Here, it has to be pointed out that when momentum transfer is dealt with, pressure drop instead of momentum transfer coefficient is directly calculated in most of the literature.

6.2 In the evaporator

6.2.1 Between the refrigerant and pipe wall

Local heat transfer coefficient in the two-phase flow region

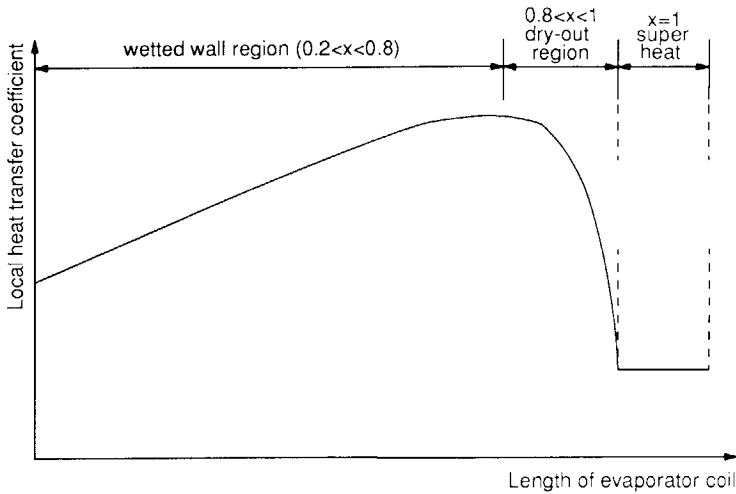


Fig. 6-1 Variation of the heat transfer coefficient in the two-phase flow region with the quality of refrigerant.

The heat transfer process taking place in the evaporator pipes is in the form of a horizontal two-phase flow. As mentioned in chapter 2, the flow patterns in refrigeration system evaporators are mostly annular flow. Heat is transferred by conduction and convection through the liquid film and meanwhile vapour is generated continuously at the interface. The bulk vapour in the core region is normally assumed to be at the saturated equilibrium state appropriate to the local pressure. As the refrigerant velocity is rather high and the liquid film is thin in the evaporator pipes, the heat transfer across the liquid film due to conduction and convection is so efficient that nucleate boiling is often suppressed. Thus, hereafter only convective boiling is concerned. On the other hand, in a dry-expansion evaporator, the refrigerant must be completely evaporated at the end of the coil. Thus along the evaporator coil, first a thin liquid film covers the inside tube surface, then the film becomes patchy, and finally it dries out completely. In such a process, the heat transfer coefficient undergoes a gradual change as shown in Fig. 6-1. In the wetted wall region the coefficient increases with the quality. When the quality is greater than a certain value (about 0.8) that is called dry-out quality, the coefficient drastically decreases to the value

of the single phase region. **Sthapak** et al [6.1] investigated the heat transfer in the dry-out region of a horizontal refrigerant tube and gave a complicated correlation. However, a simple way to account for the dry-out effect without causing large deviation is to make an interpolation for the heat transfer coefficient in the dry-out region as follows (see [6.2])

$$\alpha_e = \begin{cases} \alpha_{tp}(x) & \text{(wetted wall region: } 0.2 < x < x_d) \\ \alpha_{tp}(x_d) - [(x - x_d)/(1 - x_d)]^2 (\alpha_{tp}(x_d) - \alpha_s) & \text{(dry-out region: } x \geq x_d) \end{cases} \quad (6.2)$$

where the dry-out quality x_d is calculated as below (see [6.3])

$$x_d = 7.943 [\text{Re}_v (2.03\text{E}+4 \text{Re}_v^{-0.8} \Delta T - 1)]^{-0.161} \quad (6.3)$$

with $\text{Re}_v = \frac{G_d}{\mu_v}$ as the Reynolds number for the total mass flow rate considered as only vapour flow and $\Delta T = T_{pw} - T_e$.

Now it can be found that the main task of calculating the heat transfer coefficient in the two-phase flow region is to find a good correlation for $\alpha_{tp}(x)$. In the literature, many correlations about $\alpha_{tp}(x)$ can be found. However, they can be classified into five types.

a. Type 1

This is the most commonly used type which simply employs the Martinelli parameter X_{tt} to correlate the heat transfer coefficient for single-phase flow to that for two-phase flow

$$\alpha_{tp}(x) = a \left(\frac{1}{X_{tt}} \right)^b \alpha_l \quad (6.4)$$

α_l is the heat transfer coefficient for the liquid portion of the total mass flow if it were flowing in the pipe alone.

$$\alpha_l = 0.023 (\lambda_l / d) [G(1-x)d/\mu_l]^{0.8} (\text{Pr}_l)^{0.3} \quad (6.5)$$

The reason why to use the Martinelli parameter has been explained in [6.4]. The constants a and b in (6.4) have different values from different sources, depending on the specific conditions to be concerned.

b. Type 2

As nucleate boiling on the inside pipe wall is absolutely omitted in (6.4), it may give an incorrect prediction of the heat transfer coefficient when the refrigerant velocity is low and convective boiling is not dominating. Thus it is proposed to add an extra term to (6.4) by including a boiling number

$$\alpha_{tp}(x) = a [Bo + b (\frac{1}{X_{tt}})^c] \alpha_l \quad (6.6)$$

In this type of correlations, the boiling number is dominating when nucleate boiling plays a main role. When the heat flux is relatively small and nucleate boiling is suppressed on a thin film, convective heat transfer becomes dominant and the Martinelli parameter is then in action. Similarly, the constants a, b, c in (6.6) could be different in different cases.

c. Type 3

This type of correlation just uses a boiling number and a Reynolds number

$$\alpha_{tp}(x) = \frac{\lambda_l}{d} a (\text{Re}_l^2 Bo)^b \quad (6.7)$$

In contrast to (6.4) and (6.6), (6.7) is independent of quality and depending instead on quality change per unit length (see the definition of boiling number in the nomenclature).

d. Type 4

All the other correlations using self-defined dimensionless numbers belong to this group.

As an overview to the existing correlations found from the literature, Table 6-1 gives a list of authors as well as their experimental conditions. The selection of a appropriate correlation depends on two aspects of consideration: 1) the valid range of the selected

correlation should fit the application range; 2) the selected correlation should be simple so that, if any further validation to the correlation is made through own experiments, there will not be too many evaluated constants. **Van der Meer** [6.16] ever pointed out in his thesis that one should carry out his own measurements to obtain a useful correlation instead of just directly using a heat transfer correlation from literature. The reason is because all existing correlations are based on measurements on special test stands and conditions and to different degree show some deviations from reality. Moreover, the measured pipe wall and fluid temperatures which are used to obtain the heat transfer coefficients might be influenced by the methods of doing experiments. The more important point is that the definition of temperature difference used in modelling may be different from that when the correlations were obtained.

Table 6-1 Overview of the existing correlations from the literature.

Year	Author	Correlation type	Test system & fluid	Used by
1956	Dengler & Addoms [6.5]	1	ver. tube, d=25.4mm, water	-
1956	Guerrieri & Talty [6.6]	1	ver. tube, d=19.0mm, various organics	-
1957	Pierre [6.7]	3	hor. tube, d=18 & 22mm, R-22	Domanski [6.15]
1959	Bennett et al [6.8]	1	ver. annulus, d=0.623-0.866in, water	-
1962	Schrock & Grossman [6.9]	2	ver. tube, water	-
1962	Collier & Pulling [6.10]	2		-
1963	Chen [6.11]	4		-
1966	Chaddock & Noerager [6.12]	1	hor. tube, d=0.46in, R12	Fischer [6.2]
1976	Shah [6.13]	4	statistical work	-
1978	Dembi & Dhar [6.14]	4	statistical work	van der Meer [6.16]

From this point of view, we decided to select the first type as the basic correlation for our model. There are only two constants: a and b in (6.4), which can be more accurately determined through own experiments. The validation procedure will be presented in chapter 7. Fig. 6-2 shows the comparison of the first type of correlation (with a=3.4 and b changeable) to the **Dembi** correlation. It can be found that differences between them are existing for different b values. **Guerrieri** suggested a=3.4 and b=0.45 and the calculated heat transfer coefficient is about 30% lower than that predicted by the **Dembi** correlation. This deviation is consistent with the conclusion of **van der Meer** [6.16]. Although **Dembi** et al declared that their data (about 1600 points) covered almost all the flow patterns and heat transfer mechanisms to be expected in horizontal boiling flows, **van der Meer** found the predicted values by the **Dembi** correlation are almost greater by a factor of 2 than his laboratory experimental results on an air cooler. He attributed such a difference to several causes:

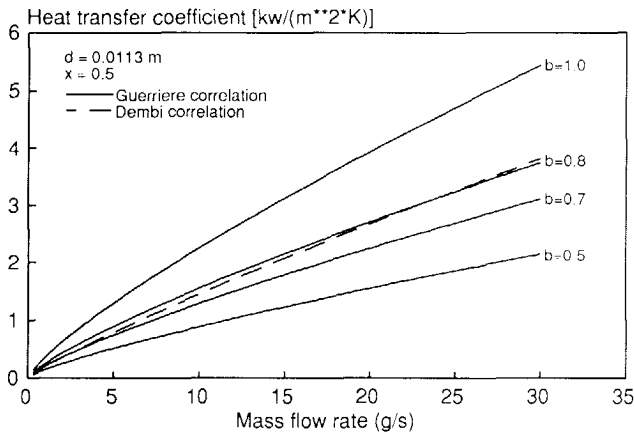
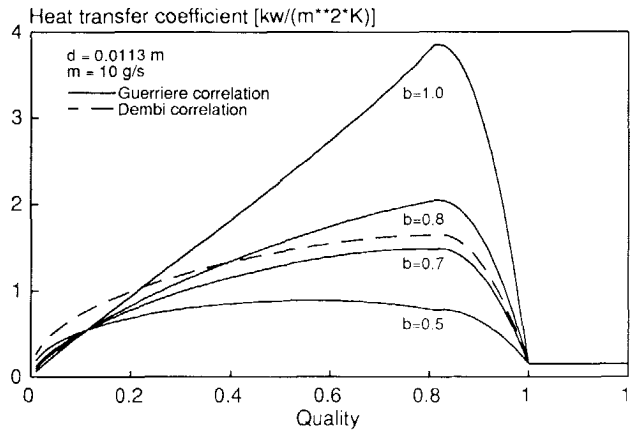


Fig. 6-2 Comparison between the **Guerriere** and **Dembi** correlations. Top: as a function of quality; bottom: as a function of mass flow rate.

- I having used an average temperature difference to calculate the effective mean heat transfer coefficient in his own calculation, which might be different from that ever used by **Dembi**.

II having used an incorrect correlation of pressure drop, that helps calculate the average evaporation temperature based on the measured refrigerant pressure at the outlet of the evaporator.

III the "rib effect" of the evaporator pipes on the refrigerant pressure drop.

In view of such uncertainties, it is really necessary to validate the selected correlation through own experiments in order to have a reliable correlation.

Average heat transfer coefficient in the two-phase flow region

Above the local heat transfer coefficient is described which is important to the distributed dynamic model of the evaporator. However, the steady-state evaporator model is lumped and therefore an average heat transfer coefficient is needed. In order to get an average value, integration of (6.2) over the whole two-phase flow region with respect to quality x is necessary. This method was adopted by both **van der Meer** [6.16] and **Fischer et al** [6.15]

$$\bar{\alpha}_e = \frac{1}{1-x_{in}} \left[\int_{x_{in}}^{x_d} \alpha_{tp}(x) dx + \int_{x_d}^1 \{ \alpha_{tp}(x_d) - [(x-x_d)/(1-x_d)]^2 (\alpha_{tp}(x_d) - \alpha_s) \} dx \right] \quad (6.8)$$

Substituting (6.4) into (6.8) and working out the integration

$$\bar{\alpha}_e = \frac{1}{1-x_{in}} \left[\frac{C}{C_1+1} (x_d^{(C_1+1)} - x_{in}^{(C_1+1)}) - \frac{C C_2}{C_1+2} (x_d^{(C_1+2)} - x_{in}^{(C_1+2)}) + C_3 (1 - x_d) \right] \quad (6.9a)$$

where

$$C = 0.023 a (\lambda_l / d) \left[\text{Gd} / \mu_l \right]^{0.8} (\text{Pr}_l)^{0.3} \left(\frac{\rho_l}{\rho_v} \right)^{0.5b} \left(\frac{\mu_v}{\mu_l} \right)^{0.1b} \quad (6.9b)$$

$$C_1 = 0.9 b \quad (6.9c)$$

$$C_2 = 0.8 - 0.9 b \quad (6.9d)$$

$$C_3 = \alpha_{tp} (x_d) - [\alpha_{tp} (x_d) - \alpha_s] / 3 \quad (6.9e)$$

The constants **a**, **b** in (6.9) will be also checked in chapter 7

Heat transfer coefficient in the single-phase flow region

In the single-phase flow region or superheat region, the **Dittus-Boelter** correlation is adopted to calculate the heat transfer coefficient (see [6.16]).

$$\alpha_s = 0.023(Re)^{0.8} (Pr)^{0.4} \lambda_g / d \quad (6.10)$$

$$\text{where } Re = \frac{4 \dot{m}_g}{\pi d \mu_g}; \quad Pr = \frac{v_c}{\lambda_g} \frac{c_p}{\lambda_g}$$

Compared to that of the two-phase flow region, this correlation is more reliable, because the influencing factors are less in the case of a single-phase flow. The reliability of (6.10) is taken for granted when the validation of the heat transfer coefficient in the two-phase flow region will be carried out in chapter 7. As the refrigerant in the single-phase flow region is considered incompressible, the mass flow rate is the same over the whole region in both steady-state and dynamic cases. Moreover, the effect of temperature variation on the physical properties is not so big. Therefore, there is no essential difference between the local and average values of α_s .

Total pressure drop in the two-phase flow region

In chapter 2 it was assumed that the refrigerant temperature keeps constant along the evaporator pipe length. However, in reality there always exists a temperature gradient due to pressure drop. This temperature gradient can be added on later just after the average evaporation temperature T_e is determined. The pressure drop results from momentum transport

between the refrigerant and pipe wall. In contrast to the heat transfer coefficient described above, the local variation of the pressure drop in the evaporator coil is not significant, because its absolute value is small. The author's experience is that the total pressure drop of an evaporator coil ($L=15\text{m}$ and $d=0.0113\text{m}$), with refrigerant mass flow rate of 80 g/s , is about 0.2 bar . On the other hand, the contribution of return bends to the total coil pressure drop can approach 50 percent (see [6.17]). A very accurate calculation of the local pressure

drop without correctly considering the bend influence is actually futile. In order to save computation times, only the total pressure drop in the two-phase flow region is calculated in the steady-state and dynamic models of the evaporator. For calculating the local refrigerant temperatures, assumption is made that the pressure drop is linearly distributed over the whole region.

The pressure drop in the two-phase flow region can be regarded as composed of three principle components: the friction and acceleration components in the straight pipes plus the total loss in the return bends. A great amount of research has been conducted, and many empirical or semi-theoretical correlations have been available. Among them, the **Lockhart-Martinelli** correlation [6.18] is the most popular. However, it is subjected to local pressure drops in straight tubes. **Van der Meer** [6.16] used the **Brauer** correlation [6.19] in his thesis, which also predicts local pressure drops. Due to the complexity of those correlations, overall integration of them, as has been made for the heat transfer coefficient above, seems mathematically impossible. In the literature, the only one that accounts for the total pressure drop in evaporator coils is the **Pierre** correlation [6.20], [6.21].

Pierre combined the three components together and obtained the following equation:

$$\Delta P_{tp} = \left\{ \underbrace{\xi_{str}}_{\text{friction}} + \underbrace{\left[\left(\frac{x_2 - x_1}{x_m} \right) + \frac{N_b}{2} \xi_b \right]}_{\text{acceleration}} \underbrace{\frac{d}{L_e}}_{\text{return bends}} \right\} (\dot{m}/A)^2 L_e / (\rho_m d) \quad (6.11a)$$

where the friction factor in the straight pipe is:

$$\xi_{str} = c (Bo / Re_l)^{0.25} \quad (6.11b)$$

$$Re_l = \frac{\dot{m} d}{A \mu_l} \quad (6.11c)$$

where the viscosity μ_l is that of a pure refrigerant without accounting for the oil effects which are however included in the constant c . **Pierre** suggested $c = 0.0185$ in the case of oil-free and $Re_l / Bo > 1.0$; $c = 0.053$ in the case of oil-present and $Re_l / Bo > 2.0$, on the basis of his experiments. However, under different operation conditions, c could be different and

needs to be determined through own experiments, because of the differences of oil concentration, pipe dimension and roughness.

x_l , x_2 and x_m are the entering, leaving and average vapour quality respectively. N_b is the number of return bends.

$$\rho_m = \frac{1}{x_m / \rho_v + (1-x_m) / \rho_l} \quad (6.11d)$$

$$\xi_b = \xi_{b,f} + \xi_{b,o} \quad (6.11c)$$

the factor $\xi_{b,o}$ accounting for the oil effects takes values as below

$$\xi_{b,o} = \begin{cases} 0.8 \text{ to } 1.0 & (\text{oil-free}) \\ 1.1 \text{ to } 1.3 & (\text{oil-present}) \end{cases} \quad (6.11f)$$

the factor $\xi_{b,f}$ accounting for friction is calculated

$$\xi_{b,f} = 2 \xi_{str} L_b / d \quad (6.11e)$$

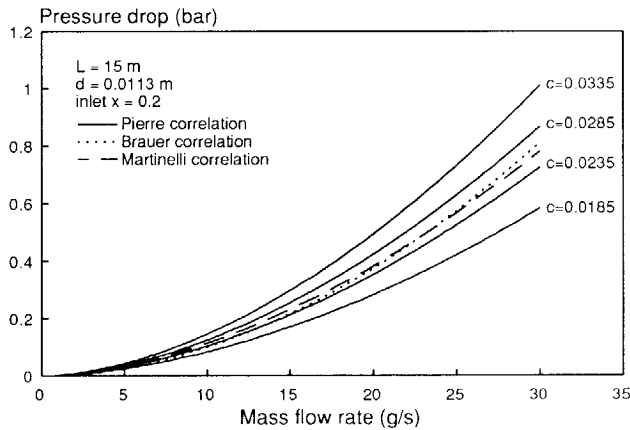


Fig. 6-3 Comparison of the **Pierre** correlation to those of **Brauer** and **Martinelli**.

Fig. 6-3 shows the comparison of the **Pierre** correlation to those of **Brauer** and **Martinelli**. As the **Brauer** correlation calculates local pressure drops, the pipe used in the comparing calculation is divided into nine elements and the total pressure drop is the summation of those of the nine elements. It is apparent from the figure that the **Pierre** correlation can fit the **Brauer** and **Martinelli** correlations by modifying the constant c in (6.11b).

Total pressure drop in the single phase flow region

The pressure drop in the single-phase flow region is calculated with a correlation in [6.22]

$$\Delta P_{sp} = 0.5 \rho_g \xi_{sp} L_{sp} u_{sp}^2 / d \quad (6.12a)$$

The friction factor ξ_{sp} is

$$\xi_{sp} = \begin{cases} 64/Re & (Re < 2320) \\ 0.316 Re^{-0.25} & (2320 \leq Re \leq 8E4) \\ 0.0054 + 0.3964 Re^{-0.3} & (Re > 8E4) \end{cases} \quad (6.12b)$$

6.2.2 Between the pipe walls

When the evaporator pipe wall was modelled in chapter 2, there was a heat conduction term, Q_{pw} , that may play an important role specially for those pipe elements with considerable temperature differences. Since the pipes are connected by the fins, heat conduction takes place between one pipe element and its neighbours. Besides, there exist axial heat flows along the pipes.

Axial heat conduction (see Fig. 6-4):

$$Q_{pw,i} = \pi(D^2 - d^2)/4 (\lambda_{pipe} / \Delta z_i) [T_{pw}(i+1,j,k) - T_{pw}(i,j,k)] \quad (6.13)$$

Heat conduction via the fins is calculated by using the solution of [6.22]:

$$Q_{pw,j} = (\lambda N \delta)_{fin} S_j [T_{pw}(i,j+1,k) - T_{pw}(i,j,k)] \quad (6.14)$$

where

$$S_j = \frac{2 \pi}{\arccos [\Delta z_j / (2D_j^2) - 1]} \quad (6.15)$$

and N_{fin} is the number of fins per pipe length of Δz_i .

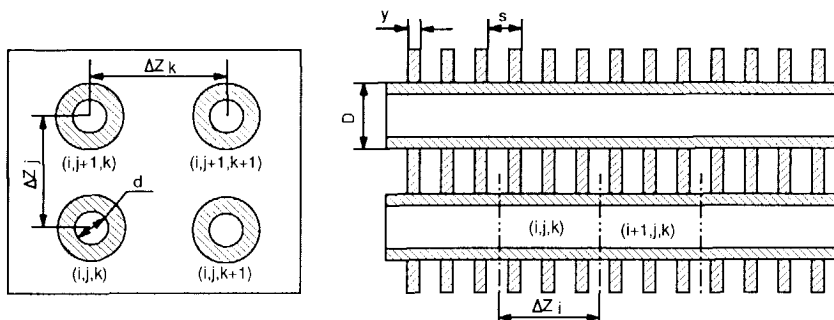


Fig. 6-4 Structure of the square pitched pipes and the plate-fins.

6.2.3 Between the pipe wall and air

Investigations on the heat and mass transfer coefficients for plate-fin-tube heat exchangers have brought out quite a lot of correlations in the past years. However, few of them have ever taken into account the effect of number of rows of tubes and the effect of the interaction between heat and mass transfer, as **McQuiston** [6.23, 6.24] did. On the top, he had done a lot of investigations in this area for more than ten years. Hereafter, the correlations of **McQuiston** are adopted. Unlike the two-phase flow heat transfer coefficient inside the evaporator pipe, the air side heat transfer coefficients, as introduced below, will not be validated by our own experiments. There are two reasons for this: 1) simultaneous validations of the inside and outside heat transfer coefficients are very difficult to realize, because the local pipe wall temperature is not easy to measure on a real air cooler; thus we have to assume a correct coefficient on one side and check the coefficient on another side; 2) the uncertainties inside the pipe are more than those outside, such as oil effect, flow pattern, return bend influence, slip effect and so on; as compared to the inside heat transfer coefficient, the outside ones are more reliable, because the operation conditions, under which the correlations were obtained, usually are similar to the conditions, to which the correlations are applied.

Total heat flux (sensible heat + latent heat):

$$q_{a,t} = \frac{(S_{pipe} + \eta_{fin} S_{fin})}{\pi D \Delta z_i} \alpha_{a,t} (h_{pw} - h_a) \quad (6.16)$$

where the total heat transfer coefficient is:

$$\alpha_{a,t} = G_a j_t / Sc_a^{2/3} \quad (6.17a)$$

and h_{pw} is the air enthalpy calculated according to the pipe surface temperature and 100 % relative humidity when the surface temperature is lower than the dew point. the air mass flux G_a must be calculated by using the front free flow area of an air cooler.

The j_t factor is calculated as

$$j_t = f(JP \cdot J_t(s)) \quad (6.17b)$$

Function $f()$ is expressed as

$$f(JP \cdot J_t(s)) = \left[\frac{1 - 1280 N_{row} Re_t^{-1.2}}{1 - 5120 Re_t^{-1.2}} \right] [0.0014 + 0.2618 JP \cdot J_t(s)] \quad (6.17c)$$

$$JP = Re_2^{-0.4} (S/S_t)^{-0.15} \quad (6.17d)$$

where S/S_t is the ratio of the total surface area to the tube surface area without fins.

$$J_t(s) = [0.95 + 4.0E-5 Re_3^{1.25}] \left[\frac{s}{s-y} \right]^2 \quad (6.17e)$$

Re_t is the Reynolds number based on longitudinal tube spacing

$$Re_t = G_a \Delta z_k / \mu_a \quad (6.17f)$$

Re_2 is the Reynolds number based on tube diameter

$$Re_2 = \frac{G}{a} \frac{D}{\mu_a} \quad (6.17g)$$

Re_3 is the Reynolds number based on fin spacing

$$Re_3 = \frac{G}{a} \frac{s}{\mu_a} \quad (6.17h)$$

Sensible heat transfer:

$$q_{a,s} = \frac{(S_{pipe} + \eta_{fin} S_{fin})}{\pi D \Delta z_i} \alpha_{a,s} (\theta_{pw} - \theta_a) \quad (6.18)$$

where the sensible heat transfer coefficient is

$$\alpha_{a,s} = \frac{G}{a} \frac{c_{p,a}}{Pr_a} j_s \quad (6.19a)$$

The j_s factor is calculated as

$$j_s = f(JP \cdot J_s(s)) \quad (6.19b)$$

$$J_s(s) = 0.84 + 4.0E-5 Re_s^{1.25} \quad (6.19c)$$

The **McQuiston** correlations are compared to those of **Briggs and Young**, and **Kutateladze** in Fig. 6-5. A good agreement among them can be found in cases without dehumidification. However, a considerable deviation appears when there is dehumidification. Such a deviation increases with air mass flux (the normal value in practice is around 4 kg/(m² s)). It demonstrates that the condensation of water vapour on the outside surface of the evaporator influences the heat transfer coefficients.

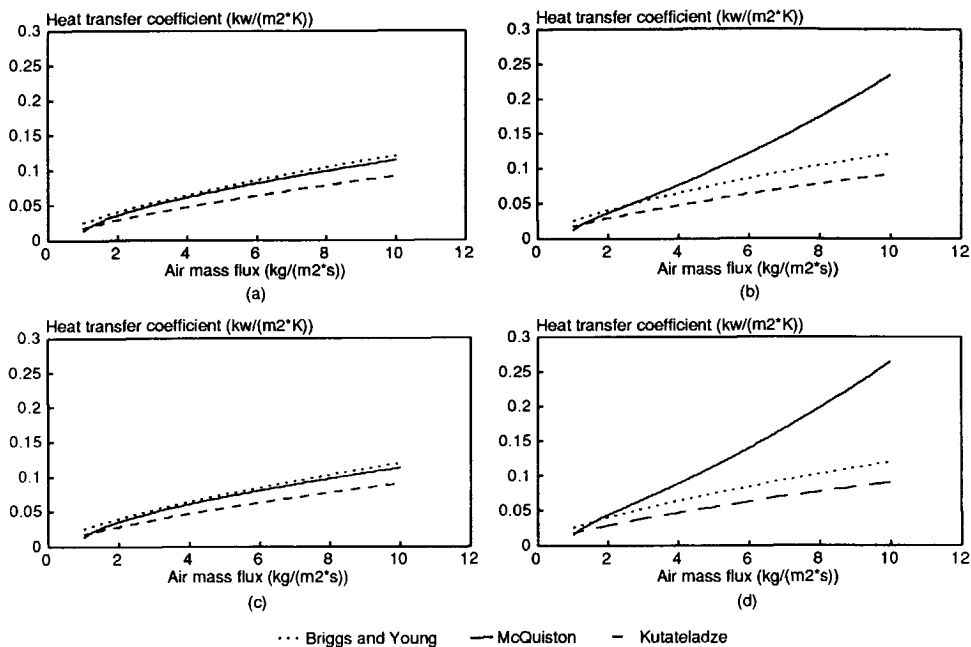


Fig. 6-5 Comparison of the **McQuiston** correlations to the other two.
 a) sensible heat transfer coefficient without dehumidification;
 b) sensible heat transfer coefficient with dehumidification;
 c) total heat transfer coefficient without dehumidification;
 d) total heat transfer coefficient with dehumidification;

Mass transfer:

After the total heat transfer and sensible heat transfer are calculated, the water condensation rate can be easily worked out as follow

$$\dot{m}_w = (q_{a,t} - q_{a,s})/\gamma \quad (6.20)$$

Fin efficiency:

The fin efficiency η_{fin} is expressed as follows (see [6.16] and Fig. 6-4)

$$\eta_{fin} = \frac{\text{tgh}\{0.5(\Delta z_j - D) [2\psi\alpha_a / (\lambda_{fin} y)]^{0.5}\}}{0.5(\Delta z_j - D) [2\psi\alpha_a / (\lambda_{fin} y)]^{0.5}} \quad (6.21)$$

where ψ is 0.85 for fins with cylindrical base.

6.2.4 Heat transfer coefficient in off-periods

During an off-period, the refrigerant stands still inside the evaporator pipes and the heat transfer process is the type of pool boiling. It has been well established that there are three basic modes of pool boiling: natural convection; nucleate boiling; and film boiling (see Fig. 6-6). Each of the modes occurs over a range of superheats measured at the surface of pipe. In the case of an air cooler evaporator during off-periods, the heat transfer process is dominated by natural convective and nucleate boiling, as the temperature difference between the pipe wall and refrigerant can never be high enough to come into the film boiling region.

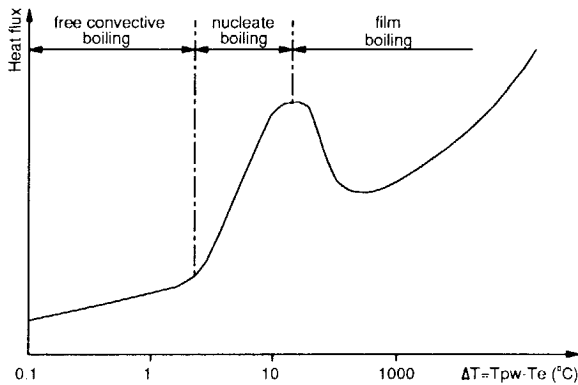


Fig. 6-6 Three modes of pool boiling.

Natural convective boiling

Natural convective boiling takes place inside the evaporator pipes, after the system is switched off for some time when the temperature difference between the pipe wall and refrigerant is less than 2 °C. Since correlations for the heat transfer coefficients for horizontal pipes are not available in the literature, the correlation for a horizontal plate is made use of (see [6.22]).

$$\alpha_{nat} = \begin{cases} 0.6 \lambda_l Ra_l^{1/4} / L_d & (Ra < 10^7) \\ 0.15 \lambda_l Ra_l^{1/3} / L_d & (Ra \geq 10^7) \end{cases} \quad (6.22)$$

$$L_d = \pi D$$

Nucleate boiling

Nucleate boiling occurs as soon as the compressor is switched off. At that moment, the temperature difference between the pipe wall and refrigerant is relatively high. The correlation given in [6.25] is used to calculate the heat transfer coefficient.

$$\alpha_{nuc} = \frac{c_l^3 (T_{pw} - T_e)^2 g^{0.5} (\rho_l - \rho_v)^{0.5} \mu_l}{\gamma^2 Pr_l^{5.1} C_{wl}^3 \sigma^{0.5}} \quad (6.23)$$

6.2.5 Effects of oil presence on the inside transfer coefficients

The above correlations for the transfer coefficients on the refrigerant side are all for cases of oil-free refrigerants, except the **Pierre** correlation. However, refrigerants commonly used in direct expansion evaporators are highly miscible in lubrication oils. The presence of oil in the refrigerant results in deviations of the real heat transfer coefficient or pressure drop from those for oil-free refrigerants. A lot of investigations have been involved in studying the effects of oil. A detailed review of those investigations was given by **Green** [6.26]. Applicable correlations to calculate the oil effects can hardly be found but only rough graphs or qualitative analysis. Below several conclusions drawn from the literature study are listed:

Effects on the heat transfer coefficients

- 1) The presence of oil tends to promote an annular flow pattern and then increases the boiling liquid contact area within the evaporation pipes. The result of a greater contact area is the increase in the heat transfer coefficient based on the inner tube area, which people normally use.
- 2) Because of the increase of the refrigerant viscosity caused by the presence of oil, the local heat transfer coefficient of the liquid area is reduced.

- 3) At high vapour velocities, oil tends to delay wall dry-out, resulting in an increase in the heat transfer coefficient. Oil can also increase the heat transfer coefficient in the superheat region. The magnitude of this effect can be up to 50%.

Schlager et al [6.27] gave a graphic illustration (Fig. 6-7) of the boiling heat transfer enhancement factor due to the presence of oil. Such a variation shown in Fig. 6-8 is the result of a combination of all the oil effects on the heat transfer coefficient. On the basis of the information given in Fig. 6-7, we are able to estimate the oil effect on the two-phase flow heat transfer coefficient on the refrigerant side.

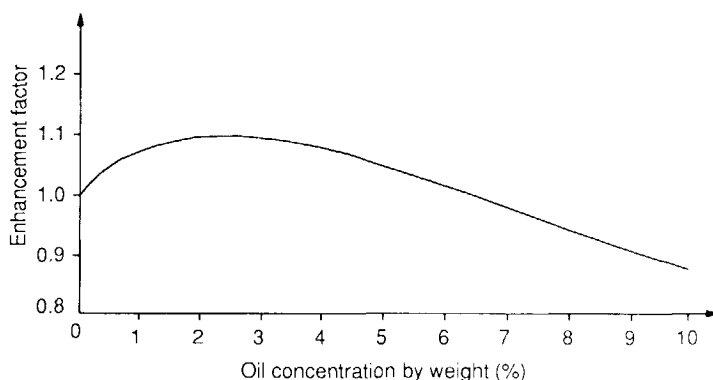


Fig. 6-7 Variation of the heat transfer coefficient enhancement factor with the oil concentration. Enhancement factor is defined as the ratio of the heat transfer coefficient with oil-presence to that with oil-free.

Effects on the pressure drop

The oil effect on the pressure drop is obvious. As the viscosity of refrigerant becomes greater, the pressure drop within the evaporator pipes is markedly increased by the presence of oil. Such an effect is taken into account in the **Pierre** correlation.

6.3 In the condenser

6.3.1 Condensation zone

Heat transfer coefficient between the refrigerant and tubes

The energy balance for the tube-and-shell condenser has clearly been presented in chapter 3. The most important part of the heat transfer taking place in the condenser is that transferred to the tube bundle in the condensation zone. This amount of heat includes two components: sensible heat of de-superheating and subcooling; latent heat of condensation. To calculate the heat transfer coefficient between the refrigerant and tubes, the Nusselt equation is in common use. However, the outside surface of the tubes is extended by using low-fins in order to intensify the heat transfer efficiency. The original Nusselt equation for condensation on a vertical plate has to be modified in view of low-finned tube geometries, tube bundles in square or triangular pitch, and total refrigerant enthalpy drop. **Beatty** and **Katz** [6.28] derived a modified Nusselt equation for a single low-finned tube. Then **Katz** et al [6.29] applied the **Beatty** and **Katz** equation to tube bundles of both square and triangular pitch. And **Kirkbride** [6.30] suggested the sensible heat transfer due to de-superheating and subcooling be accounted for by adding extra term to the enthalpy difference. With all these modifications, the final correlation of heat transfer coefficient for the condensation of refrigerant on bundles of low-finned tubes is as follows (see [6.3]):

$$\alpha_{con} = 0.725 C_n (1/M)^{0.25} \left[\frac{\lambda_l^3 \rho_l^2 g \Delta h}{D_{eq} \mu_l (T_c - T_{tube})} \right]^{0.25} \quad (6.25a)$$

where

$$[1/D_{eq}]^{0.25} = 1.3 \eta_{tube} A_{fin} / (A_{tot} L^{0.25}) + A_{tube} / (A_{tot} D_{tube}^{0.25}) \quad (6.25b)$$

$$L = \pi (D_{fin}^2 - D_{tube}^2) / (4 D_{fin})$$

$$M = \begin{cases} N_{tube} & N_{tube} \leq 20 \text{ in both pitch} \\ 0.815 N_{tube}^{0.52} & N_{tube} > 20 \text{ in square pitch} \\ 0.400 N_{tube}^{0.54} & N_{tube} > 20 \text{ in triangular pitch} \end{cases} \quad (6.25c)$$

$$C_n = \exp[-0.155 + 0.21 \ln(M)] \quad (6.25d)$$

$$\Delta h = h_{mv} - h_{subl} \quad (6.25e)$$

Heat transfer coefficient between the cooling water and tubes

The cooling water inside the tubes may be in laminar flow, turbulent flow or transition region. In [6.22], correlations are given to calculate the heat transfer coefficient for all the three cases.

Laminar flow ($Re \leq 2300$):

$$Nu = [3.65 + \frac{0.19 (Re Pr d / L)^{0.8}}{1 + 0.117 (Re Pr d / L)^{0.467}}] \quad (6.26a)$$

Turbulent flow ($Re > 10^4$) and transition region ($2300 < Re \leq 10^4$):

$$Nu = \frac{\xi/8 (Re - 1000) Pr}{1 + 12.7 (\xi/8)^{0.5} (Pr^{2/3} - 1)} [1 + (d/L)^{2/3}] \quad (6.26b)$$

were $\xi = (1.82 \log_{10} Re - 1.64)^2$. The heat transfer coefficient $\alpha_w = \frac{\lambda_w Nu}{d}$ and the Reynolds number Re is based on the pipe inner diameter d .

Heat transfer coefficient between the refrigerant and shell wall

As normally the condensation temperature is higher than the surrounding air temperature, heat can be transferred through the shell wall to the outside. Moreover, condensation may take place on the inside surface of the shell. To calculate the heat transfer coefficient, the correlation for the condensation of still saturated vapour inside a horizontal tube is adopted (see [6.31], [6.32]).

$$\alpha_{shell,c} = \lambda_{r,l} / \delta_{film} \quad (6.27)$$

where δ_{film} is roughly assumed to be 1 mm, because this part of heat transfer is unimportant.

Heat transfer coefficient between the shell wall and air

The heat transfer between the shell wall and surrounding air is a free convection problem outside a horizontal cylinder. The correlation given in [6.22] can be used for the purpose.

$$\alpha_{sh,atm} = \lambda_{air} / D_{sh} C_1 C_2 Ra \quad (6.28)$$

The constants C_1 and C_2 are as below

Ra	C_1	C_2
$10^{-2} - 10^{-1}$	0.675	0.058
$10^{-1} - 10^2$	1.020	0.148
$10^2 - 10^4$	0.850	0.188
$10^4 - 10^7$	0.480	0.250
$10^7 - 10^{12}$	0.125	0.333

6.3.2 Subcooling zone

Heat transfer coefficient between the refrigerant liquid and tubes

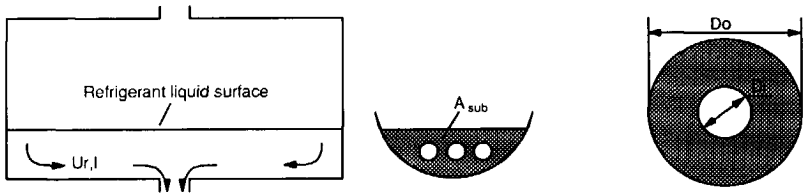


Fig. 6-8 Refrigerant flow pattern in the subcooling zone which can be represented by a system of concentric pipes (right).

The tubes merged in the subcooled liquid are identical to those in the condensation zone. But their heat transfer mechanism is different. The heat transfer in this zone occurs without

phase change and thus its coefficient should be much lower than the other. However, it is not real natural convection either, because the subcooled refrigerant liquid is not absolutely still. Such a situation is even more obvious when the liquid level becomes lower. The liquid motion velocity in the horizontal direction may not be negligible, that can be calculated as below (see Fig. 6-8)

$$u_{r,l} = \frac{\dot{m}_{r,out}}{A_{sub} \rho_{r,l}} \quad (6.29)$$

As an approximation, the heat transfer coefficient for forced convective flow in concentric pipes (see [6.22]) is adopted. It is supposed that heat is transferred through both inner and outer pipes which however have the same temperature. In the present case, the temperatures of the shell and tubes are obviously different. However, we assume such a difference would not cause big errors.

For laminar flow ($Re = u_{r,l} D_{hydr} / \nu_{r,l} < 2300$):

$$Nu = [Nu_{\infty} + f(D_i/D_o)] \frac{0.19 (Re Pr D_h/L_{sh})^{0.8}}{1 + 0.117 (Re Pr D_h/L_{sh})^{0.467}} (Pr/Pr_{tube})^{0.11} \quad (6.30a)$$

$$Nu_{\infty} = 3.66 + [4 - \frac{0.102}{(D_i/D_o) + 0.02}] (D_i/D_o)^{0.04} \quad (6.30b)$$

$$f(D_i/D_o) = 1 + 0.14 (D_i/D_o)^{0.1} \quad (6.30c)$$

For turbulent flow ($Re = u_{r,l} D_{hydr} / \nu_{r,l} > 2300$):

$$Nu = \frac{0.86(D_i/D_o)^{0.84} + [1 - 0.14(D_i/D_o)^{0.6}]}{1 + D_i/D_o} Nu_0 \quad (6.30d)$$

where Nu_0 is calculated by using (6.26) and the hydraulic diameter $D_{hydr} = D_o - D_i$.

Heat transfer coefficient between the refrigerant liquid and shell wall

The correlation in this case is the same as above.

6.4 On the connection lines

The components in a refrigerating machine are connected by pipes. In order to return the oil mixed in the refrigerant back to the compressor, an oil separator is equipped between the compressor and condenser. Usually, some control and safety devices are also assembled somewhere in the system. Depending on the specific location of the system, the connection lines can be longer or shorter and may have bends. Generally speaking, the situations on the connection lines are very diverse and complex. Therefore, we decided to use two very simple equations to calculate the heat transfer and pressure drops on the connection lines of the system.

$$Q_{1-2} = A [0.5 (T_{1,ro} + T_{2,ri}) - T_{amb}] \quad (6.31)$$

$$\Delta P_{1-2} = [\Sigma k + L/d \xi] 0.5 \rho_r v_r^2 = B [\dot{m}_r / \rho_r^{0.5}]^m \quad (6.32)$$

where Σk represents the summation of the local pressure drops due to sudden contractions or enlargements; $L/d \xi$ represents the pressure drop along the connection line between components 1 and 2.

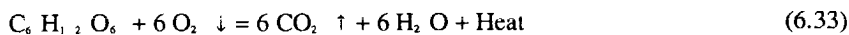
The constants A and B will be determined through experiments in chapter 7 and are assumed independent of mass flow rate.

6.5 In the refrigerated room

6.5.1 Micro-climate

Heat transfer coefficient between the product and air

Most of agricultural products are still alive even though they have been harvested. The metabolism process of them during storage produces heat and water. The characteristic reaction of metabolism is usually described as below



The reaction rate of metabolism is dependent upon the temperature of product, the composition (concentrations of CO₂ and O₂) and velocity of micro-climate air. If the composition effect is left aside for the time being, there exists an empirical correlation to calculate the heat production rates based on the product temperature (see [6.33]):

$$Q_{prod} = A e^{-B/T_{prod}} M_{prod} \quad (6.34)$$

For apples, $A = 1.5545E7$ (kw/kg), $B = 7632.9$ (K).

This amount of heat is removed by the cold air through the micro-climate. The heat transfer coefficient on the surface of product is calculated by **Fockens** [6.34] as follows

$$Nu = 1.064 Re_0^{0.59} Pr^{1/3} \quad (6.35)$$

where $Re_0 = \frac{v_0 D_{prod}}{\nu}$ and $Nu = \frac{\alpha D_{prod}}{a}$. The velocity v_0 is the air flow velocity outside the box, as shown in Fig 6-9.

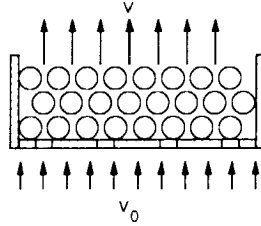


Fig. 6-9 Air velocities in the macro-climate and micro-climate.

Moisture transfer coefficient between the product and air

Besides heat, the product also releases moisture that is carried away by the air. For the moisture transfer, the surface of the product plays an important role. **Fockens** and **Meffert** [6.35] proposed four model-surfaces (see Fig. 6-10):

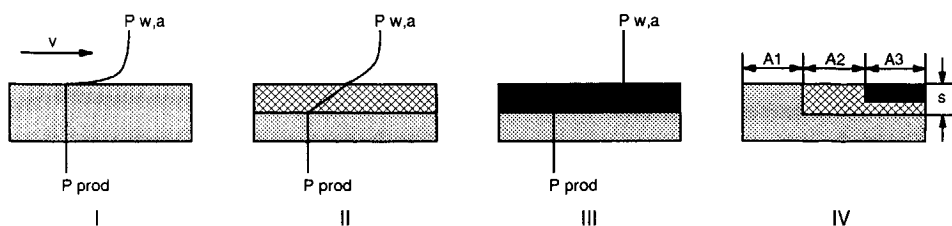


Fig. 6-10 Four models of product surface proposed by Fockens.

1. a wet surface covered by a thin layer of water or air saturated with water vapour;
2. a wet surface covered by a porous layer and the pores are filled with air;
3. a surface covered by a layer which is impervious to water vapour;
4. a surface which is a combination of the surfaces 1, 2, 3, the areas of these surfaces being A_1 , A_2 , and A_3 respectively.

Then the moisture transfer flux is calculated by using a partial pressure difference of water vapour for the most complicated case: model IV

$$m_w = \left[\xi_1 \frac{\beta}{R T} + \xi_2 \frac{\beta}{R T} \frac{1}{1/\beta + \mu s/\delta} \right] (P_{prod} - P_{w,a}) \quad (6.36)$$

$$\xi_1 = A_1 / (A_1 + A_2 + A_3)$$

$$\xi_2 = A_2 / (A_1 + A_2 + A_3)$$

where T is the mean absolute temperature of the boundary layer. To be simple, the average temperature between T_{prod} and $T_{a,mic}$ can be used to substitute it. The saturated water vapour pressure on the product surface P_{prod} is that corresponding to T_{prod} . The mass transfer coefficient β depends on the Reynolds number of the air flow along the surface. In the case of air flowing through a bed of nearly spherical bodies, β is given in [6.34] as follows

$$\beta = 0.989 \text{Re}_0^{0.59} \text{Sc}_2^{1/3} \delta/D_{prod} \quad (6.37)$$

The partial pressure of water vapour in the air is related to the absolute humidity by the state equation

$$P_{w,a} = \frac{P_{a,mi} w_a}{(R_a / R_w) + w_a} \quad (6.38)$$

Pressure drop through ball-like products

In chapter 5, when the velocity of air in the micro-climate was calculated, a pressure-velocity relation was made use of. It was assumed that the friction force produced by the ball-like products dominates the momentum transport in the micro-climate and thus inertia force was just neglected. The air flow in the micro-climate is more or less like a flow through a porous object. **Fockens** derived a correlation to calculate the pressure drop of a bed of balls by setting up two models: channel model and ball model. He demonstrated that these two models were able to give the same correlation as follows

$$\Delta P = k_1 \frac{\eta L}{D^2} v_0 \frac{(1-\epsilon)^2}{\epsilon^3} + k_2 \frac{L}{D} \frac{1}{2} \rho v_0^2 \frac{1-\epsilon}{\epsilon^3} \quad (6.39)$$

This correlation is valid for both laminar and turbulent flows. The check of flow patterns is based on a Reynolds number defined as $Re_0 = v_0 D_{prod} / \nu$. The constants k_1 and k_2 need to be determined experimentally and related to the surface roughness and shape of the products, and **Fockens** suggested $k_1 = 150$ and $k_2 = 3.5$.

6.5.2 Macro-climate

Heat transfer coefficient between the air and walls

In the macro-climate, the air is in contact with the walls of the room and the product boxes. If neglecting natural convection effect, the heat transfer between the air and walls can be regarded as a forced convection problem along a fixed plate. **Smith** et al [6.36] give an analytical solution to this problem. The overall heat transfer coefficient of a plate with length of L is

$$Nu = 0.28 Re^{0.5} Pr^{0.5} \quad (6.40)$$

where L is the characteristic dimension in the Reynolds number and Nusselt number. Because the air velocity varies in places in the room, a module-velocity should be used to calculate the Reynolds number in (6.40):

$$v = (v_1 + v_2 + v_3)^{1/2} \quad (6.41)$$

Concerned with moisture transfer, it is postulated that all the solid wall are impervious to water vapour.

6.5.3 Outside of the room

There are two components in the heat transfer from the atmospheric surrounding to the refrigerated room: heat from the air by natural convection; heat from the sun by radiation. To determine these two components, information is needed about weather and the position of the earth. Detailed recordings as well as calculations about them can be found in [6.37]. Here we assume the atmospheric temperature and the solar radiations to each of the six walls of the room are well known. Meanwhile, it is assumed that there is no wind (if there is wind and the heat transfer on the outside surface of the room is in forced convection, Eq. (6.40) can be put in use).

Natural convective heat transfer coefficient between the room's walls and air

The refrigerated room has four vertical walls and two horizontal walls. If the temperature of the wall surface and the atmospheric temperatures are known, the natural convective heat transfer coefficient between the walls and surrounding air can be calculated by using the correlations given in [6.22], which are subjected to vertical as well as horizontal plates.

Vertical plate:

$$Nu = \left\{ 0.825 + \frac{0.387 Ra^{1/6}}{[1 + (0.492/Pr)^{9/16}]^{8/27}} \right\}^2 \quad (6.42)$$

This correlation is valid for both laminar and turbulent flows with $Ra = 0 - 10^{12}$ and $Pr = 0 - \infty$. The characteristic length is the height of the plate.

Horizontal plate:

$$\text{Nu} = \begin{cases} 0.700 \text{ Ra}^{1/4} & (\text{laminar flow, Ra} < 4\text{E}7) \\ 0.155 \text{ Ra}^{1/3} & (\text{turbulent flow, Ra} \geq 4\text{E}7) \end{cases} \quad (6.43)$$

This correlation is valid for the case that air is above the horizontal plate. The used characteristic dimension should be the average of the length and width of the plate.

Absorption and reflection of the walls to the solar radiation

In principle, the solar energy transferred to an object can be divided into three parts: absorbed, penetrating, and reflected. In case of solid objects, the penetration rate of solar radiation is almost null. Thus

$$Q_{solar,tot} = Q_{solar,ref} + Q_{solar,abs} \quad (6.44)$$

The absorbed energy is quickly transformed into heat energy within a very short distance in the wall behind the surface. The absorption rate of a material is defined as the ratio of $Q_{solar,abs}$ to $Q_{solar,tot}$ and depends upon the roughness, physical properties, surface temperature of the plate and the radiation wave length. The details on this problem can be found in [6.38].

6.6 Closure

Above all the transfer coefficients, which are used in the steady-state and dynamic modelling of the refrigeration system, have been described and the appropriate correlations have been selected from the literature. These are programmed as auxiliary subroutines in the simulation codes. However, as pointed out before, the selected correlations are obtained by different investigators based on different experimental conditions. The validation to them is always required in order to make reliable simulations under the concerned specific operation conditions. The next chapter is therefore devoted to this part of work.

References

- 6.1 **Sthapak B.K., Varma H.K., Gupta C.P.:** "Heat transfer coefficients in dry-out region of horizontal tube water heated R-12 evaporator", *ASHRAE Transactions*, Vol.82, Part 2 1976.
- 6.2 **Fischer, S.K., Rice, C.K.** "The Oak Ridge heat pump models: I. a steady-state computer design model for air-to-air heat pumps", ORNL/CON-80/R1, Department of Energy, Oak Ridge National Laboratory, Oak Ridge, Tennessee 37830, August 1983.
- 6.3 **Conde, M.R.** "A steady-state mathematical simulation model for air-to-water heat pumps", Report, ETH Zurich, July 1985.
- 6.4 **Collier, J.G.** "Convective boiling and condensation", McGraw-Hill Book Company Limited, 1972.
- 6.5 **Dengler, C.E., Addoms, J.N.** "Heat transfer mechanism for vaporization of water in a vertical tube", *Chem. Eng. Progress Symp. Series*, Vol. 52(18), pp. 95-103, 1956.
- 6.6 **Guerrieri, S.A., Talty, R.D.** "A study of heat transfer to organic liquids in single-tube, natural circulation, vertical tube boilers", *Chem. Eng. Progress Symp. Series: Heat Transfer*, Louvisville, No.18, Vol.52, pp.69-77, 1956.
- 6.7 **Pierre, B.** "The coefficient of heat transfer for boiling freon-12 in horizontal tubes", *SF Review* Vol.2, Svenska Flaktfabriken A.B., Stockholm, Sweden, 1955.
- 6.8 **Bennett, J.A.R., Collins, J.G., Pratt, H.R.C., Thornton, J.D.** "Heat transfer to two-phase gas liquid system", *AERE-R3159*, 1959.
- 6.9 **Schrock, V.E., Grossman, L.M.** "Forced convection boiling in tubes", *Nuclear Sci. Eng.*, Vol.12, pp.474-481, 1962.
- 6.10 **Collier, J.G., Pulling, D.J.** "Heat transfer in two-phase gas-liquid systems, part II, further data on steam-water mixture", *AERE-R3809*, 1962.
- 6.11 **Chen, J.** "A correlation for boiling heat transfer to saturated fluids in convective flow", *ASME 63-HT-34*, 1963.
- 6.12 **Chaddock, J.B., Noerager, J.A.** "Evaporation of refrigerant R12 in a horizontal tube with constant wall heat flux", *ASHRAE Transactions*, Vol.72, Part 1, pp.90-103, 1966.
- 6.13 **Shah, M.M.** "A new correlation for heat transfer during boiling flow through pipes", *ASHRAE Transactions*, Vol.82, Part 2, pp.66-86, 1976.
- 6.14 **Dembi, N.J., Dhar, P.L., Arora, C.P.** "Statistical analysis of heat transfer data for convective boiling refrigerants in a horizontal tube", *Letters in Heat and Mass Transfer*, Vol.5, pp.287-296, 1978.
- 6.15 **Domanski, P., Didion, D.** "Computer modelling of the vapour compression cycle with constant flow area expansion device", *NBS Building Science Series 155*, Washington DC, May 1983.
- 6.16 **Van der Meer, J.S.** "Simulation of a refrigerant evaporator", Ph. D. Thesis, Delft University of Technology, the Netherlands, October 1987.

- 6.17 **Geary, D.F.** "Return bend pressure drop in refrigeration systems", *ASHRAE Transactions*, Part 1, pp.250-265, 1975.
- 6.18 **Hsu, Y.Y., Graham, R.W.** "Transport processes in boiling and two-phase systems", Hermisphere Publishing Corporation, 1976.
- 6.19 **Storek, H., Brauer, H.** "Reibungsdruckverlust der adiabaten gas-flüssigkeit-strömung in horizontalen und vertikalen rorhen", *VDI Forschungsheft, No.599*, VDI-Verlag GmbH Düsseldorf, pp.1-36, 1980.
- 6.20 **Pierre, B.** "Flow resistance with boiling refrigerants - part I", *ASHRAE Journal*, pp.58-65, September 1964.
- 6.21 **Pierre, B.** "Flow resistance with boiling refrigerants - part II", *ASHRAE Journal*, pp.73-77, October 1964.
- 6.22 **VDI-Wärmeatlas**, "Berechnungsblätter für den wärmeübergang", VDI-Verlag GmbH, Düsseldorf, 1984 (in German).
- 6.23 **McQuiston, F.C.** "Finned tube heat exchangers: state of the art for the air side", *ASHRAE Transaction*, Vol.87, Part 1, pp.1077-1085, 1981.
- 6.24 **McQuiston, F.C.** "Correlation of heat, mass and momentum transfer coefficients for plate-fin-tube heat transfer surfaces with staggered tubes", *ASHRAE Transaction*, Vol.84, Part 1, pp.294-301, 1978.
- 6.25 **Rohsenow, W.M.** "Handbook of heat transfer", McGraw-Hill Book Company, New York, 1973.
- 6.26 **Green, G.H.** "Influence of oil on boiling heat transfer and pressure drop in refrigerants R12 and R22", *ASHRAE Journal*, pp.57-61, December 1965.
- 6.27 **Schlager, L.M., Pate, M.B., Bergles, A.E** "Evaporation and condensation of refrigerant-oil mixtures in a smooth tube and a micro-fin tube", *ASHRAE Transactions*, vol.94, Part 1, 1988.
- 6.28 **Beatty, K.O., Katz, D.L.** "Condensation of vapours on outside of finned tubes", *Chemical Eng. Progress*, Vol.44/1, 1948.
- 6.29 **Katz, D.L., Young, E.H., Balekjian, G.** "Condensing vapours on finned tubes", *Petroleum Refiner*, Vol.33/11, 1954.
- 6.30 **Kirkbride, C.G.** "Heat transfer by condensing vapour on vertical tubes", *Industrial and Engineering Chemistry*, 26/4, 1934.
- 6.31 **Dikken, R.A.** "A dynamic simulation of a refrigerated room, using a steady-state model of the refrigerating machine", Report No. S-866, Delft University of Technology, the Netherlands, September 1988.
- 6.32 **Kraaijeveld, B.** "Niet-stationair simulatiemodel voor een kondenser", Report S-766, Delft University of Technology, the Netherlands, March, 1985 (in Dutch).
- 6.33 **Rudolphij, J.W.** "Listing of the product properties", private letter, January, 1987.
- 6.34 **Fockens, F.H.** "Fysische transportverschijnselen tijdens het afkoelen van tuinbouwprodukten", Ph.D. Thesis, Delft University of Technology, the Netherlands, June, 1967 (in Dutch).

- 6.35 **Fockens, F.H., Meffert, H.F.** "Biophysical properties of horticultural products as related to loss of moisture during cooling down", *J. Sci. Fd. Agric.*, vol.23, pp.285-298, 1972.
- 6.36 **Smith, J.M., Stammers, E., Janssen, L.P.B.M.** "Fysische transport-verschijnselen", Delftse Uitgevers Maatschappij b.v., 1986 (in Dutch).
- 6.37 "Verkort referentiejaar voor buitencondities", ISSO-publikatie No.12 (in Dutch).
- 6.38 "Zontoetredingsfactoren", ISSO-publikatie No.2 (in Dutch).

Chapter
SEVEN
Validation of the Models

7.1 General

By so far, the theoretical part of the investigation has been described, which is composed of the steady-state and non-steady-state modelling of the refrigerating machine and refrigerated room. In principle, the models developed in the preceding chapters are based on the fundamental laws of physics and therefore should correctly predict the real behaviour of the system. However, such an inference is mostly not true in practice. There are two reasons for it: 1) in making the models, the fundamental laws were not exactly applied. To overcome the difficulties in solving the governing equations, assumptions are always necessary. For example, we have assumed that the superheated vapour in the condensation zone of the condenser was perfectly mixed in order to derive an ordinary differential equation that is much easier to be solved than a partial differential equation. 2) although the models are on the basis of the physical rules, they are not completely "white". A certain number of empirical or semi-empirical correlations to calculate the transfer coefficients for heat, mass and momentum exist in the models. Those correlations are usually obtained by other investigators under the specific experimental circumstances of their own. Even though we have attempted to select those which have similar operational conditions to ours, deviations are almost unavoidable. Moreover, the correlations themselves are not 100 % accurate. From this point of view, we may say that our models are in fact "grey" models. Therefore, experimental validation of the models is necessary before they can be put to use. This chapter is intended to fulfill this task.

7.2 Contents of the experiments

Steady-state experiments for the determination of empirical constants

In order to guarantee a wide validation range of the empirical constants to be determined, the experimental conditions are required to scatter and the number of steady-state tests have to be large enough. Only with a number of representing test data, can a regression process result in a good fitting for the correlation which includes empirical constants. Thus we decided to do 10 steady-state tests with cyclic refrigerant mass flow rate varying from ± 20 g/s to ± 90 g/s.

Steady-state experiments to validate the steady-state models

This group of experiments is intended to check the steady-state models which have been supplemented with empirical constants determined experimentally. The requirements towards this set of tests are almost the same as above. However, a validation is not a fitting process but a comparison. Thus a great number of steady-state tests are not necessarily required. In our case, 6 sets were planned.

Non-steady-state experiments to validate the dynamic models

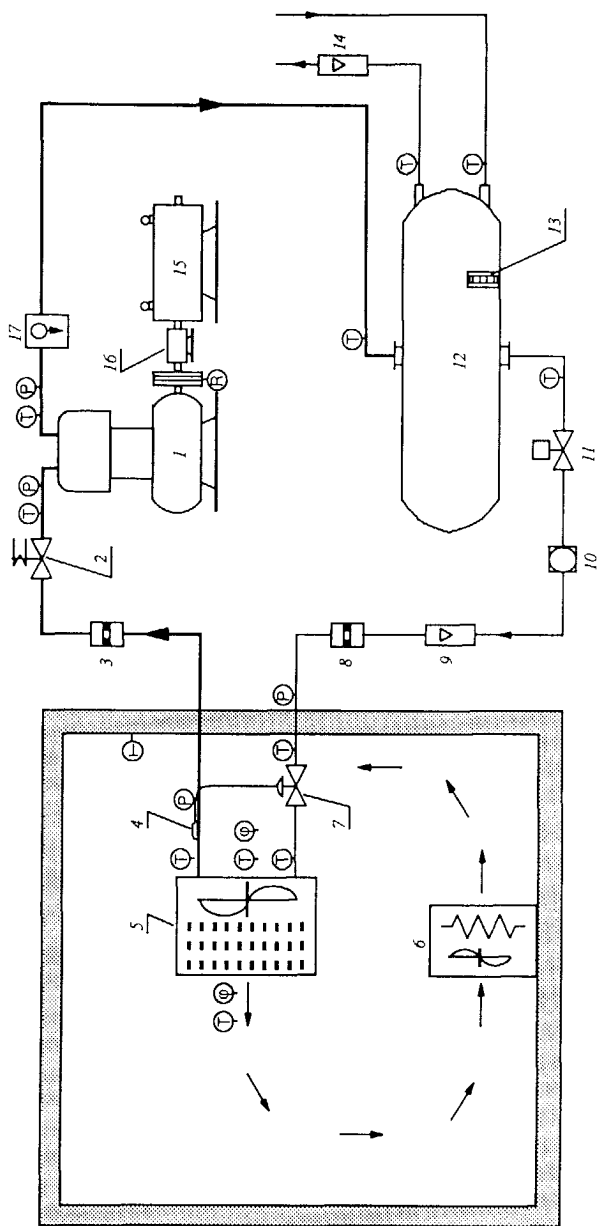
The non-steady-state experiments are the main part of our experimental work. In contrast with the steady-state tests, a non-steady-state test should consist of three stages: initialization, stimulation, and response. All these three stages have to be recorded with respect to time during the test. Usually, step changes are used as stimuli just for the purpose of validation of a dynamic model. The number of non-steady-state tests are thus counted with the number of step changes. In our case, 5 types of step changes were schemed.

Measurement of the air flow pattern in a cold room

This experiment is particularly aimed at checking the application of PHOENICS to a refrigerated room. Different from the other experiments, the measurement of air flow is carried out in a spatial domain instead of time. For a certain cold room with a constant ventilation rate and a chosen arrangement of products, its flow pattern is almost monotonous and therefore the measurement can be steady-state.

7.3 Description of the experiment plant

In order to fulfill the experiments listed above, a sophisticated test plant has been set up in the laboratory. This plant has five main components: evaporator, condenser, compressor, thermostatic expansion valve, and cold room. Besides, a number of auxiliary devices are assembled on the plant for the purposes of safety, control and measurement. Several possibilities to change operation conditions are also provided, which include rotational speed of the compressor, electrical input of the heating, water supply of the condenser, screw position of the TEV. To realise automatic capacity controls, the plant is rigged with a



1. Compressor, Bock I4, (Q=10 kw, W=3 kw, at $T_c=30^\circ\text{C}$, $T_e=-10^\circ\text{C}$, RPM=1125 1/min)
2. Safety valve
- 3, 8. Orifice flow meter, Viertelkreisdruck DIN 1952,
4. Alphaline flow meter, Viertelkreisdruck 1151DP, Rosenmount
5. Bulb feeder of the TEV
6. Evaporator, Helpman Lex-18 (10 kw at $T_e=10^\circ\text{C}$, $dT=10^\circ\text{C}$)
7. Heating, Sinus (8.826 kw)
8. Thermostatic expansion valve (TEV), Danfoss, TEF5, orifice No.2
9. Float flow meter, Fischer & Porter, Model 10A5001 (0 - 300 l/hr for water, 0 - 254 l/hr for F12)
10. Glass Viewer
11. Sononoid valve
12. Condenser, home-made, water-cooled, shell-and-tube
13. Liquid level viewer
14. Float flow meter, Fischer & Porter,
15. tube: FP-1"-35-g-10/83, float: GGV164 (1355 l/hr water)
16. Motor, Siemens, Type 1GC3 162-5NF50-6RU1 B3, (RPM 50-1500 1/min, 380V, 50Hz, 34A, 0.5-15kw)
17. Torque transducer, Kyowa, TP-10KMCB
- Oil separator, AC&R, S-5692

Fig.7-1 Schematic diagram of the test plant

two-stage thermostat. Because of the cost of loads or dummy loads, an empty cold room containing several obstacles is used for the validation of the air flow pattern. Fig. 7-1 shows the scheme and the specifications of the test plant and Fig. 7-2 is its photograph.

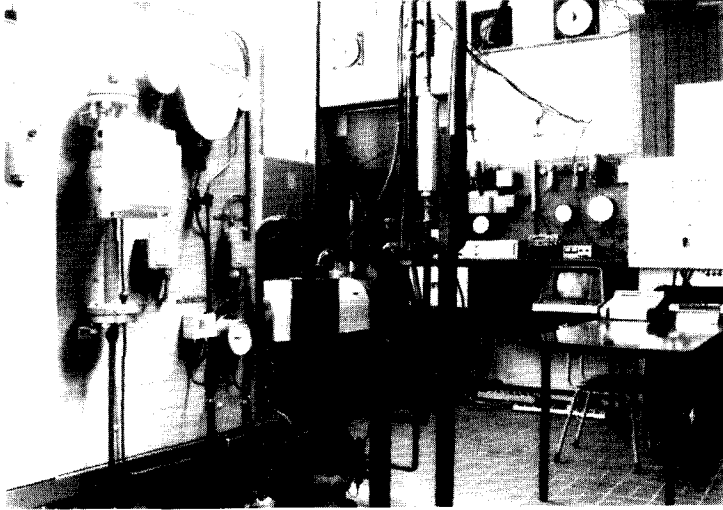


Fig. 7-2 Photograph of the test plant.

7.4 Measurement instruments

Temperature

Copper-Constantan thermocouples are used as the temperature measurement device. All the thermocouple threads are connected to the datalogue which internally has an electronic zero-point compensation and can register signals with minimum voltage: $1 \mu\text{V}$. This type of thermocouples have an accuracy of 0.1°C (note: all the accuracy figures presented in this thesis are in terms of standard deviation). However, depending on the way of fitting, a systematic error due to the thermal conductivity of the probe is to be expected. From earlier research it follows that this error does not exceed $+0.1^\circ\text{C}$ for those lower than ambient temperature and -0.1°C for those higher than ambient temperature.

Pressure

Pressures are measured with strain gauge pressure transducers (Transamerica, type BHL-4000). The accuracy of this type of pressure transducers is: full range output: $5V \pm 1\%$ at $+25^{\circ}\text{C}$ and rated supply. In our case, the pressure transducers measuring the compressor suction pressure and the evaporator inlet and outlet pressures have a pressure full-range: 0 - 5 bar; the one measuring the compressor discharge pressure has a pressure full-range: 0 - 20 bar. Pressure measurement using this type of transducers may be suitable in the determination of low side pressures, such as the compressor suction pressure, but not for the compressor discharge pressure. The reason for this is that 1% of deviation of the output voltage corresponds to 0.05 bar of pressure for a pressure full-range: 0-5 bar, and 0.2 bar for a pressure full-range: 0-20 bar. Therefore, for high pressure measurements, this type of pressure transducer is actually inaccurate. However, we did not have alternatives in the circumstance concerned.

Flow

Two types of flow meters are applied: float type and orifice type. The float type flow meters are used to measure the water flow and steady-state refrigerant flow. While, the orifice type flow meters are for measuring the gas and liquid refrigerant flows under dynamic conditions, because they can output analogue signals continuously. The orifice flow meters are calibrated with one of the float flow meters.

The float flow meters are the Fischer & Porter variable area flow meters (Model 10A5000 and 1-A3500) with an accuracy of 1% of maximum flow rate. In our case, the float flow meter measuring the refrigerant flow has a maximum flow rate of 254 liter/hour for R12; that measuring the water flow has a maximum flow rate of 1355 liter/hour for water.

The orifice flow meters consists of a Viertelkreisdüse orifice (Model DIN 1952) and an Alphaline $\sqrt{\Delta P}$ flow transmitter (Model 1151DP) made by Rosemount Inc.. The accuracy of the flow meters is $\pm 0.25\%$ of calibrated span for a range of 20% to 100% of flow (the output is linear with the input pressure for the range of 0% to 20% of flow). Because the orifice flow meters are calibrated by the float flow meter with maximum flow rate: 254 liter/hour, the calibrated span is 0 - 254 liter/hour.

Air velocity

For measuring air velocities, a hot wire anemometer is put in use. Its main advantages are: the probe is very small (diameter 5 μm) so that the flow pattern to be measured is not influenced by the probe itself; the probe responses very fast and is also sensitive so that air flows with high turbulent frequency or low velocity can be measured. The calibration of the anemometer was done in a wind tunnel (maximum velocity 8 m/s) with a pito-meter. The calibration accuracy was 8%.

Air humidity

Air humidity measurements are necessary for the validation of the evaporator models which account for air de-humidification. The humidity of air is measured with a MBW dew-point indicator (model DP 3) which has the working range of $-40\text{ }^{\circ}\text{C}$ to $60\text{ }^{\circ}\text{C}$ and the accuracy of $\pm 0.4\text{ }^{\circ}\text{C}$. The measuring principle is that the air to be measured is directed over a mirror cooled by a Peltier battery down to the temperature of which dew or ice falls out and the measured mirror temperature corresponds with the dew point of the air. To establish a constant dew density, a monitoring device consisting of a photoelectric arrangement controls the Peltier battery current until equilibrium is reached. With the measured air temperature at the same point, the relative humidity can be calculated.

Shaft power

A Kyowa torque transducer (model TP-10KMCB) is arranged to measure the instantaneous shaft power of the compressor. The output signal of the transducer is integrated and averaged every 2 seconds by an analog integrator and then transmitted to the datalogue. The product of the measured shaft torque and rotational speed is then the shaft power of the compressor.

Rotational speed

A Philips timer/counter (model PM6624) is used to measure the rotational speed of the compressor, which has a frequency range up to 80 MHz and is able to measure frequency, ratio, period, time interval. The accuracy of this instrument is ± 1 count \pm time base error.

7.5 Determination of several empirical constants

As stated before, the theoretical models always include a certain amount of empirical constants which are difficult to obtain from the basic physical equations, such as mass and energy conservation equations. Thus experiments are needed to determine them. Usually, empirical constants can be classified into three groups: 1) the constants which have already been determined by the precedent investigators through their own experiments. This type of empirical constants can be found in the correspondent literature and usually do not need to be re-checked with extra experiments. 2) the constants which have ever been found by others, but under different operation conditions than the applied situations. In other words, the validation ranges of the constants are incompatible with the applied situations. Then, experiments are necessary in this case. 3) the constants which are to a large extent dependent on the concrete plants themselves, for instance, the constants encountered in the correlations for calculating the pressure losses on the connection lines. Different plants would have different connection circuits and thus different pressure drops on them. In this case, experiments should be done on the concerned plant and the obtained data are only applicable to this plant.

Tab. 7-1 *Experimental results for determining the empirical constants.*

Items	test 1	test 2	test 3	test 4	test 5	test 6	test 7	test 8	test 9	test 10
Compressor:										
$T_{r,i}$ (°C)	1.00	12.10	5.10	16.12	4.28	11.77	7.29	15.98	2.16	-2.50
$T_{r,o}$ (°C)	84.98	70.34	87.46	89.34	75.40	83.50	82.43	66.27	74.39	95.62
$P_{r,i}$ (bar)	1.150	2.289	1.494	2.343	1.575	2.124	1.58	2.677	1.475	0.924
$P_{r,o}$ (bar)	8.771	8.648	8.944	11.19	8.208	10.205	7.442	8.260	7.993	7.578
m_r (g/s)	21.60	53.60	53.00	85.30	33.50	68.80	71.90	68.30	32.10	34.90
W (kw)	1.386	1.934	2.935	4.020	1.617	3.063	3.404	1.729	1.574	2.493
RPM (1/min)	703.0	704.6	1196.4	1198.8	704.6	1021.3	1384.0	715.0	711.7	1389.0
Condenser:										
$T_{r,i}$ (°C)	71.18	65.10	79.78	84.64	66.90	78.10	77.26	62.70	65.39	84.14
$T_{r,o}$ (°C)	33.90	34.20	35.16	44.74	32.30	40.87	26.30	30.40	28.10	27.91
$T_{w,i}$ (°C)	18.72	18.18	18.40	18.60	18.22	18.50	20.62	21.60	20.64	22.62
$T_{w,o}$ (°C)	37.60	35.14	37.20	46.88	33.94	42.70	29.22	33.19	31.98	30.68
m_w (g/s)	31.0	104.8	97.2	102.4	106.7	89.6	346.0	222.0	110.0	182.0
H_{lev} (m)	0.039	0.039	0.039	0.039	0.039	0.039	0.039	0.039	0.039	0.039
TEV										
$T_{r,i}$ (°C)	29.52	32.42	32.94	42.86	29.60	38.83	25.34	29.42	25.76	25.60
$T_{r,o}$ (°C)	-19.86	1.24	-5.26	10.20	-11.10	3.63	-1.78	7.15	-13.02	-17.02
$P_{r,o}$ (bar)	8.438	8.165	8.462	10.426	7.838	9.606	6.856	7.672	7.622	7.202
m_r (g/s)	21.60	53.60	53.00	85.30	33.50	68.80	71.90	68.30	32.10	34.90
Evaporator:										
$T_{r,i}$ (°C)	-21.96	-1.37	-10.79	4.51	-13.41	-1.77	-6.89	5.24	-15.51	-22.78
$T_{r,o}$ (°C)	-3.44	12.22	4.60	18.10	2.22	12.27	7.61	17.17	-0.48	-5.37
$P_{r,o}$ (bar)	1.229	2.717	1.833	3.201	1.720	2.616	2.115	3.392	1.616	1.140
$T_{a,i}$ (°C)	-1.27	15.52	7.98	23.16	4.81	16.67	11.96	21.32	2.35	-1.03
$T_{a,o}$ (°C)	-2.86	11.02	3.62	15.61	2.26	10.75	5.52	14.94	-0.38	-5.12
$\phi_{a,i}$ (%)	60.52	44.68	41.23	35.06	53.96	39.18	37.45	41.99	55.22	50.63
V_a (m ³ /s)	1.172	1.172	1.172	1.172	1.172	1.172	1.172	1.172	1.172	1.172
Cold Room:										
T_{amb} (°C)	25.95	23.95	24.95	25.45	25.25	26.10	27.75	28.00	27.05	28.40
Q_{heat} (kw)	1.195	6.036	6.036	10.886	3.116	8.886	8.886	8.886	3.116	3.116

Therefore, the prepared test plant was firstly used to determine the empirical constants mentioned above. The simple way to find those constants is to make a number of steady-state tests which should be so scattered that most of the normally encountered operation conditions are covered. In our case, 10 steady-state tests were made. Since we have arranged quite enough measuring points for all kinds of quantities, all the uncertain empirical constants involved in the previous chapters can be entirely determined with the 10 groups of experimental data. Tab. 7-1 shows the test results as well as the ambient conditions.

The above experimental data are intended to determine the following empirical constants:

- the constants **A**, **B**, **m** in Eqs. (6.31) and (6.32) which calculate the heat transfer and pressure drops along the connection lines.
- the constants **a**, **b** in Eqs. (6.4) and (6.9) which calculate the heat transfer coefficient in the two-phase flow region of the evaporator.
- the constant **c** in Eq. (6.11) which calculates the pressure drop in the two-phase flow region of the evaporator.
- the interfacial momentum-transport coefficient f_i in Eq. (2.9).

7.5.1 Constants A, B, m in Eqs. (6.31) and (6.32)

As the connection lines of a refrigerating system are very different and complex, we intend to use two simple correlations as (6.31) and (6.32) to calculate the heat transfer and pressure drops on them, although it is possible to separately consider all the elements, such as valves, measuring instruments, pipes, on the connection lines. However, the generality of Eqs. (6.31), (6.32) requires three constants to be fixed through experiments. In a normal refrigerating system as shown in Fig. 7-1, the connection lines can be divided into four parts: between compressor and condenser; between condenser and TEV; between TEV and evaporator; between evaporator and compressor. These four parts thus need different constants.

The determination of **A** in Eq. (6.31) is based on the energy balance principle as follows

$$A [0.5(T_{1,ro} + T_{2,ri}) - T_{amb}] = \dot{m}_r (h_{1,ro} - h_{2,ri}) \quad (7.1)$$

where "1" and "2" represents the components connected by the connection line concerned. As the inlet and outlet properties as well as the mass flow rate of the refrigerant are measured through the experiments, the constant **A** can be easily figured out. The 10 sets of experiments can provide 10 different constants. But we make use of the average of the ten.

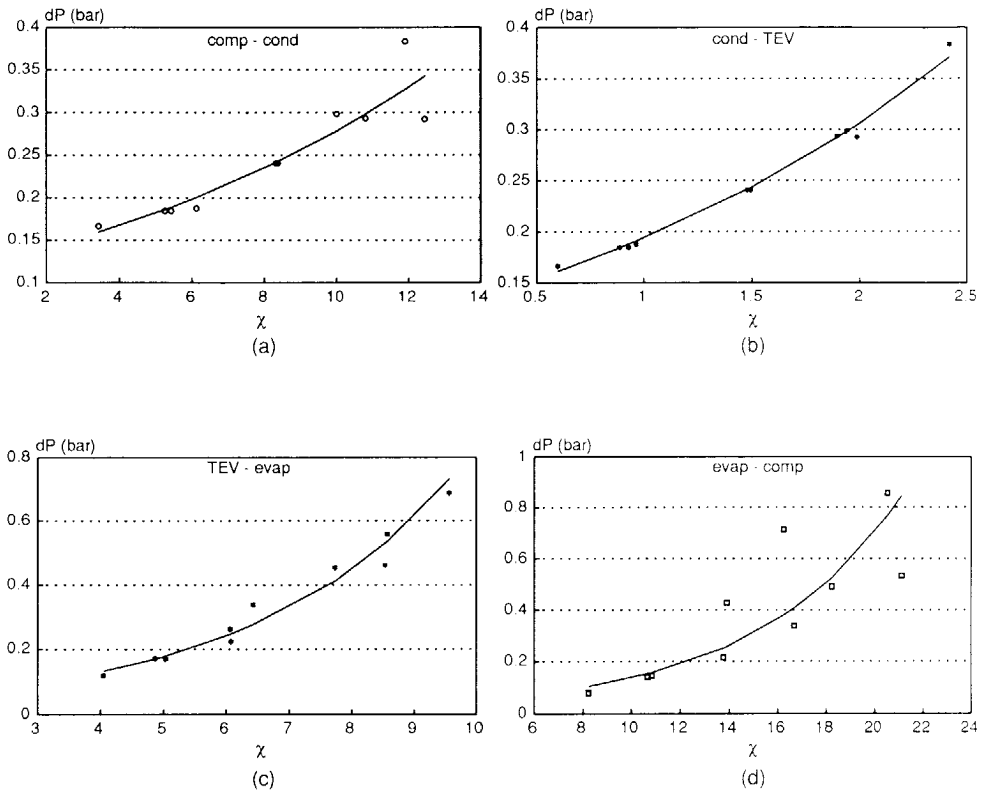


Fig. 7-3 Experimentally fitted curves of the correlations between pressure drop and mass flow rate on the connection lines ($x = 1000 \text{ m}/\sqrt{\rho}$).

Between the compressor and condenser

Besides the pipe, there is also an oil separator between the compressor and condenser. The following correlation for calculating the pressure drop is obtained from regressing the 10 sets of test results (see Fig. 7-3a).

$$\Delta P_{\text{comp-cond}} = 6828.1 (1000 \text{ m}/\rho^{0.5})^{0.646} \quad (7.2)$$

where ρ is the refrigerant density referred at the inlet of the condenser.

For sake of simplicity, the heat transfer through this line to the ambience is included in the compressor model. Thus the discharge temperature calculated by the compressor model is regarded as the condenser inlet temperature.

Between the condenser and TEV

The connection line between these two components is rather long and complicated. However, the refrigerant flow is of single-phase and thus simple. Fig. 7-3b is the fitted curve of the relation between the pressure drop and mass flow rate. The curve is expressed in the following formula.

$$\Delta P_{cond-tev} = 20673.4 (1000 \dot{m}/p^{0.5})^{0.591} \quad (7.3)$$

The density used above is calculated at the outlet of the condenser.

The constant **A** for calculating the heat transfer is determined as 0.0308 (kw/°C).

Between the TEV and evaporator

Although the pipe between these two components is very short, the velocity of the refrigerant flow is quite high because of the refrigerant flashing. Moreover, the flow is in form of two-phase. The pressure drop in this part of line to some extent influences the distribution of refrigerant to the evaporator circuits (see [7.1]). Based on the test results shown above, the following correlation has been obtained (also see Fig. 7-3c).

$$\Delta P_{tev-evap} = 607.3 (1000 \dot{m}/p^{0.5})^{2.099} \quad (7.4)$$

where p is calculated at the inlet of the evaporator as below

$$p = \frac{1}{x/\rho_v + (1-x)/\rho_l} \quad (7.5)$$

As this part of line is insulated very well and short, the heat transfer is neglected in the model.

Between the evaporator and compressor

As there is a safety valve on the line, the pressure drop is considerably large, which results in a big influence on the suction state and mass flow rate of the compressor. In most cases, the pressure drop on this connection line surpasses that in the evaporator and therefore the latter seems to be less important in calculating the suction pressure. Viewing at this point, a proper consideration and prediction of the pressure of this part is rather decisive to the simulation results. The experimental regression formula is as follows (see Fig. 7-3d)

$$\Delta P_{\text{evap-comp}} = 49.46 (1000 \text{ m} / \sqrt{\rho})^{0.5 \cdot 1.659} \quad (7.6)$$

Due to the unknown dynamic behaviour of the safety valve, we have experienced that the pressure drop during dynamic processes is likely to be unstable. Thus, Eq. (7-6) sometimes, such as, during on-off processes, cannot deliver a good prediction. Nevertheless, the safety valve is not a standard component in a refrigerating system. Thus we did not pay too much attention to it. For the dynamic validation of the model in 7.7, the measured pressure drop between the evaporator and compressor will be used anyhow, in order to avoid the uncertainty.

The constant **A** for calculating the heat transfer is determined as 0.0024 (kW/°C).

7.5.2 Constants a, b, c in Eqs. (6.4), (6.9), (6.11)

As the evaporator used in the test plant is a normal air cooler instead of a plant specially for testing heat transfer coefficients, the pipe wall temperature and its distribution cannot be measured. Meanwhile, it is also not possible to exactly measure the heat transfer area, because the length of evaporation region is not known. What we are able to measure are the inlet and outlet temperatures, pressures, humidities and so on. In such a case, we have to presume the other empirical correlations from the literature are correct and only focus on one or two which are the most suspicious. For the time being, Eqs. (6.4), (6.9) and (6.11) need to be validated through our own experiments. On the basis of the 10 test results, we have found that Eq. (6.4) with $a=3.0$ and $b=0.45$ predicts pretty good local heat transfer coefficient in the two-phase flow region in the range of mass flow rate from 30 g/s to 100 g/s. However, these two constants cannot be directly used in Eq. (6.9), because the refrigerant quality is not linearly distributed along the two-phase flow region (see Fig. 7-4). However, a linear distribution of quality is the condition for deriving Eq.(6.8). Thus, different a and b rather than 3.0 and 0.45 have to be adopted. We found $a=2.7$ and $b=0.30$ result in good predictions.

Even though the pressure drop in the evaporator coils is much less than that of the connection line between the evaporator and compressor in the case of the present test plant, it is still important to the behaviour of the TEV as well as the temperature difference for

calculating heat transfer. Therefore, Eq. (6.11) to calculate the pressure drop of the two-phase flow region should be checked also by the experiments. We determined the constant c in Eq. (6.11) as 0.1 according to the above test results.

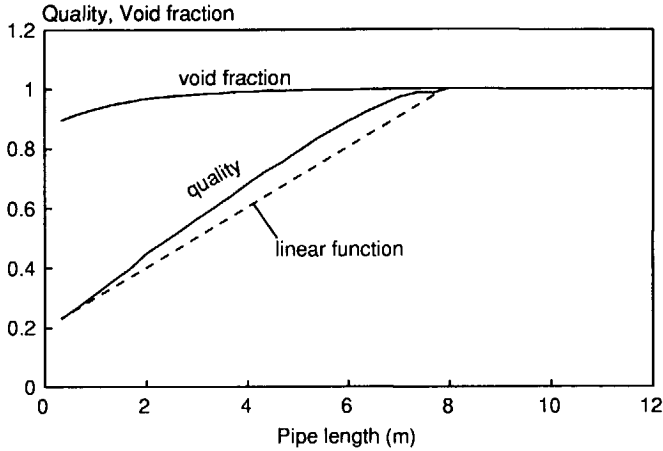


Fig. 7-4 Non-linearly distributed quality and void fraction in an evaporator pipe.

7.5.3 Interfacial momentum-transport coefficient f_i in Eq. (2.9)

The interfacial momentum-transport coefficient f_i mentioned in section 2.5 cannot be determined with the steady-state tests, because the void fraction model (VFM) is not involved in the steady-state model. According to the description in chapter 2, the constant f_i can influence the refrigerant liquid mass content inside the evaporator. Thus, if we use a certain value for f_i and run the dynamic model for a steady-state operation, we can obtain a certain amount of refrigerant liquid content in the evaporator (when the simulation time is long enough). Then we suddenly stop the compressor and switch to the off-period simulation. It is apparent that different amounts of liquid content can lead to different dynamic processes of the off-period, because the times for evaporating the liquid refrigerant in the evaporator are different. By comparing a set of experimental results with on-off periods, we are able to determine a correct f_i . Fig.7-5a shows the influence of different f_i on the dynamic behaviour of the evaporator pressure during an off-period. It can be found that the bigger the interfacial momentum-transport coefficient f_i , the quicker the liquid refrigerant is completely evaporated. A complete evaporation occurs when the refrigerant pressure is lower than the saturated pressure corresponding to the refrigerant temperature. Clearly,

$f_i=300$ is a better experiment-fitting choice (in fact, $f_i=3000$ could be also a possible choice). From Fig. 7-5b, it can be found that f_i does not really affect the on-period dynamic behaviour (all the lines are almost overlapped), when the compressor is suddenly started.

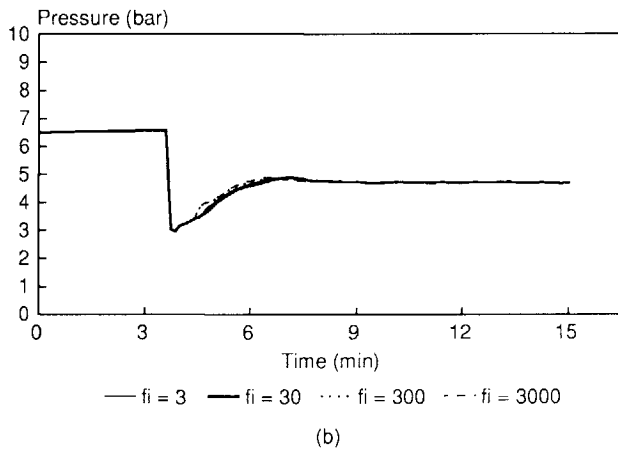
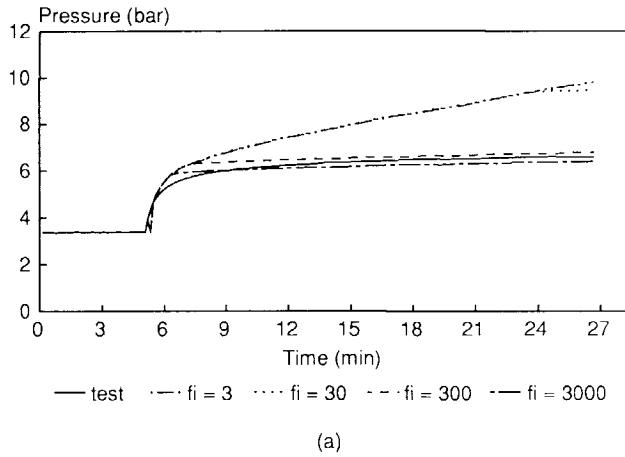


Fig. 7-5 Effects of different interfacial momentum-transport coefficient f_i on the pressure behaviour of evaporator during off- and on- periods. a) from on-period to off-period; b) from off-period to on-period.

7.6 Validation of the steady-state model

The steady-state model as an initial program for the dynamic model has been validated with 6 series of tests which have quite wide operational ranges. The comparison between the simulations and tests is illustrated in Table 7-2. Each of the steady-state tests took about 5 hours with the following parameters kept constant:

- the rotational speed of the compressor
- the mass flow rate of water of the condenser
- the inlet temperature of water of the condenser
- the volume flow of air of the evaporator fans
- the electrical power of the heating in the cold room
- the ambient temperature

Table 7-2 *Steady-state behaviour of the refrigerating system from both simulations and experiments*

		run 1		run 2		run 3		run 4		run 5		run 6	
		test	simu	test	simu	test	simu	test	simu	test	simu	test	simu
Compressor	$T_{r,i}$ (C)	7.00	7.05	15.09	14.48	6.60	7.09	16.60	15.57	2.58	3.74	2.24	3.10
	$T_{r,o}$ (C)	81.12	78.06	60.05	60.39	61.00	62.35	60.37	61.69	60.08	61.37	81.30	78.86
	$P_{r,i}$ (bar)	1.560	1.586	2.617	2.618	2.163	2.221	2.594	2.541	1.485	1.580	1.295	1.340
	$P_{r,o}$ (bar)	8.032	8.192	7.817	7.972	8.139	8.339	7.682	7.860	6.854	7.128	7.892	8.047
	\dot{m}_r (g/s)	72.90	70.80	67.40	65.58	51.20	52.99	64.20	62.73	33.30	35.96	54.60	54.83
	W (kw)	3.724	3.399	1.693	1.964	1.838	1.922	1.726	1.924	1.491	1.523	3.129	2.906
	η_{vol}		0.723		0.840		0.794		0.837		0.754		0.692
	η_{ad}		0.709		0.751		0.733		0.750		0.719		0.700
	RMP (1/min)	1465.0	1465.0	712.0	712.0	704.2	704.2	711.0	711.0	704.6	704.6	1389.0	1389.0
Condenser	$T_{r,i}$ (C)	81.12	78.06	60.05	60.39	61.00	62.35	60.37	61.69	60.08	61.37	81.30	78.86
	$T_{r,o}$ (C)	28.39	30.72	28.30	29.78	29.39	31.47	28.00	29.33	24.90	26.40	27.74	30.20
	T_{mv} (C)		54.44		45.04		45.20		45.10		39.44		51.74
	T_c (C)		32.05		31.06		33.09		30.53		27.16		31.58
	P_c (bar)	7.747	7.856	7.540	7.656	7.906	8.069	7.405	7.551	6.662	6.905	7.656	7.760
	\dot{Q}_{con} (kw/m C)		7.578		8.115		9.865		8.111		9.854		8.923
	\dot{Q}_{sub} (kw/m C)		0.0349		0.0328		0.0277		0.0317		0.0203		0.0284
	H_{liq} (m)	3.90	3.90		0.039	0.039	0.039	0.039	0.039	0.039	0.039	0.039	0.039
	\dot{Q}_c (kw)		11.94		10.30		8.282		9.947		5.827		9.308
	$M_{r,i}$ (kg)		8.112		8.134		8.093		8.145		8.213		8.124
	$M_{r,v}$ (kg)		3.377		3.432		3.650		3.376		3.129		3.373
	$T_{w,i}$ (C)	22.24	22.24	21.69	21.69	20.50	20.50	22.01	22.01	22.10	22.10	20.95	20.95
	$T_{w,o}$ (C)	32.44	31.80	31.23	30.84	32.74	32.93	30.60	30.12	26.70	27.03	31.67	31.39
	\dot{m}_w (g/s)	296.0	296.0	268.0	268.0	158.0	158.0	285.0	285.0	283.0	283.0	212.0	212.0
	\dot{Q}_w (kw/m C)		2.525		2.311		1.545		2.415		2.325		1.926
	$T_{p,6}$ (C)		32.02		31.04		33.08		30.51		27.15		31.57
	$T_{p,1}$ (C)		31.25		30.39		32.51		29.89		26.85		30.96
TEV	$T_{r,i}$ (C)	27.30	28.02	27.70	26.78	27.79	28.69	27.40	26.47	23.20	25.21	26.34	29.34
	$T_{r,o}$ (C)	-1.10	-0.43	5.80	6.09	-1.28	-0.53	7.78	7.51	-12.68	-11.12	-7.87	-6.93
	$P_{r,i}$ (bar)	7.462	7.547	7.262	7.361	7.673	7.808	7.128	7.264	6.469	6.699	7.419	7.495
	$P_{r,o}$ (bar)	2.974	3.041	3.716	3.750	2.957	3.031	3.952	3.920	1.988	2.104	2.361	2.440
	\dot{m}_r (g/s)	72.90	71.29	67.40	65.74	51.20	52.87	64.20	62.72	33.30	36.32	54.60	54.94
	DTSS	21.29	21.29	19.48	19.48	17.87	17.87	19.78	19.78	22.03	22.03	21.40	21.40

To be continued

Continuing

		run 1		run 2		run 3		run 4		run 5		run 6	
		test	simu	test	simu	test	simu	test	simu	test	simu	test	simu
Evaporator	$T_{r,i}$ (C)	-6.89	-6.48	3.96	4.00	-3.93	-3.19	6.56	5.93	15.28	-13.72	-13.46	-13.41
	$T_{r,o}$ (C)	7.63	7.78	16.15	15.86	5.98	6.68	18.82	17.91	0.28	1.67	1.46	2.35
	$P_{r,i}$ (bar)	2.444	2.478	3.506	3.511	2.705	2.774	3.805	3.731	1.806	1.913	1.932	1.936
	$P_{r,o}$ (bar)	2.113	2.139	3.271	3.272	2.502	2.560	3.581	3.528	1.636	1.731	1.658	1.703
	$\alpha_{2,ph}$ (kw/m C)		0.603		0.551		0.470		0.528		0.157		0.494
	$\alpha_{1,ph}$ (kw/m C)		0.179		0.174		0.142		0.169		0.0102		0.144
	L_{evap} (m)		6.274		8.602		8.636		8.608		9.119		4.782
	$T_{a,i}$ (C)	12.28	12.18	20.30	19.92	9.12	9.49	22.86	21.89	3.26	3.28	5.06	6.22
	$T_{a,o}$ (C)	5.44	5.73	13.97	13.34	4.50	4.88	16.21	15.30	0.38	0.19	-0.01	1.10
	$\phi_{a,i}$ (%)	35.05	34.43	41.52	40.62	49.63	47.34	41.74	43.46	54.89	54.69	42.13	38.51
	$\phi_{a,o}$ (%)	55.81	53.22	61.98	61.66	66.34	64.86	63.10	65.58	67.52	68.26	58.25	55.23
	$\alpha_{a,s}$ (kw/m C)		0.508		0.501		0.511		0.499		0.516		0.514
	δ_{fr} (m)	0.000	0.000	0.000	0.000	0.000	0.000	0.000	0.000	0.000	0.000	0.000	0.000
	\dot{V}_a (m/s)	1.172	1.172	1.172	1.172	1.172	1.172	1.172	1.172	1.172	1.172	1.172	1.172
	\dot{Q}_a (kw)		9.197		8.603		6.951		8.279		4.607		7.563
Room	\dot{Q}_{heat} (kw)	9.046	9.145	9.046	9.489	6.196	6.581	9.046	9.379	3.276	4.408	6.196	7.220
	$T_{w,in}$ (C)		12.67		20.07		10.20		21.86		4.19		7.13
	$T_{w,out}$ (C)		18.93		21.87		18.88		22.77		15.13		18.45
	T_{ab} (C)	24.60	24.60	23.50	23.50	26.75	26.75	23.60	23.60	25.05	25.05	28.70	28.70

The real measurement time was however 10 minutes during which the datalogue sampled once every 8 seconds. The averaged values of the samples were taken as the final measurement results. As there was no special water supply to humidify the inside air of the cold room, the air was almost dry after 5 hours of refrigeration. Thus no water condensation took place on the outside surface of the evaporator. No water supply was installed because real products generating water vapour were impossible to be used in the laboratory (deteriorating too quickly) and dummy products were too expensive. This was accepted for lack of time. The model is, in fact, able to solve instantaneous heat and moisture transfer, but could not be validated for the latter. Thus further investigations and tests are necessary. Moreover, frost-formation was avoided in the experiments since the model temporarily cannot yet tackle it.

The steady-state simulations were carried out corresponding to the experiments on a SUN workstation (386i). For one complete simulation, it needs ± 20 minutes of CPU with the iteration accuracy: 0.1 °C for temperature; 0.05 bar for pressure; 1.e-4 kg/kg for absolute humidity; and 1.0% for energy balance. Generally speaking, the simulation results are in pretty good agreement with the experimental ones. The several relatively obvious disagreements can be explained as follows.

- The predicted compressor shaft power as shown in Table 7-2 is $\pm 10\%$ different from the measured. There could be two reasons for it: a) the fitted performance curve for the compressor based on the experimental results might be not accurate enough; b) the assumption,

that the adiabatic shaft power efficiency is only dependent on pressure ratio, is not very true. The details on the compressor modelling can be found in Appendix 1.

- The predicted subcooling temperature is higher than the measured by ± 2 °C. This deviation can be explained by the low refrigerant side heat transfer coefficient.
- The predicted refrigeration capacity of the evaporator is sometimes different from the predicted heat load of the cold room. The reason is that the iterative convergence in steady-state simulations is controlled by checking the temperature difference (0.1 °C check accuracy, see chapter 4) in the model. Although 0.1 °C is quite small for temperature, its effect on the air side heat balance is still considerable. Therefore, it is suggested to directly check the air side heat balance to control the convergence for steady-state simulations.
- The predicted heat load for the cold room is higher than the measured specially when the air temperature is very low, because the heat leakage through the room walls is not taken into account in the experiments. However, under very low inside temperatures, this amount of heat is quite considerable.

7.7 Validation of the dynamic model

One of the most effective methods to check a dynamic model is to compare the responses of the system to a *step change* stimulus from both simulations and experiments. The step changes should be practically typical to the concerned system. In the case of refrigerating systems, four types of step change are interesting:

- a) step change of the rotational speed of compressor
- b) turn-off of the system
- c) turn-on of the system
- d) step change of the heat load supplied to the system

These step changes are the basic elements encountered in the commonly used refrigeration control systems, such as, on-off, multi-stage variation of RPM, continuous variation of RPM. Therefore if our model is able to pass the validations with all the types of step changes mentioned above, it can be applied to study the system performance under non-steady-state conditions with variable refrigeration loads and control devices.

In the following figures, the fitted curve for the compressor shaft power is not used to calculate the C.O.P., because of its inaccuracy in the lower region. Instead, the measured values are used for the purpose.

A step increase of the rotational speed of the compressor

The first test for the validation of the dynamic model is one with a step increase of the rotational speed of the compressor. This step change was realised with the help of a potential meter connected to the power line of the compressor motor. The changed value of the rotational speed was measured by the PHILIPS timer meter (see section 7.4). To avoid the disturbances from the previous non-steady-state conditions, the system was operated under a constant surrounding condition for 5 hours until a steady-state was reached. After about 5 minutes of recording the steady-state conditions, the step change was imposed and the dynamic behaviour was recorded by the datalogue every 8 seconds. The measurement lasted about half an hour.

Similar to the test, the simulation was started with a pre-prediction by using the steady-state model in order to obtain a good initial condition for the dynamic model. Then the dynamic model was initiated under the same surrounding conditions, that is, to simulate a steady-state operation using the dynamic model. Such a simulation was carried on until the non-steady-state behaviour disappeared. At the very moment, the same step change of the rotational speed of the compressor as during the test was imposed to the simulation. In order to save the computational times, different integration time increments were adopted for the components. For example, a time step of 8 seconds was used for the cold room, because it has relatively slower transient behaviour. And 1.6 seconds was used for the evaporator, while 0.2 second was for the condenser. The reason that the smallest time step was applied to the condenser was because of the specific operation conditions of the condenser. It was found that the last several water passes of the condenser had a pipe wall temperature very close to the condensation temperature. Thus if a too big time step had been used, the pipe wall temperature would have been higher than the condensation temperature and there would be no condensation occurring on these pipes. This phenomenon would lead to an instability of the simulation.

Fig.7-6 presents the experiment and simulation results. The step change of the rotational speed of the compressor was from 712 (1/min) to 1463 (1/min). The heat transfer of the evaporator Q_{evap} was calculated based on the inlet and outlet temperature difference of the air. The heat transfer of the condenser Q_{cond} was according to the inlet and outlet temperature difference of the cooling water. Accordingly the C.O.P shown in the figure is of the air-side.

The comparison of the test and simulation results shows a rather good agreement. However, some deviations can be seen either. For instance, the predicted inlet refrigerant temperature of the evaporator is different from the experiment by almost 4 °C and the simulated discharge temperature of the compressor has much quicker behaviour. The air of the evaporator also

behaves faster than the reality. All these deviations can be explained with the following arguments:

- After the step change of the compressor RPM, the mass flow rate of refrigerant inside the evaporator coil is already beyond the validation range of correlation (6.4), so that the predicted heat transfer coefficient is bigger and accordingly the evaporation temperature is higher.
- The compressor is considered as an instantaneous element in the model, that means it has no heat capacity. However, in practice the compressor is built up with quite a lot of metal which can store heat. Its transient behaviour would make the refrigerant temperature at discharge react slowly, when the RPM is suddenly increased.
- The thermal masses of the evaporator, such as, those of the coils and fins, are smaller in the model than in reality. Thus the response of the air to the step change of RPM is too fast.

A step decrease of the rotational speed of the compressor

This test is just an opposite situation of the first one. The experimental procedure is exactly the same as above, only except that the rotational speed of the compressor was changed from 1465 (1/min) to 707 (1/min). Fig. 7-7 shows the comparison between the experiment and simulation. As the variation of the mass flow rate is within the validation range of eq. (5.6), the predicted evaporation temperature is in pretty good agreement with the test. The reasons for the other deviations could be the same as above.

Turn-off and Turn-on of the compressor

This test is a combination of two step changes. Therefore it took longer time (about 3 quarters of an hour) than the others. The preparation for this test was the same as above. However, at the moment when the recording time was about 5 minutes, the compressor was forced to stop. At the same time the solenoid-valve (No.11 in Fig. 7-1) was closed so that there was no mass exchange between the low and high pressure sides. Nevertheless, the water supply to the condenser, the fans on the evaporator, as well as the heating were continuously in operation. The off-period took about 25 minutes and then the compressor was started again. At time = 42 minutes, the whole experiment was stopped.

The simulation of on-off operations is the most difficult, because the variations of the thermodynamic state of the system are very sharp. Such steeply changing behaviour of the system necessities a very careful consideration of the integration time step of simulation. Not only the implementation of the model is difficult, but also the realisation of the

experiment is not so easy, because, during the very short time of turn-on, some devices operates abnormally. For instance, the safety valve produces quite larger pressure drop after a turn-on than it works under steady-state conditions. Another uncertainty is the solenoid-valve between the condenser and TEV, which probably does not open instantaneously after a sudden turn-on. However, the dynamic behaviour of these auxiliary devices are not taken into account in the model. Therefore, the discrepancy of the simulation from the test (see Fig. 7-8) are not easy to explain. Nonetheless, one phenomenon can still be explained, that is, the C.O.P difference between the simulation and test at the beginning of the on-period. As the evaporator thermal mass is too small in the model, the refrigerant temperature decrease at the beginning of the on-period is immediately transferred to the air side, so that the air temperature also drops down and the air side C.O.P is higher, according to the model. But in practice the refrigerant temperature decrease cannot be felt by the air so quickly due to the large thermal mass of the evaporator. Thus the experimental C.O.P is lower than the simulated one. The effect of a small thermal mass of the evaporator can also be seen at the beginning of the off-period. Because of the quick response of the air to the refrigerant side change, the refrigeration capacity at the beginning of the off-period is smaller than that of the test. However, the smaller refrigeration capacity at the beginning of the off-period is compensated by the larger one of the on-period. Therefore, the average C.O.P over a long time, during which many on-off cycles take place, might not differ in the simulation and test.

A step increase of the heat load

To emulate the real situations in refrigerated stores, where the heat loads change with the input and output of products, a step change of the heat load was adopted. The realisation of this step change was through changing the electrical supply to the heating (No.6 in Fig. 7-2) from 3.116 kw to 8.886 kw. In this case, the walls of the cold room play an important role, because the room is almost empty. Thus, when the air temperature is higher than the wall temperatures, the walls could refrigerate. Fig.7-9 shows the comparison between the simulation and test. The existing difference of the evaporation temperature is also due to the small evaporator thermal mass. The deviation of the mass flow rate is then because of the incorrect evaporation temperature.

A step decrease of the heat load

Fig. 7-10 is the results related to a step decrease of the heat load. It can be found that the same problems, as in the case of a step increase of the heat load, appear in the simulation results. Thus the explanation is of the same.

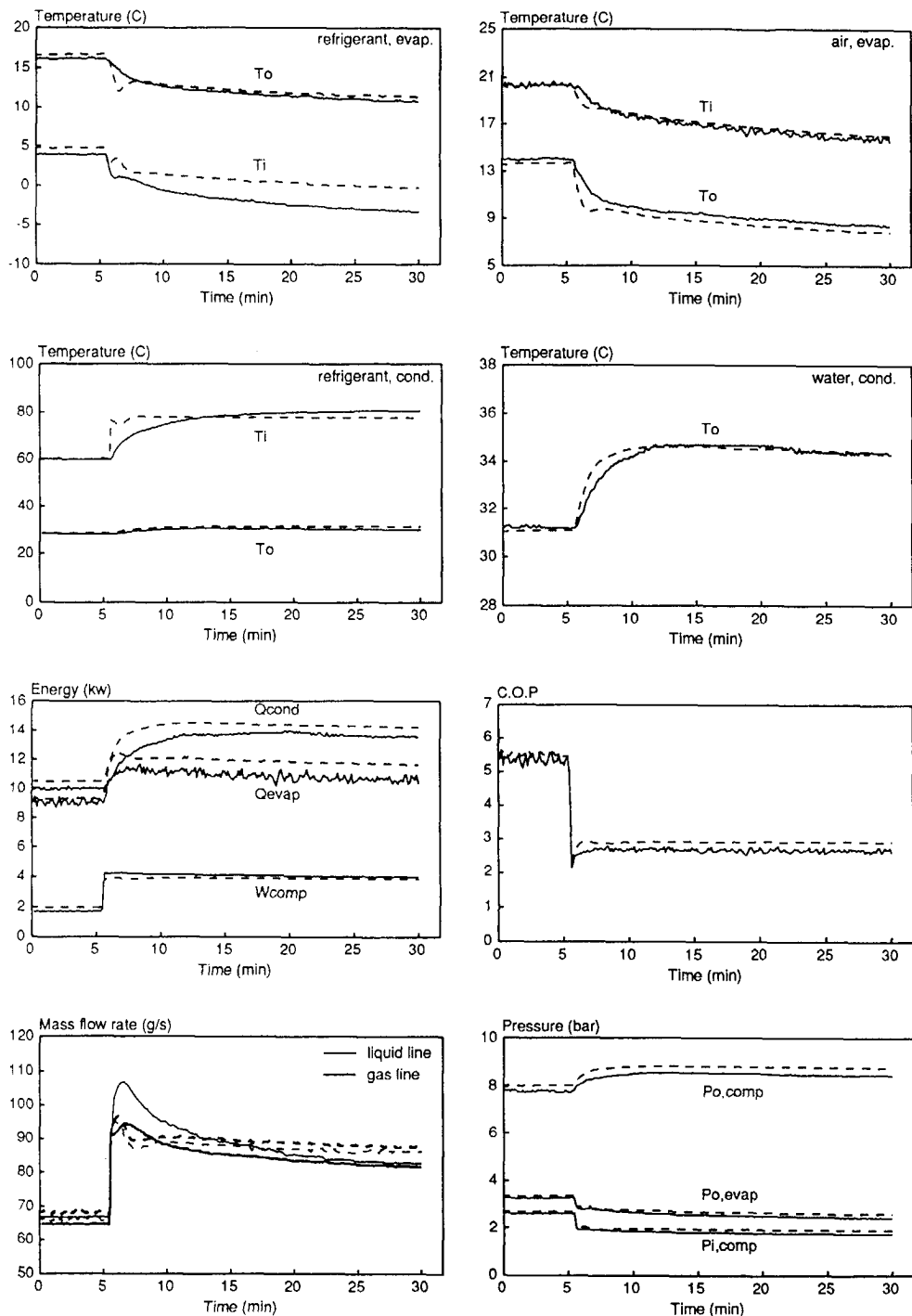


Fig. 7-6 Dynamic behaviour of the system in response to a step increase of the compressor RPM from 712 to 1463. The solid lines are all from the experiments and the broken lines are all from the simulations.

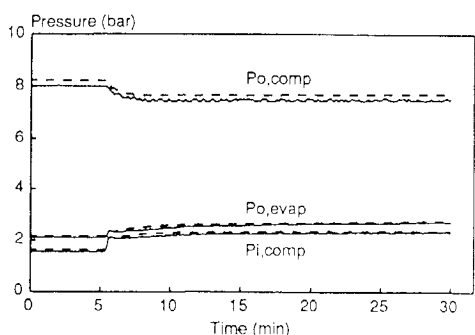
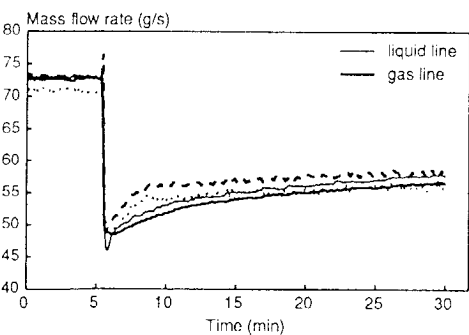
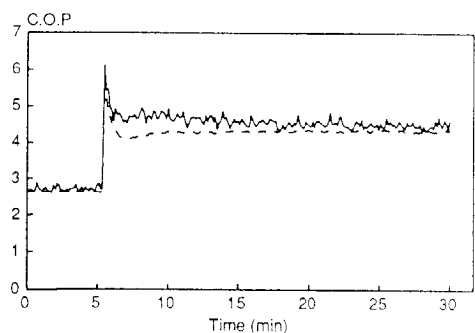
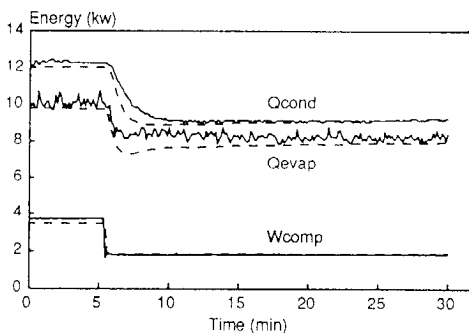
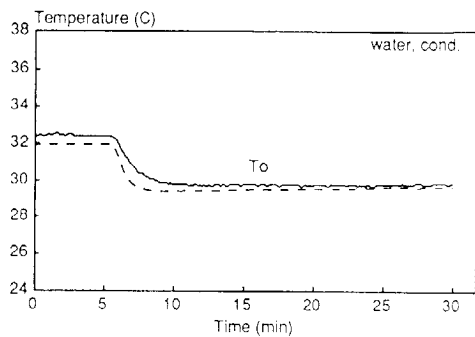
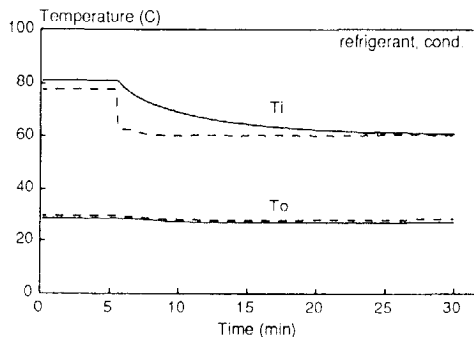
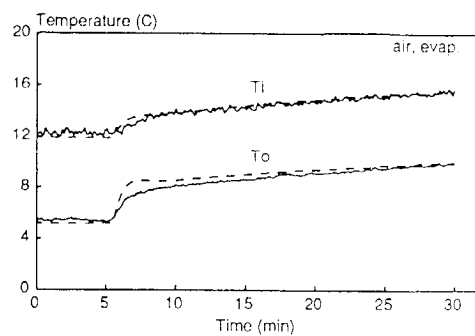
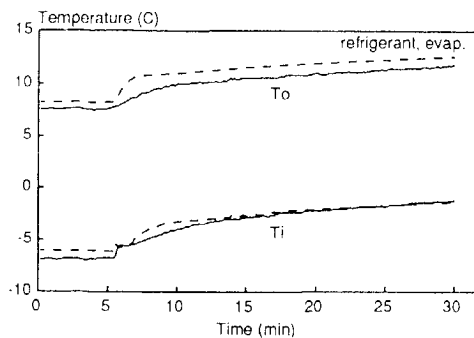


Fig. 7-7 Dynamic behaviour of the system in response to a step decrease of the compressor RPM from 1465 to 707. The solid lines are all from the experiments and the broken lines are all from the simulations.

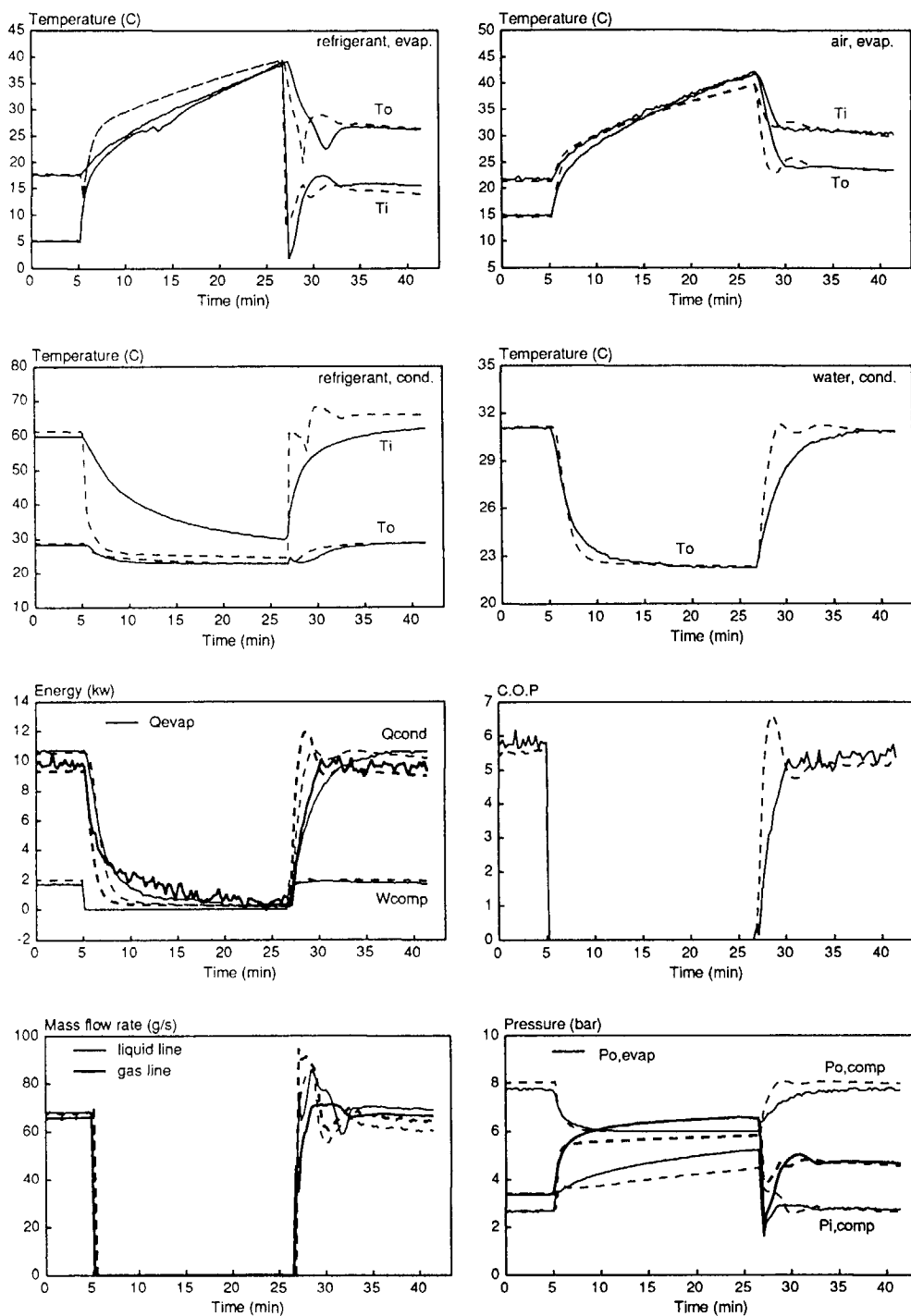


Fig. 7-8 Dynamic behaviour of the system during an on-off cycle. The solid lines are all from the experiments and the broken lines are all from the simulations.

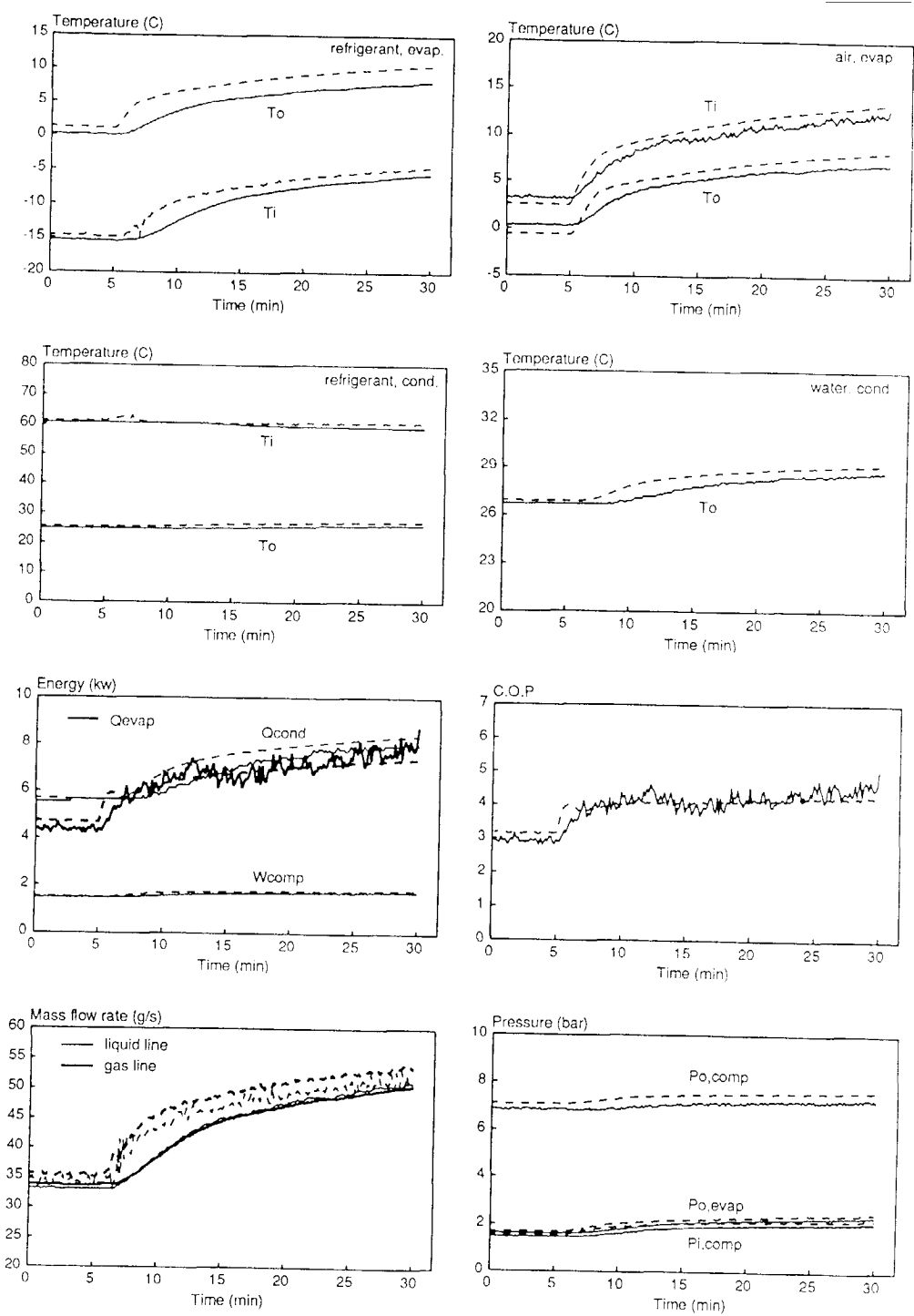


Fig. 7-9

Dynamic behaviour of the system in response to a step increase of the heat load from 3.116 kw to 8.886 kw. The solid lines are all from the experiments and the broken lines are all from the simulations.

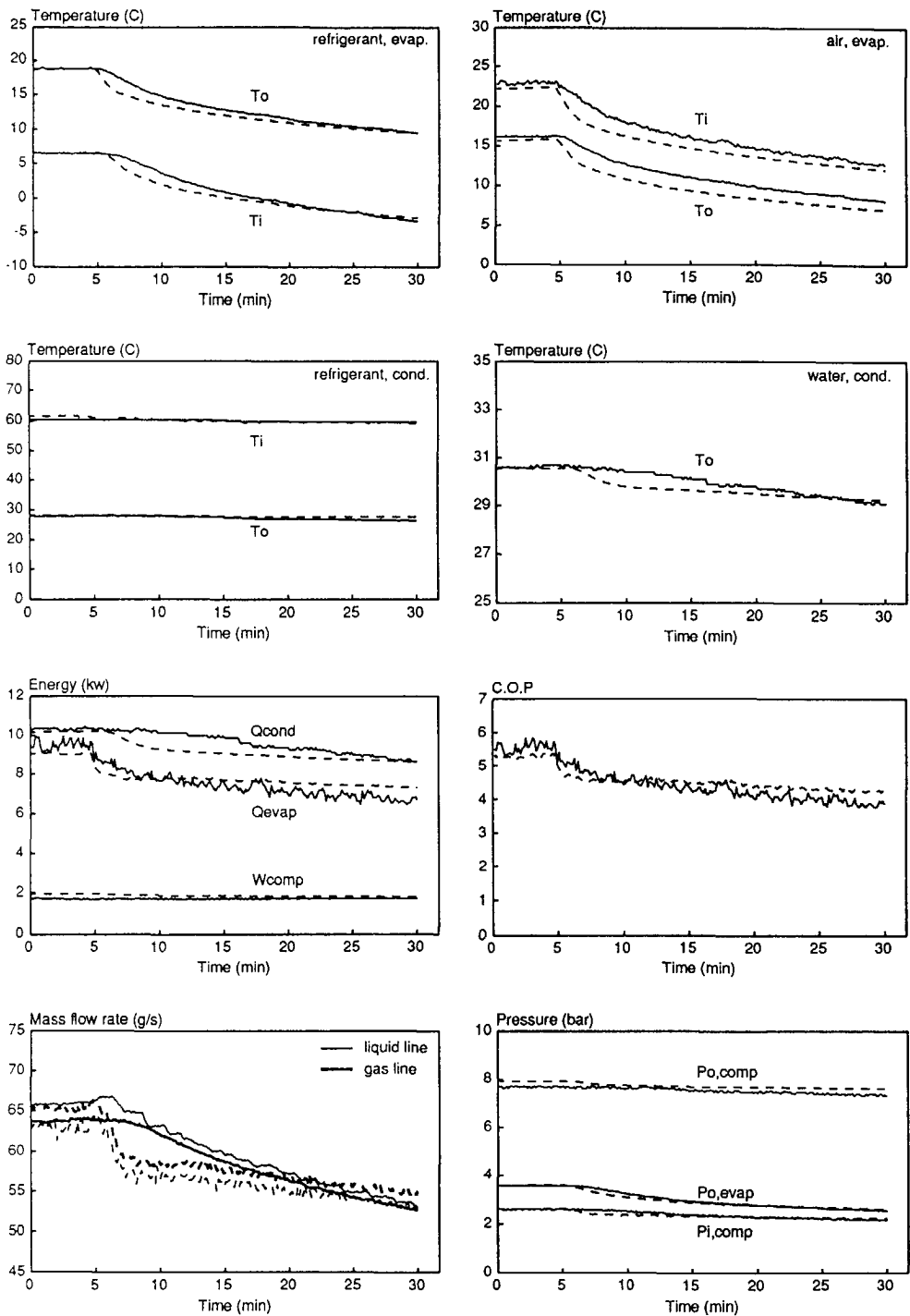


Fig. 7-10 Dynamic behaviour of the system in response to a step decrease of the heat load from 8.886 kw to 3.116 kw. The solid lines are all from the experiments and the broken lines are all from the simulations.

7.8 Validation of the air flow model (PHOENICS)

To predict the air flow pattern in the cold room, the standard computer package PHEONICS has been applied. Although this software is widely used in the world today, a specific application of it, for instance, to the cold room, still needs more data as well as validation, because the definition of a concrete problem, which possesses a lot of assumptions in order to approach the physical object with mathematical equations, is independent of the computer package itself. For example, in our case, we assumed the air flow pattern is dominated by forced convection. However, whether or not this assumption is correct should be checked with experiments. Besides, to implement PHOENICS, some of the boundary conditions have to be determined through experiments. What is concerned at present is the turbulence intensity of the fans on the evaporator. These two reasons formed the initiative of the air velocity measurements.

Fig. 7-11 illustrates the dimensions of the cold room of the test plant (see Fig. 7-1). As the purpose was to validate the model, the room was not loaded with real products. The emptiness of the room facilitated the measurements very much, because positioning the anemometer became very easy.

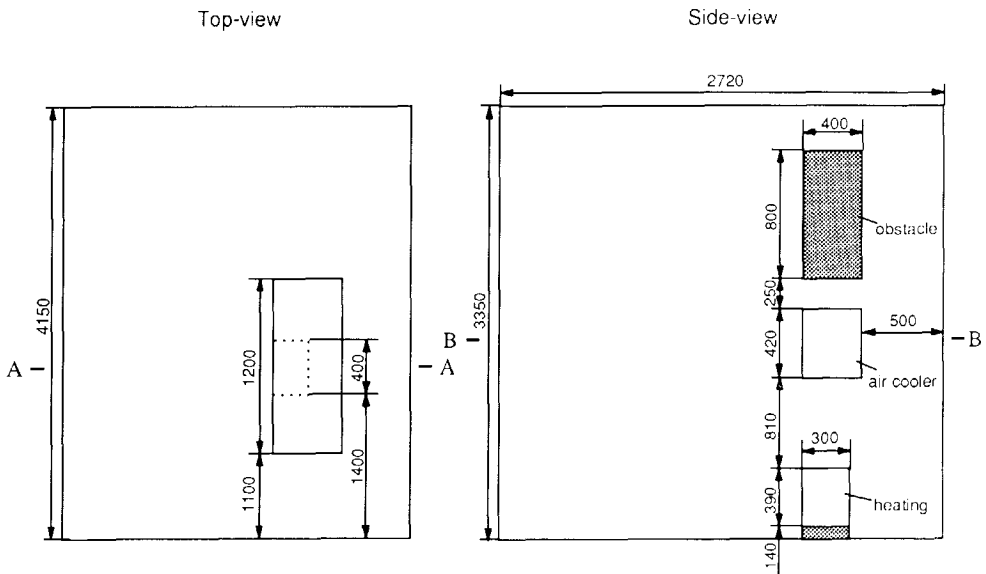


Fig. 7-11 Dimensions of the cold room

7.8.1 Measurement of the turbulence intensity produced by the evaporator fans

The air cooler evaporators are usually assembled with propeller fans behind the coils and fins. The number of fans is dependent on the capacity of the air cooler. The concerned evaporator possesses two fans with outside diameter 30 cm. Its catalogued air volume flow is 5240 m³ /hour. Since the fans are composed of several blades which are not in the form of stream line, the turbulence of the air flow produced by them is rather intensive, which is however dampened by the plate-fins and coiled pipes. Because the air cooler was treated as a block as a whole in the model, the turbulence intensity was measured immediately after the fins instead of internally.

The turbulence intensity of an air flow is usually represented by two parameters: turbulent kinetic energy: k , dissipation rate of k : ϵ . In fluid mechanics, k is defined as follows,

$$k = \frac{1}{2} \overline{u_i' u_i'} \quad (7.7)$$

where the mean square root deviation of velocity is calculated as below

$$\overline{u_i' u_i'} = \left[\frac{\sum_{i=1}^n (u_i - \bar{u})^2}{n} \right]^{0.5} \quad (7.8)$$

and the time-average velocity is

$$\bar{u} = \frac{\sum_{i=1}^n u_i}{n} \quad (7.9)$$

Technically, the instantaneous velocity u can be measured with a hot wire anemometer, provided that the sampling frequency is quick enough. Nevertheless, a normal hot wire anemometer can only measure the absolute velocity: $U = [u_x^2 + u_y^2 + u_z^2]^{0.5}$. Thus an

approximation has to be made toward Eq. (7.7), that is, $k = 0.5 \overline{U' U'}$.

The definition of ϵ is given below:

$$\varepsilon = \nu \left(\overline{\frac{\partial u'_i}{\partial x_j} \frac{\partial u'_i}{\partial x_j}} + \frac{\partial u'_i}{\partial x_j} \frac{\partial u'_i}{\partial x_j} \right) \quad (7.10)$$

From the above equation, it is found that a direct measurement of ε is technically very difficult, because the velocity gradient is hardly measurable. Therefore, we adopted an indirect measurement of ε value, that is to make use of the Prandtl's mixing length concept. Between k , ε and the Prandtl's mixing length l , there is a correlation (see [7.2])

$$\varepsilon = C_{\mu} \frac{k^{3/2}}{l} \quad (7.11)$$

where $C_{\mu} = 0.09$ and $l = 0.09H$ for a plane jet (H is the jet width).

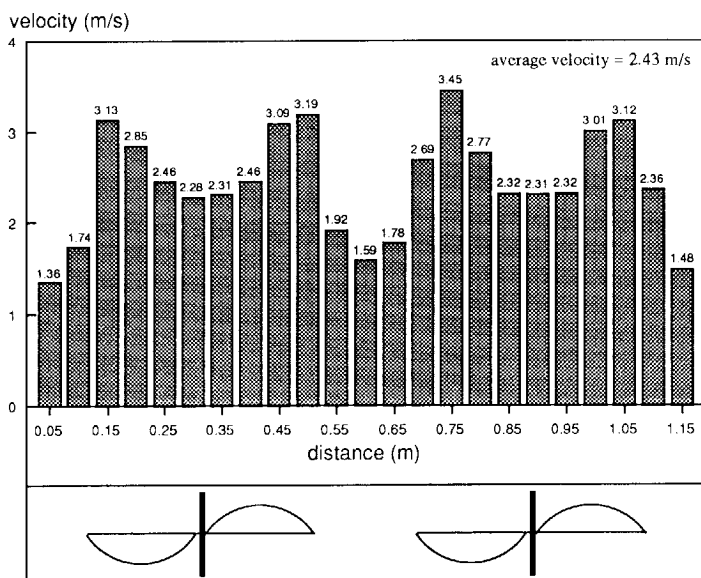


Fig. 7-12 Velocity distribution along the air cooler.

Because we are able to measure k and the height of the air cooler can be taken as H , ϵ is thus easily obtained with Eq. (7.11).

During our experiment, we used a sampling frequency of 250 (1/second). Fig. 7-12 shows the time-average velocity distribution along the air cooler and Fig. 7-13 gives the instantaneous velocity. Based on the measured results, the k and ϵ values as well as the average velocity were calculated.

$$k = 0.1266 = 0.0214 \bar{U}^2 ; \quad \epsilon = 0.1958 = 0.0136 \bar{U}^3 ; \quad \bar{U} = 2.43$$

where \bar{U} is the average value of velocity calculated from Fig. 7-2.

Besides the air cooler, the fan of the heating was also measured with the following results

$$k = 0.3586 = 0.0734 \bar{U}^2 ; \quad \epsilon = 1.0226 = 0.0947 \bar{U}^3 ; \quad \bar{U} = 2.21$$

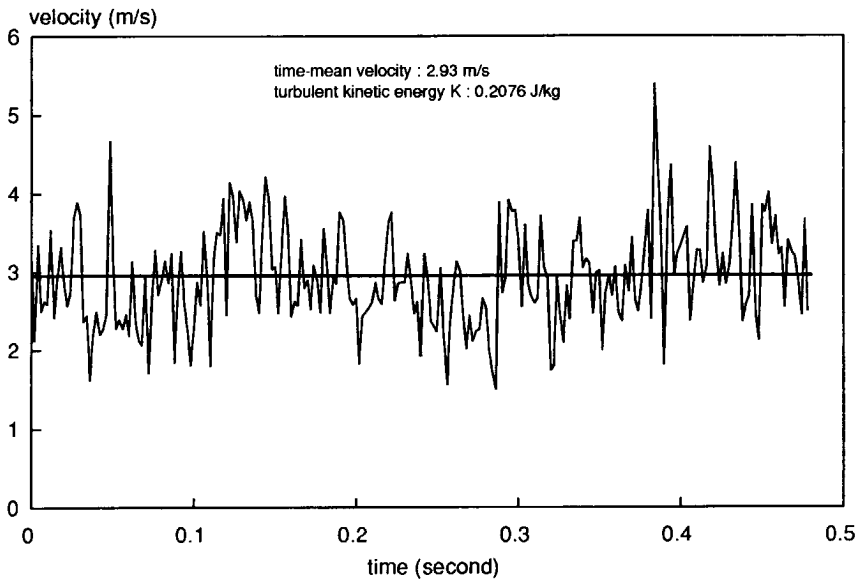


Fig. 7-13 Instantaneous velocity at the outlet of air cooler.

7.8.2 Measurement of the air flow

The air flow pattern in the cold room is actually in three dimensions. Measurement of a 3-d air flow costs a lot of efforts. Thus we attempted to measure the velocities on one "slab" of the room and to limit the measurement within 2 dimensions. However, because the anemometer we used is of a conventional type and has a characteristic of direction-dependency. Fig. 7-14 illustrates the effect of the angle between the hot wire and velocity on the output signal. It can be found that the anemometer gives a maximum output when it is perpendicular to the velocity. If the velocity is parallel with the hot wire, the output signal is zero. In other words, the anemometer always measures the module of two components of a velocity, which are perpendicular to the hot wire, and the contribution of the third component to the output is always zero. Therefore, we had to position the anemometer so carefully that it crossed the selected "slab" by 90° .

We chose plane A-A in Fig. 7-11 as the measurement "slab", because it most likely represents the main flow pattern in the room. The measurement was carried out with moving the anemometer from one point to another and totally 59 points were scanned. The integration time to obtain time-mean velocities was 300 seconds. Fig. 7-15 shows the test results (the upper figures) as well as the positions of the measurement points.

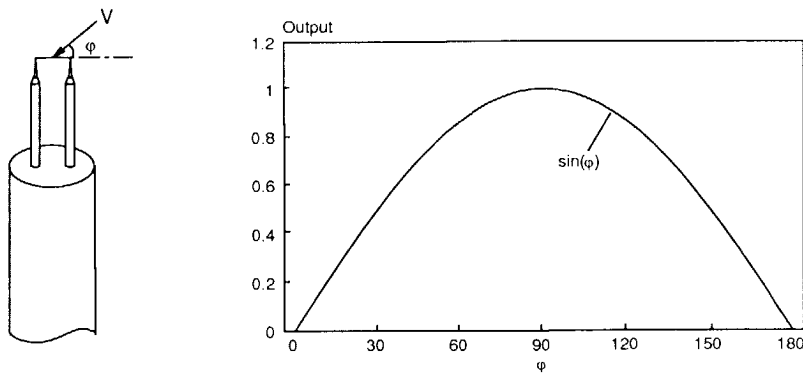


Fig. 7-14 Characteristic of the anemometer.

The simulation was made by applying the PHOENICS package on a SUN 386. The cold room was modelled as a 3-d flow problem. The measured velocities and turbulent intensities at the air cooler and heating were directly used as the boundary conditions. The wall boundary conditions were exactly the same as stated in chapter 5. The grid division was $20 \times 24 \times 20$ with

non-linear distribution (power function) near to the walls. Fig. 7-16 gives the simulation results: velocity distribution on planes A-A and B-B in Fig. 7-11. To compare the simulation result with the measurement, the velocity modules on plane A-A were calculated from the PHOENICS output file. They are also shown in Fig. 7-15 (the figures beneath the test results).

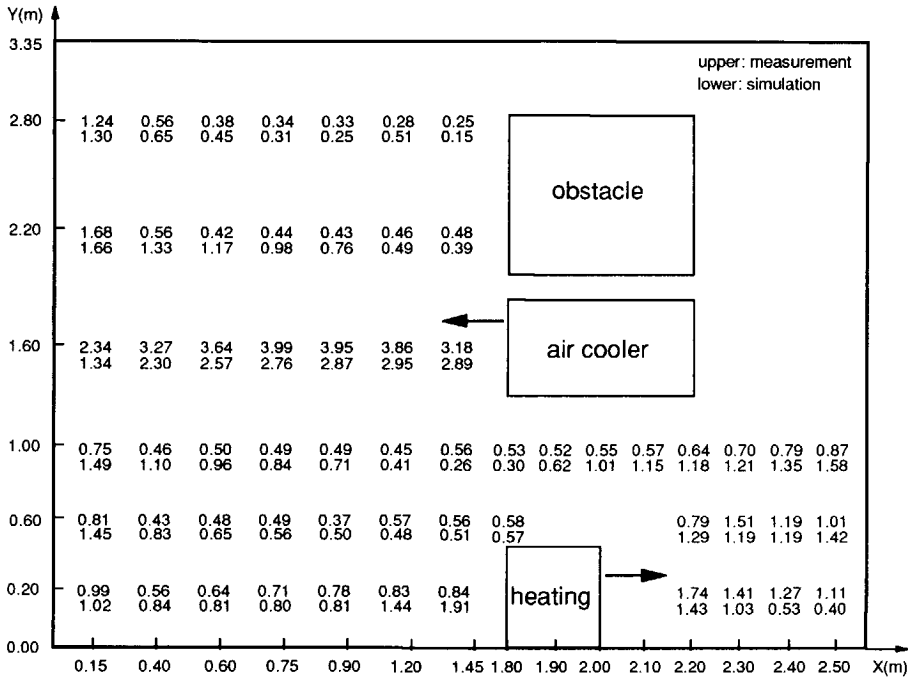


Fig. 7-15 Velocity distributions in the cold room from the measurement and simulation.

From Fig. 7-15, we can find that the main flow pattern shows an agreement between the simulation and measurement. However, the concrete figures still deviates from each other, at some points, even considerably. There are several reasons to explain:

- The averaged velocities along the air cooler as well as the heating were used as the boundary conditions. However, as demonstrated in Fig. 7-12, they are unevenly distributed and the maximum and minimum values are different by more than 2 m/s. Although plane A-A seems to

be in the middle of the air cooler, the measured velocity at height of 1.6 m are higher than the average value (2.43 m/s), due to the momentum transfer from the neighboring flow.

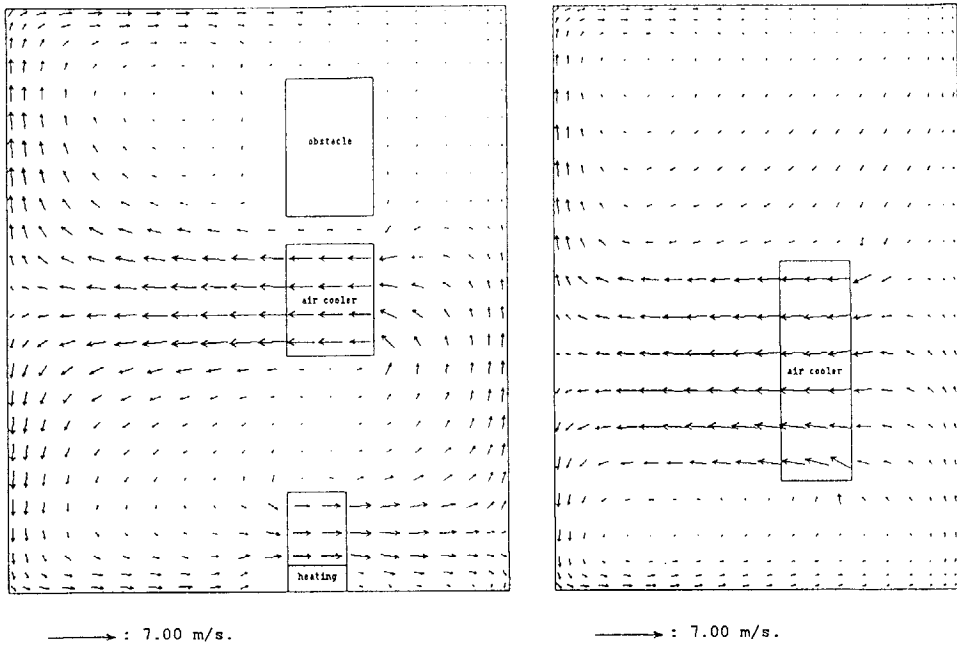


Fig. 7-16 PHOENICS simulation output. left: flow pattern on plane A-A; right: flow pattern on plane B-B (see Fig. 7-11).

- The dimensions and positions of the air cooler, heating and obstacle are not exactly identical in the model and in the reality. This is because the definition of an object in PHOENICS is on the basis of grids. An exact fitting to the reality is in fact impossible.
- The turbulence model (k- ϵ model) adopted by PHOENICS is not 100% reliable.
- There may be a lot of small eddies in the air flow, which might influence the measurement. Because the hot wire is very small, sometimes even smaller than the eddies themselves, it could be located somewhere inside the eddies and then give the very local velocities instead of the main stream velocities.

From this point of view, we may draw a conclusion that PHOENICS can successfully predict the main flow patterns in case of refrigerated rooms, but cannot deliver exact velocity values everywhere in a flow domain. Therefore, attempts to achieve a numerical agreement between simulation and experiment seem to be impossible. It also has to be pointed out that a good application of PHOENICS to a refrigerated room requires the air cooler to be experimentally studied in details, with the emphasis on its turbulence intensity and velocity distribution.

References

- 7.1 **Van der Meer, J.S.** "Simulation of a refrigerant evaporator", Ph.D. Thesis, Delft University of Technology, the Netherlands, October 1987.
- 7.2 **Markatos, N.C.** "The mathematical modelling of turbulent flows", *Encyclopaedia of Fluid Mechanics*, Vol.6, 1985, Gulf Publishing Co..

Chapter
EIGHT
Applications of the Models

8.1 General

As soon as a model is established and validated, it can be used as a flexible "test plant", on which various "experiments" or ideas can be realized. Such an "experimental" manner has a lot of advantages over a real field experiment, such as, economical, flexible, etc.

In the field of refrigeration, the use of mathematical models and computer simulations as aids in design and optimization is now increasing. The development started with compressor models (excellently recorded in [8.1]). Then models have been proposed for components such as evaporators, condensers and also even for complete refrigerating systems. The majority of such models are steady-state simulation models for design or selection of components. However, a minority of them allow non-steady-state simulations and the number and importance of these models are growing.

Following the validation in chapter 7, this chapter is intended to describe the applications of the models which have been described in chapters 2, 3, 4, 5. In principle, the models could be used for many purposes related to design and optimization. However, hereafter only two interesting examples will be given, which are:

- a) Prediction of the steady-state distribution of air velocity, temperature and humidity in a cold store, by using the distributed refrigerated room model;
- b) Study of system C.O.P with different capacity control systems, by using the dynamic models of the evaporator, condenser and refrigerated room, as well as the simple steady-state models of the TEV and compressor; the latter will be described in the appendices.

8.2 Prediction of the steady-state distribution of the air velocity, temperature and humidity in a cold store

As a branch of refrigeration applications, refrigerated storage and transportation of perishable foods play an important role in human daily life. Especially in the countries, such as the Netherlands where $\pm 10\%$ of the national income are from the production, processing and transport of agricultural products, the refrigeration applications in this area are very widespread (see [8.2]). Cold stores are however the basic elements in the distribution processes of agricultural products from producers and consumers. Thus the investigations on this subject are very significant.

One of the main problems concerned with a cold store is about how to achieve an even distribution of air quality inside. Generally speaking, air quality implies the temperature, humidity, CO_2 and O_2 concentrations of air. If the air distribution is not satisfactory and the air quality somewhere in the store is bad, the stored products may deteriorate quickly. Therefore many technical measures, such as false ceiling, pressure walls and staggered pallets (see [8.3], [8.4]), have been adopted to improve the air distributions. However, using advanced mathematical models to study this problem is just a recent event. **Van Gerwen and Oort** [8.5] tried to use PHOENICS to optimize cold stores, for example, determining the resistance coefficient of pressure wall, the air cooler flow rate, the position of air cooler, etc. Some practical improvements toward better air distribution and less energy consumption have been attained. As another contribution to this area, we have used the model developed in chapter 5 to predict the steady-state distribution of air velocity, temperature and humidity in a laboratory cold store.

8.2.1 Problem setting

Description of the cold store

The simulated cold store is a $2.8 \times 2.4 \times 2.0$ (m^3) polyurethane-insulated room which contains 24 wooden boxes with electrical heating mats inside. Fig. 8-1 is a photograph of it and Fig. 8-2 shows its dimensions and the arrangement of the boxes. To produce necessary refrigeration, a small refrigerating system is also built up with an air cooler located inside the room. The air cooler has three propeller fans behind, to re-circulate the air through and around the boxes.

Boundary conditions (steady-state):

- air velocity at the outlet of the air cooler: V_o 4.0 m/s
- air relative humidity at the outlet of the air cooler: ϕ_o 60 %
- air temperature at the outlet of the air cooler (measured): T_o -3.82°C

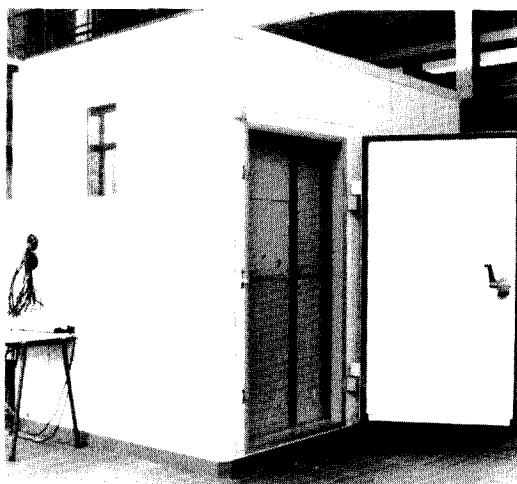


Fig. 8-1 Photograph of the cold room.

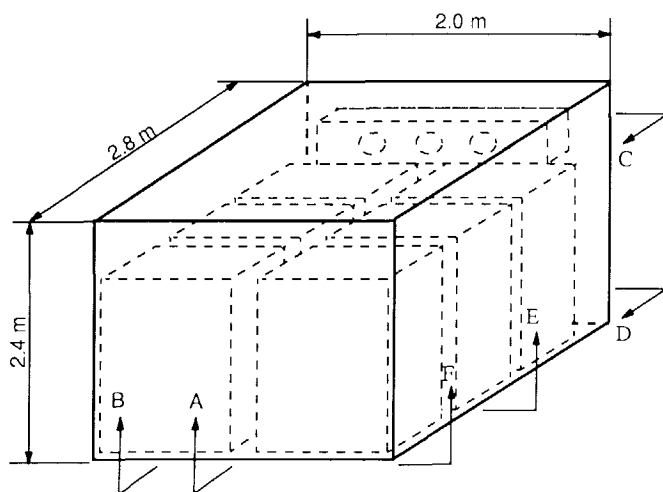


Fig. 8-2 Schematic diagram of the cold store.

- turbulent kinetic energy at the outlet of the air cooler: k_o $0.02V_o^2$
- dissipation rate of k at the outlet of the air cooler: ϵ_o $0.004V_o^3$
- ambient temperature: 25°C
- heating load in each box: 0.16 kw

Requirements:

- prediction of the steady-state air flow pattern using PHOENICS
- prediction of the steady-state air temperature distribution using own model
- prediction of the steady-state air humidity distribution using own model

8.2.2 Presentation of the results

the simulation results from PHOENICS are presented in the form of vector arrows and contours. And the output from our own model as well as the test is shown in grey-level, in order to illustrate the distribution patterns of temperature and humidity. An overview of the output is given in Table 8-1.

Table 8-1 Overview of the simulation output from both PHOENICS and own model.

Figure	Source	V	P	k	ϵ	T	ϕ	Plane in Fig.8-2
8-3	PHOENICS	x	x	x	x			A-A
8-4	PHOENICS	x	x	x	x			B-B
8-5	PHOENICS	x	x	x	x			C-C
8-6	PHOENICS	x	x	x	x			D-D
8-7	PHOENICS	x	x	x	x			E-E
8-8	PHOENICS	x	x	x	x			F-F
8-9	own model					x		B-B
8-10	own model						x	B-B
8-11	test					x		B-B

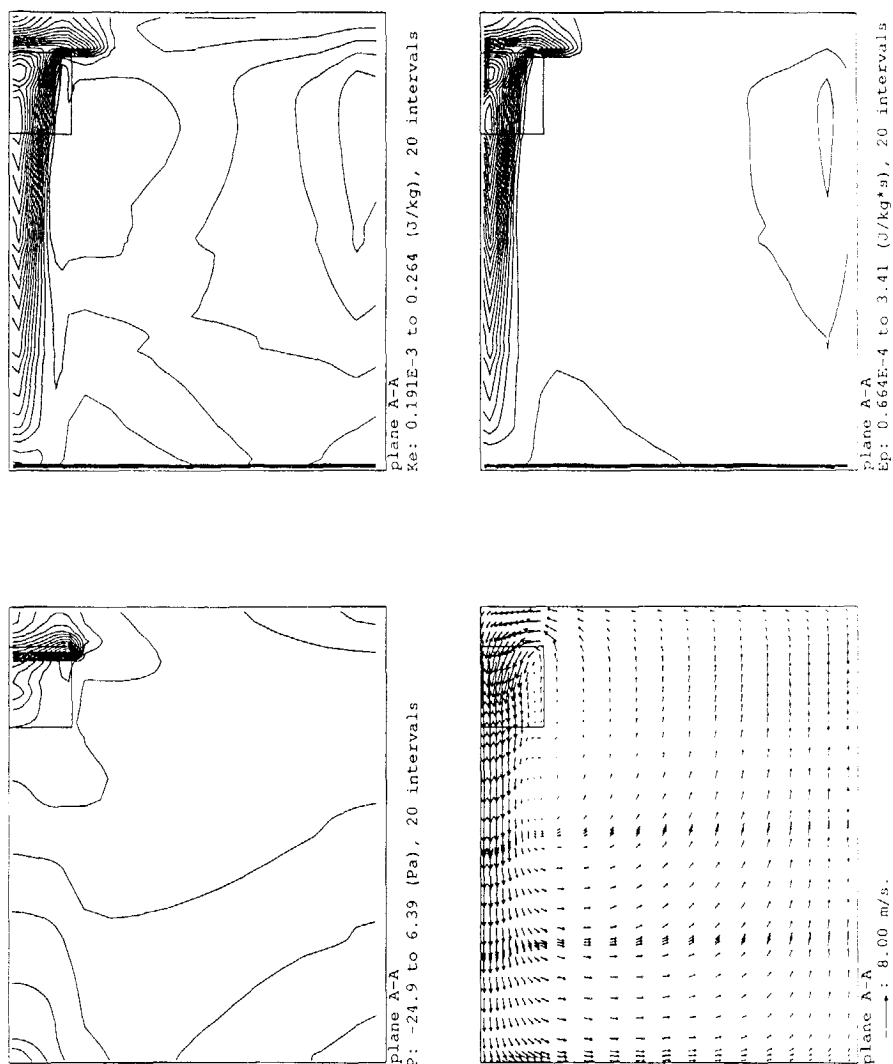


Fig. 8-3 The velocity vectors (left-bottom), pressure contours (left-top), K-value contours (right-top) and ϵ -value contours (right-bottom) on plane A-A in Fig. 8-2, plotted by using PHOTON.

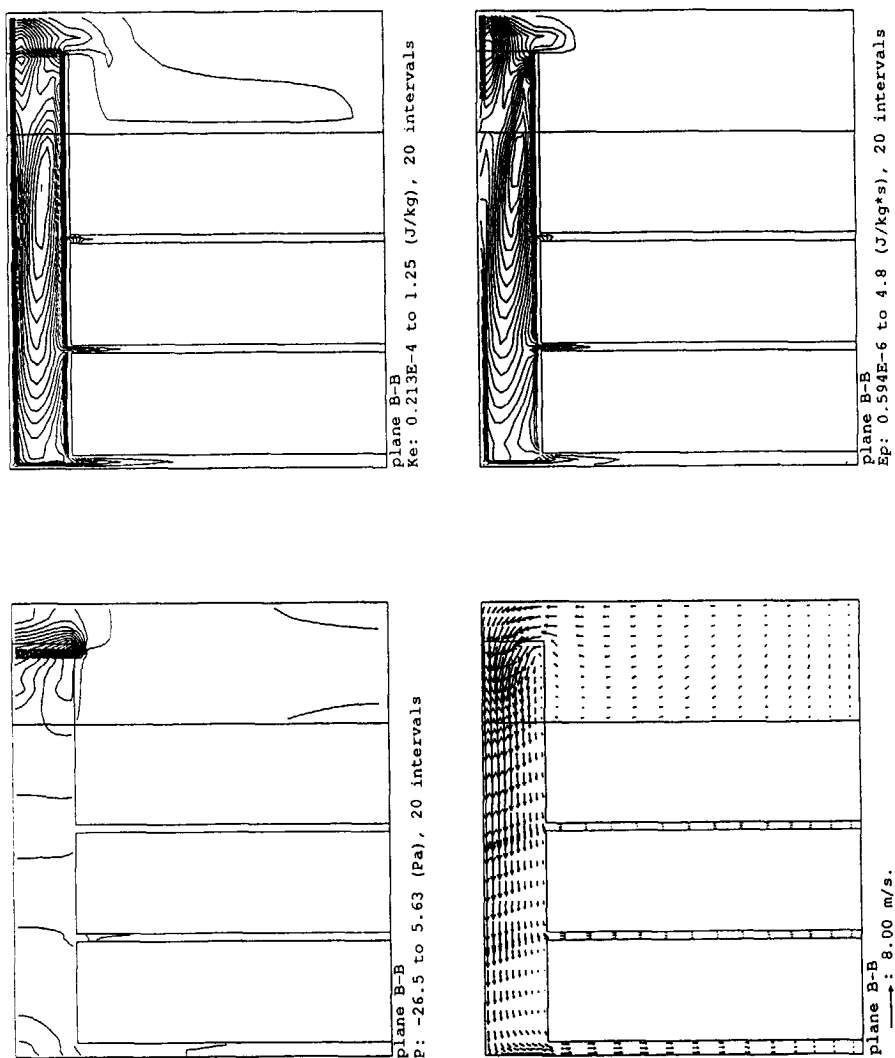


Fig. 8-4

The velocity vectors (left-bottom), pressure contours (left-top), K-value contours (right-top) and ϵ -value contours (right-bottom) on plane B-B in Fig. 8-2, plotted by using PHOTON.

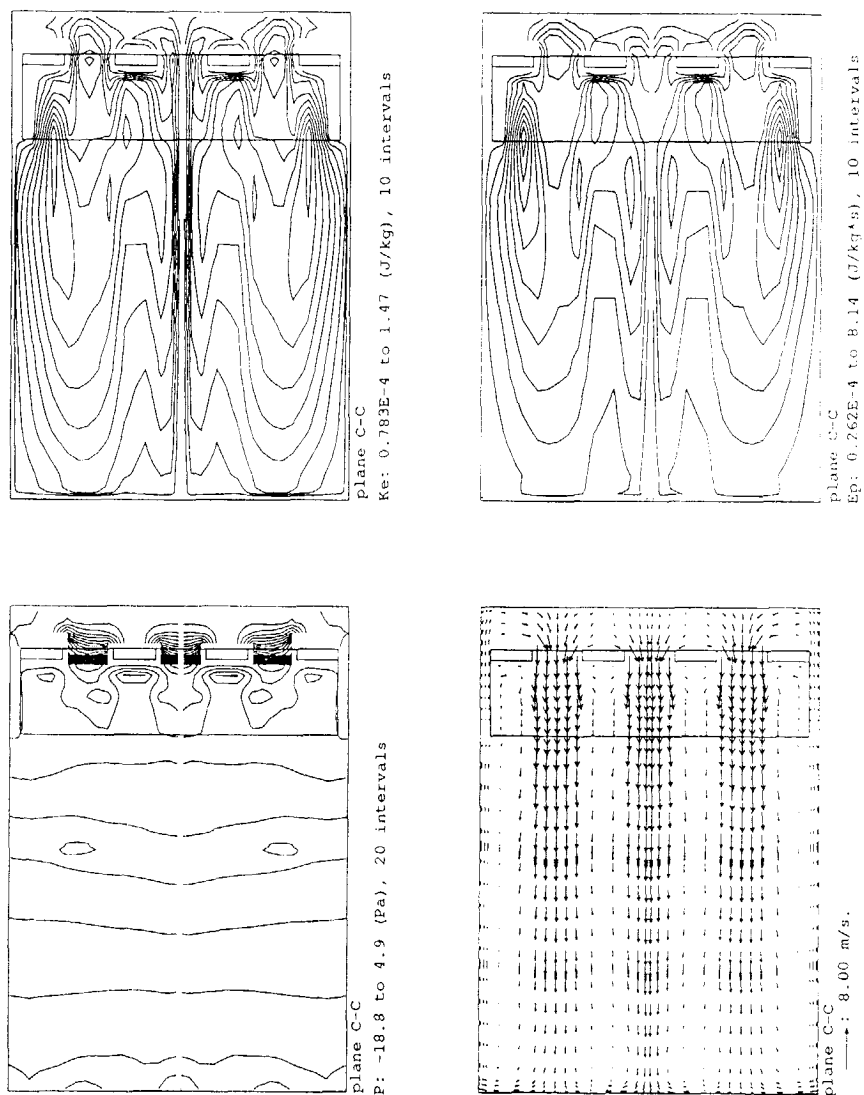


Fig. 8-5 The velocity vectors (left-bottom), pressure contours (left-top), K-value contours (right-top) and ϵ -value contours (right-bottom) on plane C-C in Fig. 8-2, plotted by using PHOTON.

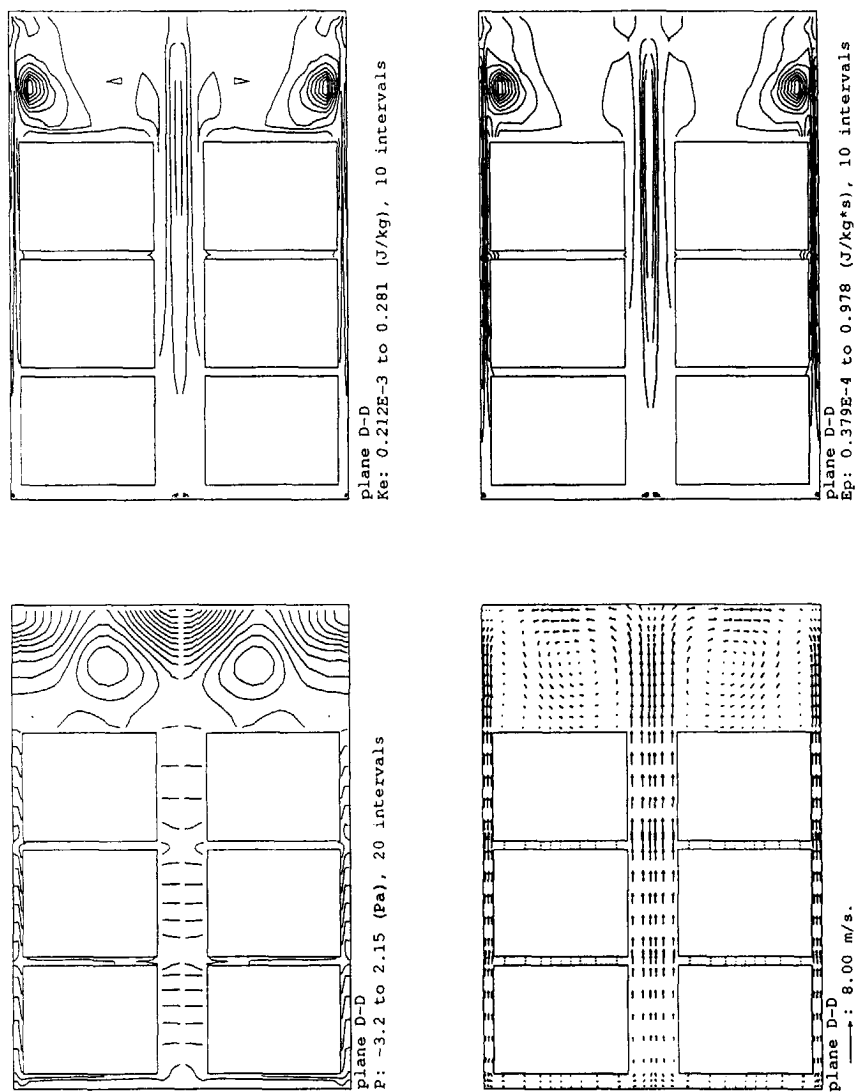
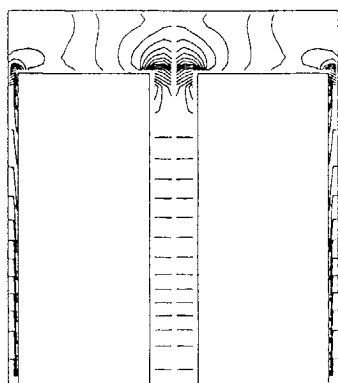
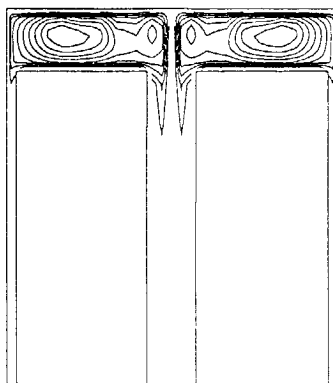


Fig. 8-6

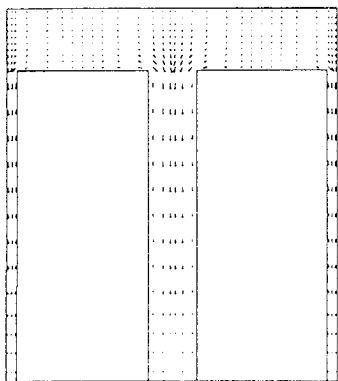
The velocity vectors (left-bottom), pressure contours (left-top), K-value contours (right-top) and ϵ -value contours (right-bottom) on plane D-D in Fig. 8-2, plotted by using PHOTON.



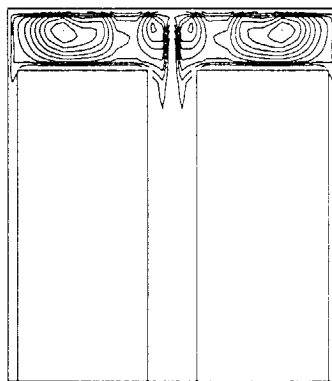
plane E-E
P: -2.2 to 0.405E-1 (Pa), 20 intervals



plane E-E
Ke: 0.695E-3 to 1.17 (J/kg), 10 intervals

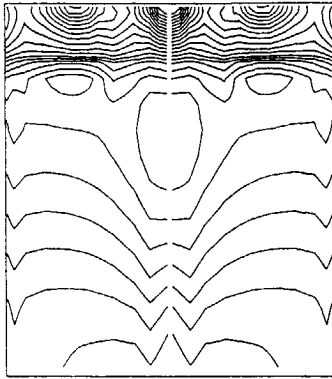


plane E-E
→: 8.00 m/s.

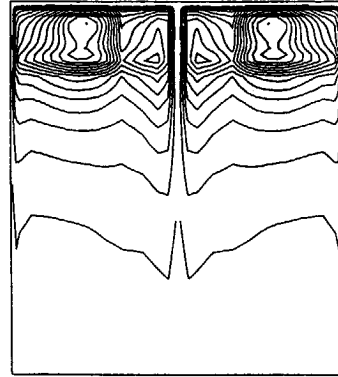


plane E-E
Ep: 0.346E-3 to 3.78 (J/kg*s), 10 intervals

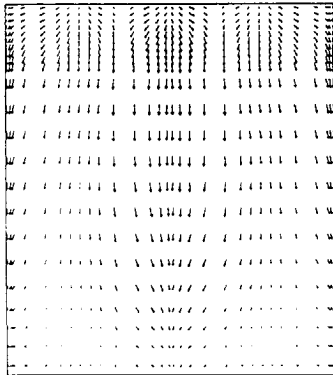
Fig. 8-7 The velocity vectors (left-bottom), pressure contours (left-top), K-value contours (right-top) and ϵ -value contours (right-bottom) on plane E-E in Fig. 8-2, plotted by using PHOTON.



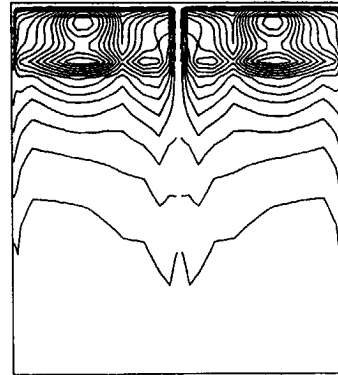
plane F-F
P: 0.241E-1 to 5.86 (Pa), 20 intervals



plane F-F
Ke: 0.569E-4 to 0.458 (J/kg), 15 intervals



plane F-F
→: 8.00 m/s.



plane F-F
Ep: 0.259E-5 to 1.33 (J/kg*s), 15 intervals

Fig. 8-8 The velocity vectors (left-bottom), pressure contours (left-top), K-value contours (right-top) and ϵ -value contours (right-bottom) on plane F-F in Fig. 8-2, plotted by using PHOTON.

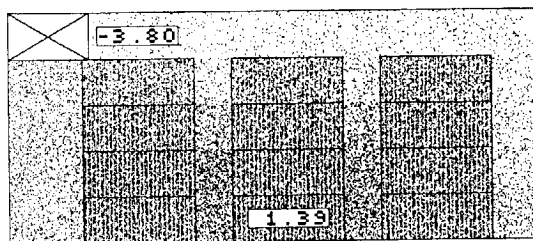


Fig. 8-9 The temperature distribution on plane B-B in Fig. 8-2, output from the own model.

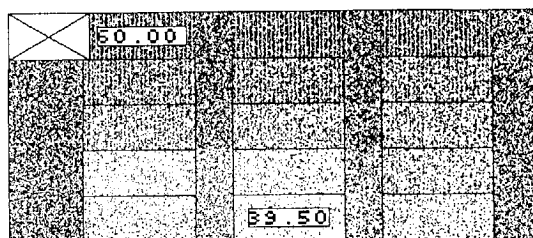


Fig. 8-10 The relative humidity distribution on plane B-B in Fig. 8-2, output from the own model.

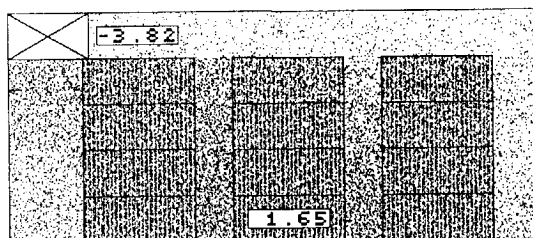


Fig. 8-11 The temperature distribution on plane B-B in Fig. 8-2, output from the measurement.

8.2.3 Discussion and conclusions

On the dominance of forced convection

In chapter 5, we assume that the transport processes in the refrigerated room are dominated by forced convection so that the governing equations (momentum and energy and mass equations) can be de-coupled. This modelling strategy is regarded as a solution to reduce the long computational times. However, this assumption requires a condition to be satisfied, that is, the dimensionless parameter Gr/Re^2 should be small enough. The details on this problem can be found in section 5.6.

In section 8.2.2, the distributions of air velocity, temperature and humidity in the cold room have been predicted by using PHOENICS and our own model. Now it is the time to check whether the criterion is satisfied or not. Eq. 5.57 gives the method of calculating the dimensionless parameter Gr/Re^2 . For the calculation, the local values of air velocity and temperature are needed. The calculated dimensionless parameter is then different at different places. To be simple, we select the boundary faces of the elements (see Fig. 8-9) as the places on which the parameter is calculated. Fig. 8-12 gives the local values of Gr/Re^2 , from which it can be found:

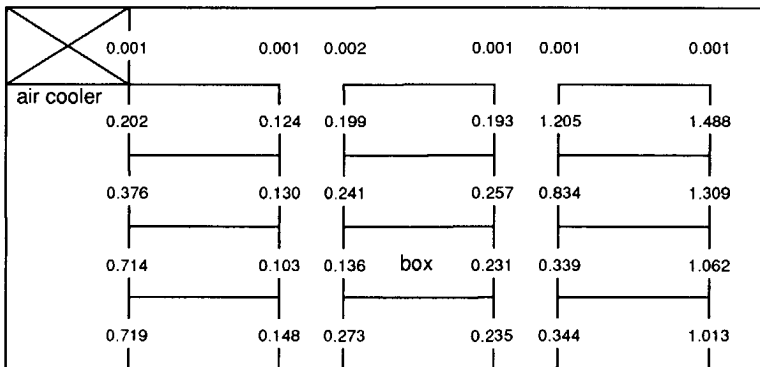


Fig. 8-12 Local values of the dimensionless parameter Gr/Re^2 introduced in section 5.6;
 $Gr/Re^2 \gg 1$: free convection is dominant;
 $Gr/Re^2 \approx 1$: free and forced convections are of comparable magnitude;
 $Gr/Re^2 \ll 1$: forced convection is dominant.

- In the macro-climate (outside the boxes), Gr/Re^2 is very small and thus the de-coupling of the governing equations is out of question. Thus the strategy of

predicting the main flow pattern by using PHOENICS without considering temperature influences is correct.

- However, at the boundary between the macro-climate and micro-climate, Gr/Re^2 is around 1; according to the criterion mentioned in section 5.6, the free and forced convections are of the same magnitude. The reason for this is that we use electrical mats to substitute real products which in fact generate much less heat than what is input to the mats. However, the air velocity through the empty boxes as used in the present cold store is higher than that through boxes filled with real products. From this point of view, we think that the values shown in Fig. 8-12 might be in the same order as real situations. Therefore, further investigations are needed to study the transport processes between macro-climate and micro-climate.

On the computational times

Using PHOENICS is a good approach to predict 3-d flow patterns in cold stores. But the computational times are considerable long: a job with $15 \times 23 \times 36$ grids and 300 sweeps costs ± 35 hours of CPU on a SUN 3/60 with operating system OS 4.03.

8.3 Study of C.O.P with different capacity control systems

As the second application example, the study of system C.O.P with different capacity control systems is described now. A better control system is essential to a refrigerating system when it operates under variable loading conditions and its performance and efficiency are concerned. In the past years, quite a lot of investigations have been done on this aspect. For example, **Wong** et al [8.6, 8.7, 8.8, 8.9] studied the influence of a control system on the system transients, reliability and energy costs. An experimental rig and an analytical model were simultaneously developed to study the behaviour of a liquid chilling system. The experimental results using variable compressor speed to affect capacity changes showed significant energy savings, although operating problems at low speed were not fully resolved. It was also found that set point accuracy and stability could be achieved at the expense of energy consumption requirement. However they did not pay much attention to compressor on-off control, although this type of control is still one of the most popular in refrigeration. Concerned with compressor on-off control systems, **Kruse** et al [8.10] compared two on-off control strategies with different on-cycle lengths, that means two compressor speeds. Their conclusion was that decreasing on-cycle length should lead to lower mean temperature difference between evaporator and condenser and thus lead to higher values of C.O.P. However, they also pointed out that some other investigations resulted in an opposite conclusion. They were doubted about that probably other factors influencing C.O.P also played a role, for instance heat losses during off-period.

Related to the matter on the effects of thermal mass (defined as the product of specific heat capacity and density) of each component on system C.O.P, no publications have been even found until now. It is obvious that more investigations are still needed in this area.

The application of the dynamic evaporator, condenser and cold room models (see chapters 2,3,5) combined with the steady-state TEV and compressor model (see Appendices 1, 2) to investigate the control problems in refrigerating systems consist of a number of simulations with different control strategies and thermal masses, as shown in Table 8-2. The simulation results are grouped into three categories (distinguished with G1, G2, G3 in Table. 8-2) in order to make a clear comparison. The control loop is illustrated in Fig. 8-13, which is a feedback system. The compressor rotational speed is supposed to be changeable in steps or continuously and the temperature sensor is presumed to be instantaneous and located at the returning point of the warm air. The refrigerating system and cold room have the same dimensions and specifications as the experimental plant in chapter 7. Below are the separate descriptions of the three categories of simulation results.

Table 8-2 Combinations of different control systems with different thermal masses.

	normal	2xCp (evap.)	2xCp (room)	5xCp (room)
on-off (rpm=700)	G2.1			
on-off (rpm=1195)	Base	G3.1	G3.2	G3.3
two-stage (rpm=100, 1195)	G2.2			
P control (gain=300)	G1.1			
PI control (gain=300)	G1.2			

normal: the specific heat capacity of each component is that of the test plant shown in Fig. 7-1;
 2xCp (evap.): the specific heat capacity of the evaporator pipes and fins is twice as much as the normal one;
 2xCp (room): the specific heat capacity of the room's wall is twice as much as the normal one;
 5xCp (room): the specific heat capacity of the room's wall is 5 times as much as the normal one.

8.3.1 Group G1: on-off (rpm=1195), P and PI control systems

In order to initiate control action, there must be a difference between the instantaneous value of the controlled condition and its desired value, that is, there must be a deviation. The relationship between the deviation and the signal sent from the logic element to the

correcting element determines the control action. The commonly encountered control actions are on-off, proportional (**P**) and proportional plus integral (**PI**) actions.

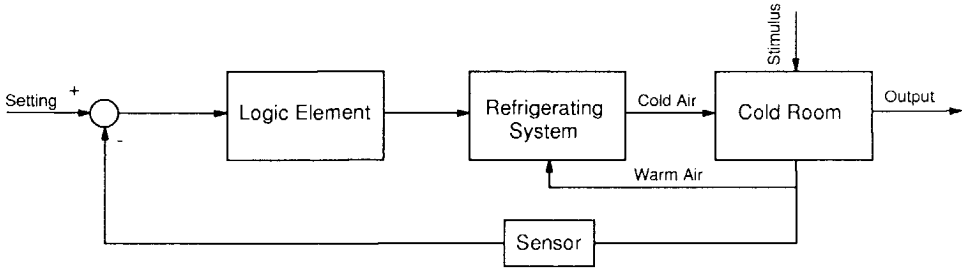


Fig. 8-13 The control system to which the models are applied.

On-off control is the most primitive form but with the minimum initial cost. In this control, the correcting element can assume one of the two positions (on and off) according to the requirements of the process. In our case, the requirement is that the returning air temperature should be within a certain range around the setting value. However, for an on-off controller, small deviations from the desired value causes just as much movement of the correcting element as large deviations and therefore the controlled condition has a permanent oscillation. To overcome this disadvantage of on-off control, proportional control is proposed.

In this control, the position of the correcting element is directly related to the deviation within a proportional band. Mathematically, proportional control action is described by the following equation (see Fig. 8-14):

$$R = \begin{cases} R_{low} & (T \leq T_{low}) \\ R_0 + K_I (T - T_{desire}) & (T_{low} < T < T_{high}) \\ R_{high} & (T \geq T_{high}) \end{cases} \quad (8.1)$$

where R is supposed to be the rotational speed of the compressor. The proportional band is defined as $[T_{high} - T_{low}]$ and K_I is called "gain". A very small proportional band is obviously tending towards on-off control action. On the other hand, a very wide proportional band may result in sluggish control, the controlled condition not being restored to the desired value quickly enough following a disturbance. Another disadvantage of proportional control is its

inability to accommodate load change without sustained deviation, usually called "offset". Thus integral action is added to proportional control, which is called proportional plus integral control or PI control.

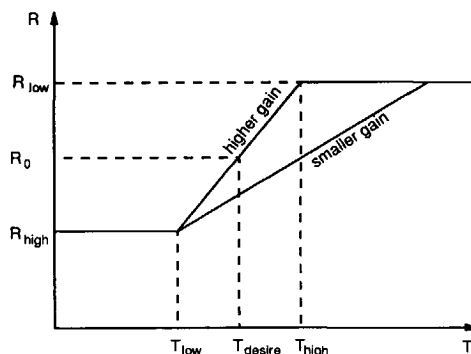


Fig. 8-14 Proportional function employed in a P control system.

In PI control, the position of the correcting element is proportional to the magnitude as well as the duration of the deviation. Mathematically, it can be described by the following equation:

$$R = R_0 + K_1 (T - T_{desire}) + K_0 \int_0^t (T - T_{desire}) dt \quad (8.2)$$

where K_1 / K_0 is called integral action time.

We have programmed these three control actions together with our own models. Following ± 5 minutes of steady-state running, the heat load of the electrical heating is suddenly decreased by 50% and at the same time, the programmed control action is in operation. Three simulations with respect to the three control strategies have been carried out and the results are shown in Fig. 8-15. It can be found that PI control is the most efficient and accurate. Not only is the returning air temperature (controlled condition) best controlled, but also the room wall temperature, which could be considered as product temperature in the case of an empty room, shows a good trajectory. The average C.O.P of PI control is 1.625 times as higher as that of on-off control and 1.13 times as that of P control. The average C.O.P was calculated based on the total air-side heat transfer of the evaporator and the total power consumption of the compressor, all over the total simulation time (50 minutes).

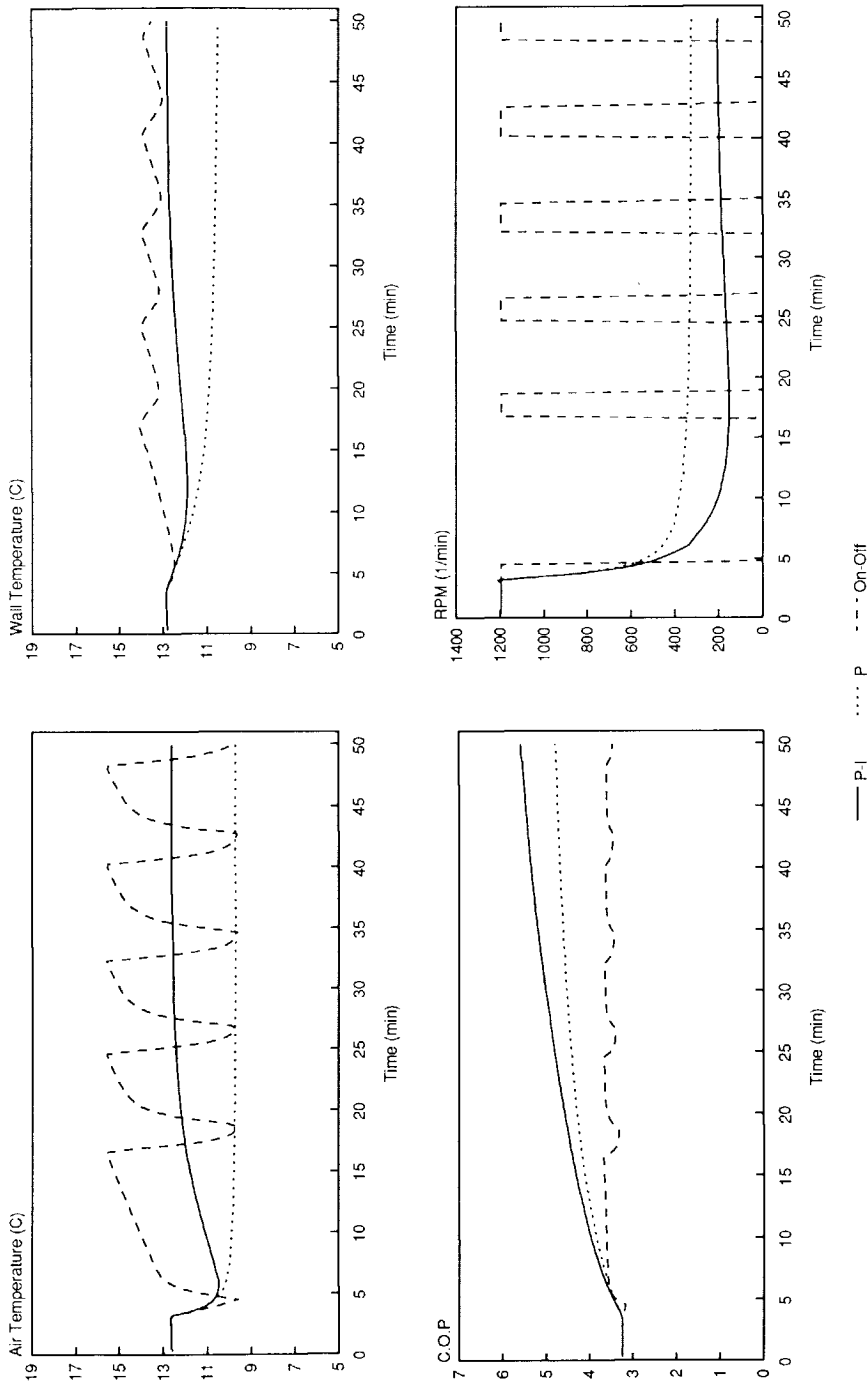


Fig. 8-15 The first group of simulation results related to the comparison of C.O.P between on-off, P and P-I controls.

During the simulations for P and PI controls, the gain K_I was 300 1/(min · °C) and the integral action time 200 seconds and there were no low- and up-limits for the rotational speed of the compressor.

8.3.2 Group G2: two-stage, on-off (rpm=700) and on-off (rpm=1195) control systems

Although on-off control is inefficient and inaccurate, it is still used popularly in the field of refrigeration for small systems (less than 20 kw of refrigeration capacity), because of its cheap initial cost. Thus a further investigation to it is not superfluous. As stated before, the effect of on-cycle length upon the system C.O.P is still arguable for the time being. Kruse et al [8.10] thought it would lead to a negative effect, while some others concluded a positive effect. Such a difference was most probably owing to inadequate study of complete refrigerating systems and lack of sufficient models.

To conduct a comparison investigation, pure experimental methods are often not appropriate, because exactly identical operation conditions, which are considered as the comparing base (for example, in comparing the mentioned three control systems, a basic condition is that the controlled returning air temperature and its oscillation band have to be identical in the three cases), are hardly realized in practice. Therefore, a validated model is very suitable for this purpose. For a simulation model, the operation conditions can exactly be adjusted.

Fig. 8-16 gives the simulation results from our models. The simulations were made following the same steps as in section 8.3.1. The stimulus was also 50% part-loading of the heating power. However, the simulation time was 100 minutes instead of 50 minutes, in order to have more on- and off-cycles. From the figure, it can be found that two-stage control is as efficient as P control but the controlled air temperature and the room wall temperature are oscillating. On-off control, with a lower compressor speed (700 1/min) and thus longer on-cycle length, has a higher C.O.P than that with a higher (1195 1/min) and shorter on-cycle length. Nevertheless, the room wall temperature shows a wider oscillation band in the case of 700 rpm, although the controlled air temperatures in both cases have the same band.

Therefore, we may conclude: 1) using two-stage control to replace P or PI controls will not decrease system C.O.P too much but can save initial capital costs quite a lot; 2) using a big refrigerating system for a small refrigeration requirement is always uneconomical.

8.3.3 Group G3: the effects of thermal mass on C.O.P

The thermal mass of a system is defined as the product of density ρ and specific heat C_p . Normally, the thermal mass determines the time constant of the system and thus the dynamic behaviour. In the case of a refrigerating system, the thermal mass is distributed among its components, such as evaporator, condenser and cold room. Different refrigerating systems

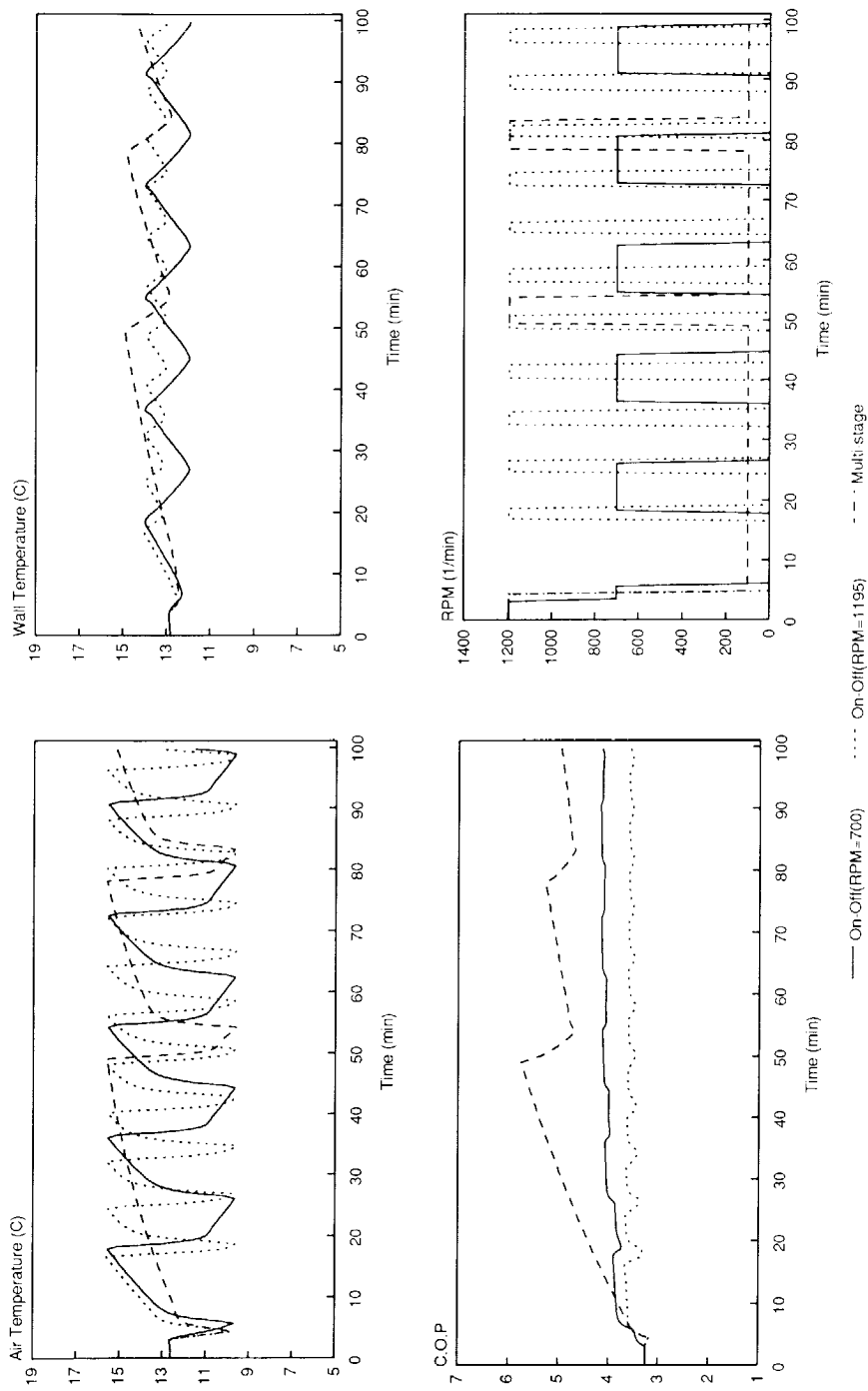


Fig. 8-16 The second group of simulation results related to the comparison of C.O.P between two stage, on-off (rpm=1195) and on-off (rpm=700) control systems.

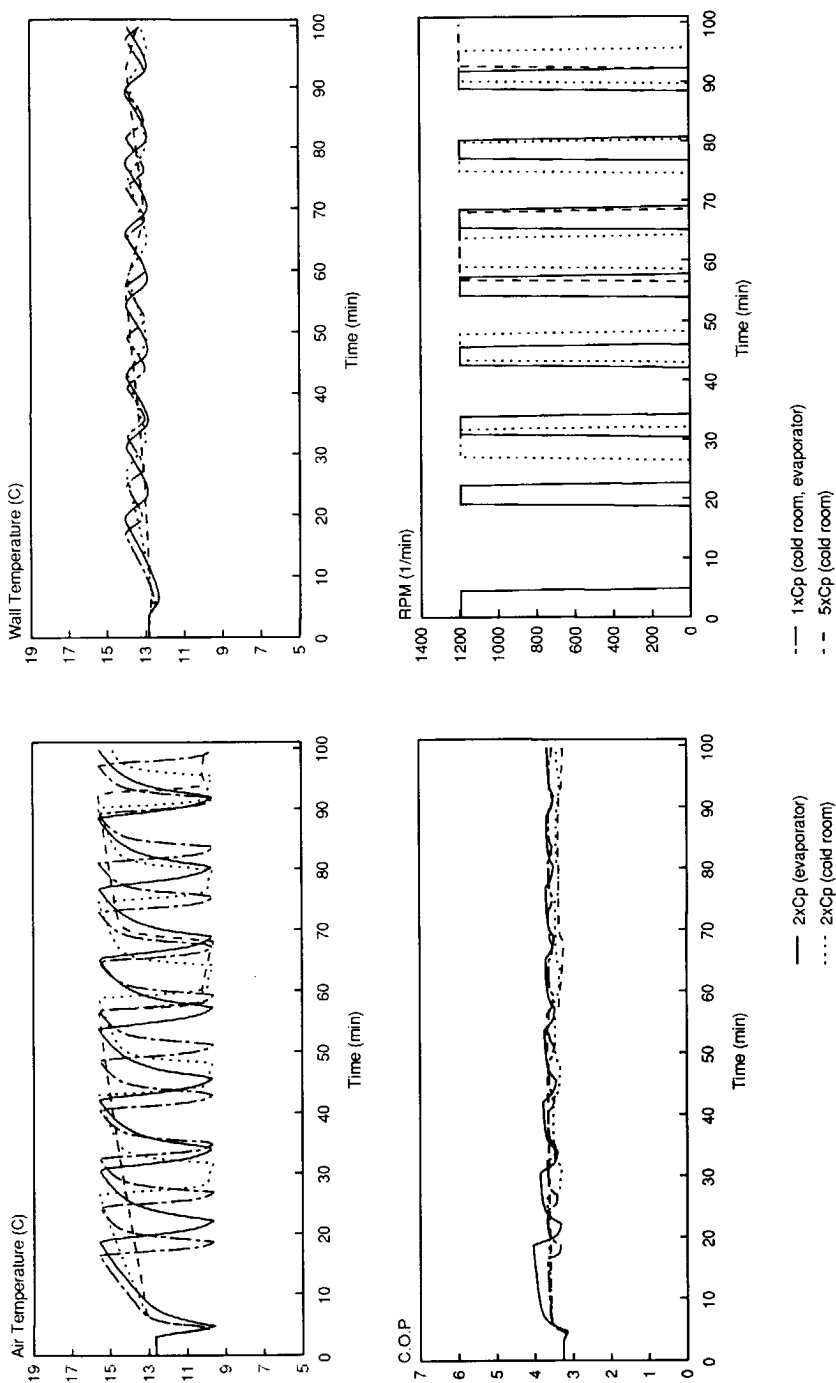


Fig. 8-17 The third group of simulation results related to the comparison of C.O.P between different thermal masses.

would have different thermal masses, depending on their capacity and scale. Generally speaking, a system with large thermal mass behaves slower than one with small thermal mass and therefore their control systems should be different to guarantee high system performance. Nevertheless, the effects of thermal mass on C.O.P are still not clear as far as the literature review shows (see [8.10]). Hereafter, we will give a group of simulation results obtained from our models, which are hoped to bring out some useful conclusions.

Fig. 8-17 gives the comparison of C.O.P between four situations corresponding to four different thermal masses. Except the thermal mass differences, the other conditions are all the same and the control is of an on-off type with $\text{rpm}=1195$ and the part-loading is 50 %. It can be found that the average C.O.P does not show big difference in the four cases, although the on-off frequency varies considerably.

The conclusions from this group of simulation results are 1) for a refrigerating system with on-off control, its thermal mass does not play an important role, as far as C.O.P is the concerned point. The reason is because the C.O.P contribution during each off-period by larger thermal mass is always compensated by the slow increase of refrigeration capacity at the beginning of each on-period (see Fig. 8-18). 2) the small negative effect ($\pm 5\%$) of larger thermal mass on C.O.P is because of the exergy losses due to the temperature differences for storing and releasing heat to and from the thermal mass.

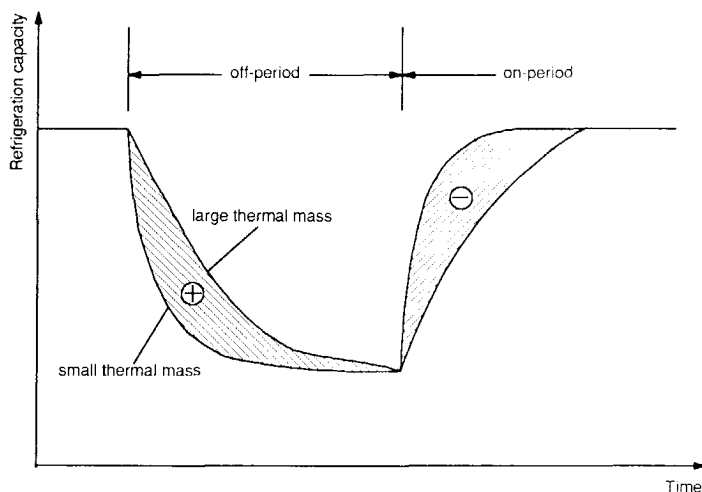


Fig. 8-18 Refrigeration capacity during off- and on-periods.

As a general overview, Fig. 8-19 shows the C.O.P values for all of the cases in Table 8-2, which are all under the same operation conditions: part-load = 50% and controlled returning air temperature = 3.2 °C.

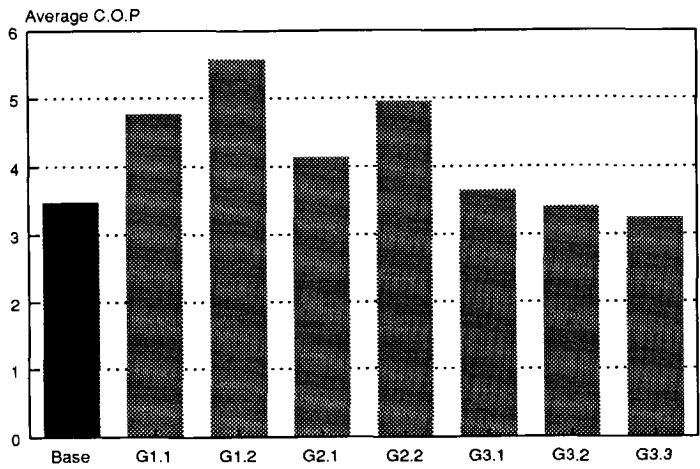


Fig. 8-19 C.O.P distribution for all of the cases shown in Table 8-2.

References

- 8.1 *Proceedings of the Purdue Compressor Conferences* published bi-annually since 1972, Purdue University, West Lafayette, IN, USA.
- 8.2 *Proceedings of meetings of Commissions B1, B2, C2, D1, D2/3*, Wageningen (the Netherlands), 1988.
- 8.3 **Lorentzen, G.** "Air circulation in refrigerated ships holds", Annex 1961-3, Bull. I.I.R., pp.404-428.
- 8.4 **Fockens, F. H., Meffert, H. F. Th., Romijn, J.G., Van Nieuwenhuizen, G.H., Van Beek, G.** "Improved storage results by staggered pallet arrangement", *Proceedings of the 14th Int. Cong. of Refrig.*, Vol.4, Session D1.2, Moscow (USSR), 1975, pp.123-131.
- 8.5 **Van Gerwen, R.J.M., Van Oort, H.** "The use of fluid dynamics simulation models in cold store design", I.I.F. - I.I.R. - Commission B2 - Bristol (UK), 1989, pp.163-169.
- 8.6 **Wong, A.K.H.**, "An investigation into control of refrigeration systems with the emphasis on capacity control", Ph.D. Thesis, South Bank Polytechnic, London, 1988.
- 8.7 **Wong, A.K.H., James, R.W., Welch, T.C.** "Control of a refrigeration system using an analytical model", *Proceedings of 16th International Congress of Refrigeration*, B, Wien (Austria), 1987, pp.635-640.
- 8.8 **Wong, A.K.H., James, R.W.** "Capacity control of liquid chilling systems", *Proc. of The Institute of Refrigeration*, Session 1988-1989, London.
- 8.9 **Wong, A.K.H., James, R.W.** "Control strategies of an intelligent controller for a liquid chilling plane", *Proceedings of meetings of Commissions B1, B2, C2, D1, D2/3*, Wageningen (the Netherlands), 1988, pp.327-335.
- 8.10 **Kruse, H., Upmeier, B.** "Saving of energy by applying optimum conditions to steady state and dynamic behaviour of refrigeration components and installations", I.I.F. - I.I.R. - Commission B2, Dresden, 1984, pp.239-259.

9.1 About the models

9.1.1 The evaporator model

The evaporator was modelled differently in the steady-state and non-steady-state cases. The steady-state evaporator mode is a 3-zone model. Such a lumped model is in fact not suitable for an air-cooler evaporator which has a complicated pipe configuration. However, according to the characteristic of the steady-state model which is mainly used as a start program for dynamic simulations, the assumption of a lumped model for the evaporator was adopted in chapter 4.

However, the non-steady-state evaporator model is a pure distributed one with dividing the evaporator pipe into small elements. From the application results of this model, we found several advantages and disadvantages of this models:

Advantages:

- The void fraction propagation equation as introduced to the dynamic modelling of a dry-expansion evaporator can clearly depict the transient motion of the refrigerant liquid inside evaporator coils. The two-phase flow slip-effect is included in the parameter C_0 that may be treated separately by using standard computer packages, such as PHOENICS, to solve two-phase flow problems.
- By adoption of the distributed modelling methodology, the model is very flexible for various types of evaporator coil configurations. Meanwhile, the heat conduction through the pipes and fins can be computed more accurately.

- Integration of the energy balance equation in the two-phase flow region avoids simultaneous solution of the energy balance equation and propagation equation. This treatment to a large extent makes the model workable, which otherwise would take unacceptable computation time.
- The heat transfer coefficient in the two-phase flow region can locally be calculated according to the local vapour quality.

Disadvantages

- The model needs relatively long computation time. Therefore it is suggested to use different integration time-steps for different components in order to save computational costs. For example, in our simulations, we used 8 seconds for the cold room, 1.6 seconds for the evaporator and 0.2 second for the condenser. The small time step for the condenser model is not required because of the thermal mass, but because of a special situation caused by the relatively large condenser used in the test plant. In this situation, the condensation temperature is very close to the pipe wall temperature of the last water pass; a big time step could result in an oscillation of the condensation temperature around the pipe wall temperature; thus the simulation becomes unstable.
- For lack of the knowledge on the boiling heat transfer inside horizontal pipes without forced fluid flow, the off-period model has made use of the correlations developed for horizontal plates. Thus the deviation of the simulations from the reality is bigger in off-periods than in on-periods.
- Frost-formation is not yet taken into account in the model

Based on the evaluation to the model, it is suggested that the complex distributed non-steady state model be useful only for short-term simulations, such as, 1 hour (rather than days or years). In case of long-term simulations, combination of a steady-state refrigerating machine model with a dynamic refrigerated room model is feasible.

9.1.2 The condenser model

The condenser was modelled in the same way in both the steady-state and non-steady-state situations. The condenser model took the form of lumped models. On the refrigerant side, two lumped control volumes were defined, assuming that the superheated refrigerant vapour above the liquid zone is perfectly mixed and homogeneous and that the temperature gradient from the superheat temperature to the condensation temperature takes place only in the thermal boundary layer. On the water side, control volumes were divided according to the water passes. Such an element division method has an advantage that each pass can be considered separately according to its local conditions. For example, the condensation heat transfer coefficient outside the pipe wall was locally calculated. The simulation results showed that the heat transfer coefficient of the first pass is much lower than that of the last pass in the mixing vapour zone, because the temperature difference between the refrigerant and pipes is bigger in the first pass than in the last (see Eq. (6.25)).

The heat transfer calculation for the thermal boundary layer affects the temperature of the mixing vapour and the condensation rate of refrigerant. For the first time, the ordinary boundary layer theory was introduced in the modelling of shell-and-tube condensers. The simulation results prove that this method is more realistic than that proposed by James et al (see [3.1]) who just simply assumed the amount of returning vapour from the boundary layer to the mixing vapour zone, which requires a measurement to be made at the specific equipment to be simulated.

The treatment of the liquid zone is geometrically very precise, for instance, the heat transfer areas are calculated on the base of the liquid level position (see Appendix 3). However, the heat transfer coefficient is not accurately calculated, more or less because of the lack of suitable correlations related to the situation where the refrigerant liquid flows semi-cross and semi-parallel with the cooling water pipes.

The condenser shell was found very important during a non-steady-state process, because it can act as a thermal "reservoir". Thus a good consideration of it in the dynamic model is necessary.

9.1.3 The refrigerated room model

The refrigerated room was modelled as a distributed model. With the help of the standard computer package PHOENICS, the complicated air flow problem in a refrigerated room has been solved, although it needs quite a lot of computation times. The assumption that the air flow in a refrigerated room is independent of the temperature and humidity distributions and thus of time is successful in working out dynamic simulations and saving computation costs. Based on the steady-state flow pattern predicted by PHOENICS, the instantaneous temperature and humidity distributions and their dynamic behaviour can be predicted by our own model.

However, there are several remaining problems which need to be pointed out. The air mass flow rate through the products was calculated with the pressure-velocity relation with constant friction factor which was given in the model as input. The free convection transport between macro-climate and micro-climate was not taken into account; however, in chapter 8 we found that to ignore this problem was irrational. These problems should be gradually solved in future investigations.

9.2 About the validation of the models

9.2.1 The steady-state validation

The steady-state model was validated with 6 series of experimental data. Generally speaking, the simulation results were in pretty good agreement with the experimental ones. However, some discrepancy was also observed:

- The predicted compressor shaft power is $\pm 10\%$ different from the measured. There could be two reasons for it: a) the fitted performance curve for the compressor based on the 10 tests might be not accurate enough; b) the assumption, that the adiabatic shaft power efficiency is only dependent on pressure ratio (see Appendix 1), is not very true.
- The predicted subcooling temperature is higher than the measured by $\pm 2\text{ }^{\circ}\text{C}$. This deviation is most likely because of the low refrigerant side heat transfer coefficient in the model.
- The predicted refrigeration capacity of the evaporator is sometimes different from the heat load of the cold room. The reason is that the heat balance between the evaporator and the cold room is represented by checking the temperature difference ($0.1\text{ }^{\circ}\text{C}$ check accuracy, see chapter 4) in the model. Although $0.1\text{ }^{\circ}\text{C}$ is quite small for temperature, its effect on heat balance is still considerable. Therefore, it is suggested to use an even smaller temperature difference to check the convergence.
- The predicted heat load for the cold room is higher than the power input (measured) of the heating in the room, specially when the air temperature is very low. The reason for this is that the heat leakage through the room walls is not taken into account in the experiments. However, the total heat load of the cold room is the summation of the heating power and the heat leakage through the walls; under very low inside temperatures, the latter is quite considerable.
- The TEV model was developed by somebody else (see Appendix 2) and is principally in agreement with the experiments. However, to determine the screw position, an input parameter for the model, a pre-calculation using experimental results is necessary.

9.2.2 The dynamic validation

The non-steady-state model was validated with 5 groups of measurement results which included an experiment with the compressor turned on and off. The following conclusions have been deduced from the validation:

- after a step increase of the compressor RPM, the mass flow rate of refrigerant inside the evaporator coil is already beyond the validation range of correlation (6.4), so that the predicted heat transfer coefficient is bigger and accordingly the evaporation temperature is higher.

- the compressor is considered as an instantaneous element in the model, that means it has no heat capacity. However, in practice the compressor is built up with quite a lot of metal which can store heat. Its transient behaviour would make the refrigerant temperature at discharge react slowly, when the RPM is suddenly increased.
- the effective thermal masses of the evaporator, such as, those of the coils and fins, are smaller in the model than in reality. Thus the response of the air to the step change of RPM is too fast.
- the simulation of on-off operations is the most difficult, because the variations of the thermodynamic state of the system are very sharp. Such steeply changing behaviour of the system necessitates a very careful consideration of the integration time step of simulation. Not only is the implementation of the model difficult, but also the realisation of the experiment is not so easy, because, during the very short time of turn-on, some devices operate abnormally. For instance, the safety valve produces quite larger pressure drop after a turn-on than it works under steady-state conditions. Another uncertainty is the solenoid-valve between the condenser and TEV, which probably does not open instantaneously after a sudden turn-on. However, the dynamic behaviour of these auxiliary devices are not taken into account in the model. Therefore, the discrepancy of the simulation from the test is not easy to explain. Nonetheless, one phenomenon is still explained, that is, the C.O.P difference between the simulation and test at the beginning of the on-period. As the evaporator thermal mass is too small in the model, the refrigerant temperature decrease at the beginning of the on-period is immediately transferred to the air side, so that the air temperature also drops down and the air side C.O.P is higher, according to the model. But in practice the refrigerant temperature decrease cannot be felt by the air so quickly due to the large thermal mass of the evaporator. Thus the experimental C.O.P is lower than the simulated one. The effect of a small thermal mass of the evaporator can also be seen at the beginning of the off-period. Because of the quick response of the air to the refrigerant side change, the refrigeration capacity at the beginning of the off-period is smaller than that of the test. However, the smaller refrigeration capacity at the beginning of the off-period is compensated by the larger one of the on-period. Therefore, the average C.O.P over a long time, during which many on-off cycles take place, might not differ in the simulation and test.

9.2.3 The validation of the air flow model (PHOENICS)

To validate the air flow model (PHOENICS), experiments were carried out in an empty room. The 2-dimensional measurements were made with a hot-wire anemometer. The following conclusions were obtained:

- the main flow pattern shows an agreement between the simulation and measurement.

- the dimensions and positions of the air cooler, heating and obstacle can not be exactly identical in the model and in the reality. This is because the definition of an object in PHOENICS is on the basis of grids. An exact fitting to the reality is in fact impossible.
- the turbulence model (k- ϵ model) adopted by PHOENICS is not 100% reliable.
- there may be a lot of small eddies in the air flow, which might influence the measurement. Because the hot wire is very small, sometimes even smaller than the eddies themselves, it could be located somewhere inside the eddies and then give the very local velocities instead of the main stream velocities.

9.3 About the applications of the models

9.3.1 Using PHOENICS to study the air distributions in cold stores

Convergence

To solve the Navier-Stokes equations, many iteration processes are employed inside PHOENICS. Accordingly, as a user, we have to be sure about the convergence if we apply PHOENICS to solve a concrete problem. In fact, to check the convergence is one of the most difficult problems encountered by users. What we have done during using PHOENICS to study the air distributions in cold stores is to follow two criteria:

- at least 600 sweeps of overall iteration have to be computed with a linear relaxation factor for pressure of 0.5 and a false time step for the other variables, calculated as follows

$$\text{false time step} = 10 \times \text{smallest cell dimension} / \text{maximum velocity}$$

- the contour shapes and ranges of the pressure, k and ϵ values should not change anymore when a convergent solution is reached.
- to check the mass balance over the whole domain.

Grid independence

The grid independence of a PHOENICS solution is another critical point. To be sure that the solutions are independent of the grid fineness, we have done a series of 2-D test computations. And two criteria were adopted:

- to compare the positions of the eddy centre appearing in the flow
- to calculate Y^+ values for the wall cells (see chapter 5)

It was found that the effect of grid fineness on the position of the eddy-centre was not obvious, but the Y^+ values were too big if the grid cells were too coarse near the walls. According our experience, a grid division 25x25 with power-law grids near the walls is satisfactory for a 2-d cold store with 3.35x2.87(m).

General conclusions

- PHOENICS can successfully predict the main flow patterns in case of refrigerated rooms, but cannot deliver exact velocity values everywhere in a flow domain. Therefore, to achieve a numerical agreement between simulation and experiment seem to be impossible. It also has to be pointed out that a good application of PHOENICS to a refrigerated room requires the air cooler to be experimentally studied in details, with the emphasis on its turbulence intensity and velocity distribution.
- Accomplishing a PHOENICS job is a trial-and-error process. There are no universal rules to determine the convergence and grid-independence of a solution. One should patiently check the in-between solutions with respect to different iteration sweeps and different grids, to find out whether or not the iteration process and grid-fineness are satisfactory.
- The computation time of PHOENICS is rather long. For an isothermal air flow with grid 15x23x36, it takes ± 35 hours of CPU to compute 300 sweeps of overall iteration on a SUN 3/60.

9.3.2 The effects of capacity control systems on the system performance

The conclusions obtained from the computer simulations related to different control systems are given in the following table where "1" denotes the best and "5" the worst.

control systems	C.O.P	control accuracy
on-off control with longer on-cycle	4	5
on-off control with shorter on-cycle	5	3
two-stage control	2	4
P control	3	2
PI control	1	1

9.3.3 The effect of thermal mass on the C.O.P with on-off control

For a refrigerating system with on-off control, its thermal mass does not play an important role, as far as C.O.P is the concerned point. The reason is because the C.O.P contribution during each off-period by larger thermal mass is always compensated by the slow increase of refrigeration capacity at the beginning of each on-period. The small negative effect ($\pm 5\%$) of larger thermal mass on C.O.P is because of the exergy losses due to the temperature differences for storing and releasing heat to and from the thermal mass.

9.4 Recommendations for further investigations

9.4.1 Long-term simulations accounting for weather and climate changes

As described in the first chapter, the coupling between a refrigerated machine and a refrigerated room can be divided into two categories, depending on which side is emphasized. If the refrigerating machine is the aimed point, then the coupling is called "quick coupling" or "short-term coupling". If the refrigerated room is the aimed point, then the coupling is called "slow-coupling" or "long-term coupling". The corresponding computer simulations are also named with the same terminology. What we have done in chapter 8 belongs to the first category of simulations, where the transient behaviour of the refrigerating machine was simulated with the consideration of capacity control systems and the simulation times were short (about one hour).

However, sometimes people are interested in a long-term simulation from which the energy consumption for refrigerating a cold store and the change of storing conditions are predicted over a period of one month or one year. In this case, not only the stored products play a role, but also the outside weather conditions are important. Because the simulation time becomes longer, the integration time step should be larger respectively, in order to save the computational time. For a short-term simulation, the integration time step can be one tenth of second; however it should be several minutes or even hours in the case of a long-term-simulation. Therefore the combination between the refrigerating machine and refrigerated room has to be different. As shown in Fig. 1-3, compared to the room, the thermal mass of the machine is small enough to be neglected, when the transient behaviour of the room is concerned. In other words, the machine instantaneously follows the room in view of a long-term observation. This means that a combination of a dynamic room model with a steady-state machine model is feasible for long-term simulations.

9.4.2 Modification of the lumped steady-state evaporator model into a distributed one

The lumped steady-state evaporator model is suitable to be used as a start program to roughly predict initial conditions for dynamic simulations. But if it is applied for the purpose

proposed in 9.4.1, there are many limitations rooted in the model. One of the most obvious is that the lumped 3-zone model cannot deal with the variation of pipe configurations of air coolers. It may apply to counter-flow type or "E-flow" type of air coolers. However, in industry and commerce, often encountered are a lot of types of air coolers which do not belong to a pure counter-flow or "E-flow" but something in combination. In such situations, a distributed model like the dynamic one developed in chapter 2 is much better, due to its flexibility.

Not only can a distributed evaporator model be used for long-term simulations, but it is useful for the optimization design of air coolers as well.

9.4.3 Extensive applications of the refrigerated room model

Extensive applications of the refrigerated room model could be another proposal for a further investigation. Simulation results could be used in the design, construction and use of various types of refrigerated warehouses, cabinets, containers and so on. For steady-state simulations, natural convection, for instance, referred to open-door cases, may be taken into account in using PHOENICS. For non-rectangular spaces, the so-called "body-fitted coordinate" may have to be used in PHOENICS.

9.4.4 Simulations using substitute fluids for CFCs

The working medium we used in the simulations until now is R12. However, with the development of new substitute fluids for CFCs, problems, such as energy penalty, re-dimensioning of refrigeration equipment, new heat and mass transfer correlations, are arising and need to be solved. Mathematical models could be one of the useful tools for the solutions. Off course, the computerization of thermodynamic property calculations of new working mediums is necessary to implement the computer models of refrigerating machines.

Appendix ONE The Compressor Model

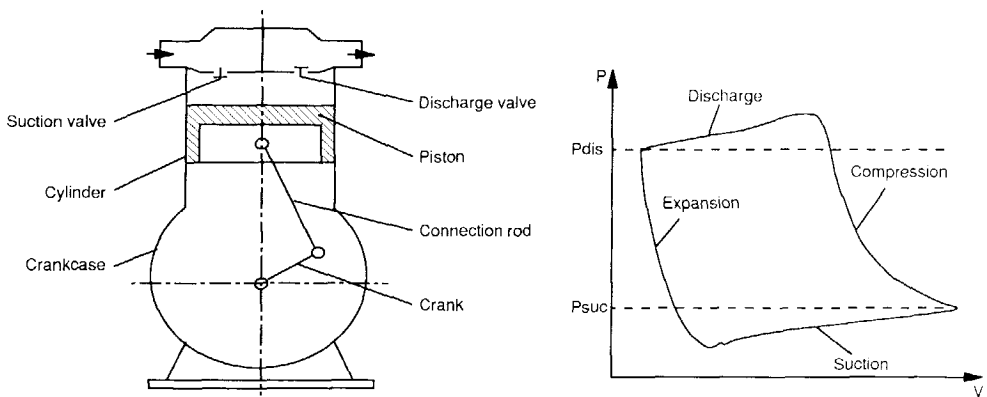


Fig. A1-1 The structure and thermodynamic processes of a reciprocating compressor.

As the compressor model is simple and derived from experiments and the TEV model is developed by somebody else, they were not introduced in the main text, except for the coupling of them with the models of the other components. Hereafter we will briefly describe these two models, in order that people can easily realise their own simulations.

The compressor functions as an energy transmitter which transforms the mechanical energy supplied by the electrical motor into the pressure (or internal) energy of refrigerant.

Through the compression process, the pressure of the superheated vapour from the evaporator can be enhanced to a high level at which condensation can happen at ambient temperature. Fig. A1-1 illustrates the structure of a reciprocating compressor which consists of cylinder, piston, crank-shaft, connection rod, suction and discharge valves. The thermodynamic processes taking place during one shaft rotation are also shown in Fig. A1-1.

Modelling of reciprocating compressors can be divided into two categories. One is for the purpose of studying compressors themselves, for instance, the motion of automatic valves, pressure pulsations, etc. This type of models should be dynamic models. A detailed description of them can be found in [A1.1]. Another category is for the purpose of simulating a complete refrigerating system in which the compressor is considered to act very fast compared to the other components and therefore a steady-state model of compressor is required.

Besides the common thermodynamic processes occurring in reciprocating compressors as shown in Fig. A1-1, different compressors could have their own characteristics of performance. Thus, a universal model valid for every compressor does not exist. Experiments are always necessary to determine those characteristics. Or sometimes people directly make use of catalogue data from manufacturers instead of doing experiments, due to possible incapacity or simplicity. In our case, we have conducted a set of steady-state experiments. Below is the description of the model.

Applying the energy conservation law to the compressor, we may have

$$\dot{m}_{comp} (h_{dis} - h_{suc}) = W_{comp} - (\alpha A)_{comp} [0.5(T_{dis} + T_{suc}) - T_{amb}] \quad (A1-1)$$

where

$$\dot{m}_{comp} = \eta_{vol} N_{cyl} \frac{\pi}{4} d_{cyl}^2 L_{cyl} n \quad (A1-2)$$

$$W_{comp} = \eta_{ad} \dot{m}_{comp} \frac{P_{suc}}{\rho_{suc}} \frac{k}{k-1} \left[\left(\frac{P_{dis}}{P_{suc}} \right)^{(k-1)/k} - 1 \right] \quad (A1-3)$$

In the equations above, three coefficients are unknown : the volumetric coefficient η_{vol} ; and the adiabatic shaft power coefficient η_{ad} ; the heat transfer coefficient times the area $(\alpha A)_{comp}$. They all need to be determined through experiments. To be simple, we assume these

coefficients are the functions of pressure ratio P_{dis}/P_{suc} . Fig. A1-2 shows the experimental results and the fitted curves which are expressed in formulas as follows.

$$\eta_{vol} = 1.11353 - 0.10954 (P_{dis} / P_{suc}) + 6.52202E-3 (P_{dis} / P_{suc})^2 \quad (A1-4)$$

$$\eta_{ad} = 0.86602 - 4.81721E-2 (P_{dis} / P_{suc}) + 3.42274E-3 (P_{dis} / P_{suc})^2 \quad (A1-5)$$

$$(\alpha A)_{comp} = 1.06648E-2 + 3.71455E-4 (P_{dis} / P_{suc}) \quad (A1-6)$$

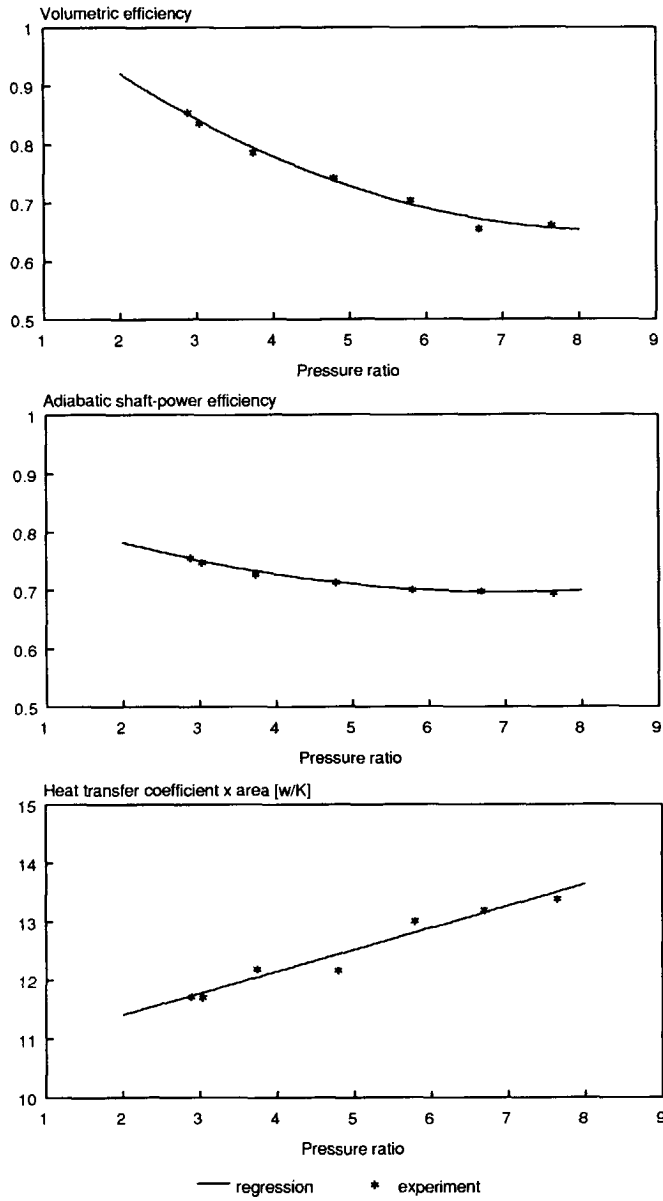


Fig. A1-2 *The experimental results and fitted curves for determining the coefficients involved in the compressor model*

Appendix TWO The TEV Model

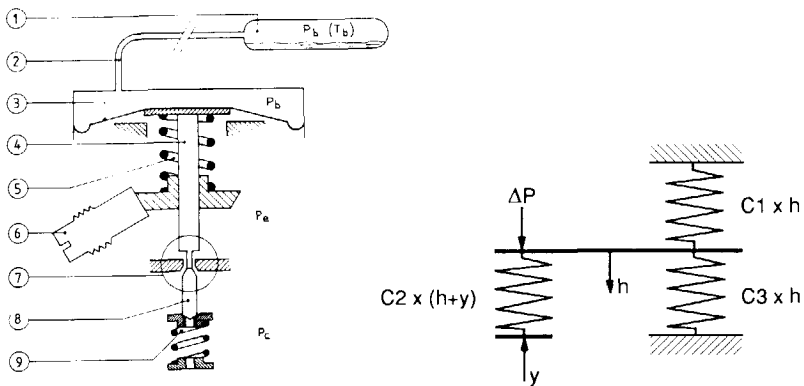


Fig. A2-1 Schematic diagram (left side) and force balance (right side) of the thermostatic expansion valve.

- | | |
|----------------------------|---|
| 1. feeler bulb | h needle displacement |
| 2. capillary tube | y position of the adjusting screw |
| 3. diaphragm | $C1$ spring constant of the diaphragm |
| 4. plate and pushrod | $C2$ spring constant (on valve body) |
| 5. spring (on valve body) | $C3$ spring constant (orifice) |
| 6. adjusting screw | ΔP pressure difference across the diaphragm |
| 7. orifice (valve opening) | |
| 8. needle | |
| 9. spring (orifice) | |

The thermostatic expansion valve (TEV) has two-fold functions: 1) to make the refrigerant decrease its pressure and temperature; 2) to control the amount of refrigerant flowing into the evaporator in order to keep the superheat at the outlet of the evaporator constant. Fig. A2-1 is a schematic diagram of the TEV which consists of two sections:

- the valve section with a needle valve and an integrated controller which is proportional.
- the sensor section which detects the refrigerant outlet temperature of the evaporator.

The feeler bulb is filled with a special liquid and its vapour in equilibrium. When the temperature of the bulb increases, the equilibrium pressure P_b rises too. This pressure is transmitted to the space above the diaphragm by the capillary tube. On the other side of the diaphragm, the evaporator pressure P_e exists, which is usually the outlet pressure of the evaporator in order to avoid the influence of pressure drop. The pressure difference $\Delta P (= P_b - P_e)$ actuate the movement of the needle and thus the opening of the valve. The moving behaviour of the needle can be adjusted by the adjusting screw. The force balance on the valve needle is illustrated in Fig. A2-1.

The mathematical model of the TEV has been well developed and validated by **van der Meer** [A2.1]. He has obtained two models for two types of thermostatic expansion valves (Danfoss TEF2 and TEF5). Below is a brief description of the second (TEF5).

According to the force balance shown in Fig. A2-1 and the experimentally determined C1, C2, C3, the displacement of the needle can be calculated as follows

$$h = \begin{cases} 0.63 \cdot \Delta P + 0.065 \cdot (-4.34 - y) + 0.32 \\ 0.49 + (h - 0.49) / 2 \\ 0.6 \end{cases} \quad \begin{matrix} (h \geq 0.49) \\ (h \geq 0.6) \end{matrix} \quad (\text{A2.1})$$

where $\Delta P = P_b - P_e$

$$P_b = 4.2 + T_b (0.097 + T_b 9.0E-4) \quad (\text{A2.2})$$

On the basis of the calculated displacement of the needle, the mass flow rate through the TEV is calculated as follows

$$\dot{m}_{tev} = 1.25 \dot{m}_{max} h / 0.6 [1.0 + 0.028 \cdot \Delta T_{sub}] \quad (\text{A2.3})$$

$$\text{where } \dot{m}_{max} = 1.45E-3 \{ \rho_l (P_c - P_e) / [1.0 + 2.2(P_c - P_e)/P_c] \}^{0.5} \quad (\text{A2.4})$$

If $P_c - P_e$ is greater than the critical pressure difference ($= [1.0 - (1.0/3.0)]P_c$), then it is substituted by the latter.

Appendix
THREE
**Calculation of the Heat Transfer
Areas in the Condenser**

In chapters 3 and 4, we did not go further with the calculation of various heat transfer areas encountered in the basic equations in order to keep the context clear. Hereafter we will concentrate on this problem which is nothing but some geometrical manipulations

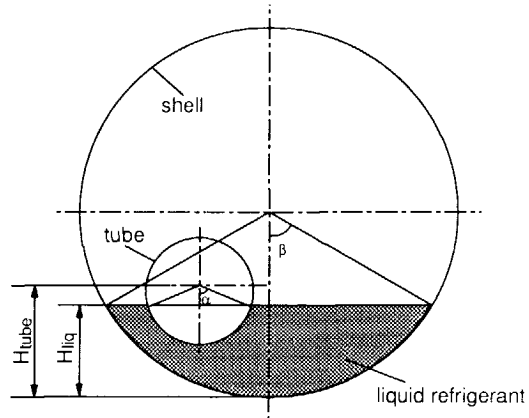


Fig. A3-1 *Cross-sectional geometry of the shell and tube condenser.*

Problem setting

Well known conditions:

1. M_{liq} mass content of the refrigerant liquid deposited in the condenser
2. T_{sub} subcooling temperature
3. various geometrical dimensions (see Fig. A3-1)

To be solved:

1. H_{liq} liquid level
2. $A_{tube,l}$ heat transfer area between one tube and the liquid refrigerant
3. $A_{tube,v}$ heat transfer area between one tube and the vapour refrigerant
4. $A_{tube,w}$ heat transfer area between one tube and the cooling water
5. $A_{r,sh1}$ heat transfer area between the liquid refrigerant and the shell
6. $A_{r,sh2}$ heat transfer area between the vapour refrigerant and the shell

Solutions:

If the mass and temperature of the refrigerant liquid are known, the volume of it can be easily calculated. Because the condenser length is fixed, the cross-sectional area (the dark part in Fig. A3-1) of the liquid volume is then as follows

$$A_{cross,liq} = M_{liq} / (L_{cond} \rho_{sub}) \quad (A3.1)$$

It is obvious that if the arc angle β is known then the liquid level H_{liq} can be directly determined by the following formula

$$H_{liq} = 0.5 d_{sh} [1 - \cos(\beta)] \quad (A3.2)$$

With this level, it is possible to calculate the cross-sectional area of the tube submerged in the refrigerant liquid, as follows

$$A_{tube,cross} = [\pi \alpha / 180 - \sin(\alpha) \cos(\alpha)] D_{tube}^2 / 4 \quad (A3.3)$$

where $\alpha = \arccos [1 - 2 (H_{tube} - H_{liq})/D_{tube}]$

With this cross-sectional area, the cross-sectional area of the refrigerant liquid can be calculated again in another way:

$$A_{cross,liq} = [\pi \beta/180 - \sin(\beta) \cos(\beta)] D_{sh}^2/4 - A_{tube,cross} \quad (A3.4)$$

The comparison between Eqs. (A3.1) and (A3.4) leads to a correct β value by means of iteration.

Now the heat transfer areas listed above can be easily calculated.

$$A_{tube,l} = \begin{cases} 0 & \text{(above the liquid level)} \\ \pi D_{tube} L_{cond} \alpha/180 & \text{(on the liquid level)} \\ \pi D_{tube} L_{cond} & \text{(below the liquid level)} \end{cases} \quad (A3.5)$$

$$A_{tube,v} = \begin{cases} \pi D_{tube} L_{cond} & \text{(above the liquid level)} \\ \pi D_{tube} L_{cond} (1 - \alpha/180) & \text{(on the liquid level)} \\ 0 & \text{(below the liquid level)} \end{cases} \quad (A3.6)$$

$$A_{tube,w} = \pi d_{tube} L_{cond} \quad (A3.7)$$

$$A_{r,sh1} = \pi d_{sh} L_{cond} \beta/180 \quad (A3.8)$$

$$A_{r,sh2} = \pi d_{sh} L_{cond} (1 - \beta/180) \quad (A3.9)$$

References

- A1.1 **Touber, S.** "A contribution to the improvement of compressor valve design", Ph.D. thesis, Delft University of Technology, the Netherlands, 1976.
- A2.1 **Van der Meer, J.S.** "Simulation of a refrigerant evaporator", Ph.D. thesis, Delft University of Technology, the Netherlands, 1987.

CURRICULUM VITAE

Hongwei Wang was born on August 13, 1962 in Shaanxi province of the People's Republic of China. From 1967 to 1977, he took his primary and secondary educations at his hometown. In 1978, he entered Xi'an Jiaotong University and studied at the department (2) of power machinery engineering. In July 1982, he was granted a bachelor degree in engineering. In the same year he was selected by the State Education Commission of China to study in the Netherlands. In 1984, he registered as a undergraduate at the Faculty of Mechanical Engineering, Delft University of Technology. He earned his degree of "werktuigbouwkundig ingenieur" in July 1985. His graduation work was performed in the Laboratory for Refrigerating Engineering and Indoor Climate Technology.

Since September, 1986, he was employed as a research assistant in the same laboratory. He was working on the project presented in this thesis under the supervision of Prof. ir. A.L. Stolk and Dr. ir. S. Touber.

He is keen about sport and music and interested in the Chinese history.

ACKNOWLEDGEMENT

I would like to express my grateful thanks to my supervisors, Prof. ir. A.L. Stolk and Dr. ir. S. Toubert for their valuable guidance and supervision throughout the promotion work. I am especially grateful to Dr. ir. S. Toubert for his effort of setting up the project and searching funding for me to participate three international conferences.

I also acknowledge the skilful assistance from the workshop technicians at the Laboratory for Refrigeration Engineering and Indoor Climate Technology of the Delft University of Technology. I owe a debt of thanks to Mr. J. Keuvelaar for his help in laying out this thesis.

I am much indebted to my wife, Xiujuan Cao, for her insistent support and encouragement during my promotion work.